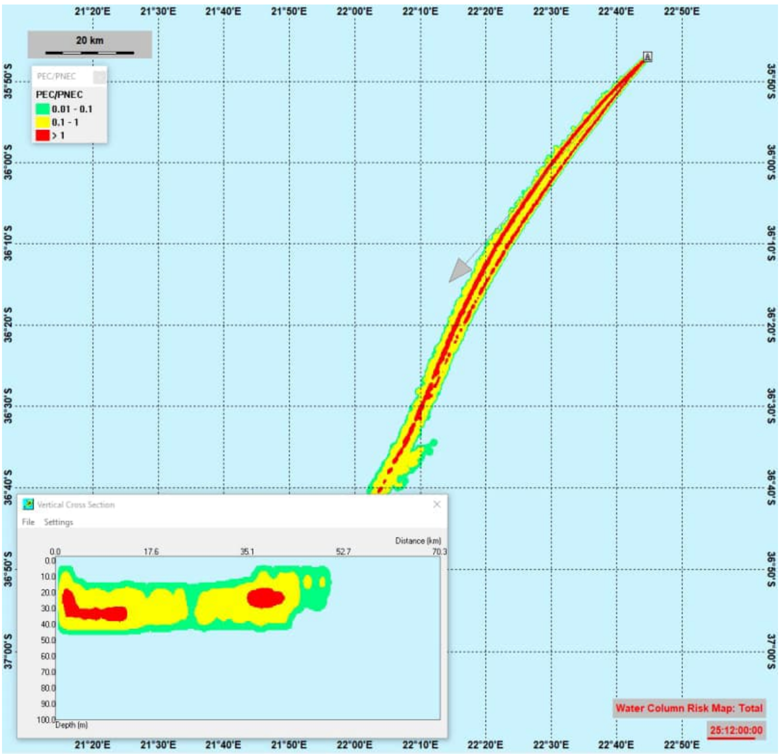

Figure 8.28 Snapshot showing the time instant with maximum EIF for the upper water column between 0-100 meters. Snapshot from 25.5 days after start, when the discharge is released from the rig. The vertical cross section shows the PEC/PNEC ratio in the water column along the grey arrow. Discharge location 4 – Winter.

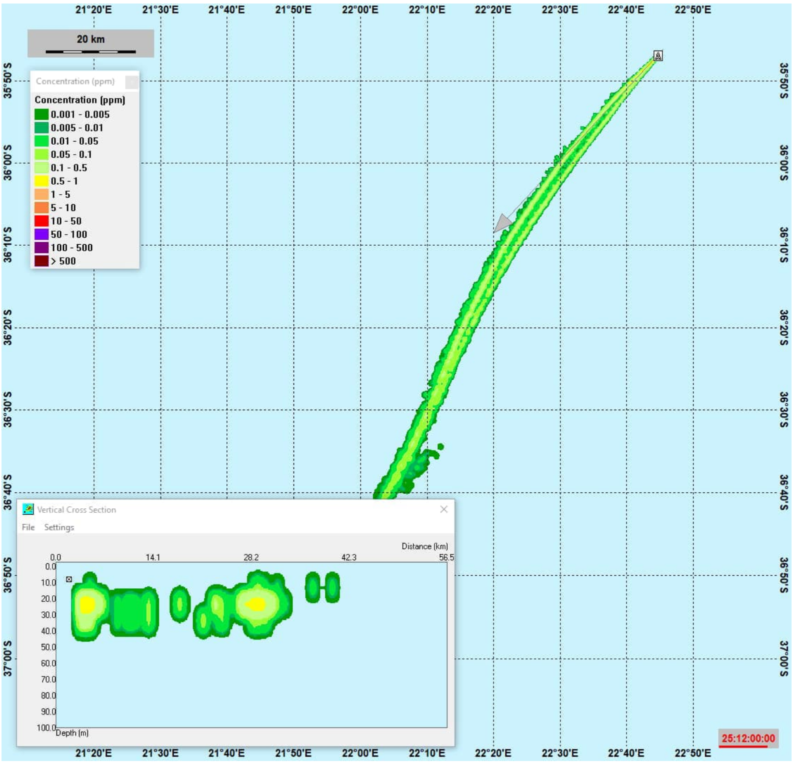

Figure 8.29 Concentration field for the component that gave the largest contribution to the environmental risk, namely the particle group Barium sulfate, at the same time-step as for maximum EIF. Discharge location 4 – Winter.

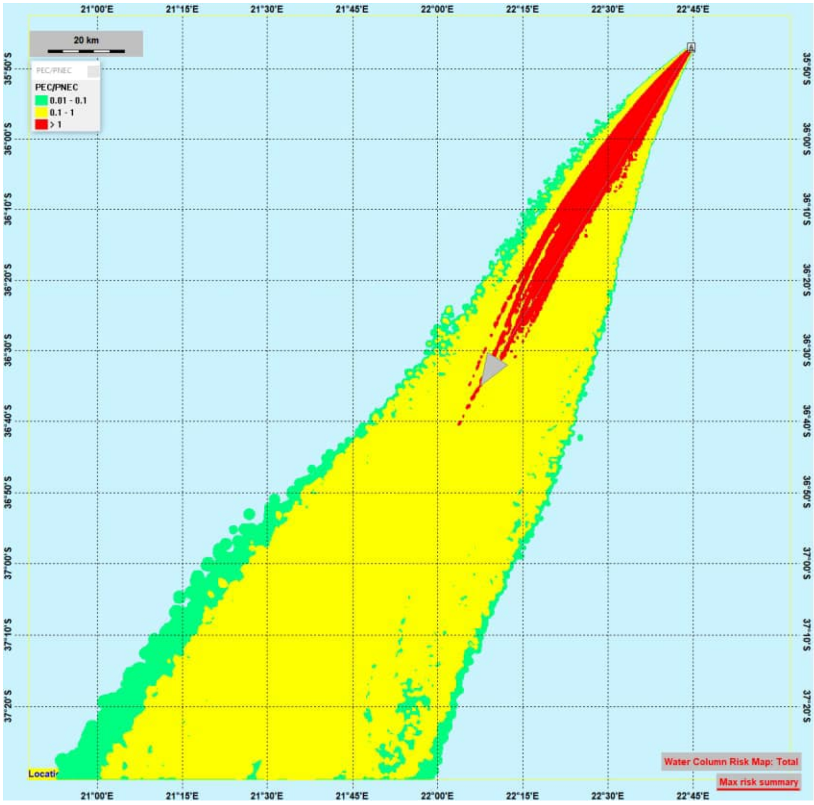

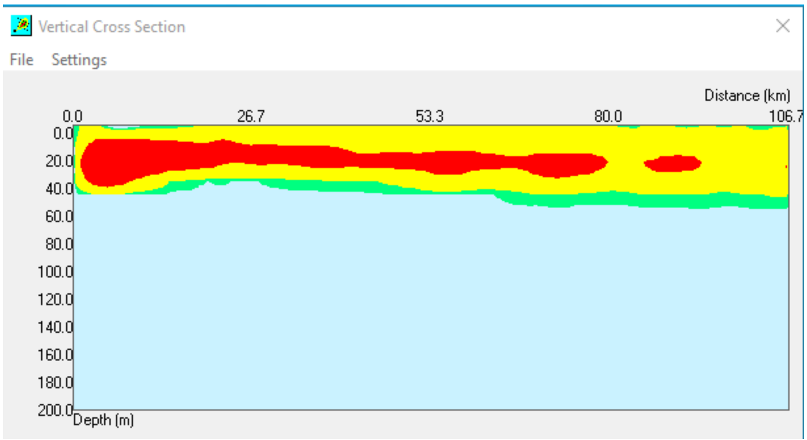

Figure 8.30 Maximum cumulative risk of drilling operations throughout the upper water column at any time for discharge location 4 (Start time August 14), discharge from rig 10 m below sea surface. Discharge location 4 – Winter.

8.3.3 Discharge location 4 - EIF results for the sediment – Winter

The maximum EIF (sea floor area 100x100 m^2) is computed with 0 impact by discharge from the rig, and 1.5 impacted by the top hole discharge. The contributions of the components of the discharge are listed in the table below (risk in % of EIF). The affected area on the sea floor is largest at the end of the transport and fate simulation, shortly after the sediment module starts. After that the sea floor will start restoration and the area (EIF) decreases. The factor affecting risk for the rig discharge is only grain size as for discharge location 4, Summer.

Table 8.10 Table and pie-chart shows contributions to EIF from the components discharged from the top hole sections to the sediment for location 4 – Winter.

Simulated instantaneous EIF:	**1.5**				
Components	Product	PNEC ppb	Contribution to risk %	Contribution max EIF	Contribution time averaged EIF
Total					
Barazan D		420	0	0	0
Soda Ash		200	0	0	0
Caustic Soda		20	0	0	0
Potassium Cloride		100	0	0	0
Starcide		49	0	0	0
Thickness		0	73.1	1.0965	1.0965
Oxygen		0	0	0	0
Grain size		0	26.9	0.4035	0.4035

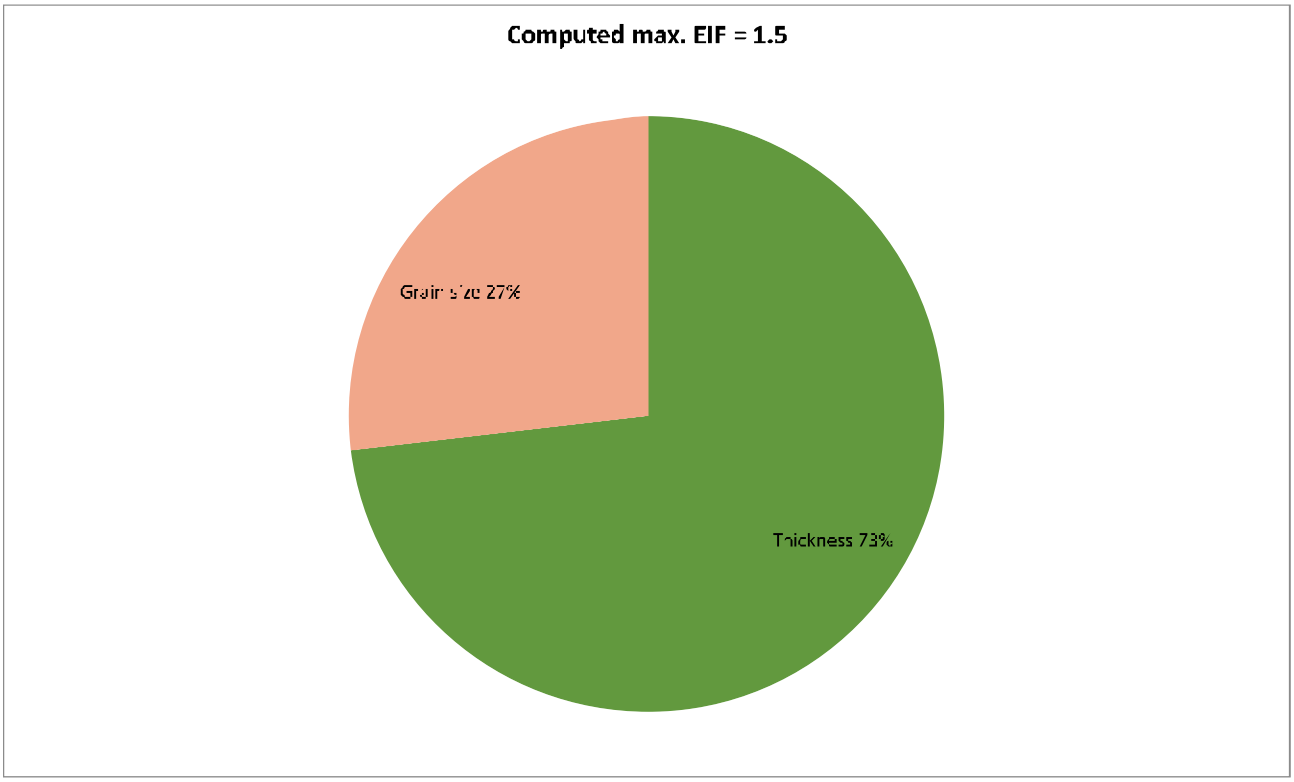

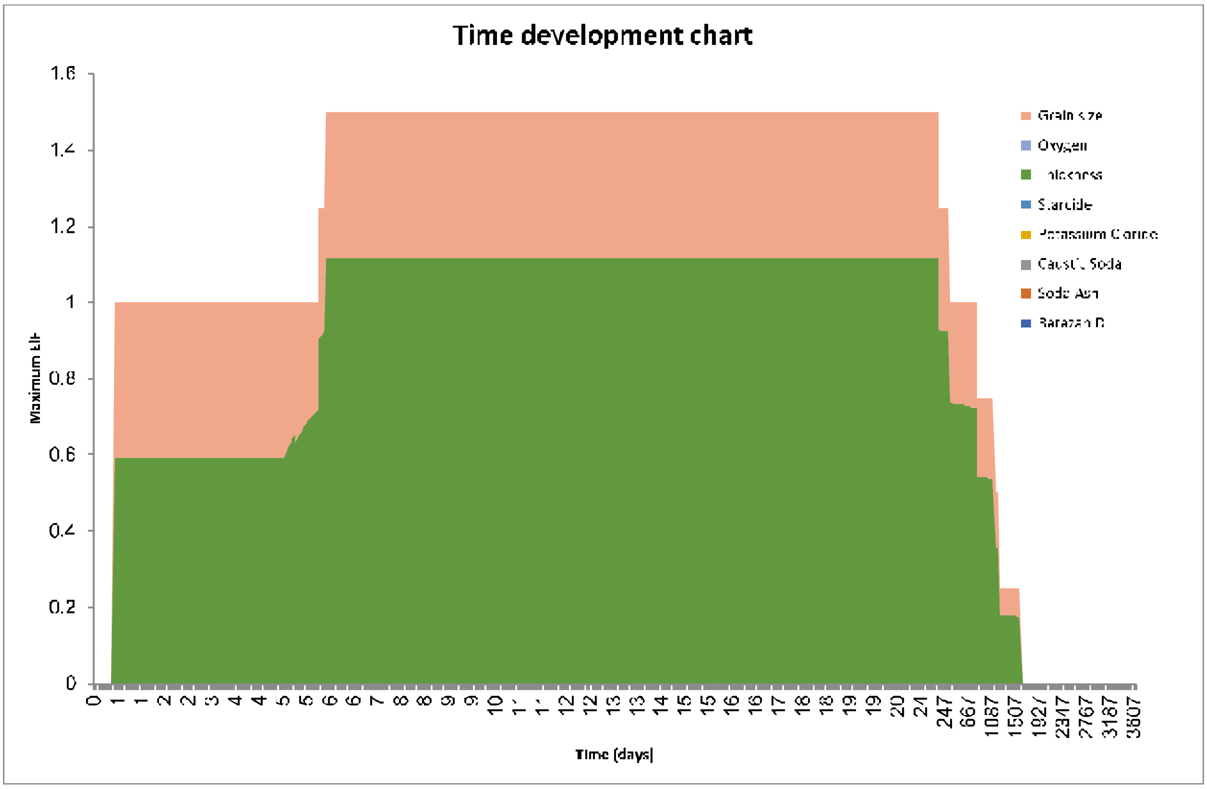

Figure 8.31 Time development of EIF for discharge from the top hole sections for the sediment for discharge location 4 – Winter.

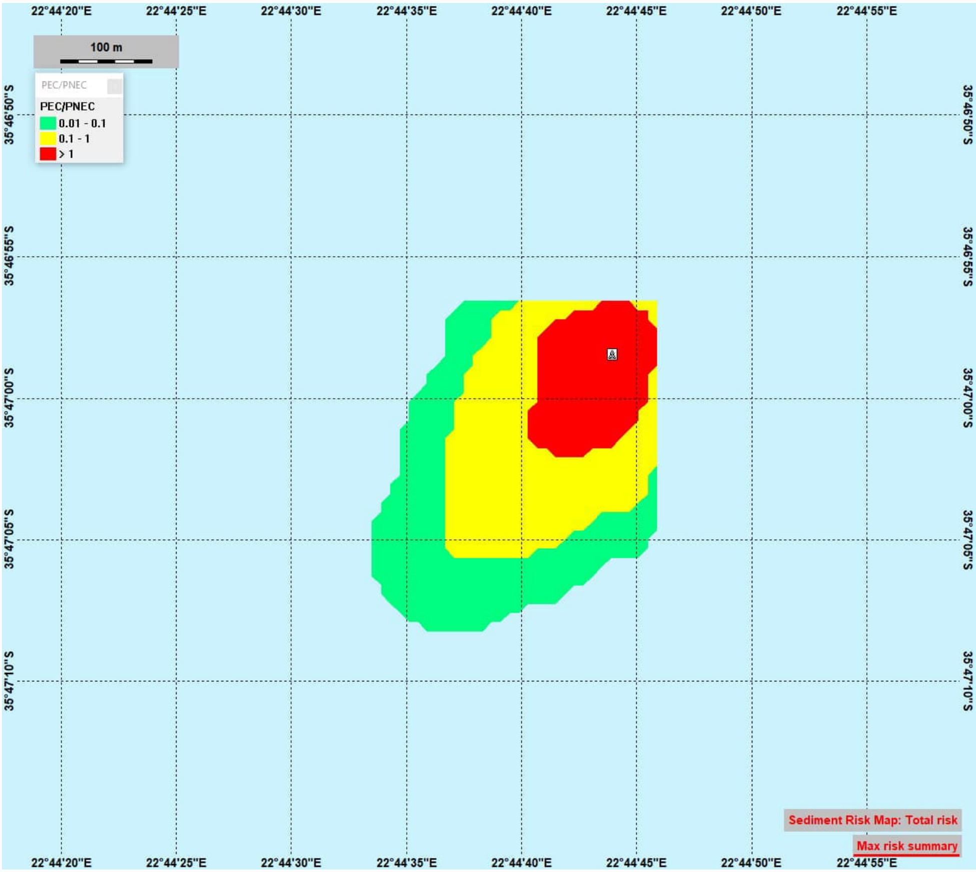

Figure 8.32 The total maximum EIF for the sediment (highest value at each location over simulation period) for discharge location 4 – Winter. (Smoothing of gridded results leads to strange straight lines north and east of the figure).

8.4 EIF results for discharge location 4, Spring

8.4.1 Discharge location 4 - Lower water-column – Spring

The maximum EIF (water volume 100x100x10 m^3) in the lower water-column 1100 - 1300 meters for discharge location 4, Spring, was 11265, while the time average EIF was 1151. The contributions of the components of the discharge are listed in the table below (risk in % of EIF).

Table 8.11 Table and pie-chart with EIF results for the lower water column, 1100 - 1300 meters. Discharge location 4 – Spring.

Computed max. EIF:	**11265**				
Time averaged EIF:	1151				
Components	Product	PNEC ppb	Contribution to risk %	Contribution max EIF	Contribution time averaged EIF
Total					
Barazan D		420	0.42	47.3130	4.8326
Soda Ash		200	0.12	13.51801356	1.3807
Caustic Soda		20	1.56	175.7341763	17.9495
Potassium Cloride		100	14.69	1654.83016	169.0243
Starcide		49	0.12	13.51801356	1.3807
Cuttings		100000	0.08	9.01200904	0.9205
Bentonite_ECHA		170	15.66	1764.10077	180.1852
Barite-Bariumsulfat		115	66.11	7447.29897	760.6670
Barite-Silica		440	1.24	139.6861401	14.2675

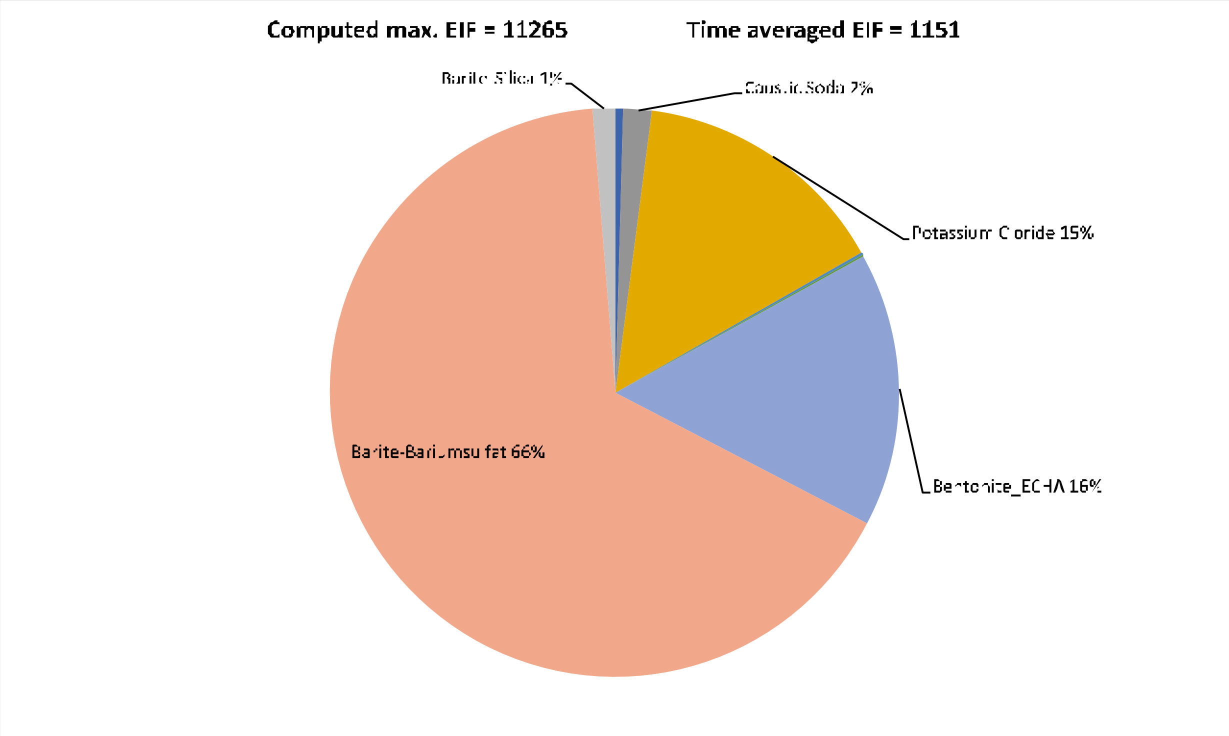

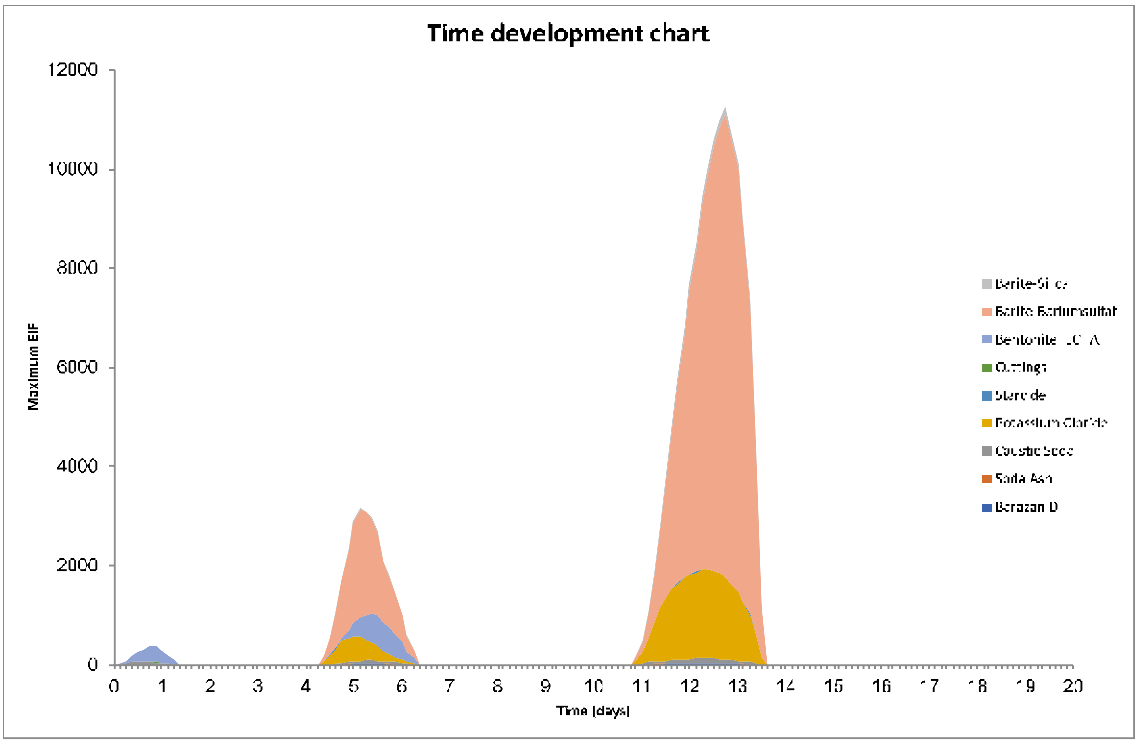

Figure 8.33 Time development of the EIF for the lower water column. Discharge location 4 – Spring.

Figure 8.34 shows the time instant with maximum EIF for the lower water column due to discharges from the top hole sections, while Figure 8.36 shows the maximum cumulative risk (foot-print) throughout the lower water column at any time during the drilling operation with discharges from the top hole sections.

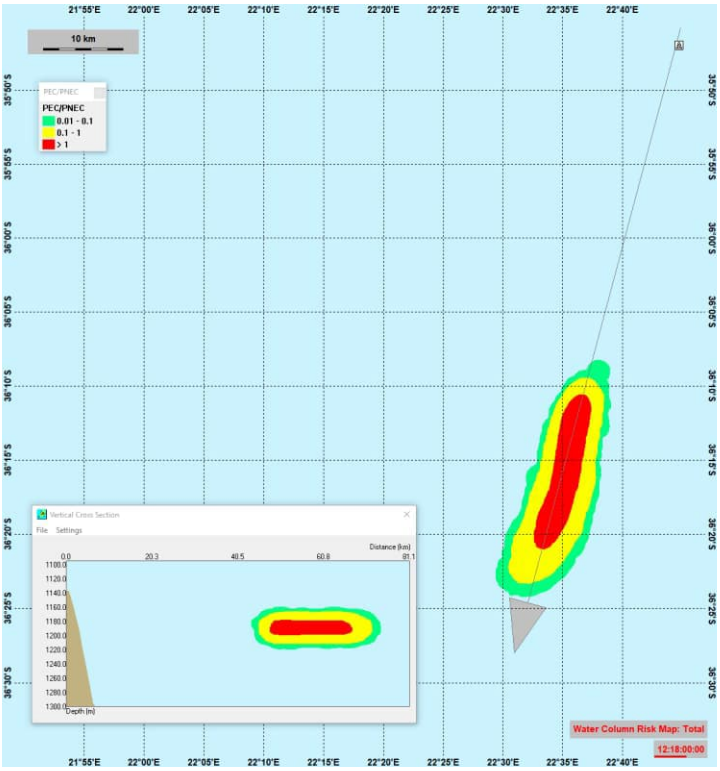

Figure 8.34 Snapshot showing the time instant with maximum EIF for the lower water column at 1100 - 1300 meters. Snapshot at day 14.5, when the discharge is from the top hole sections on the sea floor. The vertical cross section shows the PEC/PNEC ratio along the grey arrow. Discharge location 4 – Spring.

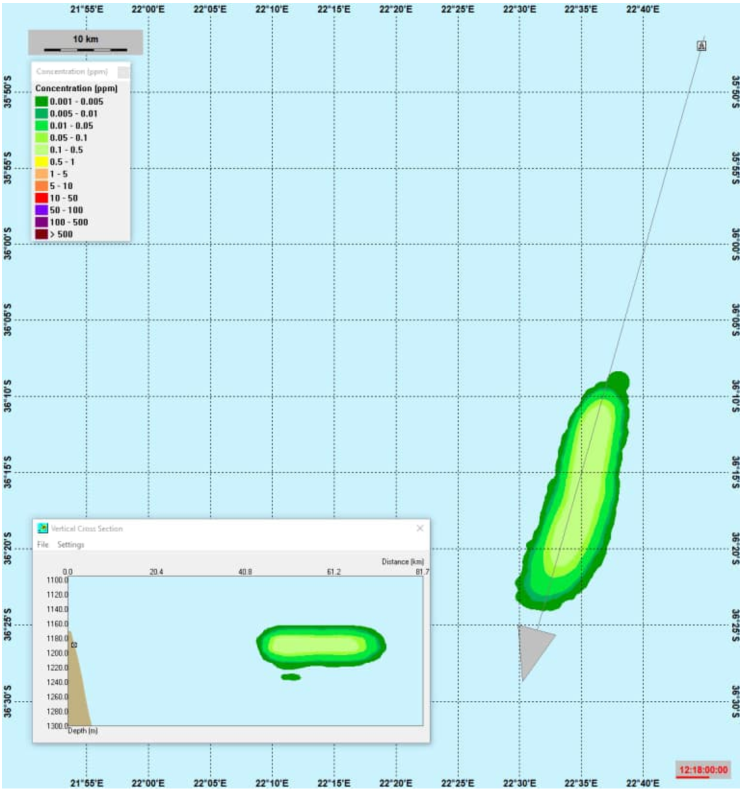

Figure 8.35 Concentration field for the component that gave the largest contribution to the environmental risk, namely the particle group barite, at the same time-step as for maximum EIF. A cross-section of the plume is shown in the smaller panel. Discharge location 4 – Spring.

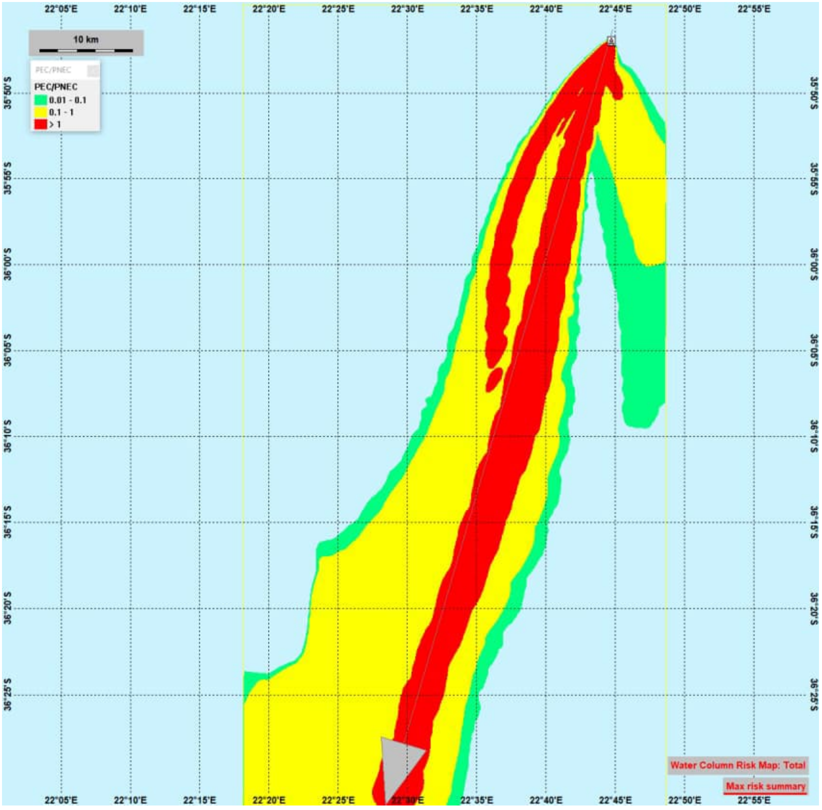

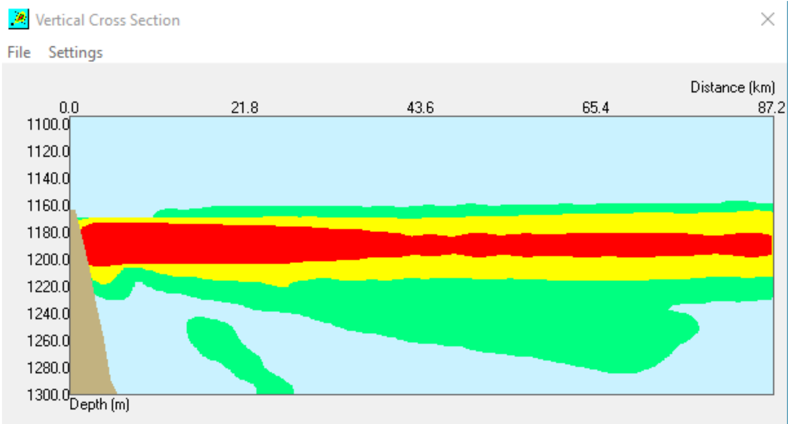

Figure 8.36 Maximum cumulative risk of drilling operations throughout the lower water column at any time for discharge location 4 (Start time October 19) Discharge at the seafloor. Discharge location 4 – Spring.

8.4.2 Discharge location 4 - Upper water-column – Spring

The maximum EIF (water volume 100x100x10 m^3) in the upper water-column 0-100 meter for discharge location 4, Spring, was 9032, while the time average EIF was 723. The contributions of the components of the discharge are listed in the table below (risk in % of EIF).

Table 8.12 Table and pie-chart with EIF results for the water column, upper 100 meter for discharge location 4, Spring.

Computed max. EIF:	9032				
Time averaged EIF:	723				
Components	Product	PNEC ppb	Contribution to risk %	Contribution max EIF	Contribution time averaged EIF
Total					
Soda Ash		200	0.03	2.7096	0.2168
Caustic Soda		20	0.34	30.70870378	2.4566
Barazan D		420	0.07	6.32238019	0.5058
Potassium Cloride		100	6.74	608.7348926	48.6983
Sodium Chloride		1000000	0	0	0.0000
GEM GP		188	0.03	2.70959151	0.2168
Clayseal Plus		562.3	0	0	0.0000
Clayseal Plus-2		0.45	1.41	127.350801	10.1876
Clay Grabber		9.8	0.31	27.99911227	2.2398
Clay Grabber 2		1.31	0.38	34.32149246	2.7456
Clay Sync II		1160	0.02	1.80639434	0.1445
Bore HIB		146	0	0	0.0000
Dextrid E		1000	0.08	7.22557736	0.5780
PAC-l		87.26	0.65	58.70781605	4.6964
Cuttings		100000	0	0	0.0000
Barite-Bariumsulfat		115	84.88	7666.337579	613.2812
Barite Silica		440	0.75	67.73978775	5.4190
Baracarb 150		115	2.16	195.0905887	15.6066
Baracarb 50		115	2.15	194.1873916	15.5343

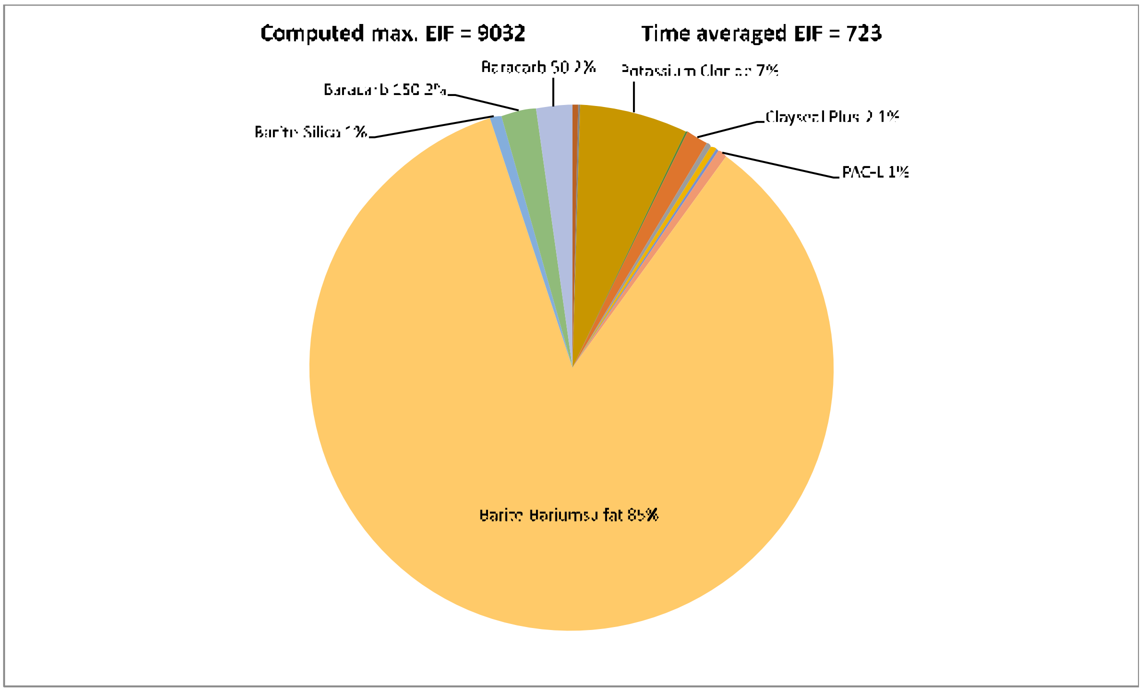

The results show that for the upper water column, effects caused by discharges of particle matter (essentially Barium sulfate 85%) are dominating the risk in the affected water volume. During the time of maximum EIF, the discharge is released from the rig 10 meters below sea-surface and sinks down in the water-column.

Figure 8.37 shows the time development for the EIF in water-column. It shows that the duration with environmental risk disappears shortly after discharge.

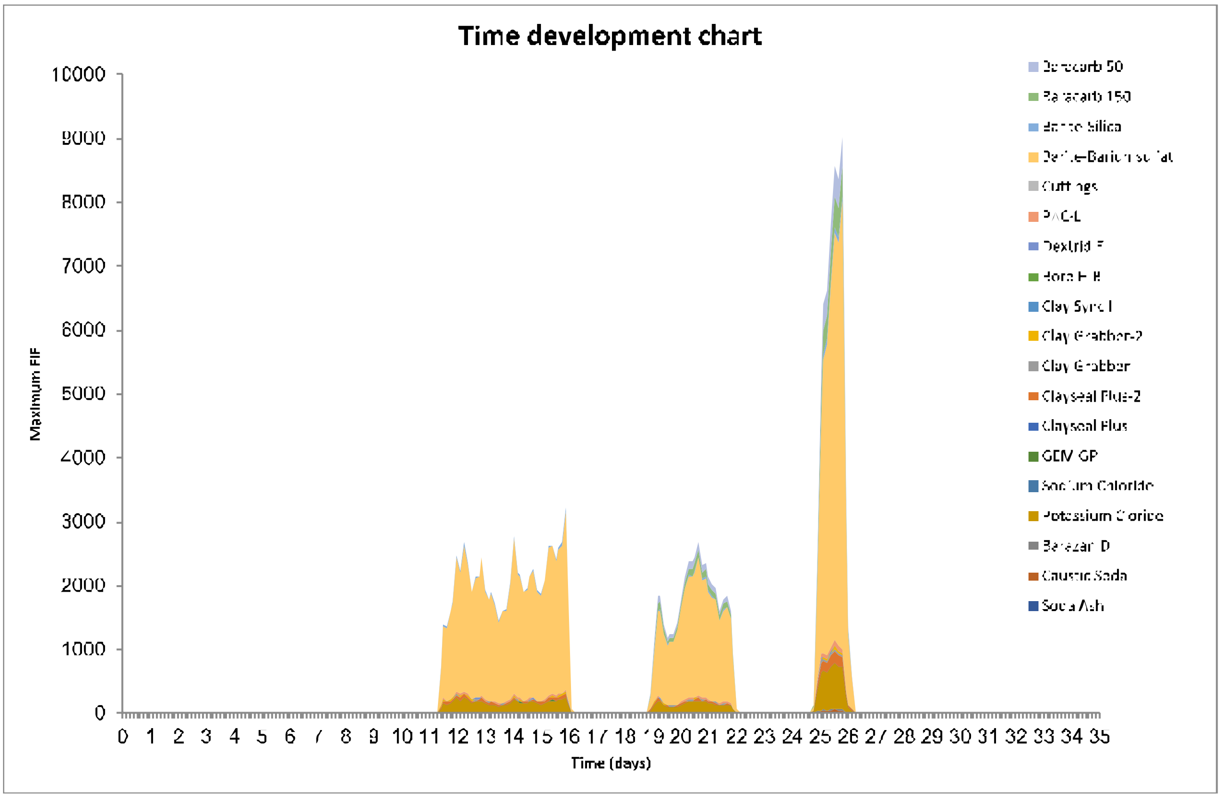

Figure 8.37 Time development of the EIF for the upper water column, for discharge location 4 Spring.

Figure 8.38 shows the time instant with maximum EIF for the upper water column due to discharges from rig 10 m below sea surface, while Figure 8.40 shows the maximum cumulative risk (foot-print) throughout the upper water column at any time during the drilling operation with discharges from the rig.

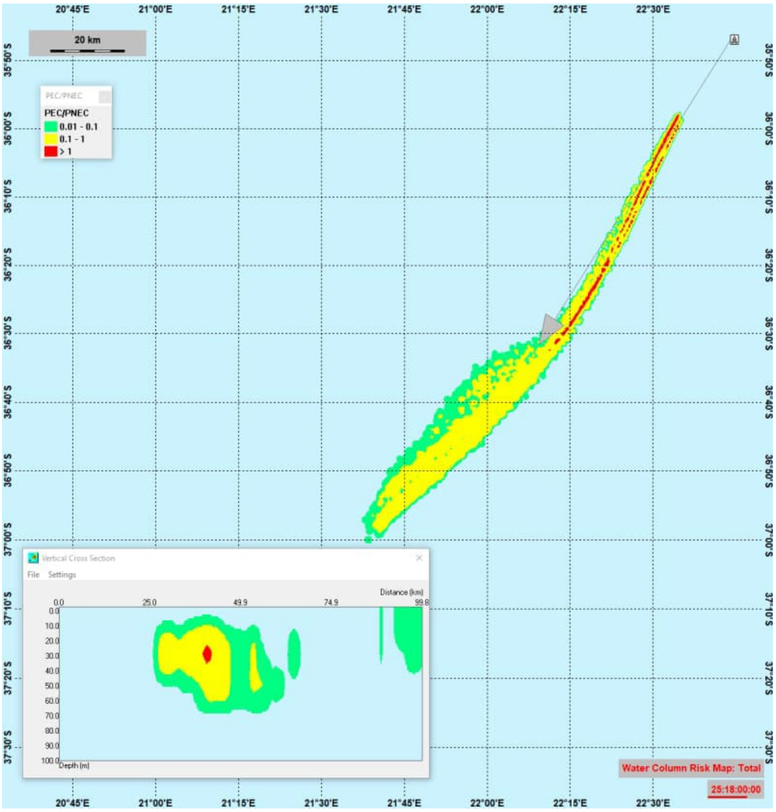

Figure 8.38 Snapshot showing the time instant with maximum EIF for the upper water column between 0-100 meters. Snapshot from 25.5 days after start, when the discharge is released from the rig. The vertical cross section shows the PEC/PNEC ratio in the water column along the grey arrow. Discharge location 4 – Spring.

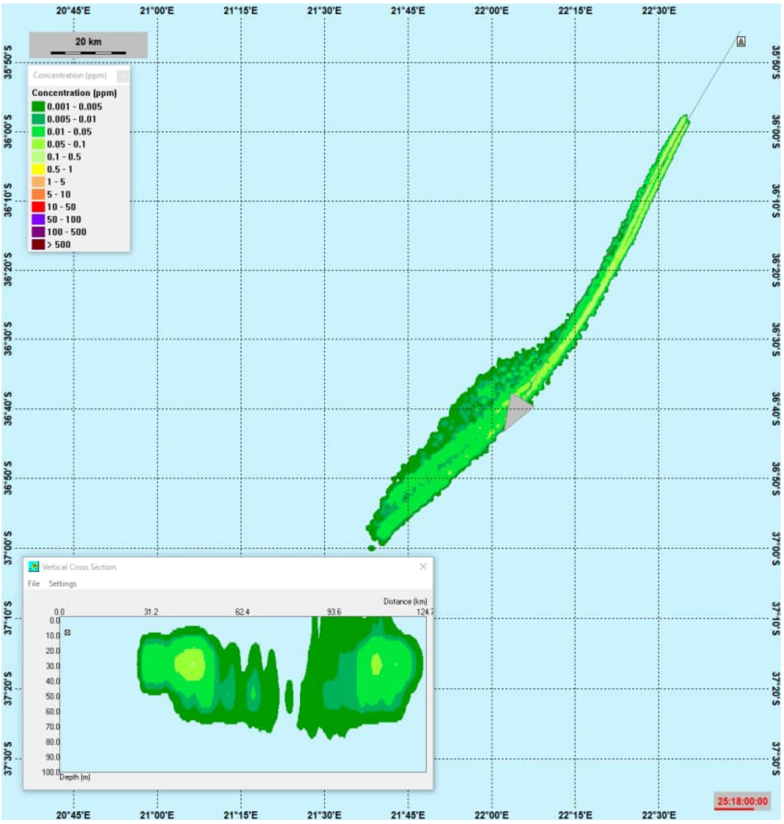

Figure 8.39 Concentration field for the component that gave the largest contribution to the environmental risk, namely the particle group Barium sulfate, at the same time-step as for maximum EIF. Discharge location 4 – Spring.

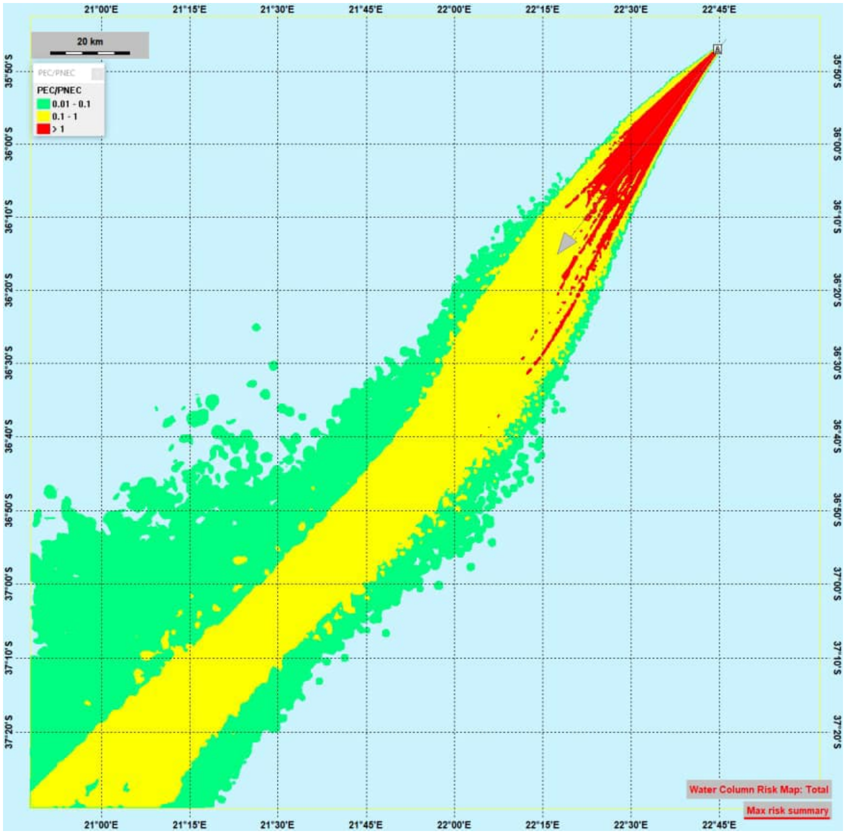

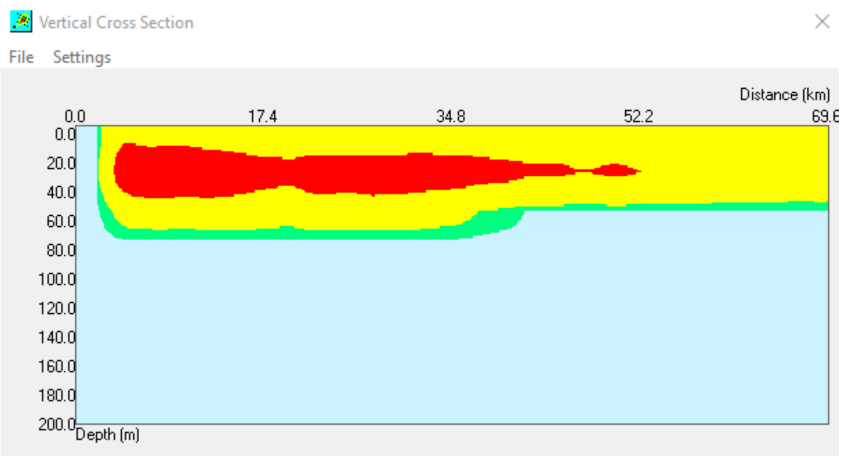

Figure 8.40 Maximum cumulative risk of drilling operations throughout the upper water column at any time for discharge location 4 (Start time October 19), discharge from rig 10 m below sea surface. Discharge location 4 – Spring.

8.4.3 Discharge location 4 - EIF results for the sediment – Spring

The maximum EIF (sea floor area 100x100 m^2) is computed with 0 impact for discharge from the rig, and 1 impacted by the top hole discharge. The contributions of the components of the discharge are listed in the table below (risk in % of EIF). The affected area on the sea floor is largest at the end of the transport and fate simulation, shortly after the sediment module starts. After that the sea floor will start to restore and the area (EIF) will get smaller. The factor affecting risk for the rig discharge is only grain size as for discharge location 4, Summer.

Table 8.13 Table and pie-chart shows contributions to EIF from the components discharged from the top hole sections to the sediment for location 4 – Spring.

Simulated instantaneous EIF:	**1**				
Components	Product	PNEC ppb	Contribution to risk %	Contribution max EIF	Contribution time averaged EIF
Total					
Barazan D		420	0	0	0
Soda Ash		200	0	0	0
Caustic Soda		20	0	0	0
Potassium Cloride		100	0	0	0
Starcide		49	0	0	0
Thickness		0	73.04	0.7304	0.7304
Oxygen		0	0	0	0
Grain size		0	26.95	0.2695	0.2695

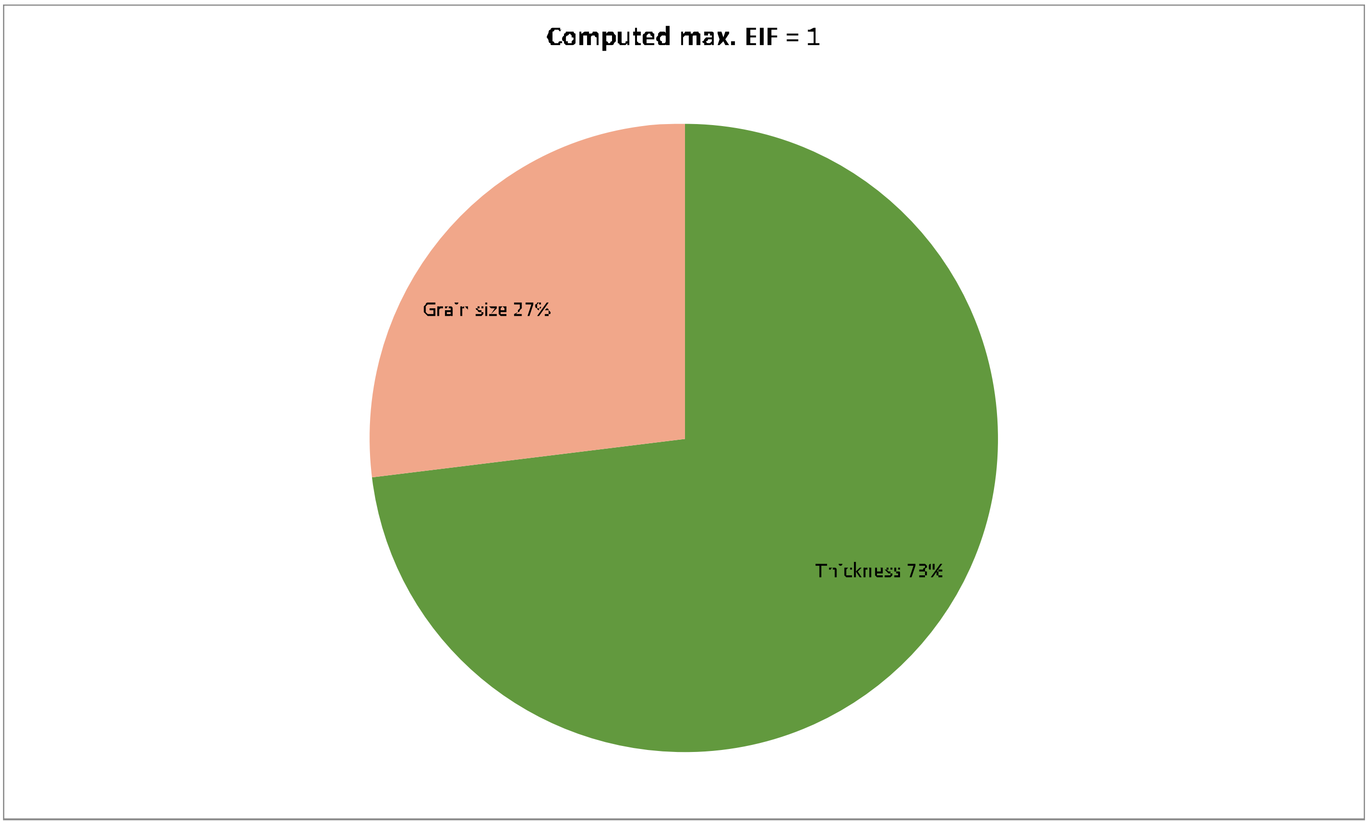

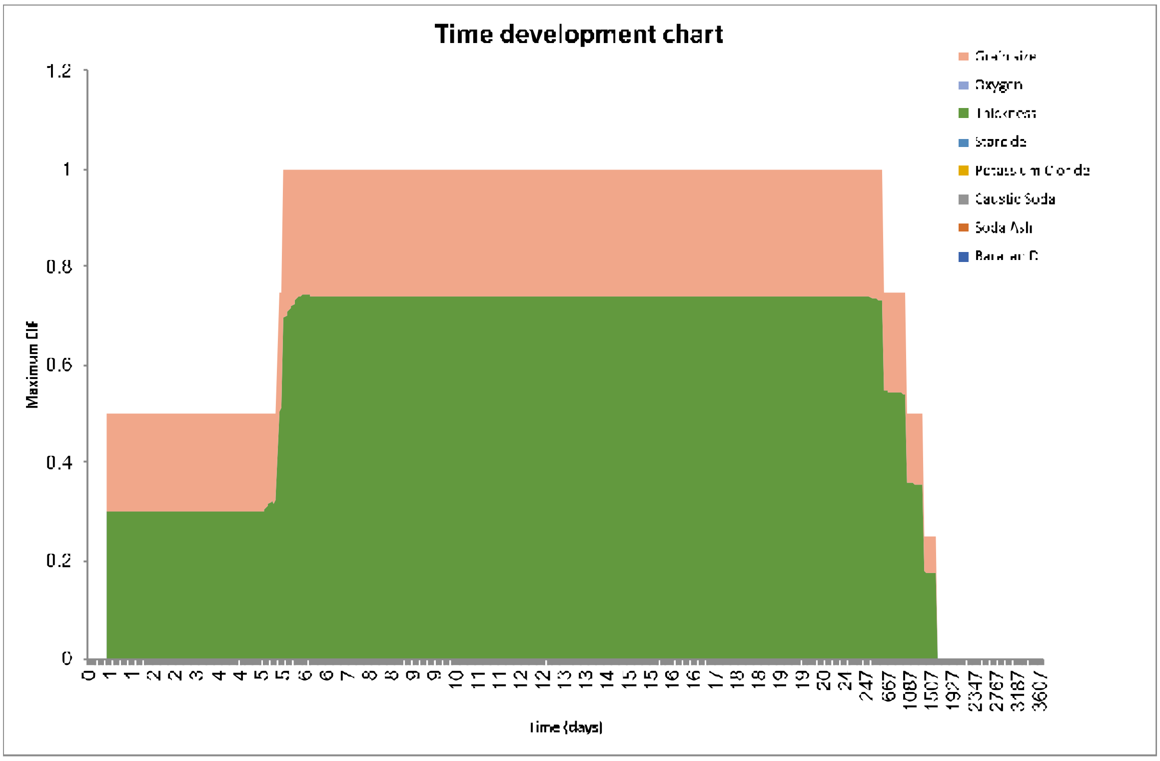

Figure 8.41 Time development of EIF for discharge from the rig for the sediment for discharge location 4 – Spring.

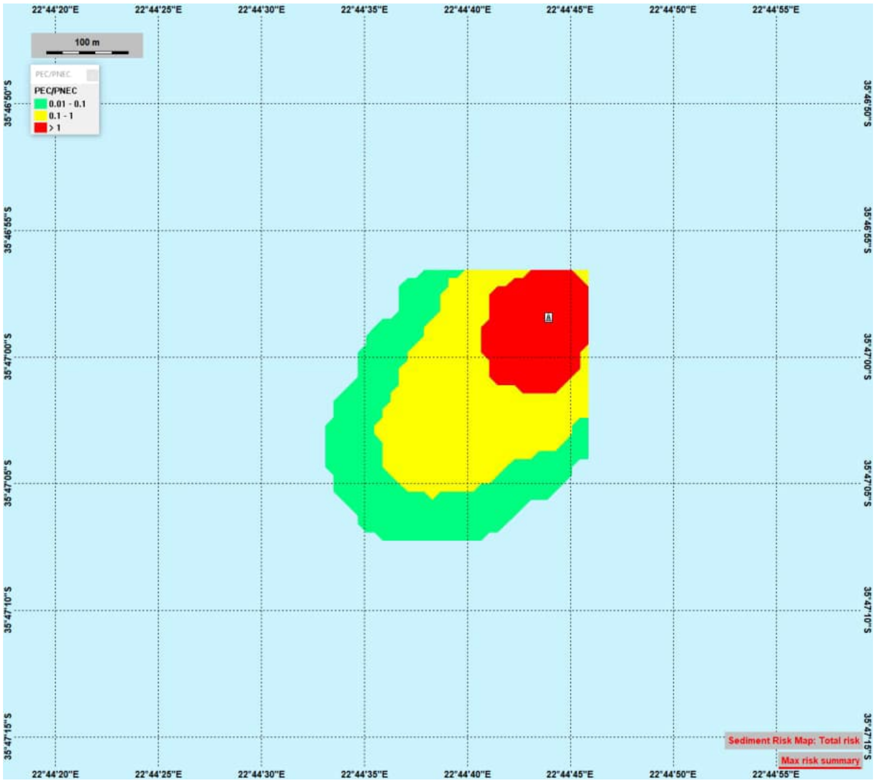

Figure 8.42 The total maximum EIF for the sediment (highest value at each location over simulation period) for discharge location 4 – Spring. Inserted figure in lower corner shows the maximum calculated EIF in sediment for discharge from the rig. Discharge location 4 – Spring. (Smoothing of gridded results leads to strange straight lines north and east of the figure).

8.5 Risk results in the water column for location 4

The EIF results are a reference water volume and sea floor area, respectively, where the risk for an environmental effect is larger than 5%. The actual risk is computed by the PNEC and risk curves for each of the components and their combination. The figures below show this environmental risk from all components in % for the water-column at the time with maximum EIF for each section. Environmental risk below 5% (not contributing to the EIF) is colored as outline only.

8.5.1 Discharge location 4 – Summer: Risk results in the lower water column

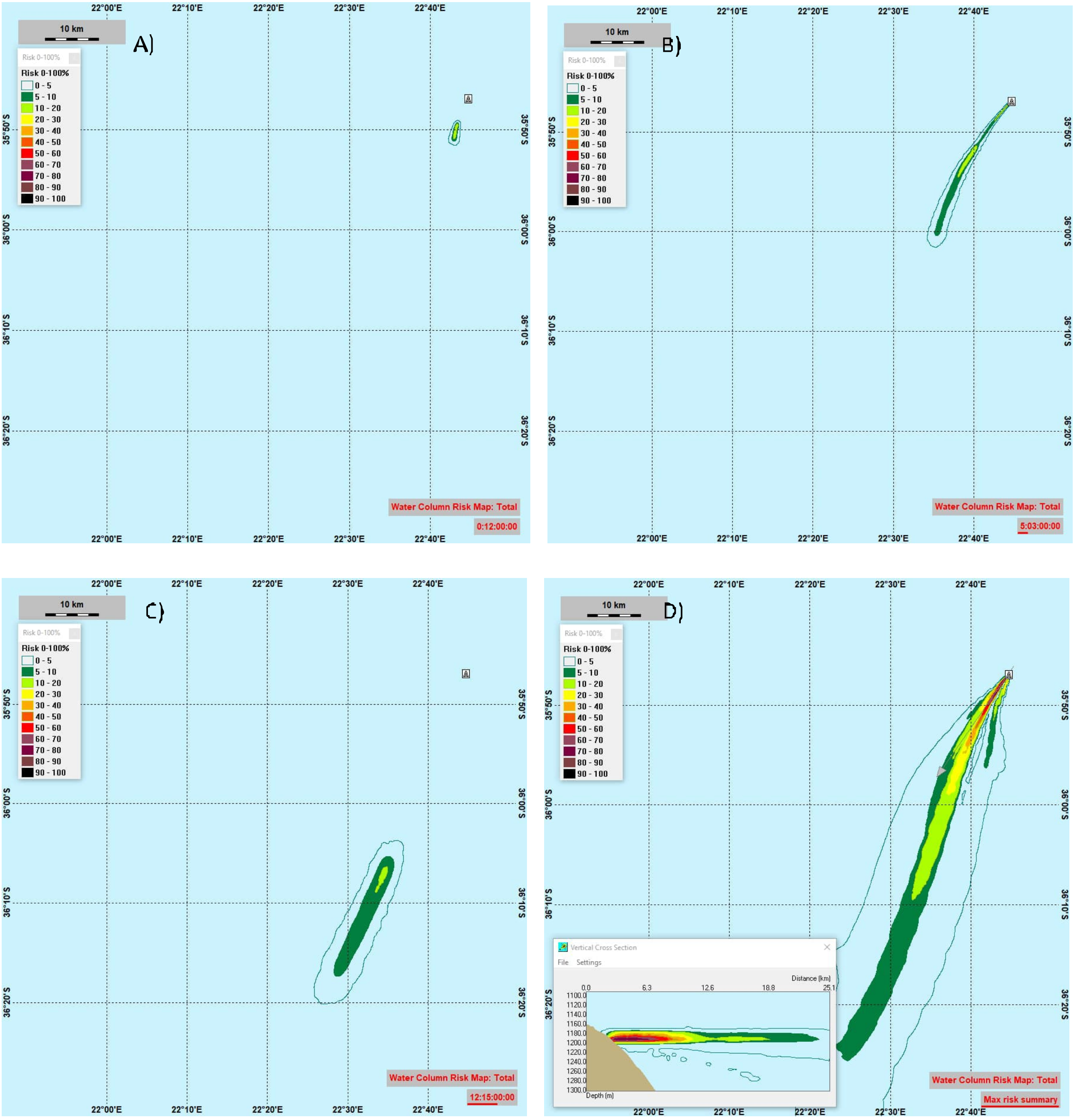

Figure 8.43 Discharge location 4 – Summer: Environmental risk > 5 % from all components for the lower water-column (1750 – 1850 meter) at the instant timestep with maximum risk for the discharges released at the sea floor: A) After Section 42", B) After Section 26". Figure C) Section 26" displacement. D) shows the total maximum risk summary for the lower water-column (highest value at each location over the whole simulation period).

8.5.2 Discharge location 4 – Summer: Risk results in the upper water column

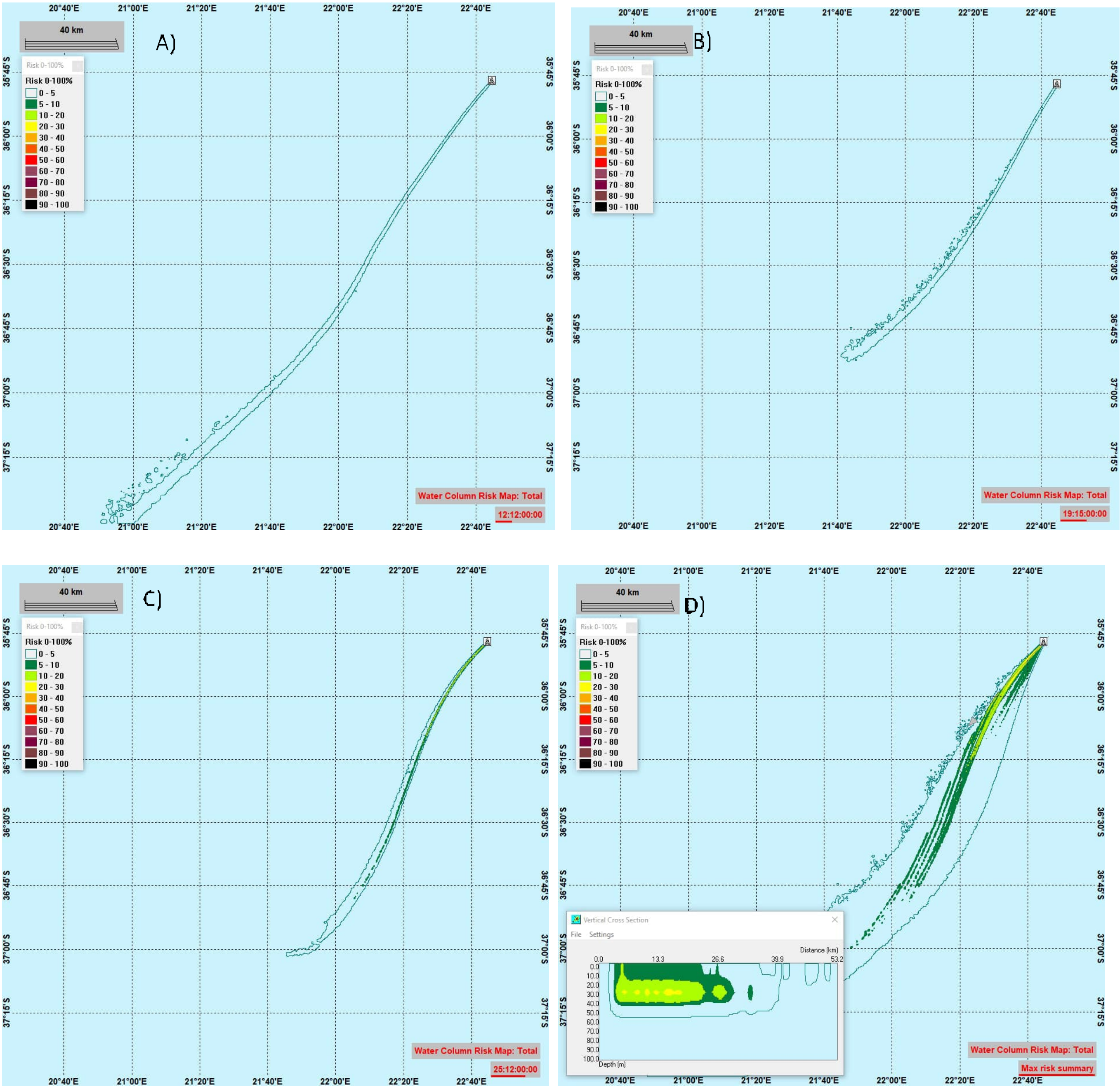

Figure 8.44 Discharge location 4 – Summer: Environmental risk > 5 % from all components for the upper water-column at the instant timestep with maximum risk for each discharge released from rig: A) Section 12 ¼" Cuttings + HPWBM, B) Section 8.5" Cuttings + HPWBM, C) Section 8.5" HPWBM, D) The total maximum risk summary for the upper water-column (highest value at each location over the whole simulation period).

8.5.3 Discharge location 4 – Autumn: Risk results in the lower water column

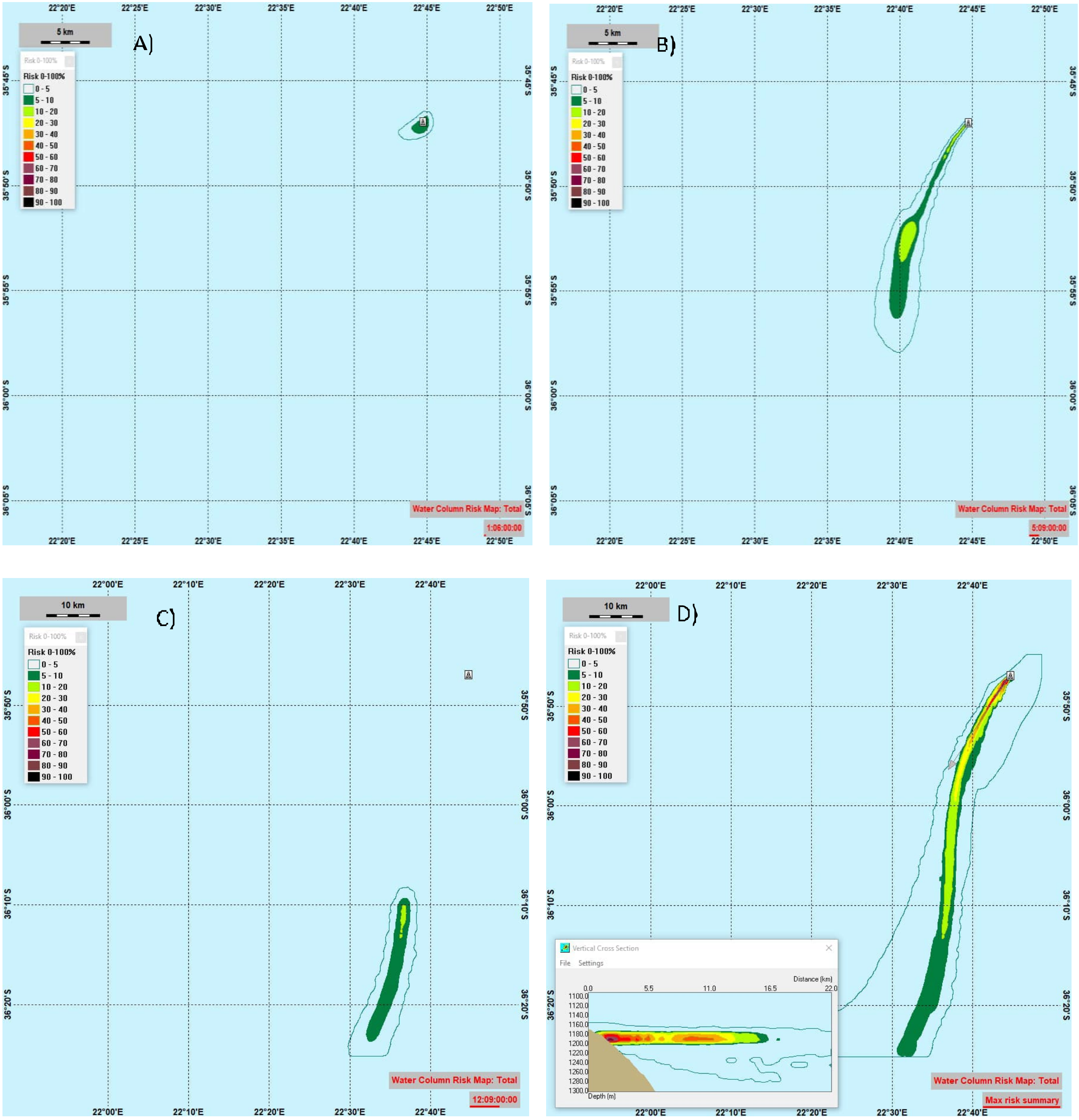

Figure 8.45 Discharge location 4 – Autumn: Environmental risk > 5 % from all components for the lower water-column (1750 – 1850 meter) at the instant timestep with maximum risk for the discharges released at the sea floor: A) After Section 42", B) After Section 26". Figure C) Section 26" displacement. D) shows the total maximum risk summary for the lower water-column (highest value at each location over the whole simulation period).

8.5.4 Discharge location 4 – Autumn: Risk results in the upper water column

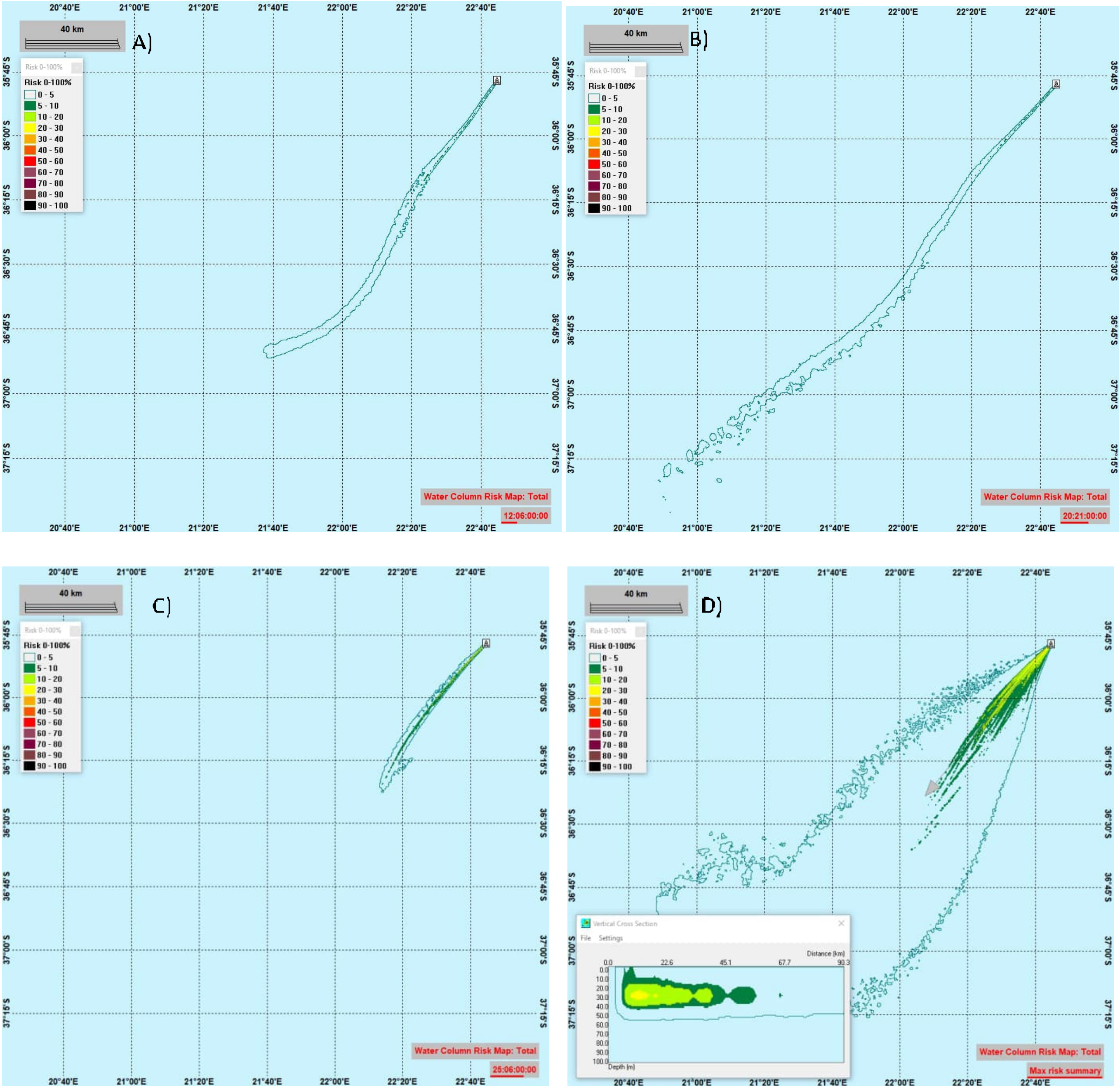

Figure 8.46 Discharge location 4 – Autumn: Environmental risk > 5 % from all components for the upper water-column at the timestep with maximum risk for the discharges released from rig: A) Section 12 ¼" Cuttings + HPWBM, B) Section 8.5" Cuttings + HPWBM, C) Section 8.5 HPWBM, D) The total maximum risk summary for the upper water-column (highest value at each location over the whole simulation period).

8.5.5 Discharge location 4 – Winter: Risk results in the lower water column

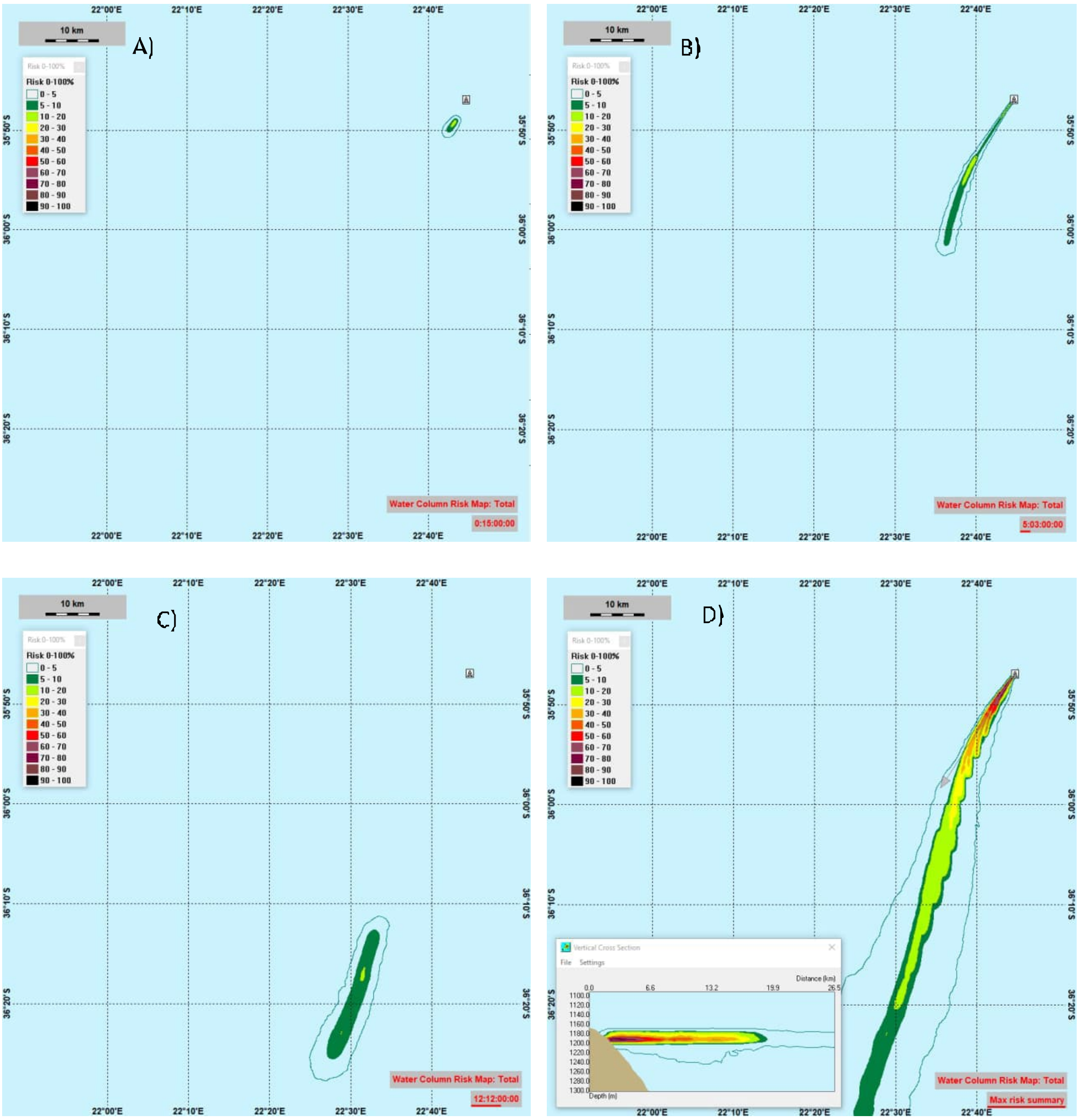

Figure 8.47 Discharge location 4 – Winter: Environmental risk > 5 % from all components for the lower water-column (1750 – 1850 meter) at the instant timestep with maximum risk for the discharges released at the sea floor: A) After Section 42", B) After Section 26". Figure C) Section 26" displacement. D) shows the total maximum risk summary for the lower water-column (highest value at each location over the whole simulation period).

8.5.6 Discharge location 4 – Winter: Risk results in the upper water column

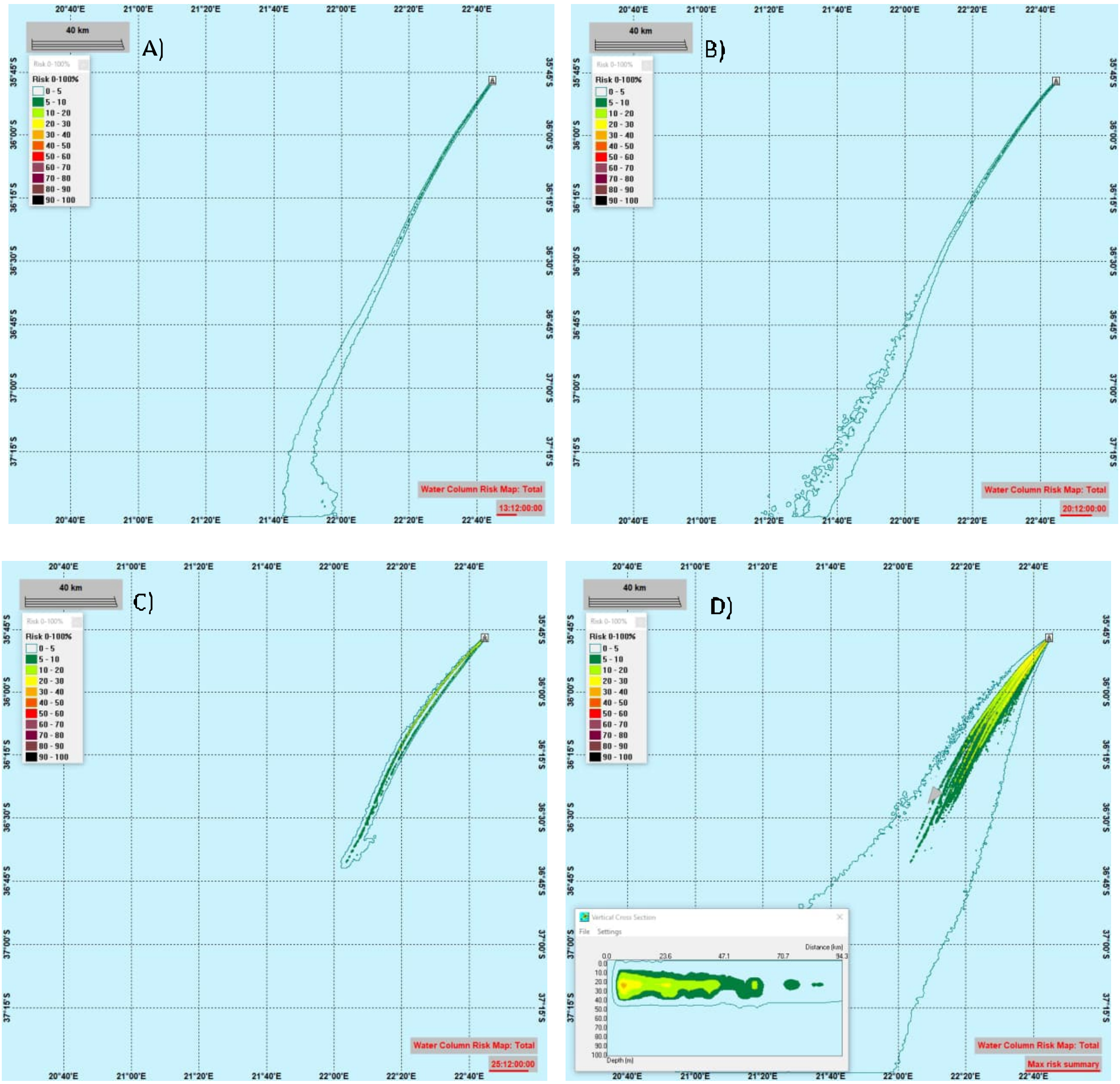

Figure 8.48 Discharge location 4 – Winter: Environmental risk > 5 % from all components for the upper water-column at the timestep with maximum risk for the discharges released from rig: A) Section 12 ¼" Cuttings + HPWBM, B) Section 8.5" Cuttings + HPWBM, C) Section 8.5 batch HPWBM , D) The total maximum risk summary for the upper water-column (highest value at each location over the whole simulation period).

8.5.7 Discharge location 4 – Spring: Risk results in the lower water column

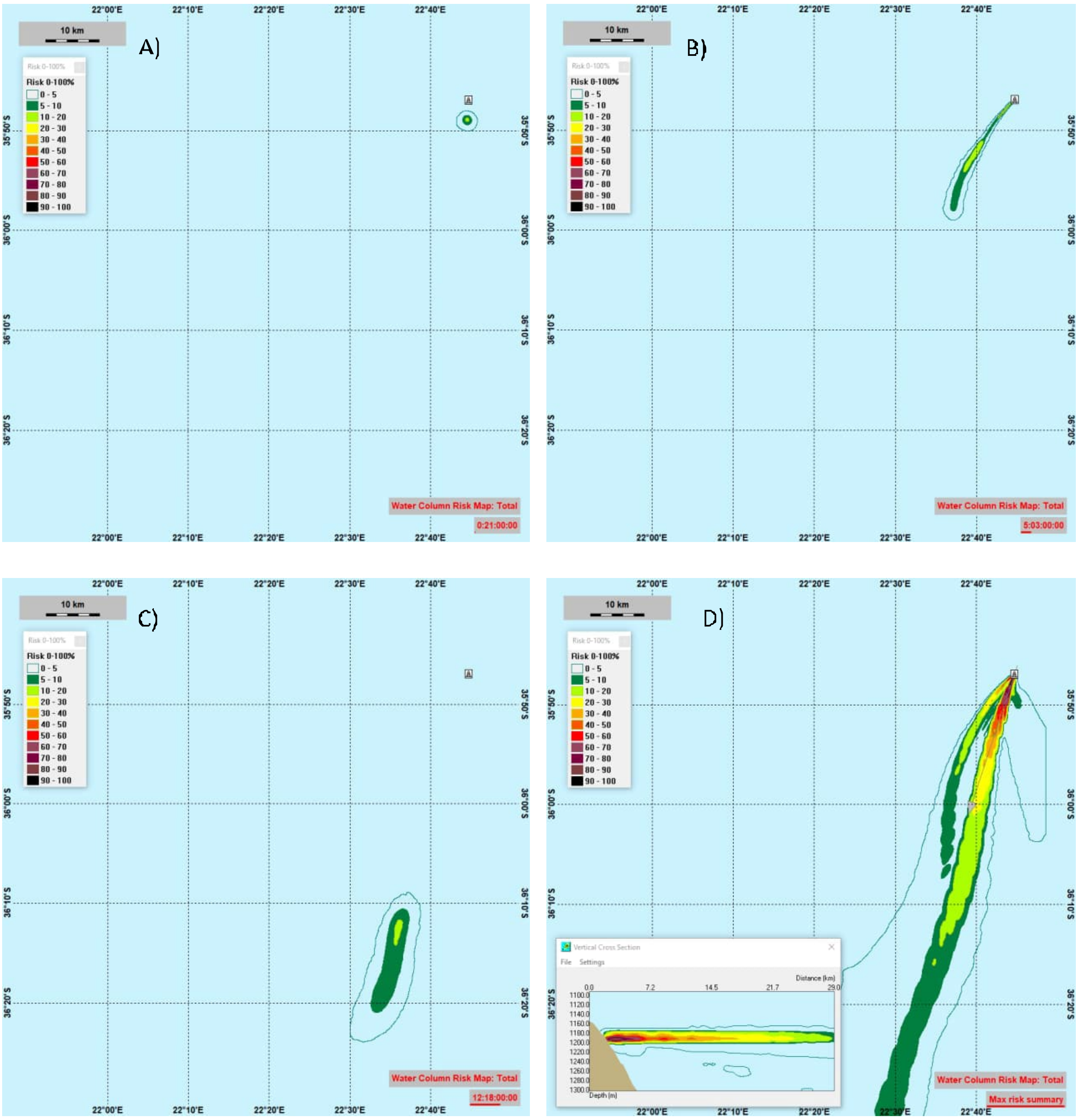

Figure 8.49 Discharge location 4 – Spring: Environmental risk > 5 % from all components for the lower water-column (1750 – 1850 meter) at the instant timestep with maximum risk for the discharges released at the sea floor: A) After Section 42", B) After Section 26". Figure C) Section 26" displacement. D) shows the total maximum risk summary for the lower water-column (highest value at each location over the whole simulation period).

8.5.8 Discharge location 4 – Spring: Risk results in the upper water column

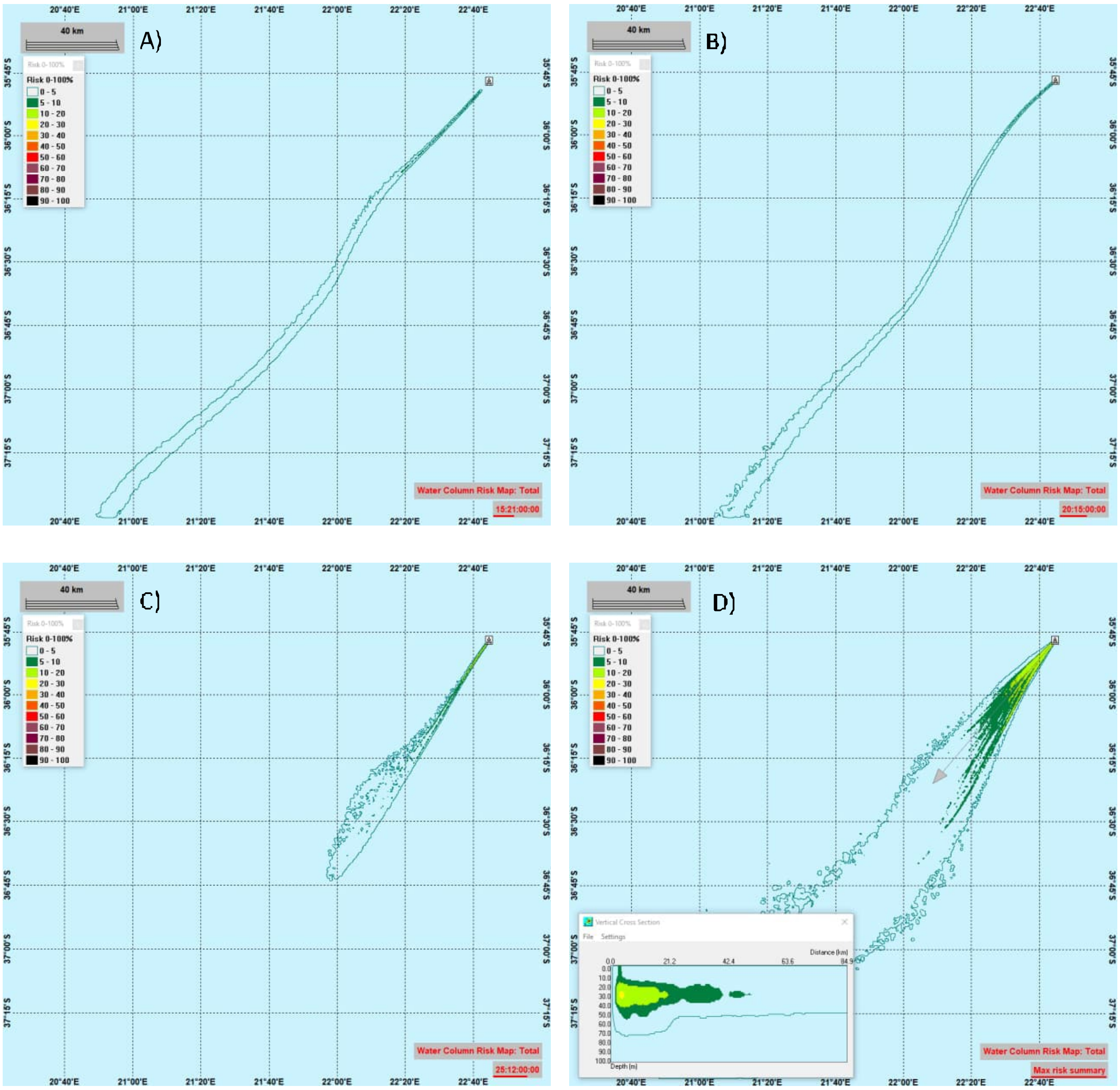

Figure 8.50 Discharge location 4 – Spring: Environmental risk > 5 % from all components for the upper water-column at the timestep with maximum risk for the discharges released from rig: A) Section 12 ¼" Cuttings + HPWBM, B) Section 8.5" Cuttings + HPWBM, C) Section 8.5 batch HPWBM , D) The total maximum risk summary for the upper water-column (highest value at each location over the whole simulation period).

8.6 Risk in the sediment for location 4

The environmental risk on the sea floor and in the sediment is presented as spatial distribution on a map and snapshots in time. The color scale is environmental risk in % as the combination of all 4 stressors toxicity, oxygen depletion, burial, and grain size change. Environmental risk below 5% (not contributing to the EIF) is colored as outline only. The figures show the risk situation at day 11 the end of all discharges on the seafloor, after 2 year and after 4 years. Simulations show that there is no risk > 5% in the sediment after 4 years. We note that changes to the sediment due to resuspension and transport by currents is not part of the simulation.

8.6.1 Discharge location 4 – Risk in sediment

Summer :

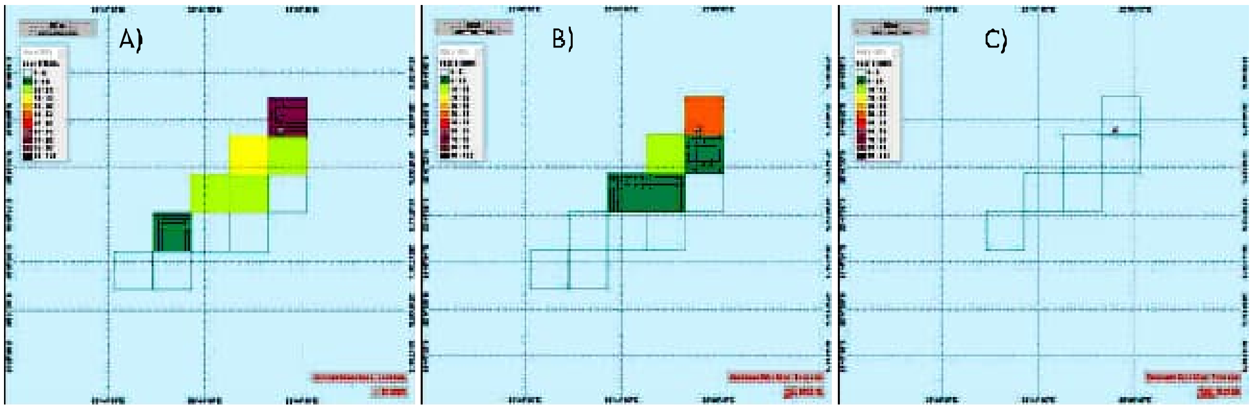

Autumn:

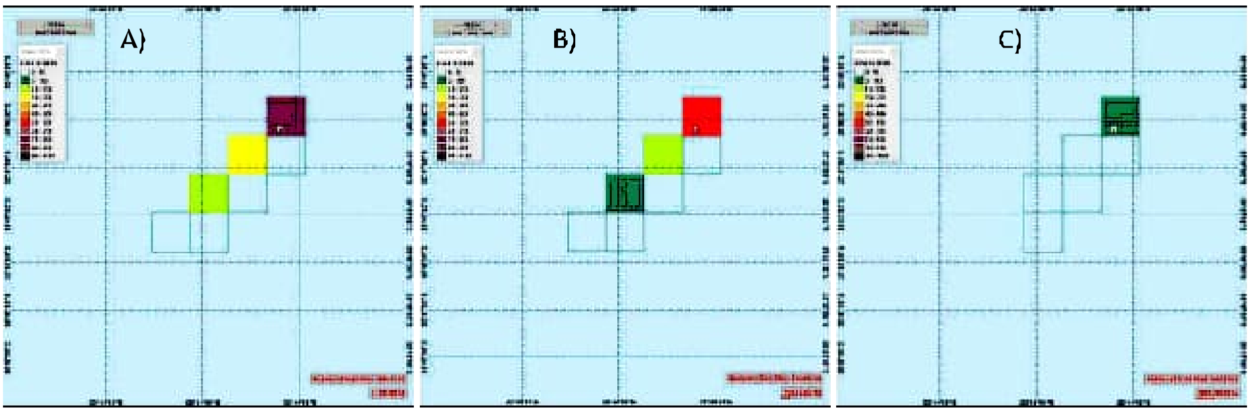

Winter:

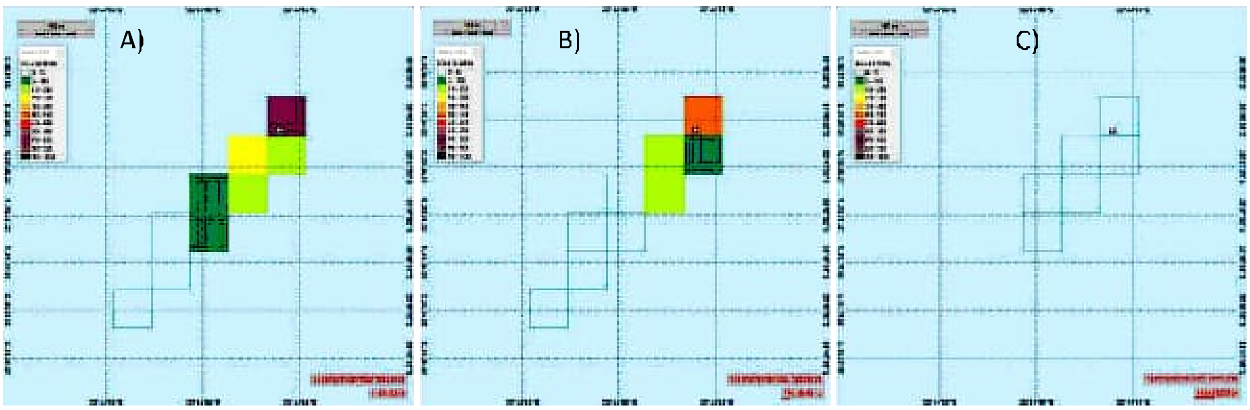

Spring:

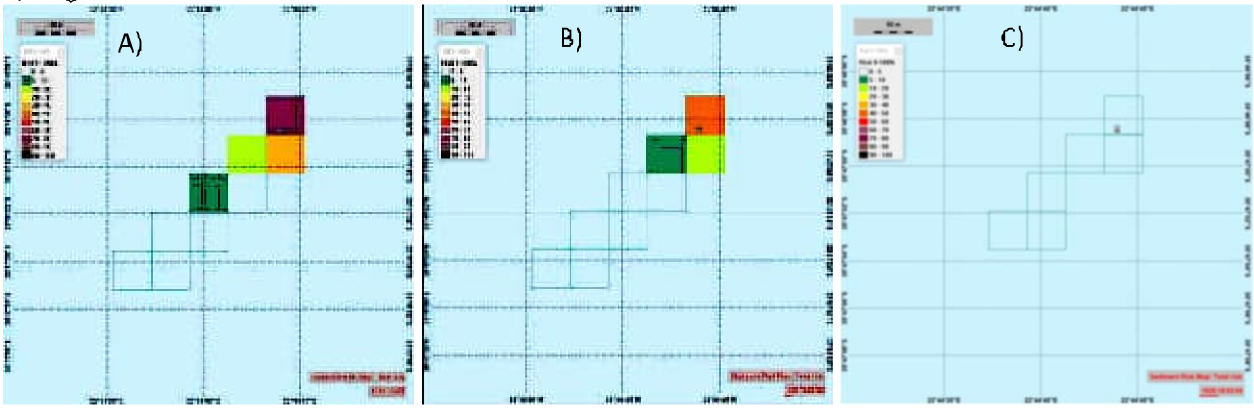

Figure 8.51 Risk % in the sediment A) Day 11, B) after 2 year, C) after 4 year for all seasons.

8.7 Deposition on the sea floor for location 4

All chemicals in the discharge with a $logP_{OW} > 3$ will attach to the particulate material in the model and eventually end up at the sea floor. This also changes the particle size distribution of the discharged matter as particles agglomerate to bigger particles which affects the transport (sinking velocity) and eventually the 'sea floor signature' of the discharge. Figure 8.52 - Figure 8.59 shows deposition on the seafloor for all particulate matter (cuttings, barite and bentonite) and any associated contaminants. The deposition is mainly caused by the cuttings particles discharged from the top hole sections on the sea floor. Discharges released from the rig gives only negligible footprint on the seafloor < 1 mm for all four seasons. The particles follow the currents and are widely dispersed higher in the water column and spreads over a larger area.

8.7.1 Discharge location 4 – Summer: Deposition on the seafloor

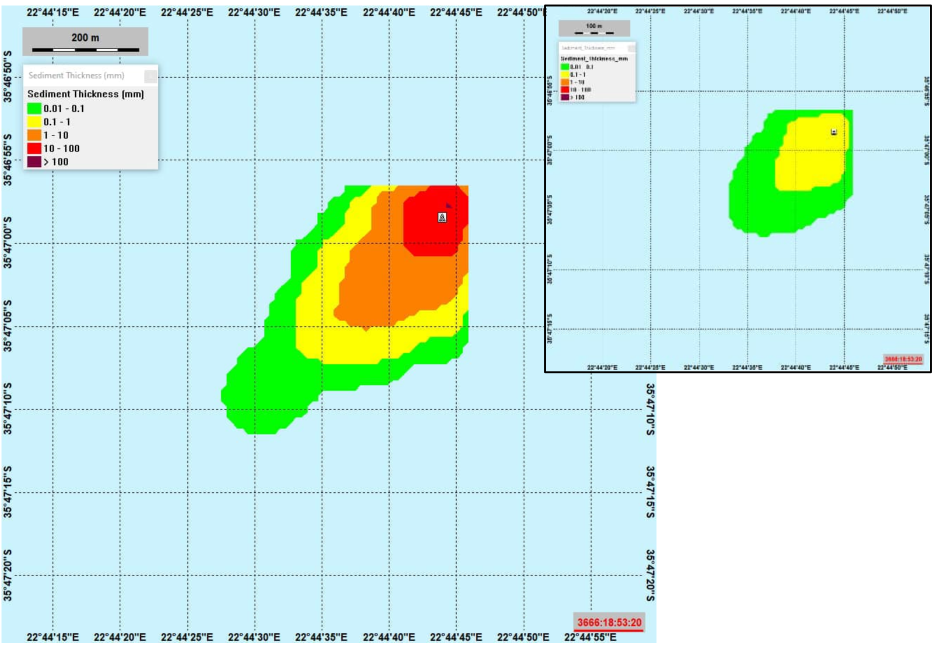

Figure 8.52 Discharge location 4 – Summer: Deposition of the total of particle matter on the sea floor (mm) (smoothed results) for discharge from the top hole sections. The inserted figure to the upper right shows deposition of barite and bentonite only. (Smoothing of gridded results leads to strange straight lines north and east of the figure).

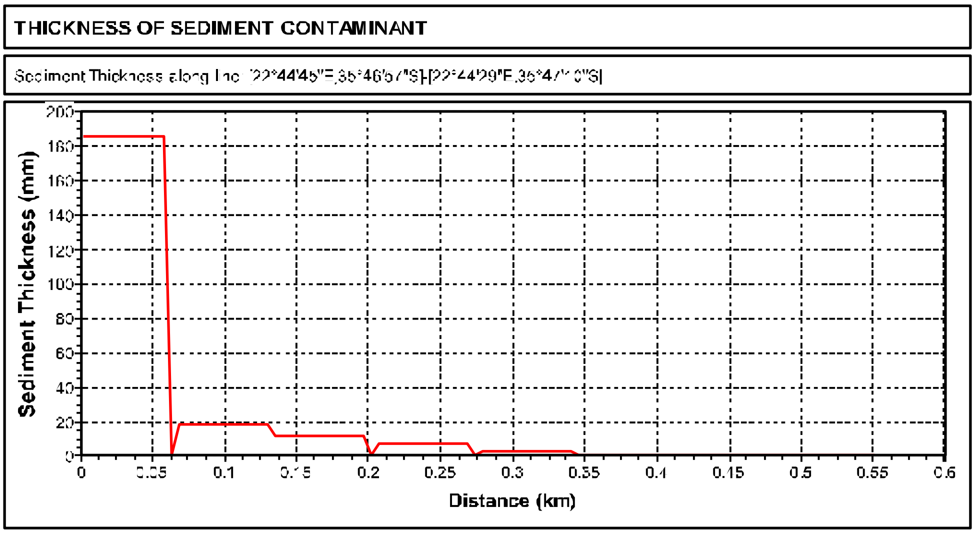

Figure 8.53 Discharge location 4 – Summer: Sediment thickness (mm) of total deposited matter on the sea floor (unsmoothed) through the release point from NE towards SW. Grid cell size 50 x 50 meters.

8.7.2 Discharge location 4 – Autumn: Deposition on the seafloor

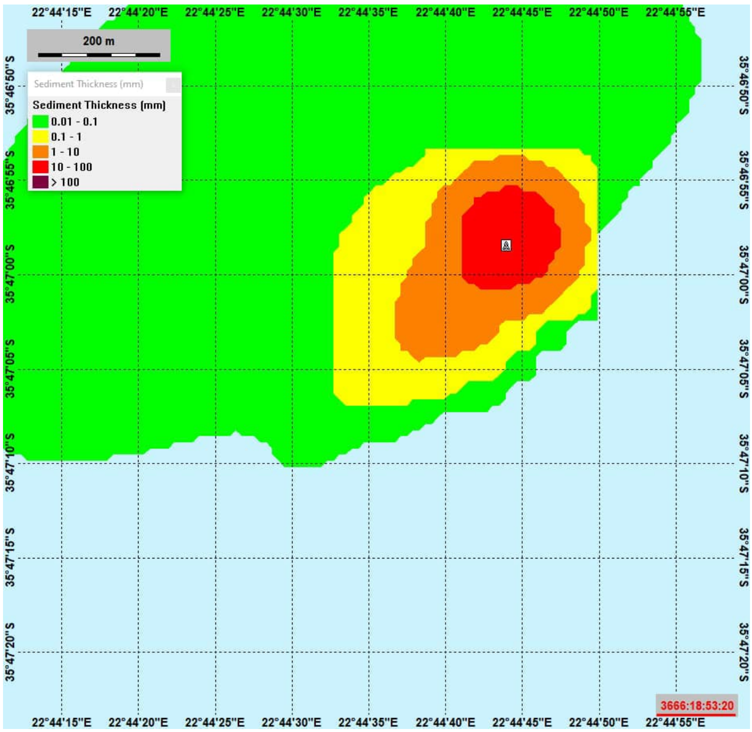

Figure 8.54 Discharge location 4 - Autumn: Deposition of particle matter on the sea floor (mm) (smoothed results) for discharge from the top hole sections.

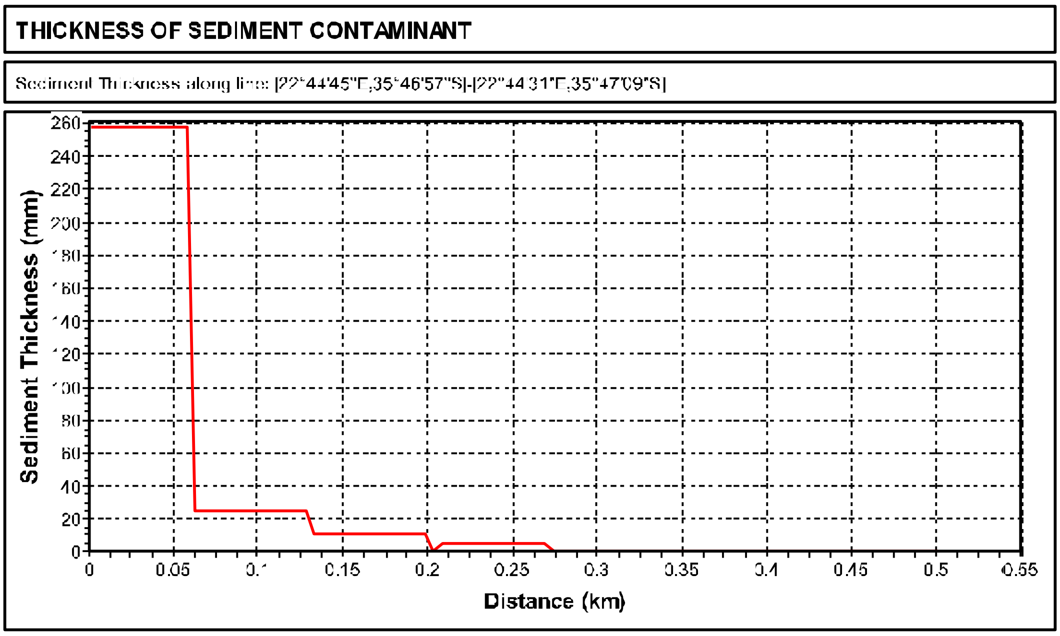

Figure 8.55 Discharge location 4 - Autumn: Sediment thickness (mm) of deposited matter on the sea floor (unsmoothed) through the release point from NE towards SW. Grid cell size 50 x 50 meters.

8.7.3 Discharge location 4 – Winter: Deposition on the seafloor

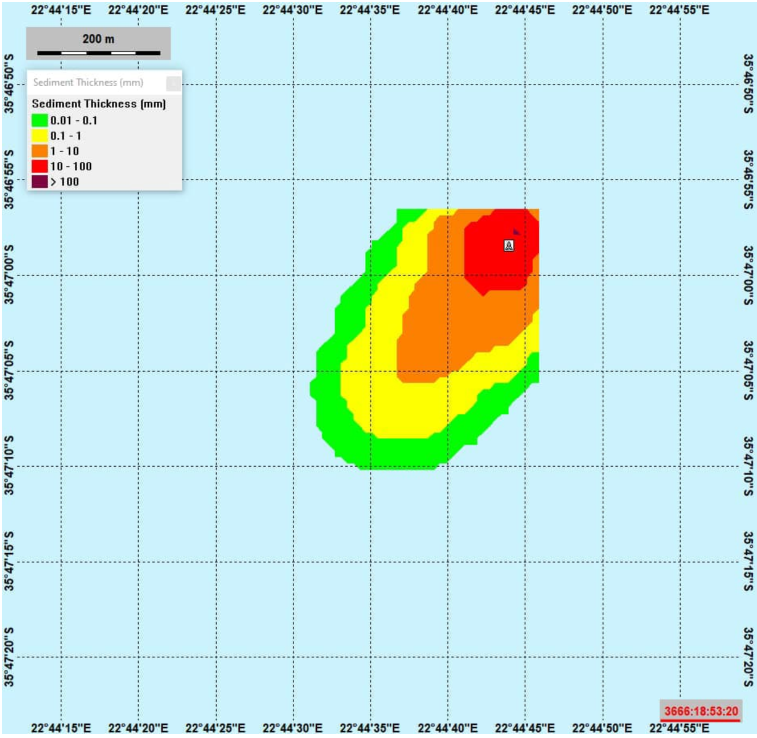

Figure 8.56 Discharge location 4 - Winter: Deposition of particle matter on the sea floor (mm) (smoothed results) for the discharge from the top hole sections. (Smoothing of gridded results leads to strange straight lines north and east of the figure).

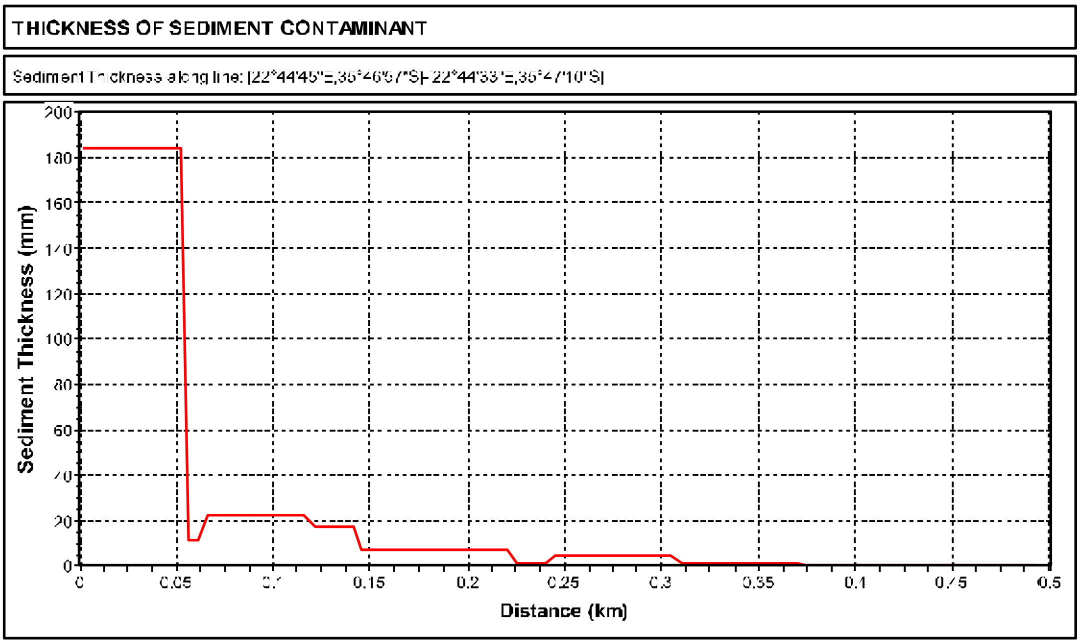

Figure 8.57 Discharge location 4 - Winter: Sediment thickness (mm) of deposited matter on the sea floor (unsmoothed) through the release point from NE towards SW. Grid cell size 50 x 50 meters.

8.7.4 Discharge location 4 – Spring: Deposition on the seafloor

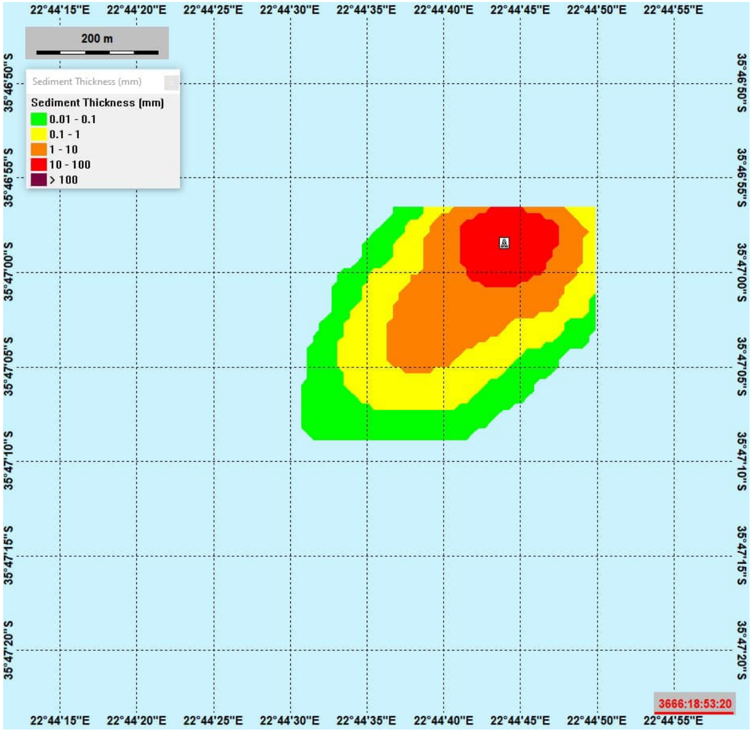

Figure 8.58 Discharge location 4 - Spring: Deposition of particle matter on the sea floor (mm) (smoothed results) for the discharge from the top hole sections. (Smoothing of gridded results leads to strange straight lines north and east of the figure).

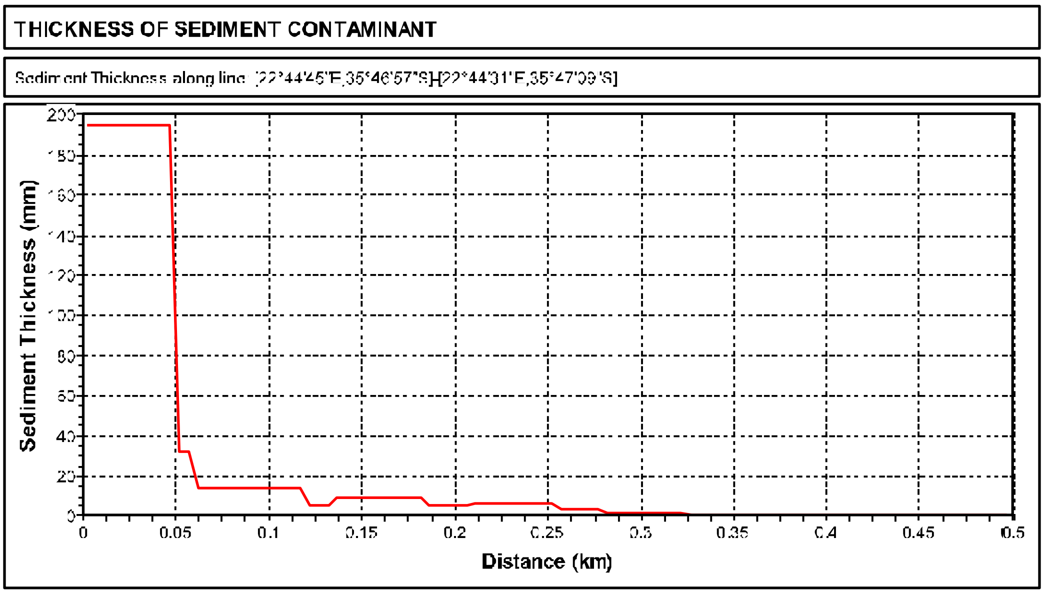

Figure 8.59 Discharge location 4 - Spring: Sediment thickness (mm) of deposited matter on the sea floor (unsmoothed) through the release point from NE towards SW. Grid cell size 50 x 50 meters.

8.8 Sediment thickness at the sea floor from cuttings (mm) for location 4

The thickness of deposited cuttings is reported as a spatial map at the end of the simulation period (10 years). At this time, bioturbation will already have reduced the maximum thickness. Thickness below 6.5 mm (the PNEC for burial) is shown as an outline. Results are shown only for cuttings, since these represent essentially all of the risk from burial.

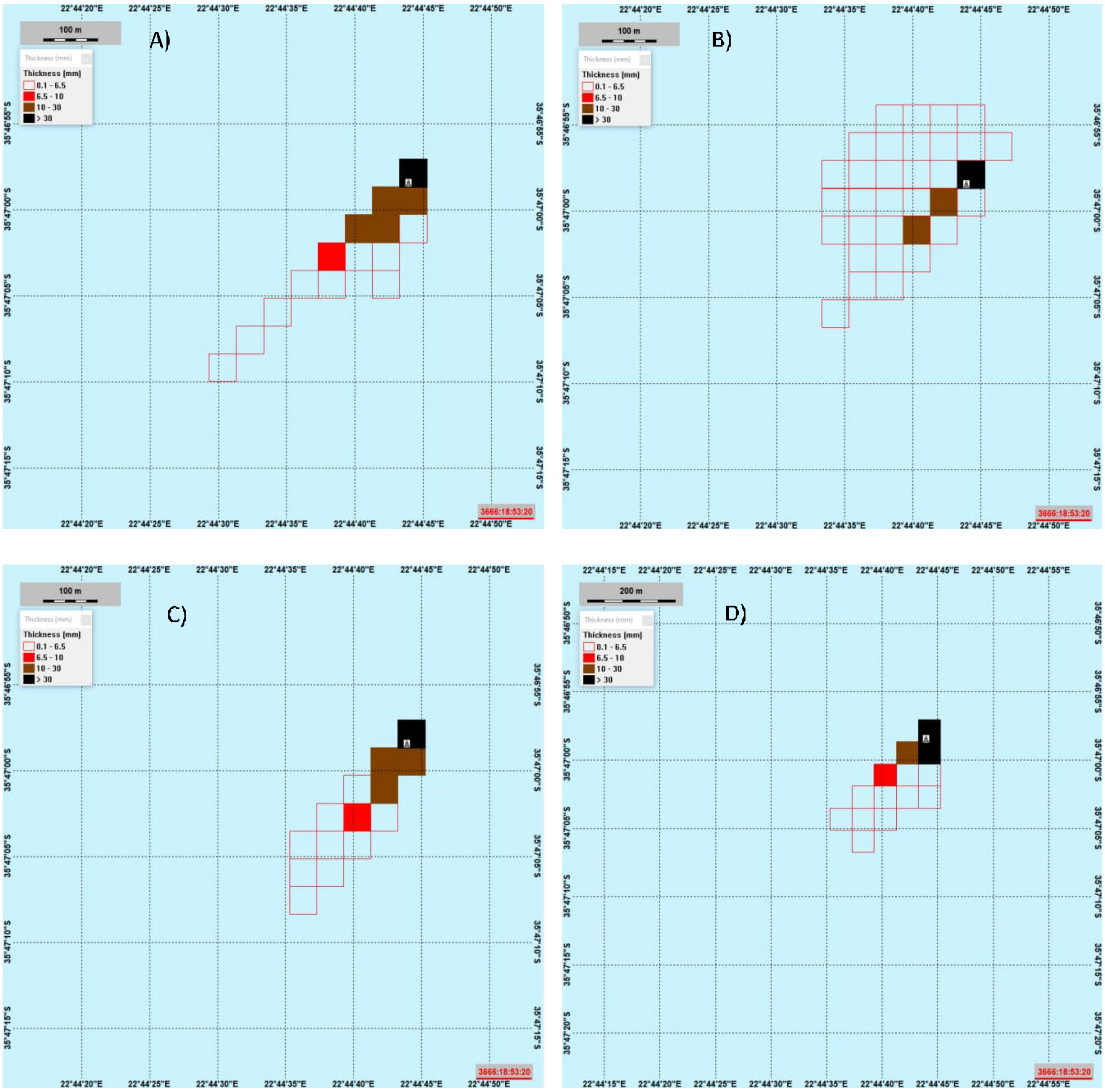

Figure 8.60 Sediment deposition at the seafloor from cuttings (thickness mm) un-smoothed. Cell-size 50 x 50 meter, PNEC level for burial is 6.5 mm. A) Summer, B) Autumn, C) Winter, D) Spring.

8.9 Grain size change for location 4

The DREAM model calculates the stresses caused by the deposition of grains with sizes that are different from the natural grain sizes on the actual location. Therefore, the actual natural grain size on the location must be input to the sediment model. The median diameter of the natural grain size on site was assumed to be about 0.35 mm (see Service Request Form).

A change in median sediment grain size caused by deposited particle matter might result in a change of benthic communities. Exposure related to grain size change is defined as the change of the median grain size in the sediment, averaged over the upper three cm of the sediment layer (including the added sediment).

Figure 8.61 shows median grain size change in the upper sediment layer caused by cuttings discharge from the rig. The particle sizes on the seabed increase in areas closest to the rig with particle sizes of as much a 4 mm being observed approximately 2 km from the rig.

Figure 8.61 Calculation of median grain size deposited at the sea floor after completion of the discharge from the rig for discharge location 4.

8.10 Oxygen change in the sediment for location 4

Environmental risk from oxygen depletion is reported as spatial distribution on a map and snapshots in time. Tones in grey show negative oxygen balances caused by biodegradation of mud chemicals. Green areas are neutral.

The figures show the risk situation at the end of discharge from the 8.5" HPWBM section discharged from rig, and after 26" displacement section discharged at the seafloor, after 3 years and at the end of the simulation period (10 years).

The PNEC for the change in oxygen content was set to 20% reduction of oxygen (in terms of mg O2/m2 sediment surface) based on NIVA Report no. 5188-2006, by considering the effect of reduced redox potential on the diversity of the benthic fauna.

The figures are very similar since the chemicals are attached to the cuttings, which are the same for all four seasons. None of the simulations gave results for oxygen change in the sediment that contributes to EIF > 1 (Risk over 5%). To give an overview of the development of oxygen change over time Figure 8.62 and Figure 8.63 are representative for all four seasons.

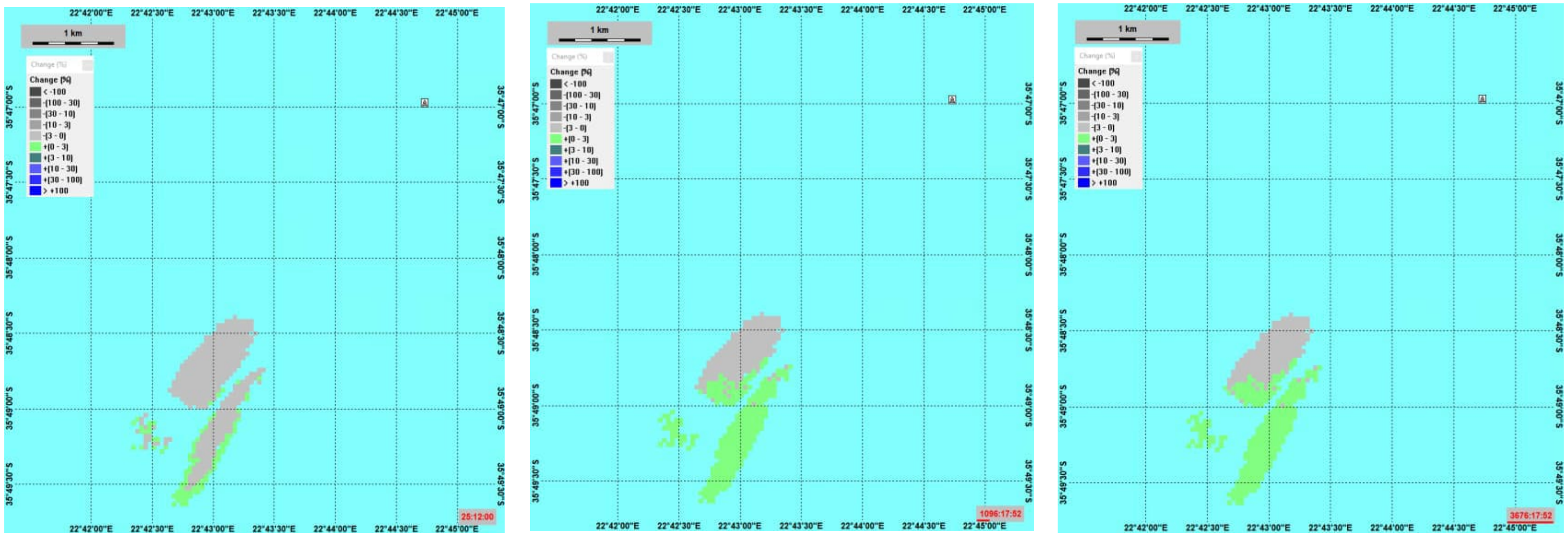

Figure 8.62 Oxygen change in the sediment layer caused by the degradation of chemicals attached to cuttings: A) timestep at the end of discharge from the 8.5" HPWBM section, B) after 3 years, C) after 10 years, for discharge location 4 discharge from rig. Summer conditions.

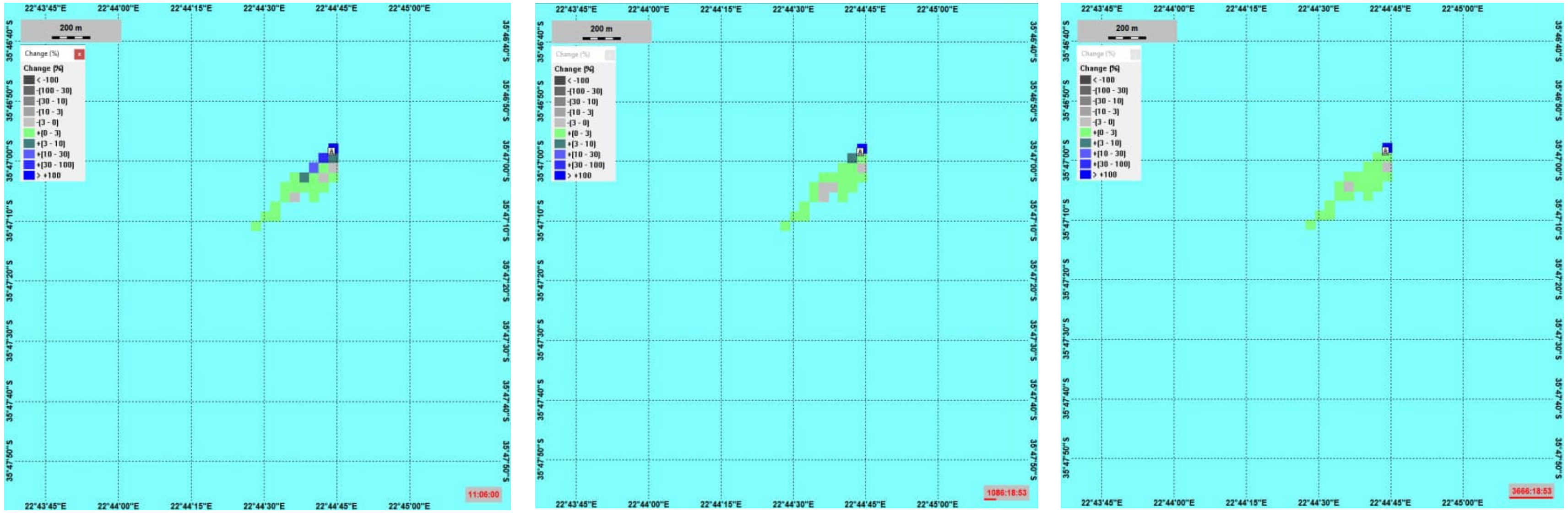

Figure 8.63 *Oxygen change in the sediment layer caused by the degradation of chemicals attached to cuttings: A) timestep after 26" displacement section discharged at the seafloor, B) after 3 years, C) after 10 years, for discharge location 4 discharge at seafloor. Summer conditions.*

9 Results for drilling discharge from location 5

9.1 EIF results for location 5 summer

9.1.1 Discharge location 5 - Lower water-column – Summer

The maximum EIF (water volume 100x100x10 m^3) in the lower water-column 1750 - 1850 meters for discharge location 5 is computed with 8605, while the time average EIF is computed with 1833. The contributions of the components of the discharge are listed in the table below (risk in % of EIF).

Table 9.1 Table and pie-chart with EIF results for the lower water column, 1750 - 1850 meters. Discharge location 5 – Summer.

Computed max. EIF:	**8605**				
Time averaged EIF:	1833				
Components	Product	PNEC ppb	Contribution to risk %	Contribution max EIF	Contribution time averaged EIF
Total					
Barazan D		420	0.4	34.4199	7.3325
Soda Ash		200	0.13	11.1865	2.3831
Caustic Soda		20	1.67	143.7031	30.6131
Potassium Cloride		100	12.69	1091.9712	232.6227
Starcide		49	0.11	9.4655	2.0164
Cuttings		100000	0.01	0.8605	0.1833
Bentonite_ECHA		170	13.88	1194.3704	254.4368
Barite-Bariumsulfat		115	70.51	6067.3671	1292.5316
Barite-Silica		440	0.6	51.6298	10.9987

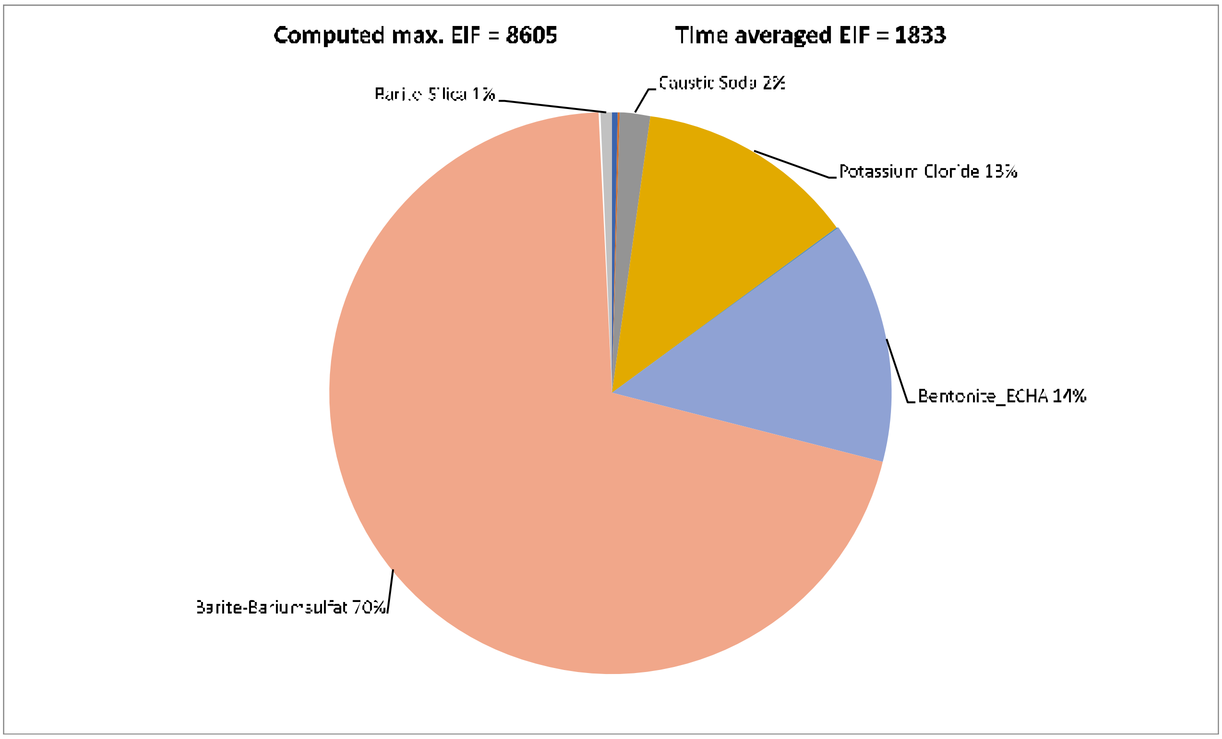

Barium sulfate is dominating the risk with 70% for the lower water column. This is caused by the amount of Barite that will be discharged on the seafloor from the displacement sections released after drilling of the 42" and 26" sections, together with Bentonite discharged during drilling.

Figure 9.1 shows the time development for the EIF in water-column. It shows the duration of risk during the discharges on the sea floor and that the risk in the water column disappears immediately afterwards.

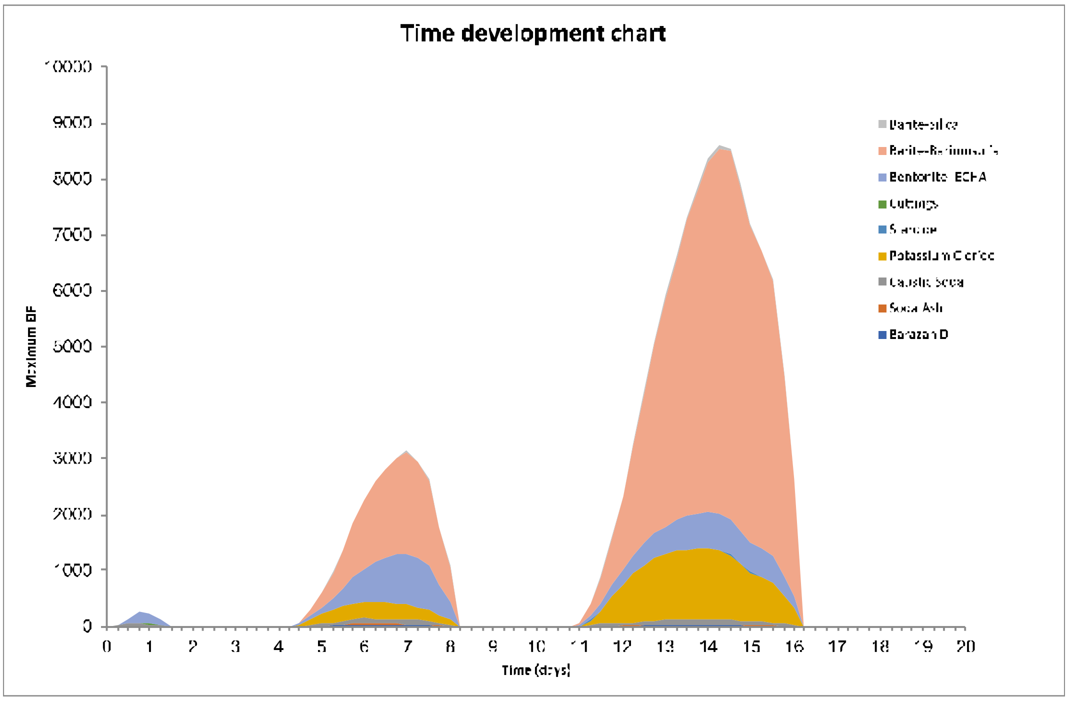

Figure 9.1 Time development of the EIF for the lower water column. Discharge location 5 – Summer.

Figure 9.2 shows the time instant with maximum EIF for the lower water column due to discharges from the top hole sections, while Figure 9.4 shows the maximum cumulative risk (foot-print) throughout the lower water column at any time during the drilling operation with discharges from the top hole sections.

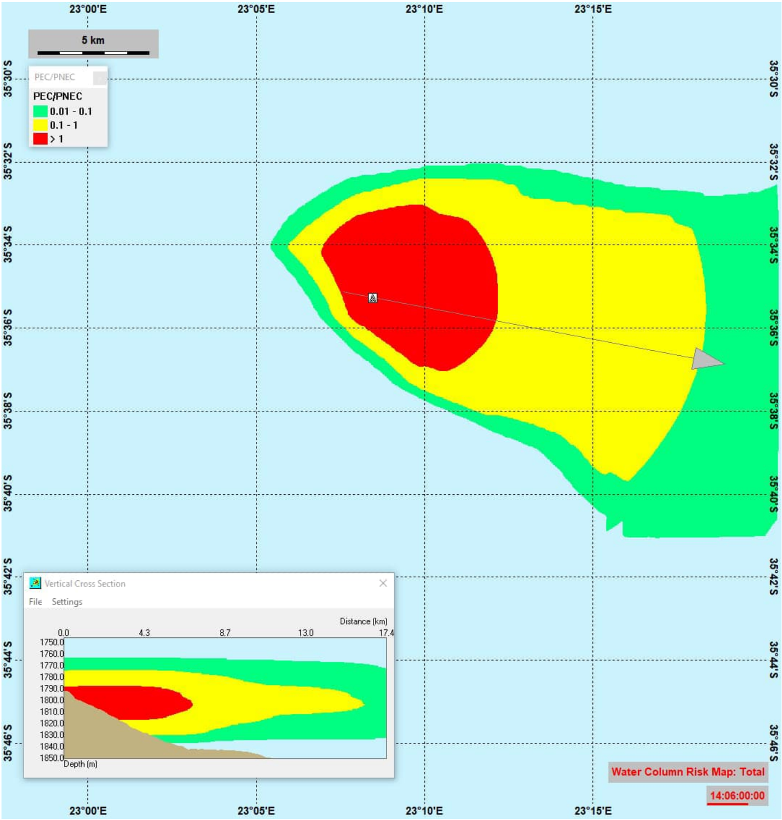

Figure 9.2 *Snapshot showing the time instant with maximum EIF for the lower water column at 1750 - 1850 meters. Snapshot at day 14.25, when the discharge is from the top hole sections on the sea floor. The vertical cross section shows the PEC/PNEC ratio along the grey arrow. Discharge location 5 – Summer.*

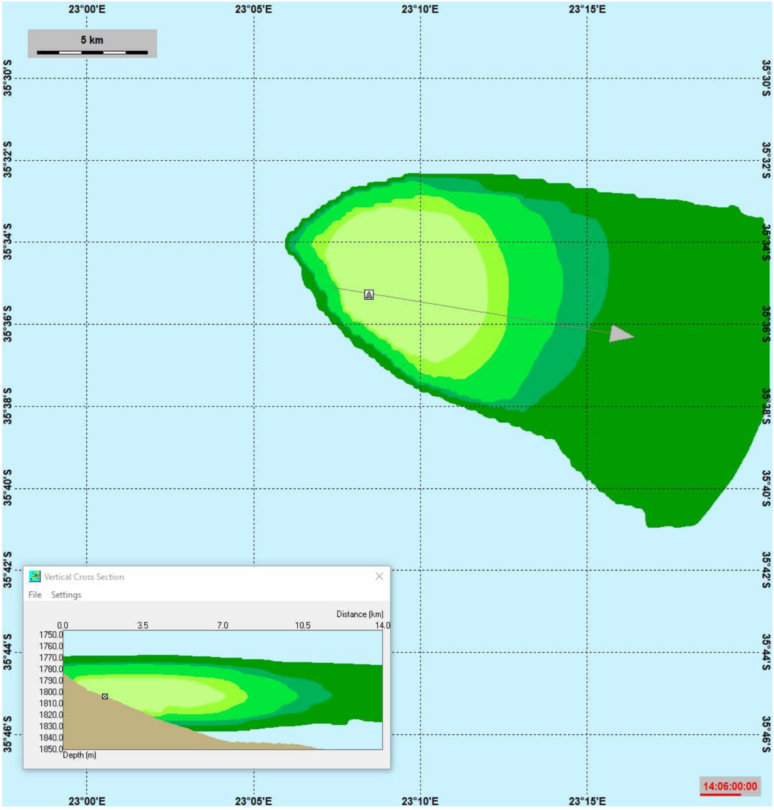

Figure 9.3 *Concentration field for the component that gave the largest contribution to the environmental risk, namely the particle group barite, at the same time-step as for maximum EIF. A cross-section of the plume is shown in the smaller panel. Discharge location 5 – Summer.*

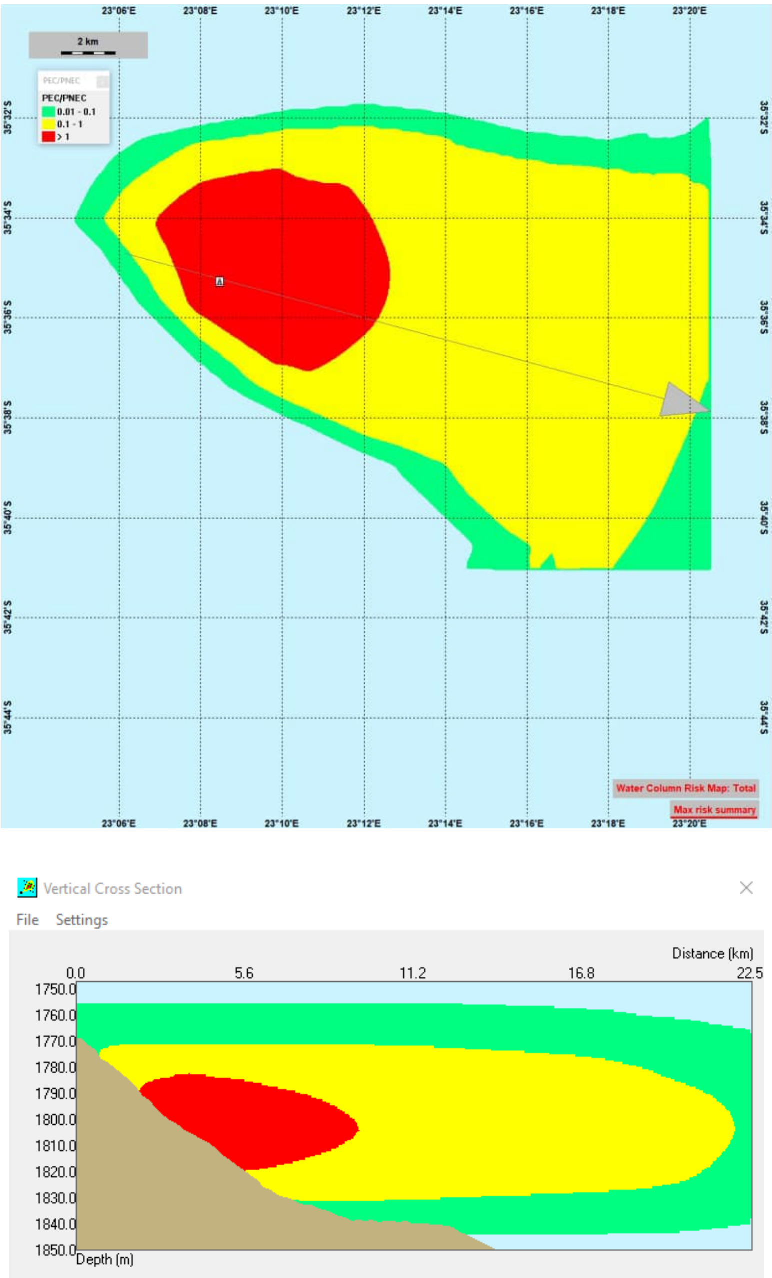

Figure 9.4 Maximum cumulative risk of drilling operations throughout the lower water column at any time for discharge location 5 (Start time December 24) Discharge at the seafloor. Discharge location 5 – Summer.

9.1.2 Discharge location 5 - Upper water-column – Summer

The maximum EIF (water volume 100x100x10 m^3) in the upper water-column 0-100 meter for discharge location 5, Summer was 10148, while the time average EIF is computed with 866. The contributions of the components of the discharge are listed in the table below (risk in % of EIF).

Table 9.2 Table and pie-chart with EIF results for the water column, upper 100 meter for discharge location 5, Summer.

Computed max. EIF:	**10148**				
Time averaged EIF:	866				
Components	Product	PNEC ppb	Contribution to risk %	Contribution max EIF	Contribution time averaged EIF
Total					
Soda Ash		200	0.03	3.0444	0.2599
Caustic Soda		20	0.4	40.5920	3.4654
Barazan D		420	0.09	9.1332	0.7797
Potassium Cloride		100	7.82	793.5732	67.7490
Sodium Chloride		1000000	0	0	0
GEM GP		188	0.03	3.0444	0.2599
Clayseal Plus		562.3	0	0	0
Clayseal Plus-2		0.45	1.65	167.4419	14.2949
Clay Grabber		9.8	0.36	36.5328	3.1189
Clay Grabber-2		1.31	0.45	45.6660	3.8986
Clay Sync II		1160	0.02	2.0296	0.1733
Bore HIB		146	0	0	0
Dextrid E		1000	0.09	9.1332	0.7797
PAC-L		87.26	0.76	77.1248	6.5843
Cuttings		100000	0	0	0
Barite-Bariumsulfat		115	81.82	8303.0894	708.8518
Barite-Silica		440	0.95	96.4060	8.2304
Baracarb 150		115	2.76	280.0847	23.9114
Baracarb 50		115	2.76	280.0847	23.9114

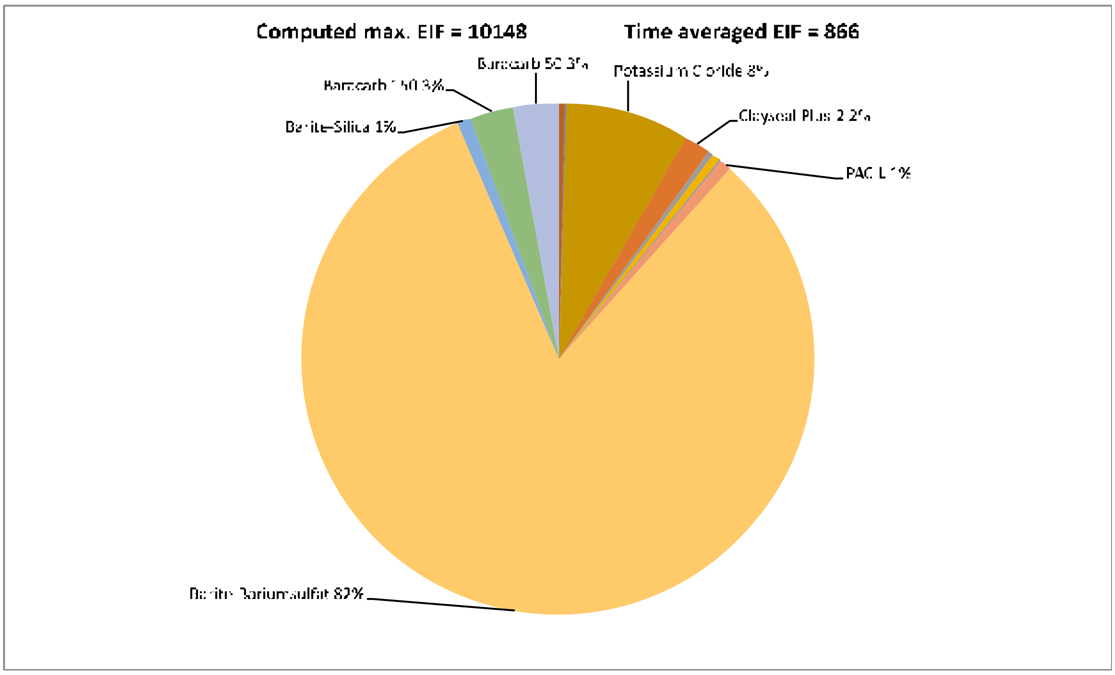

The results show that for the upper water column, effects caused by discharges of particle matter (essentially Barium sulfate 82%) are dominating the risk in the affected water volume. During the time of maximum EIF, the discharge is released from the rig 10 meters below sea-surface and sinks down to about 40 meters in the water-column. The discharge is driven by the currents in S/SW direction.

Figure 9.5 shows the time development for the EIF in water-column. It shows that the duration with environmental risk occurs in intervals lasting some days after.

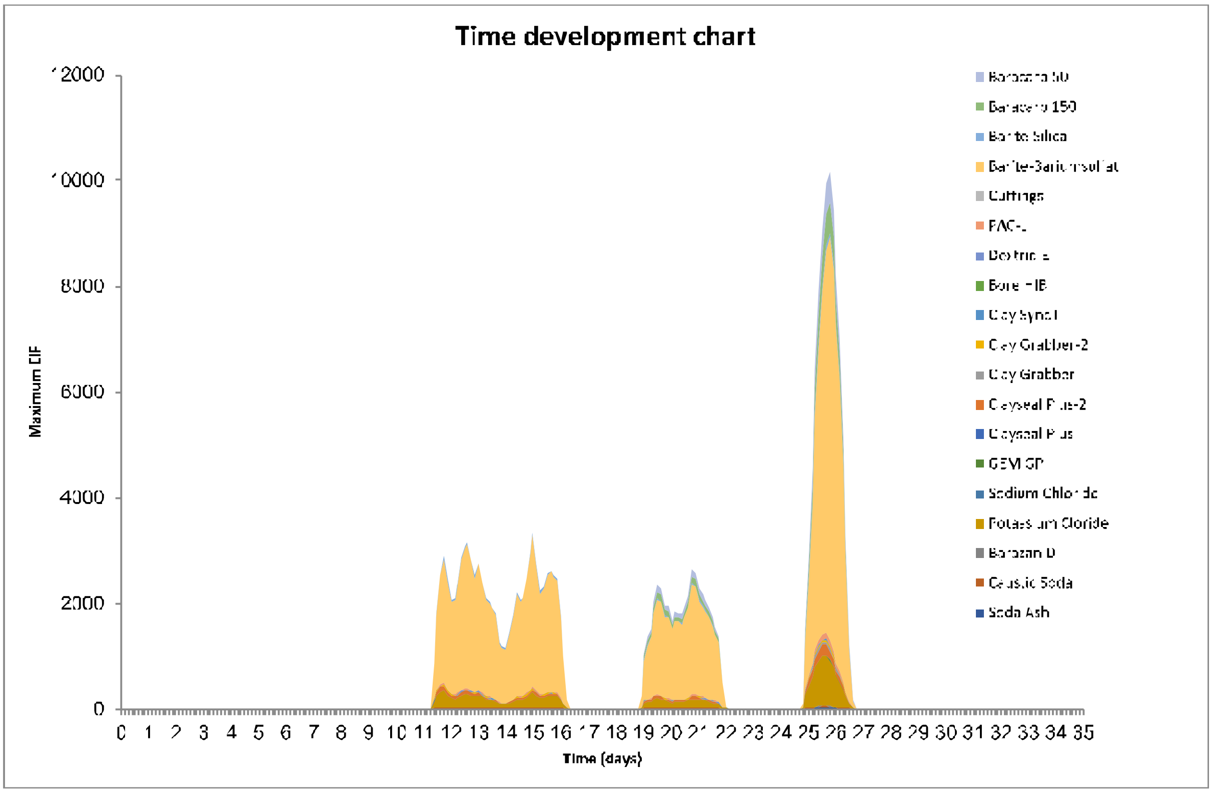

Figure 9.5 Time development of the EIF for the upper water column, for discharge location 5 Summer.

Figure 9.6 shows the time instant with maximum EIF for the upper water column due to discharges from rig 10 m below sea surface, while Figure 9.8 shows the maximum cumulative risk (foot-print) throughout the upper water column at any time during the drilling operation with discharges from the rig.

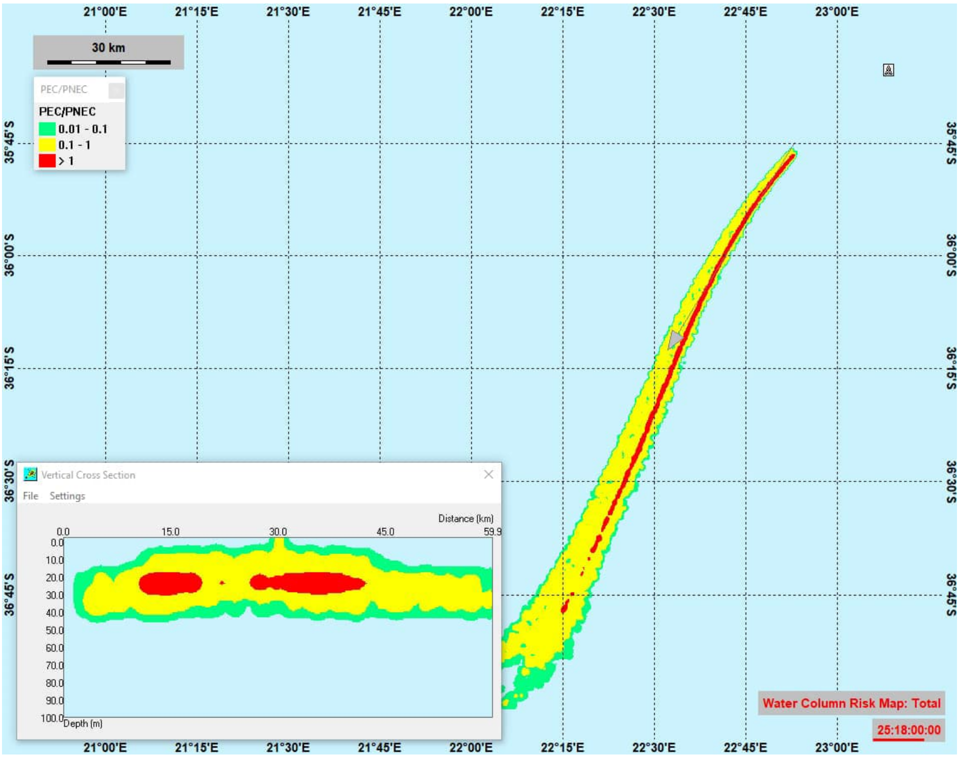

Figure 9.6 Snapshot showing the time instant with maximum EIF for the upper water column between 0-100 meters. Snapshot from 25.75 days after start, when the discharge is released from the rig. The vertical cross section shows the PEC/PNEC ratio in the water column along the grey arrow. Discharge location 5 – Summer.

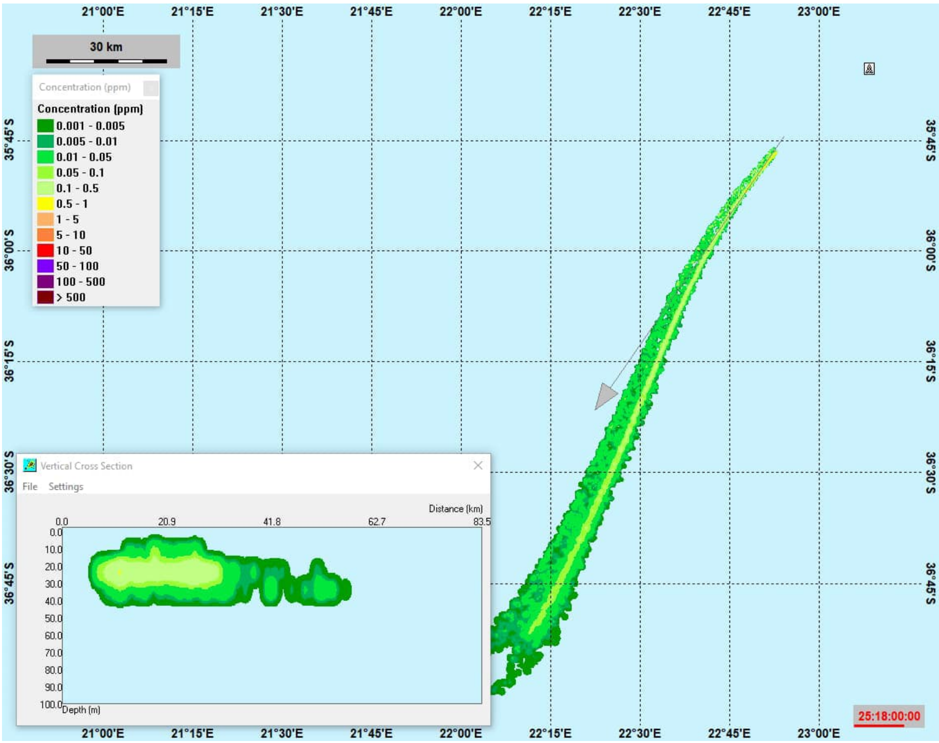

Figure 9.7 Concentration field for the component that gave the largest contribution to the environmental risk, namely the particle group Barium sulfate, at the same time-step as for maximum EIF. The discharge is spread in the upper 40 meters in the water column driven by the currents. Concentrations up to 0.5 ppm. A cross section of the plume is shown in the smaller panel. Discharge location 5 – Summer.

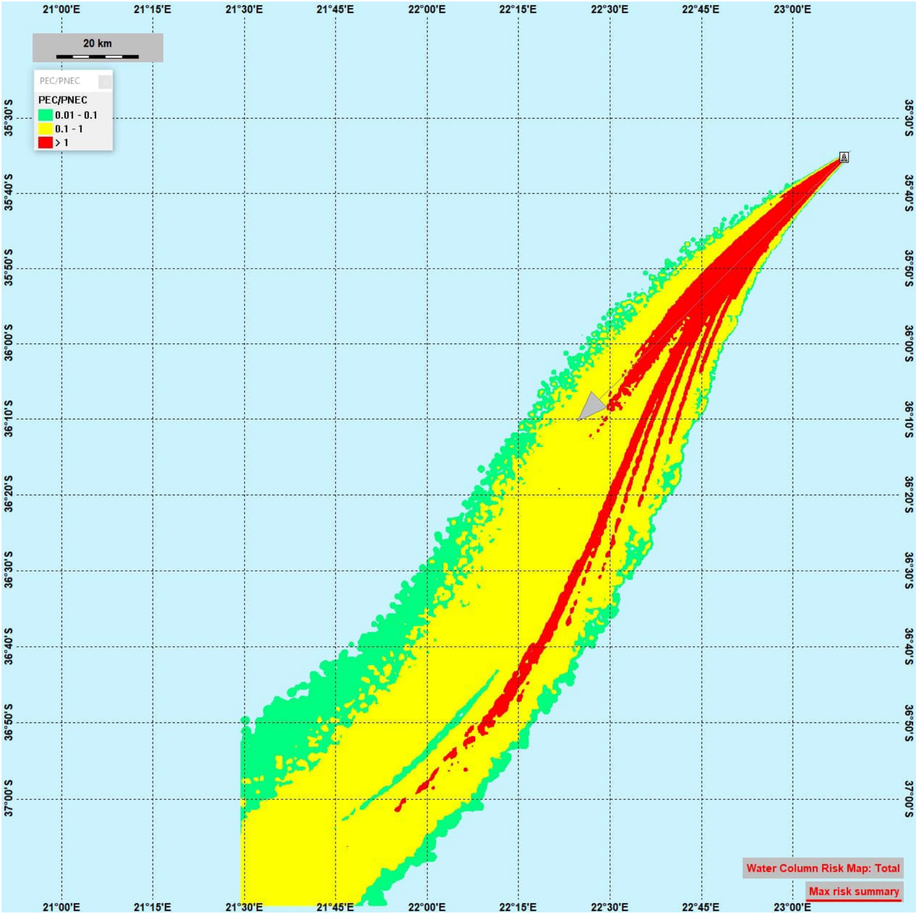

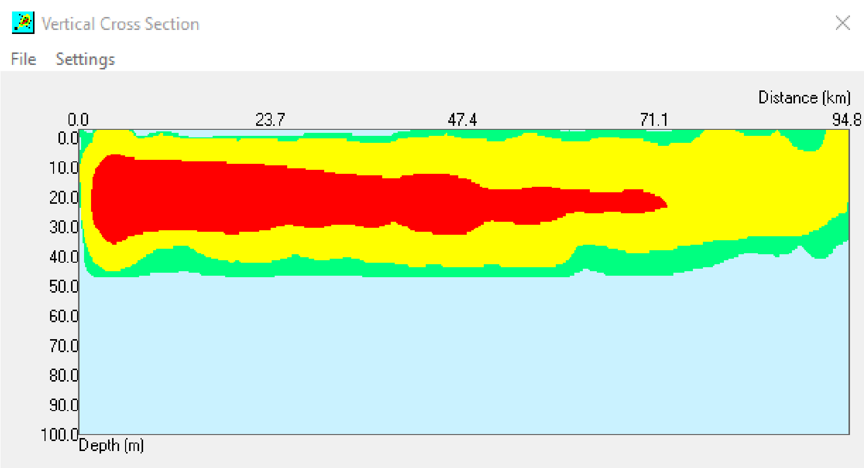

Figure 9.8 Maximum cumulative risk of drilling operations throughout the upper water column at any time for discharge location 5 (Start time December 24), discharge from rig 10 m below sea surface. Discharge location 5 – Summer.

9.1.3 Discharge location 5 - EIF results for the sediment – Summer

The maximum EIF (sea floor area 100x100 m^2) computed to 0.75 impacted by the top hole discharge see Figure 9.10 and with 0.25 impacted by discharge from the rig see Figure 9.12. The contributions of the components of the discharge are listed in Table 9.3 for the top hole sections, and Table 9.4 for the discharge from rig (risk in % of EIF). Most of the affected area on the sea floor is caused by the top hole discharges. The impact is largest at the end of the transport and fate simulation, shortly after the sediment module starts. After that the sea floor will start the restoration process and the affected area (EIF) then decreases.

Table 9.3 Table and pie-chart shows contributions to EIF from the components discharged from the top hole sections to the sediment for location 5 – Summer.

Simulated instantaneous EIF:	**0.75**				
Components	Product	PNEC ppb	Contribution to risk %	Contribution max EIF	Contribution time averaged EIF
Total					
Barazan D		420	0	0	0
Soda Ash		200	0	0	0
Caustic Soda		20	0	0	0
Potassium Cloride		100	0	0	0
Starcide		49	0	0	0
Thickness		0	64.95	0.49	0.49
Oxygen		0	0	0	0
Grain size		0	35.05	0.26	0.26

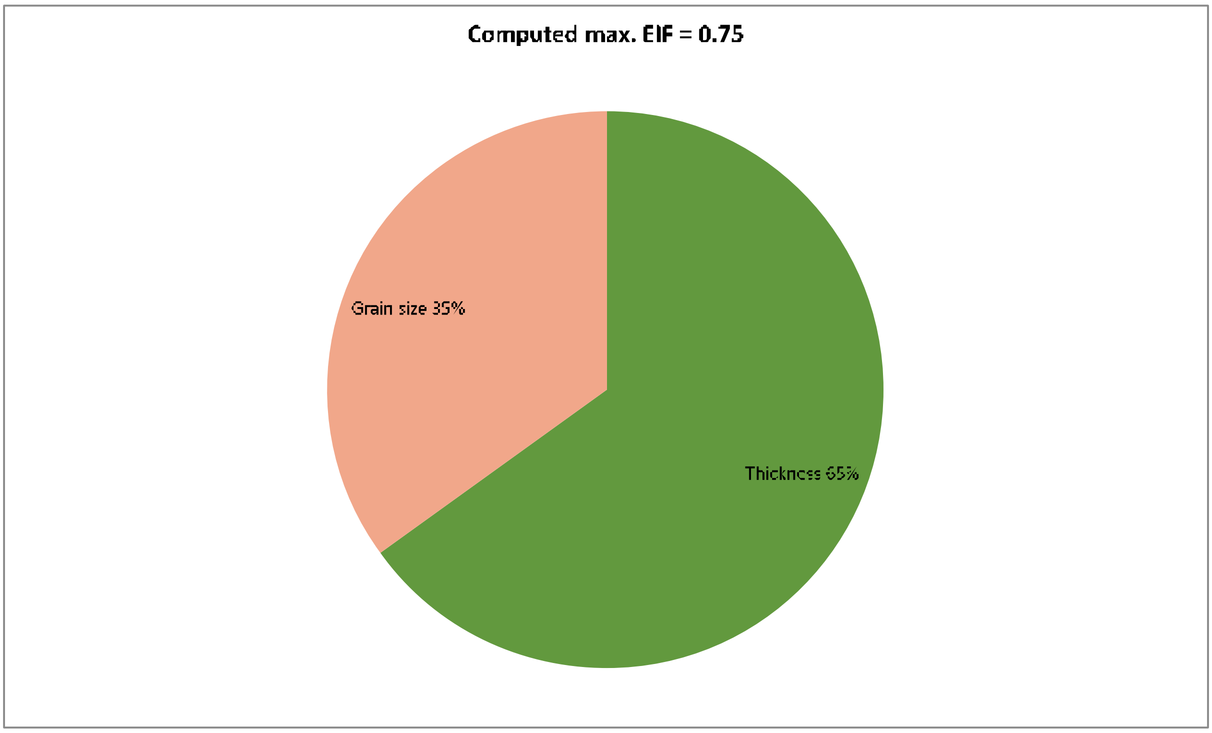

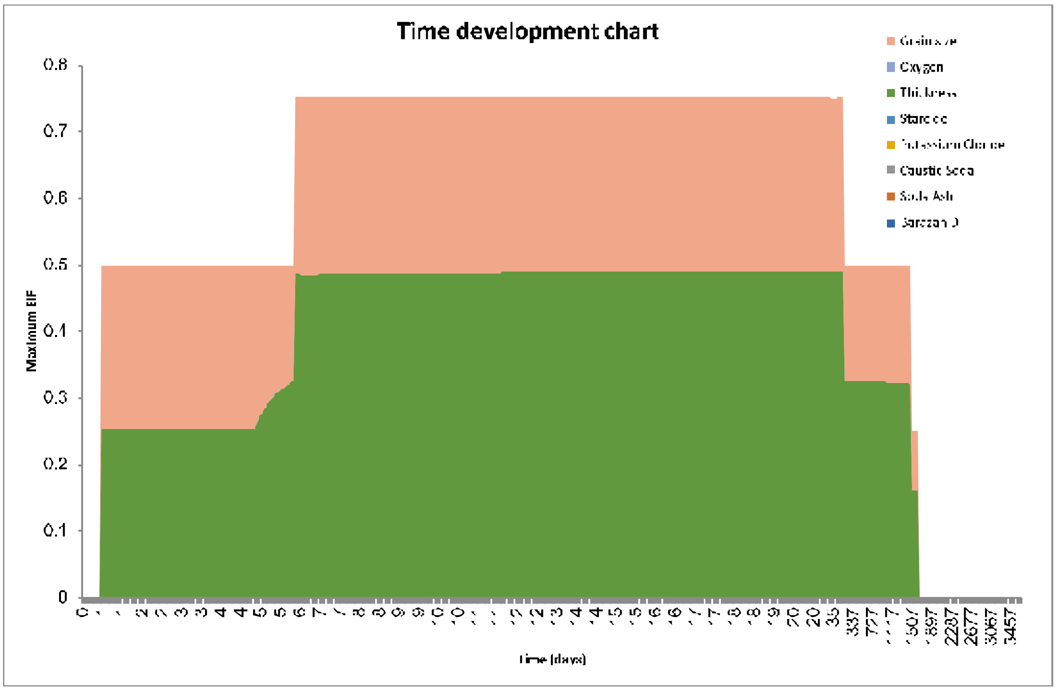

Figure 9.9 Time development of EIF for the sediment for discharge location 5 – Summer.

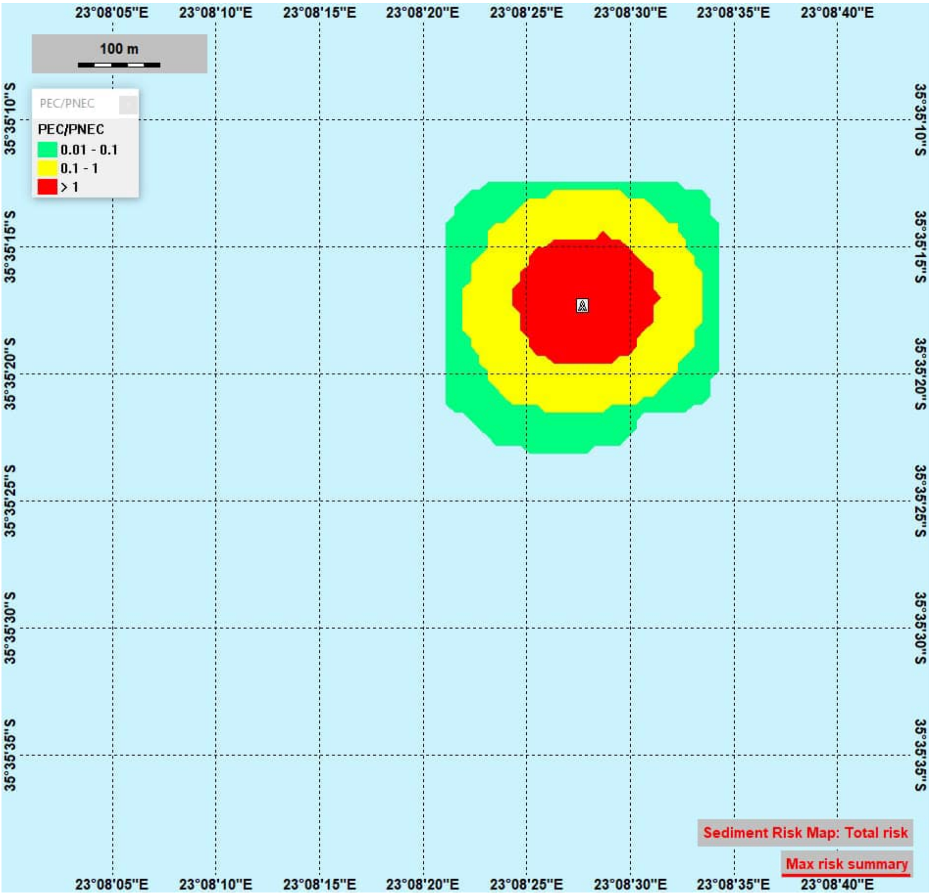

Figure 9.10 The total maximum EIF for the sediment (highest value at each location over simulation period) for discharge from the top hole drilling. Discharge location 5 – Summer.

Table 9.4 Table and pie-chart shows contributions to EIF from the components discharged from the rig to the sediment for location 5 – Summer.

Simulated instantaneous EIF:	**0.25**				
Components	Product	PNEC ppb	Contribution to risk %	Contribution max EIF	Contribution time averaged EIF
Total					
Soda Ash		200	0	0	0
Caustic Soda		20	0	0	0
Barazan D		420	0	0	0
Potassium Cloride		100	0	0	0
Sodium Chloride		1000000	0	0	0
GEM GP		188	0	0	0
Clayseal Plus		562.3	0	0	0
Clayseal Plus-2		0.45	0	0	0
Clay Grabber		9.8	0	0	0
Clay Grabber-2		1.31	0	0	0
Clay Sync II		1160	0	0	0
Bore HIB		146	0	0	0
Dextrid E		1000	0	0	0
PAC-L		87.26	0	0	0
Thickness		0	0	0	0
Oxygen		0	0	0	0
Grain size		0	100	0.25	0.25

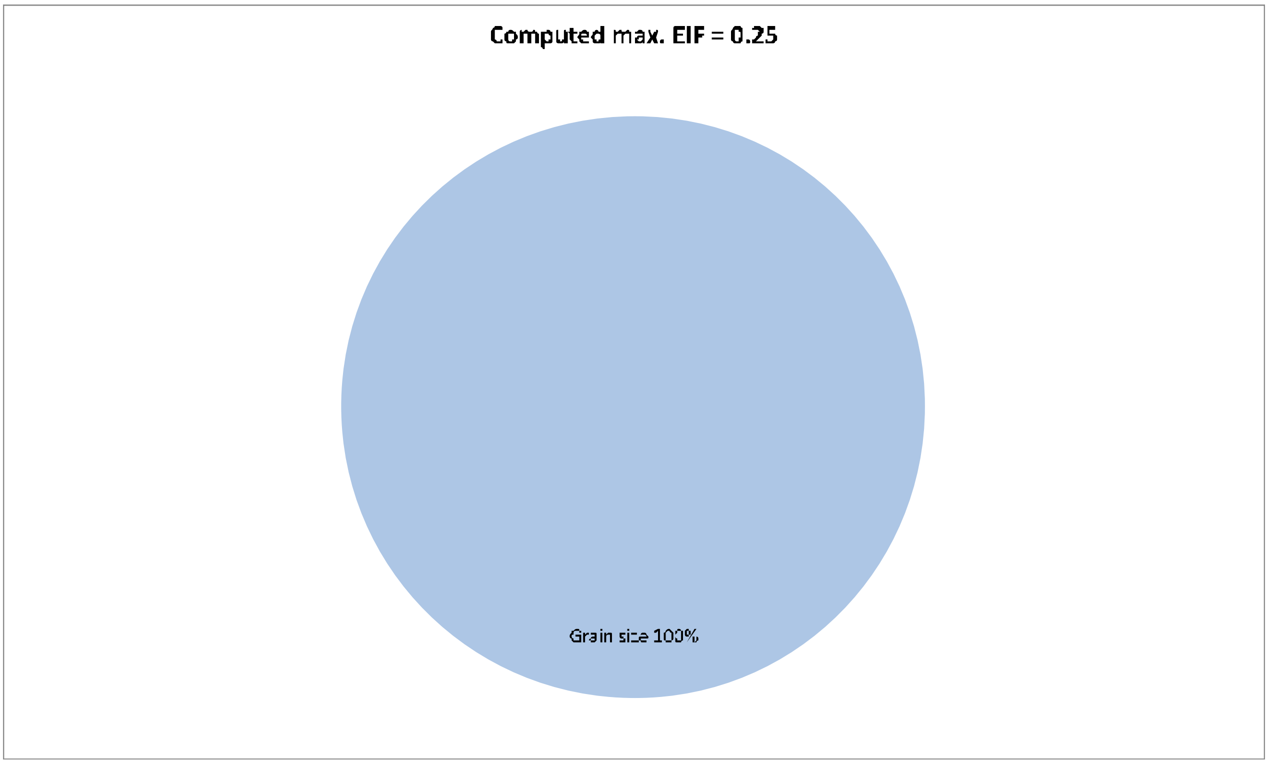

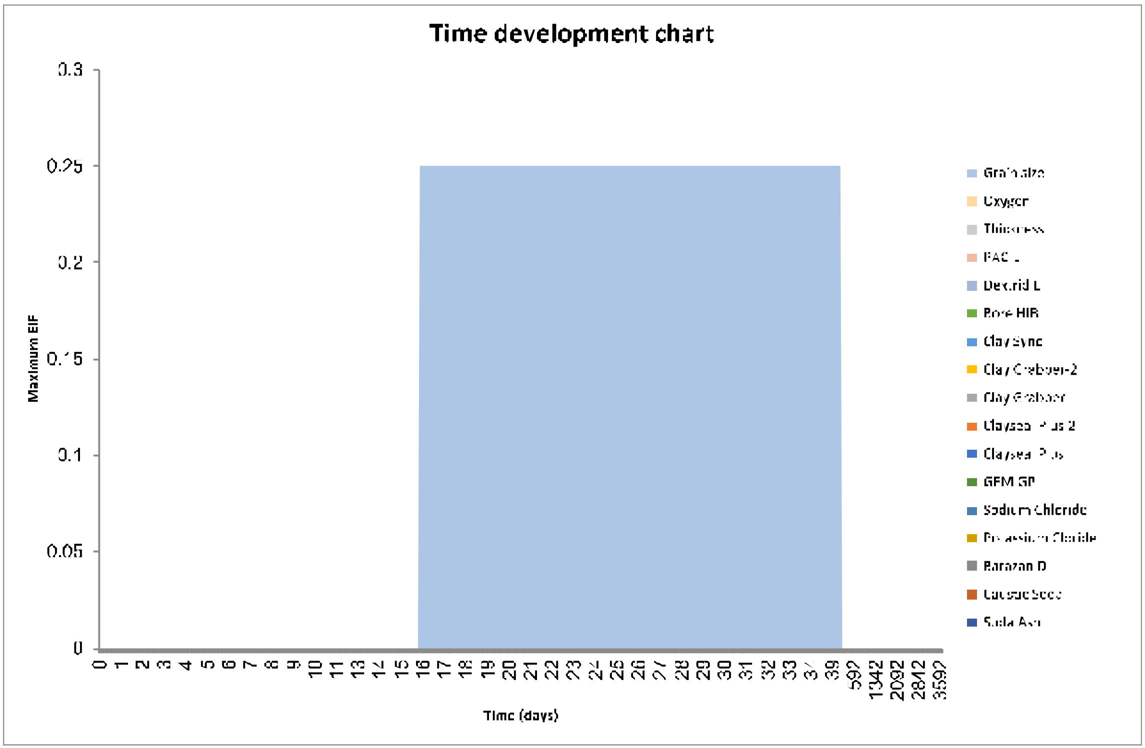

Figure 9.11 Time development of EIF for the sediment for discharges from the rig, location 5 – Summer.

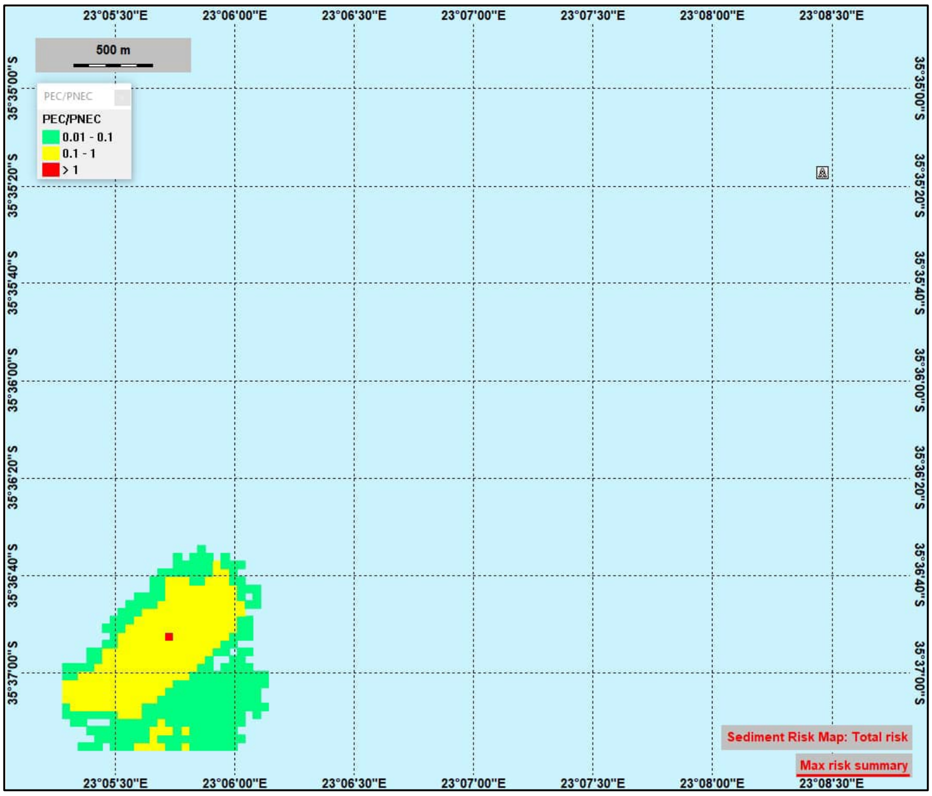

Figure 9.12 The total maximum EIF for the sediment (highest value at each location over simulation period) for discharge from the rig. The figure shows impact 4.5 km away from the release-point. Discharge location 5 – Summer (Un-smoothed results).

Simulations show that impact on the sediment caused by discharge from rig are negligible for all seasons, with EIF < 1. Therefore, only results showing impact from the top hole discharge are presented for the further scenarios.

9.2 EIF results for discharge location 5, Autumn

9.2.1 Discharge location 5 - Lower water-column – Autumn

The maximum EIF (water volume 100x100x10 m^3) in the lower water-column 1750 - 1850 meters for discharge location 5, Autumn was 8623, while the time average EIF is computed with 1825. The contributions of the components of the discharge are listed in the table below (risk in % of EIF).

Table 9.5 Table and pie-chart with EIF results for the lower water column, 1750 - 1850 meters. Discharge location 5 – Autumn.

Computed max. EIF:	**8623**				
Time averaged EIF:	1825				
Components	Product	PNEC ppb	Contribution to risk %	Contribution max EIF	Contribution time averaged EIF
Total					
Barazan D		420	0.4	34.4919	7.2990
Soda Ash		200	0.13	11.2099	2.3722
Caustic Soda		20	1.67	144.0037	30.4735
Potassium Cloride		100	12.67	1092.5308	231.1973
Starcide		49	0.11	9.4853	2.0072
Cuttings		100000	0.01	0.8623	0.1825
Bentonite_ECHA		170	13.85	1194.2819	252.7295
Barite-Bariumsulfat		115	70.55	6083.5080	1287.3692
Barite-Silica		440	0.62	53.4624	11.3135

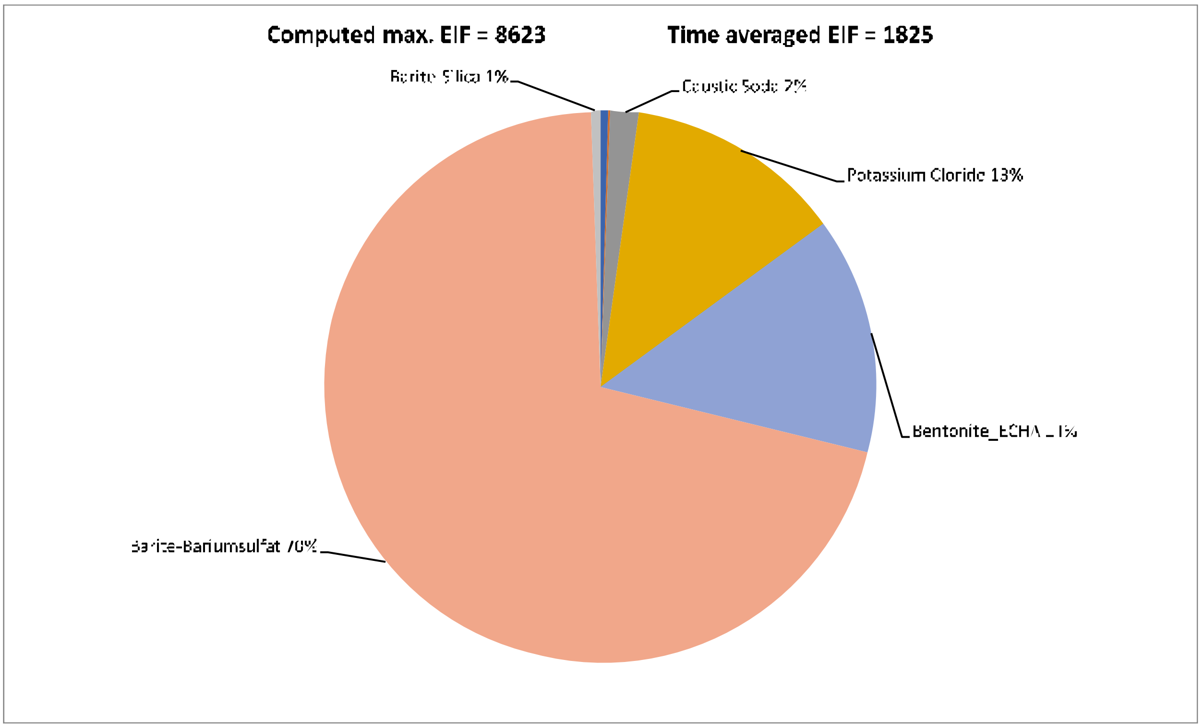

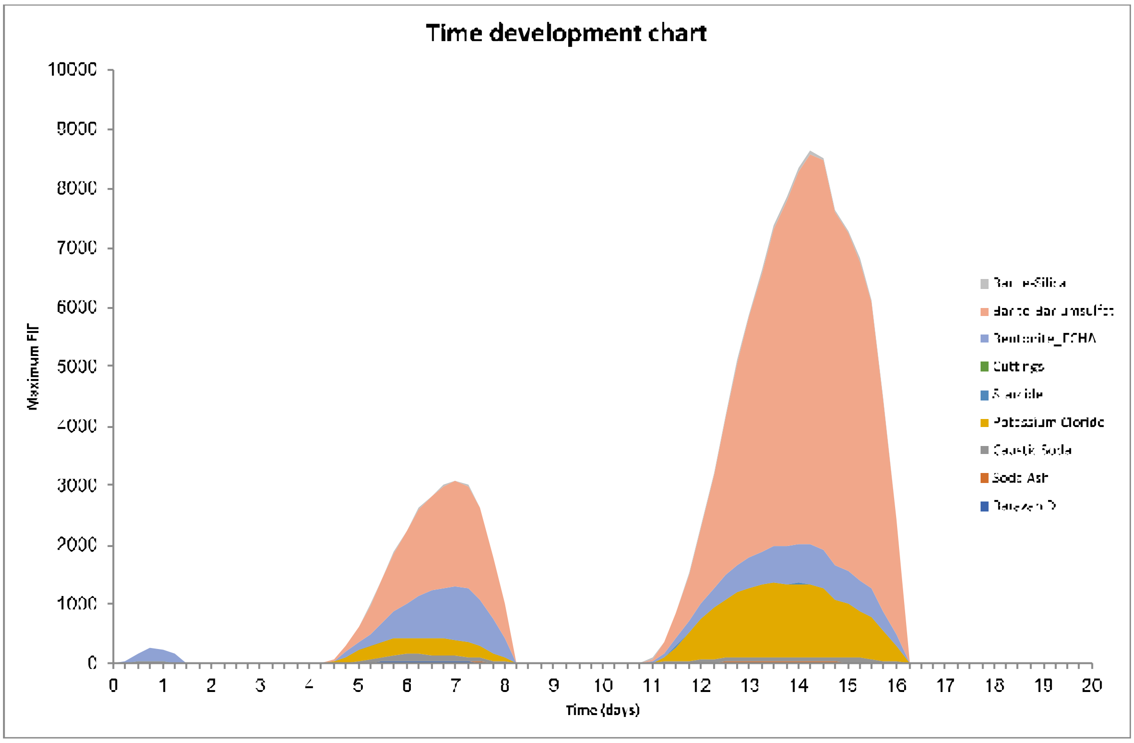

Figure 9.13 Time development of the EIF for the lower water column. Discharge location 5 – Autumn.

Figure 9.14 shows the time instant with maximum EIF for the lower water column due to discharges from the top hole sections, while Figure 9.16 shows the maximum cumulative risk (foot-print) throughout the lower water column at any time during the drilling operation with discharges from the top hole sections.

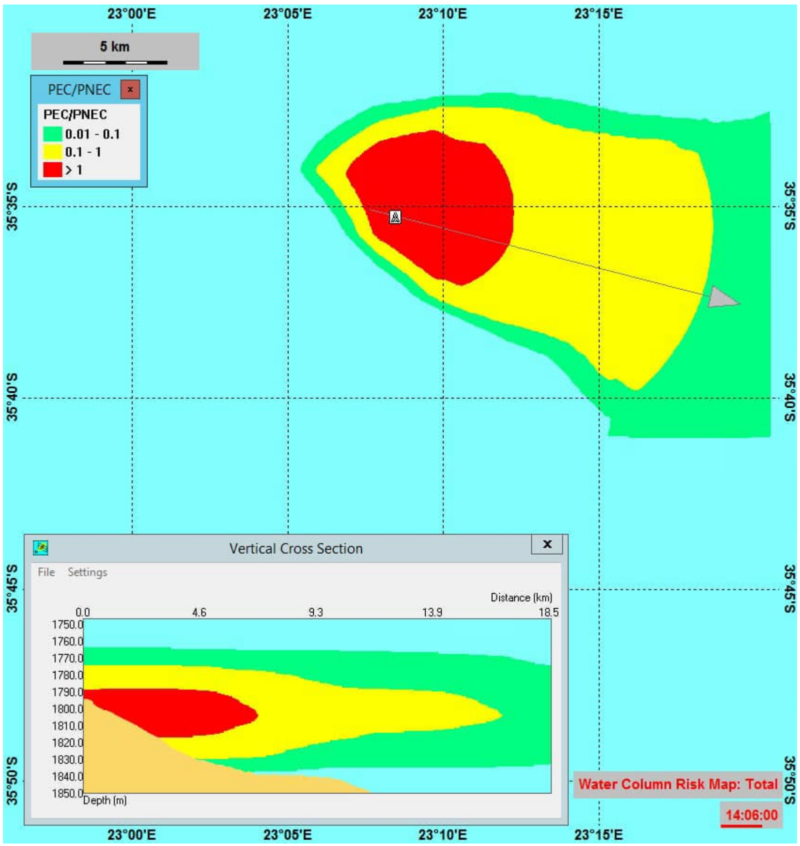

Figure 9.14 Snapshot showing the time instant with maximum EIF for the lower water column at 1750 - 1850 meters. Snapshot at day 14.25, when the discharge is from the top hole sections on the sea floor. The vertical cross section shows the PEC/PNEC ratio along the grey arrow. Discharge location 5 – Autumn.

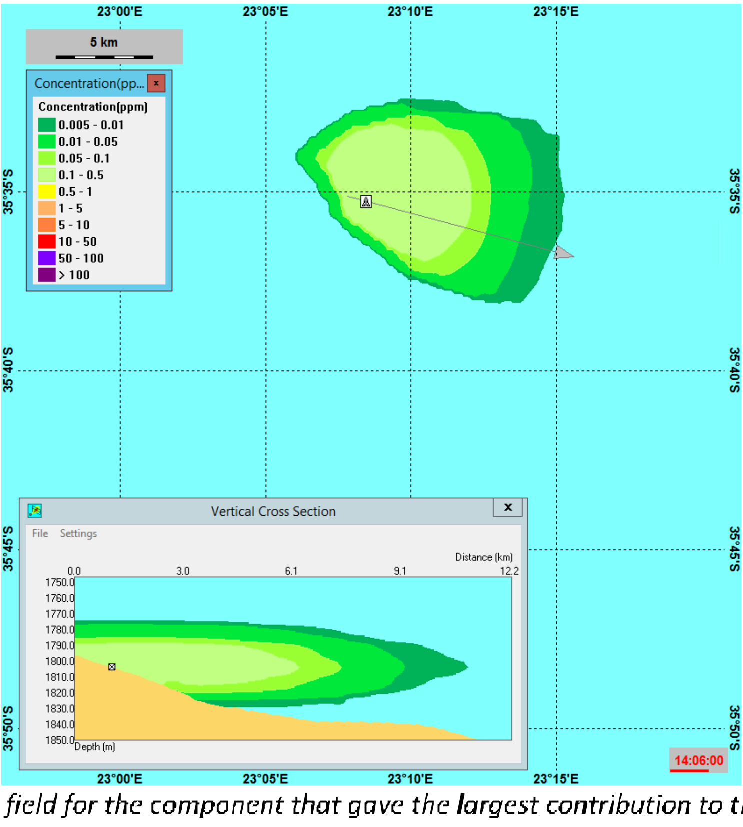

Figure 9.15 Concentration field for the component that gave the largest contribution to the environmental risk, namely the particle group barite, at the same time-step as for maximum EIF. A cross-section of the plume is shown in the smaller panel. Discharge location 5 – Autumn.

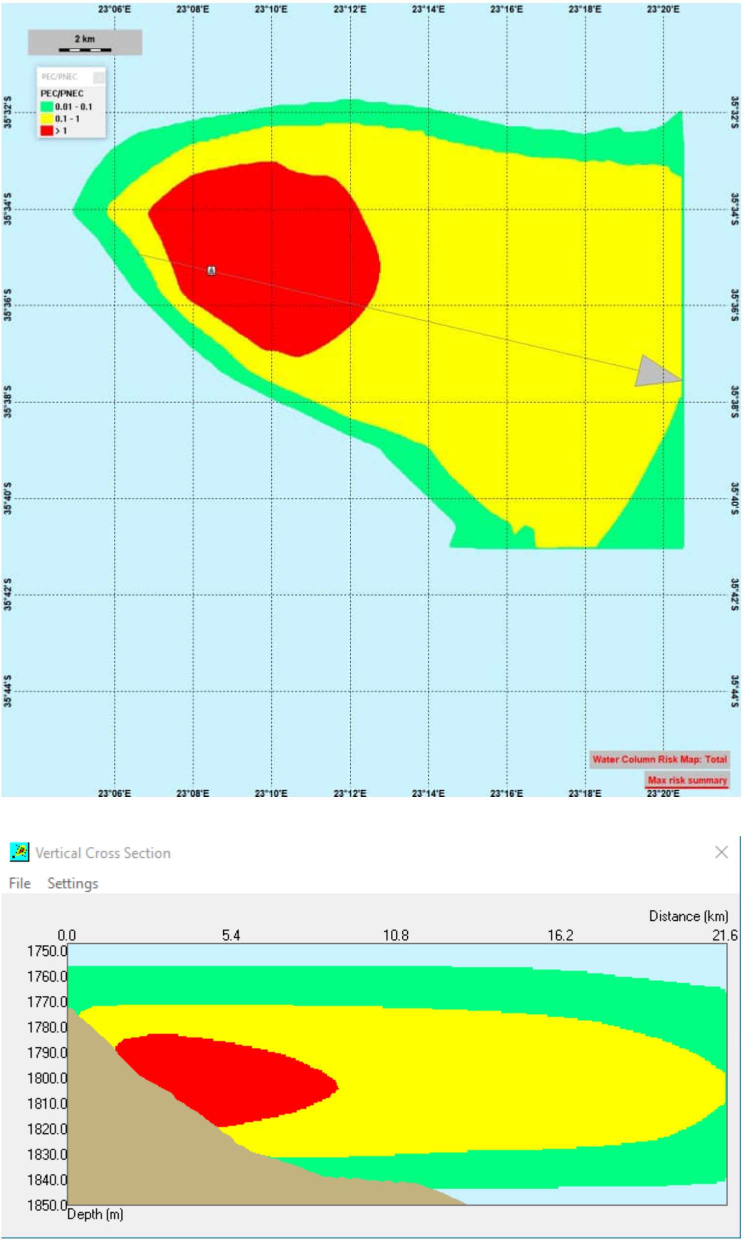

Figure 9.16 Maximum cumulative risk of drilling operations throughout the lower water column at any time for discharge location 5 (Start time March 12), discharge at the seafloor. Discharge location 5 – Autumn.

9.2.2 Discharge location 5 - Upper water-column – Autumn

The maximum EIF (water volume 100x100x10 m³) in the upper water-column 0-100 meter for discharge location 5, Autumn was 8156, while the time average EIF is computed with 655. The contributions of the components of the discharge are listed in the table below (risk in % of EIF).

Table 9.6 Table and pie-chart with EIF results for the water column, upper 100 meter for discharge location 5, Autumn.

Computed max. EIF:	**8156**				
Time averaged EIF:	655				
Components	Product	PNEC ppb	Contribution to risk %	Contribution max EIF	Contribution time averaged EIF
Total					
Soda Ash		200	0.03	2.44679877	0.196392
Caustic Soda		20	0.35	28.54598565	2.29124
Barazan D		420	0.08	6.52479672	0.523712
Potassium Cloride		100	6.97	568.4729142	45.628408
Sodium Chloride		1000000	0	0	0
GEM GP		188	0.03	2.44679877	0.196392
Clayseal Plus		562.3	0	0	0
Clayseal Plus-2		0.45	1.42	115.8151418	9.295888
Clay Grabber		9.8	0.32	26.09918688	2.094848
Clay Grabber-2		1.31	0.4	32.6239836	2.61856
Clay Sync II		1160	0.02	1.63119918	0.130928
Bore HIB		146	0	0	0
Dextrid E		1000	0.08	6.52479672	0.523712
PAC-L		87.26	0.67	54.64517253	4.386088
Cuttings		100000	0	0	0
Barite-Bariumsulfat		115	84.27	6873.057745	551.665128
Barite-Silica		440	0.79	64.43236761	5.171656
Baracarb 150		115	2.28	185.9567065	14.925792
Baracarb 50		115	2.28	185.9567065	14.925792

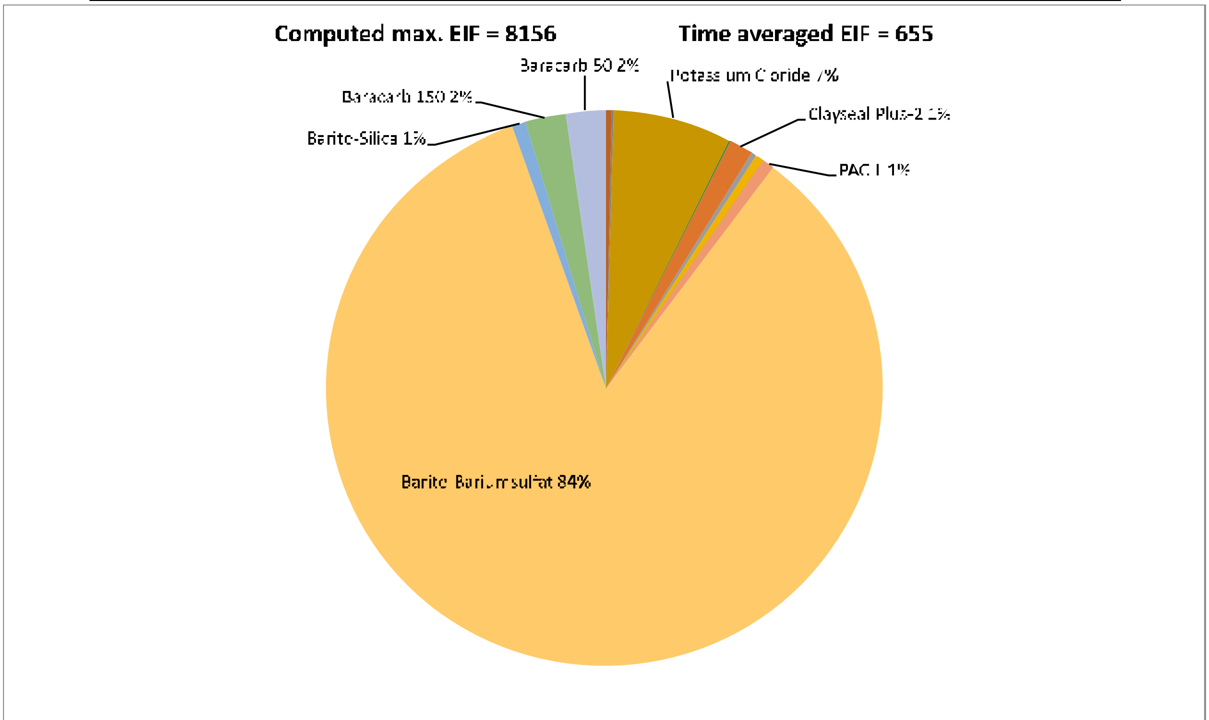

The results show that for the upper water column, effects caused by discharges of particle matter (essentially Barium sulfate 84%) are dominating the risk in the affected water volume. During the time of maximum EIF, the discharge is released from the rig 10 meters below sea-surface and sinks down in the water-column.

Figure 9.17 shows the time development for the EIF in water-column. It shows that the duration with high environmental risk lasts some days for each discharge.

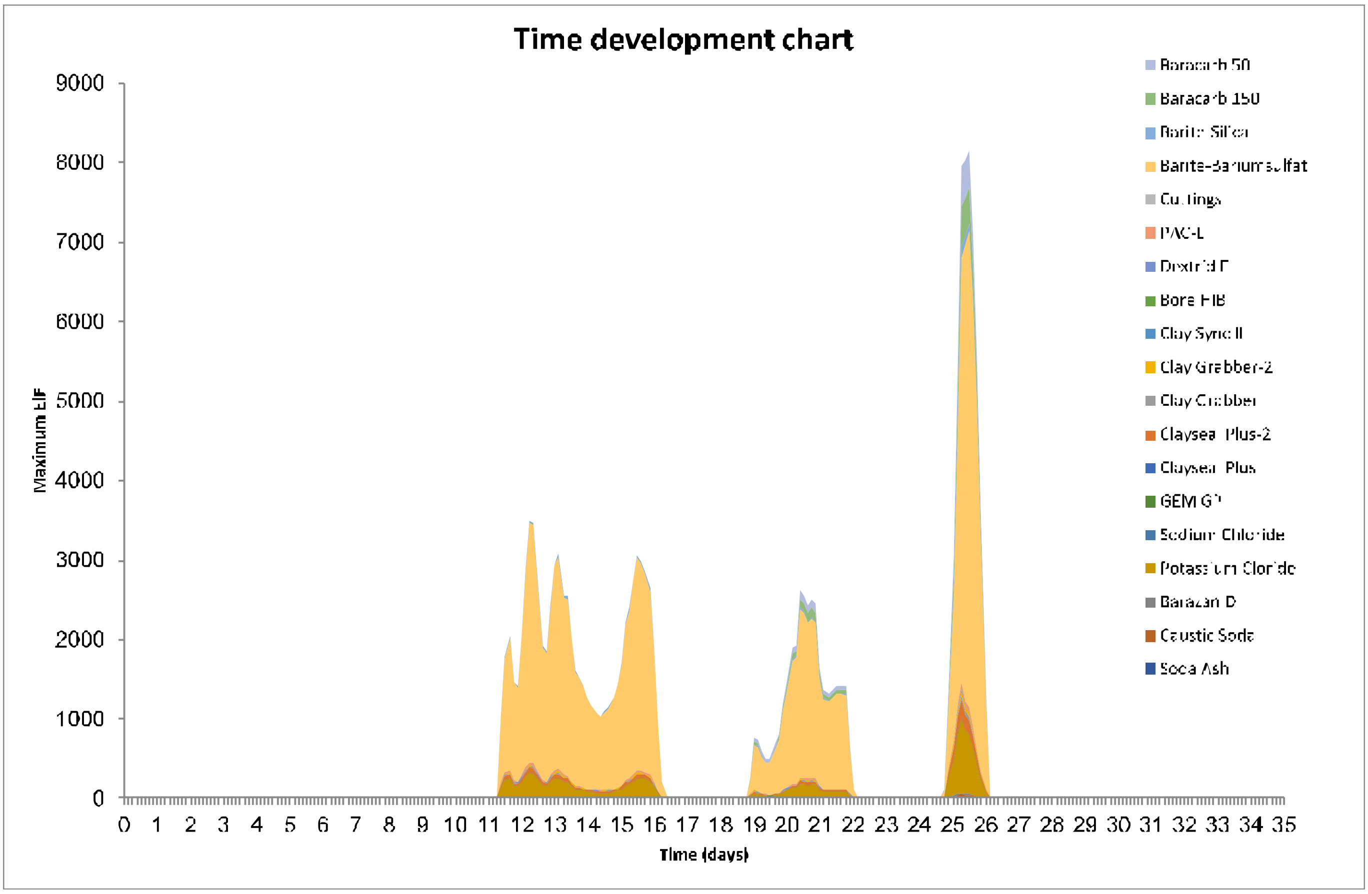

Figure 9.17 Time development of the EIF for the upper water column, for discharge location 5 Autumn.

Figure 9.18 shows the time instant with maximum EIF for the upper water column due to discharges from rig 10 m below sea surface, while Figure 9.20 shows the maximum cumulative risk (foot-print) throughout the upper water column at any time during the drilling operation with discharges from the rig.

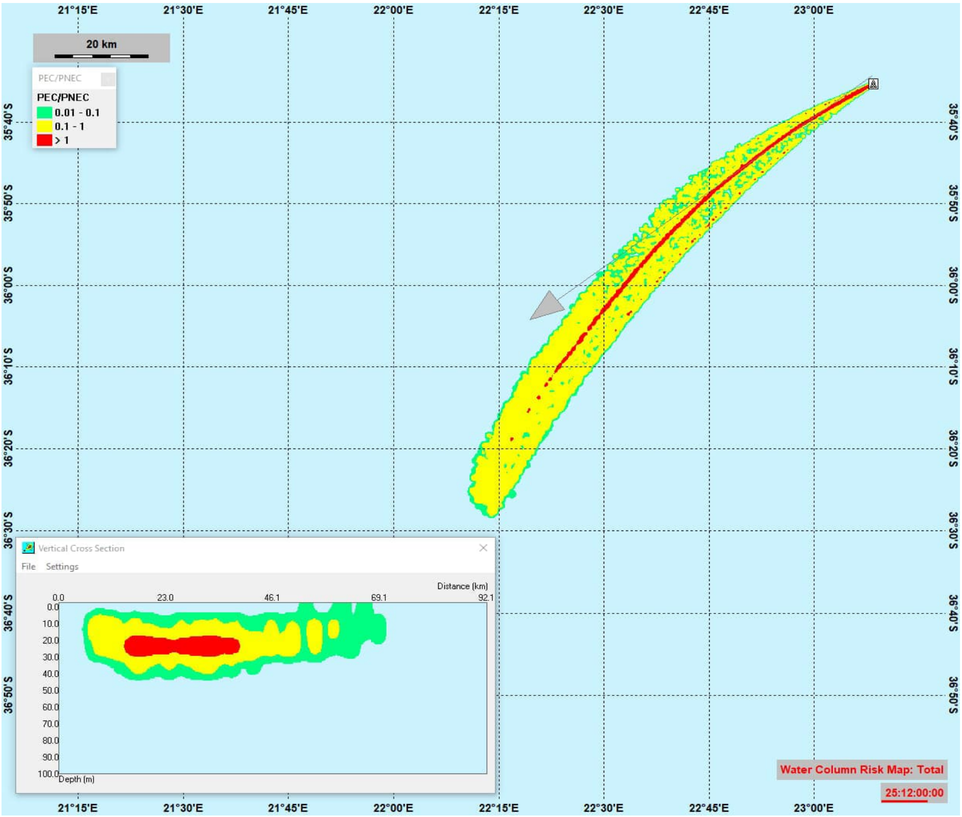

Figure 9.18 Snapshot showing the time instant with maximum EIF for the upper water column between 0-100 meters. Snapshot from 25.5 days after start, for the discharge released from the rig. The vertical cross section shows the PEC/PNEC ratio in the water column along the grey arrow. Discharge location 5 – Autumn.

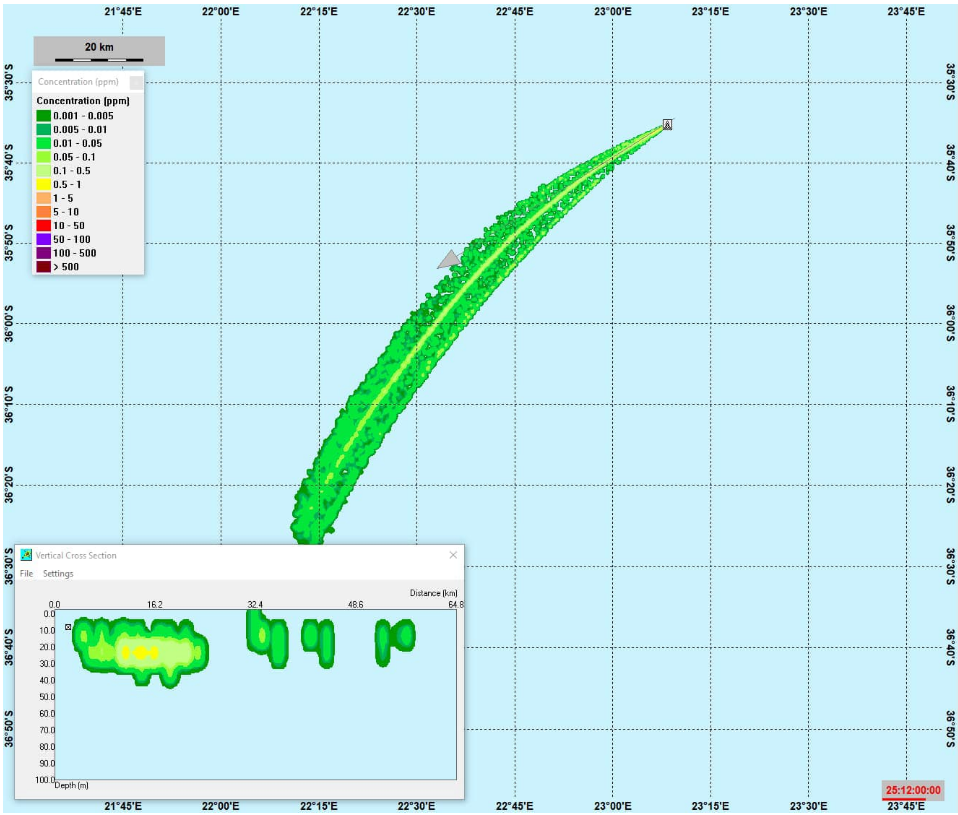

Figure 9.19 Concentration field for the component that gave the largest contribution to the environmental risk, namely the particle group Barium sulfate, at the same time-step as for maximum EIF. Discharge location 5 – Autumn.

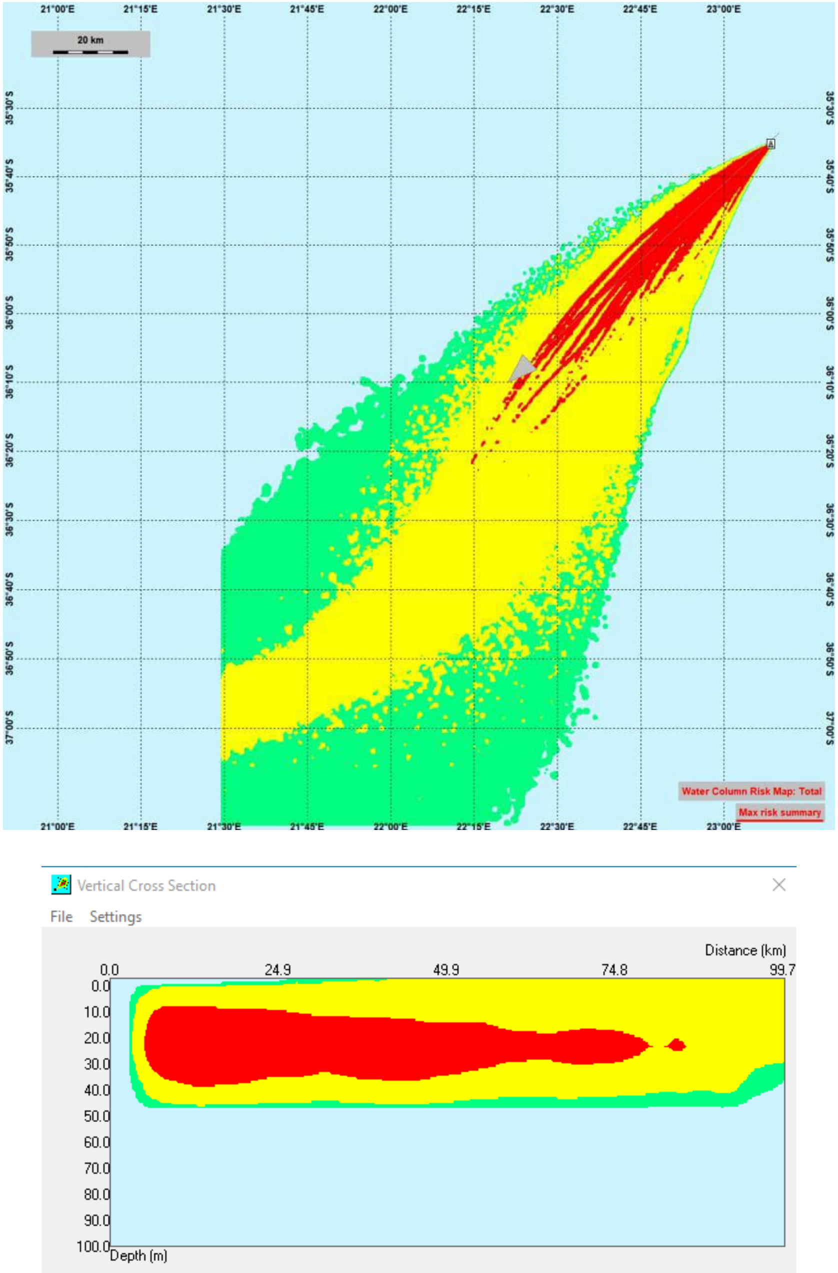

Figure 9.20 Maximum cumulative risk of drilling operations throughout the upper water column at any time for discharge location 5 (Start time March 12), discharge from rig 10 m below sea surface. Discharge location 5 – Autumn.

9.2.3 Discharge location 5 - EIF results for the sediment – Autumn

The maximum EIF (sea floor area 100x100 m^2) is computed with 1.5 impacted by discharge from the rig, and 0.75 impacted by the top hole discharge. The contributions of the components of the discharge are listed in the table below (risk in % of EIF). The affected area on the sea floor is largest at the end of the transport and fate simulation, shortly after the sediment module starts. After that the sea floor will starts restoration and the area (EIF) decreases. The factor affecting risk for the rig discharge is only grain size as for discharge location 4, Summer.

Table 9.7 Table and pie-chart shows contributions to EIF from the components discharged from the top hole sections to the sediment for location 5 – Autumn.

Simulated instantaneous EIF:	**0.75**				
Components	Product	PNEC ppb	Contribution to risk %	Contribution max EIF	Contribution time averaged EIF
Total					
Barazan D		420	0	0	0
Soda Ash		200	0	0	0
Caustic Soda		20	0	0	0
Potassium Cloride		100	0	0	0
Starcide		49	0	0	0
Thickness		0	64.38	0.48285	0.48285
Oxygen		0	0	0	0
Grain size		0	35.62	0.26715	0.26715

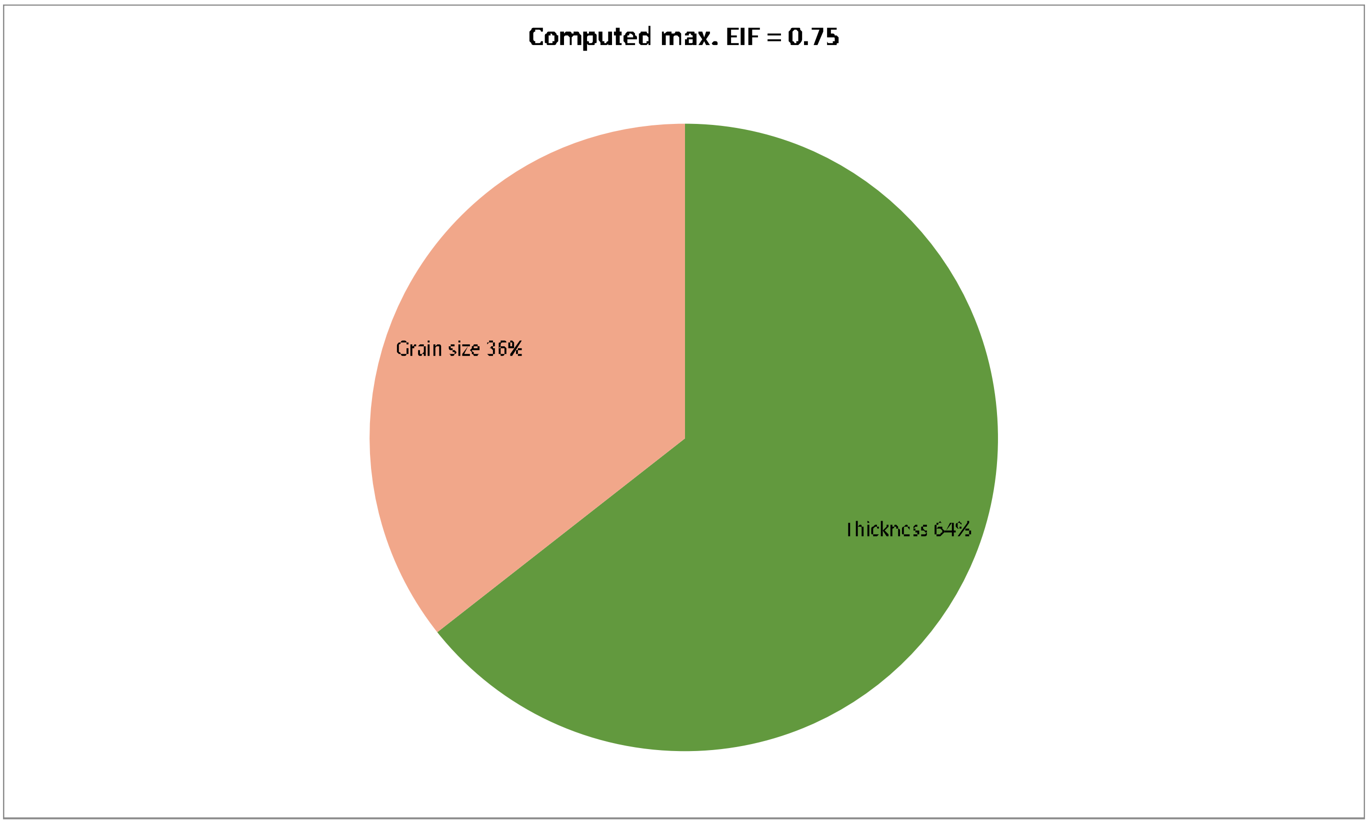

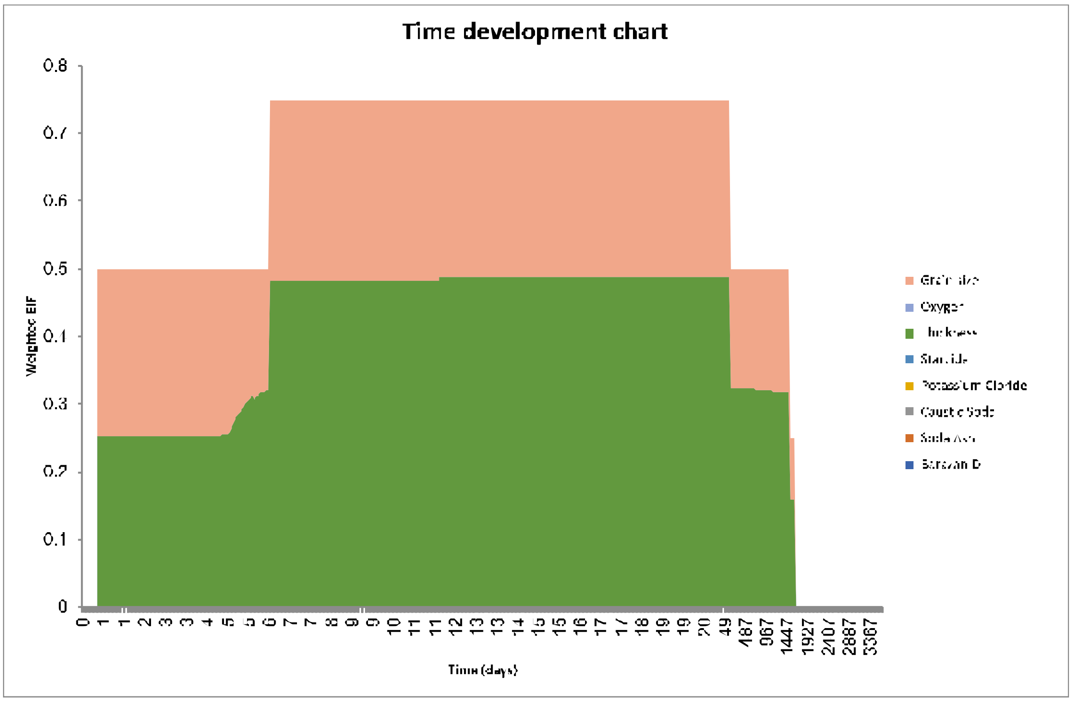

Figure 9.21 Time development of EIF for discharge from the top hole sections for the sediment for discharge location 5 – Autumn.

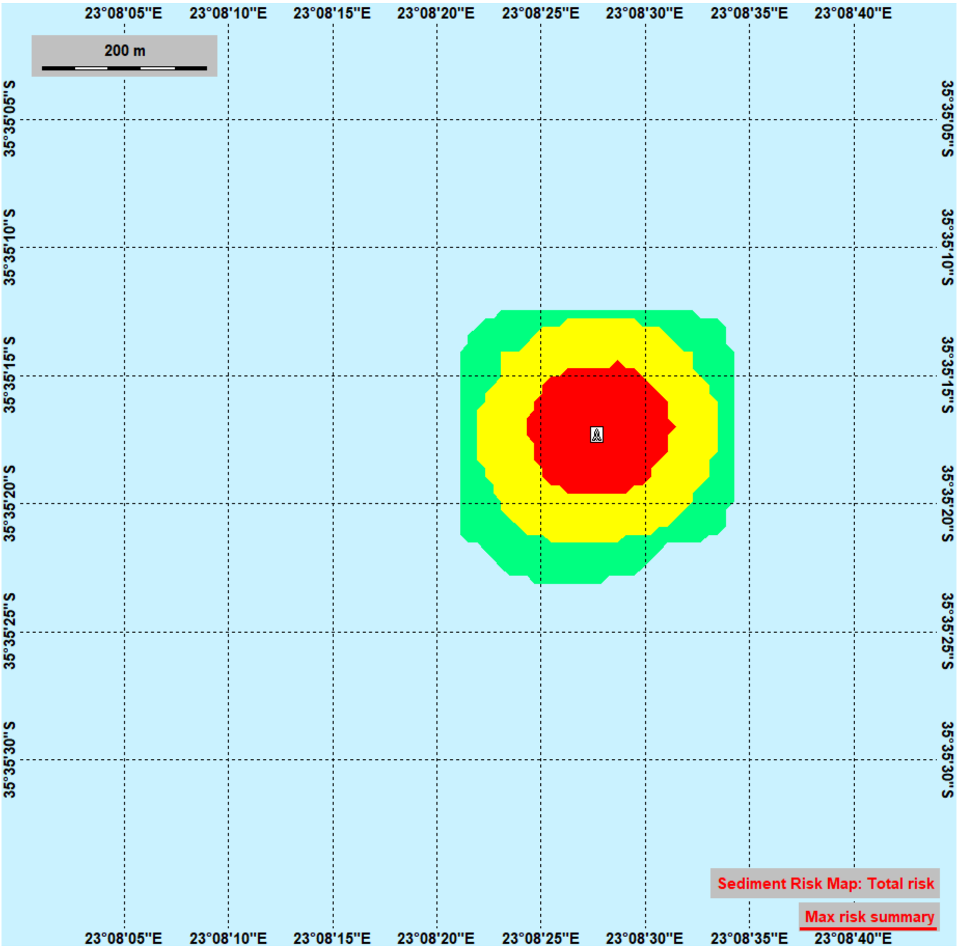

Figure 9.22 The total maximum EIF for the sediment (highest value at each location over simulation period) for discharge location 5 – Autumn.

9.3 EIF results for discharge location 5, Winter

9.3.1 Discharge location 5 - Lower water-column – Winter

The maximum EIF (water volume 100x100x10 m^3) in the lower water-column 1750 - 1850 meters for discharge location 5, Winter, was 8773, while the time average EIF was 1845. The contributions of the components of the discharge are listed in the table below (risk in % of EIF).

Table 9.8 Table and pie-chart with EIF results for the lower water column, 1750 - 1850 meters. Discharge location 5 - Winter.

Computed max. EIF:	**8773**				
Time averaged EIF:	1845				
Components	Product	PNEC ppb	Contribution to risk %	Contribution max EIF	Contribution time averaged EIF
Total					
Barazan D		420	0.39	34.21460	7.19468
Soda Ash		200	0.13	11.40487	2.39823
Caustic Soda		20	1.66	145.63136	30.62350
Potassium Cloride		100	12.65	1109.78114	233.36580
Starcide		49	0.11	9.65027	2.02927
Cuttings		100000	0.01	0.87730	0.18448
Bentonite_ECHA		170	13.59	1192.24709	250.70681
Barite-Bariumsulfat		115	70.86	6216.52895	1307.21741
Barite-Silica		440	0.59	51.76054	10.88425

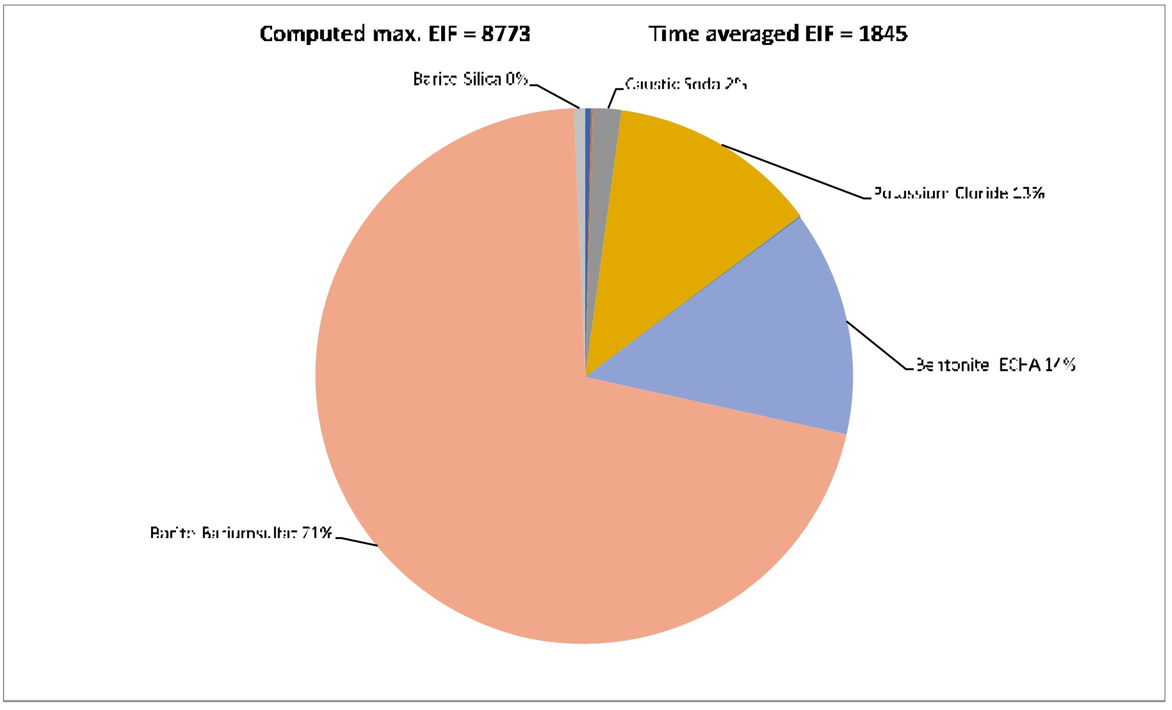

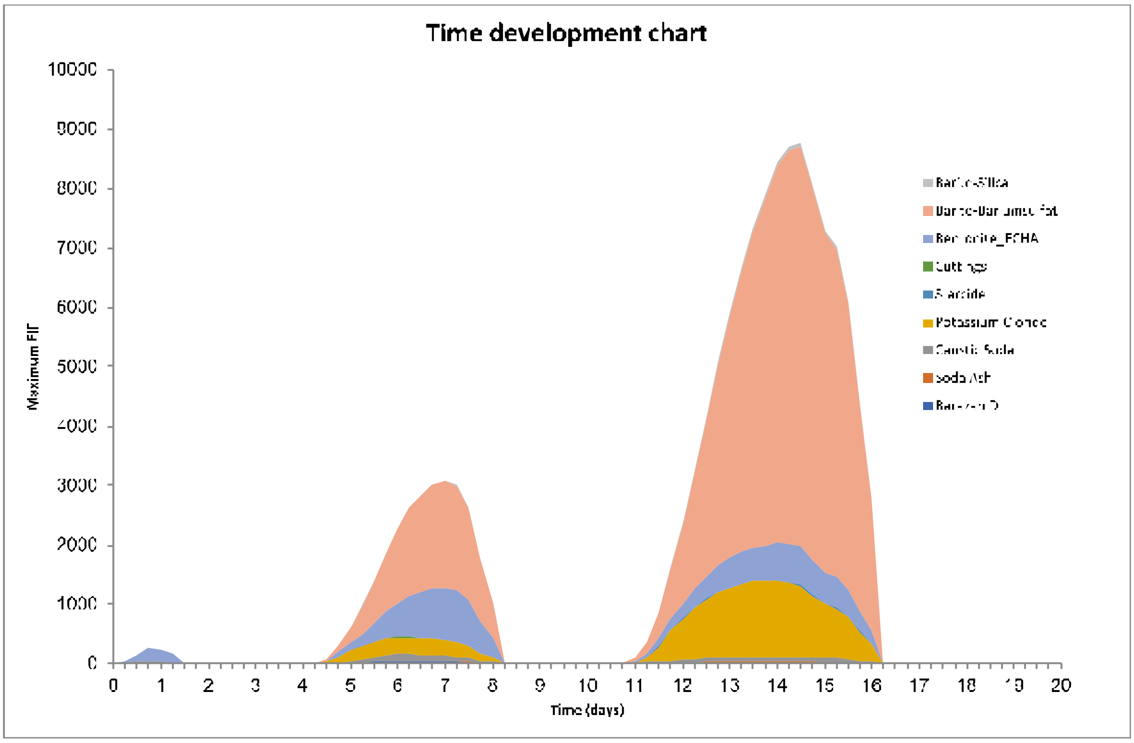

Figure 9.23 Time development of the EIF for the lower water column. Discharge location 5 - Winter.

Figure 9.24 shows the time instant with maximum EIF for the lower water column due to discharges from the top hole sections, while Figure 9.26 shows the maximum cumulative risk (foot-print) throughout the lower water column at any time during the drilling operation with discharges from the top hole sections.

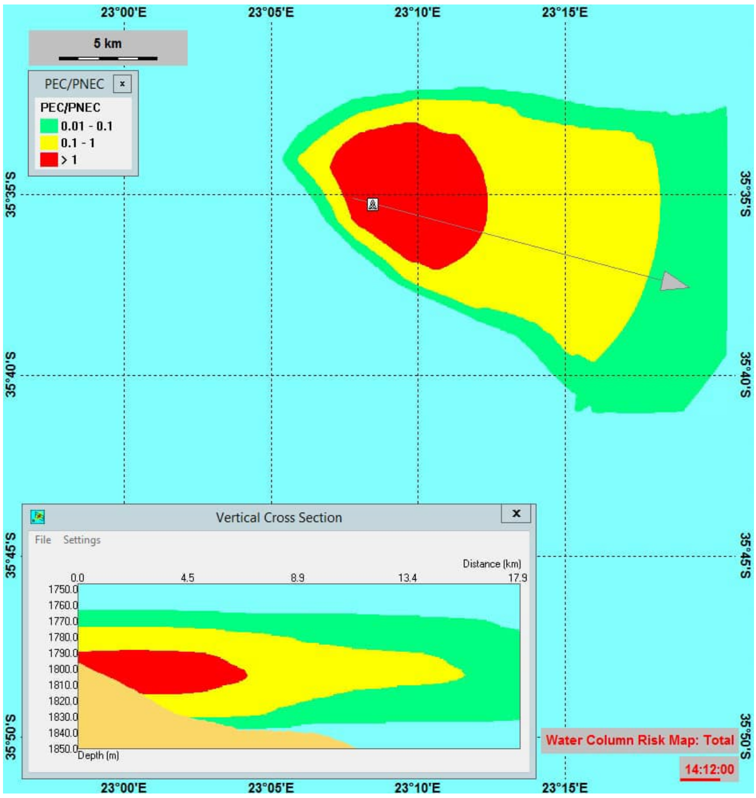

Figure 9.24 Snapshot showing the time instant with maximum EIF for the lower water column at 1750 - 1850 meters. Snapshot at day 14.5, when the discharge is from the top hole sections on the sea floor. The vertical cross section shows the PEC/PNEC ratio along the grey arrow. Discharge location 5 - Winter.

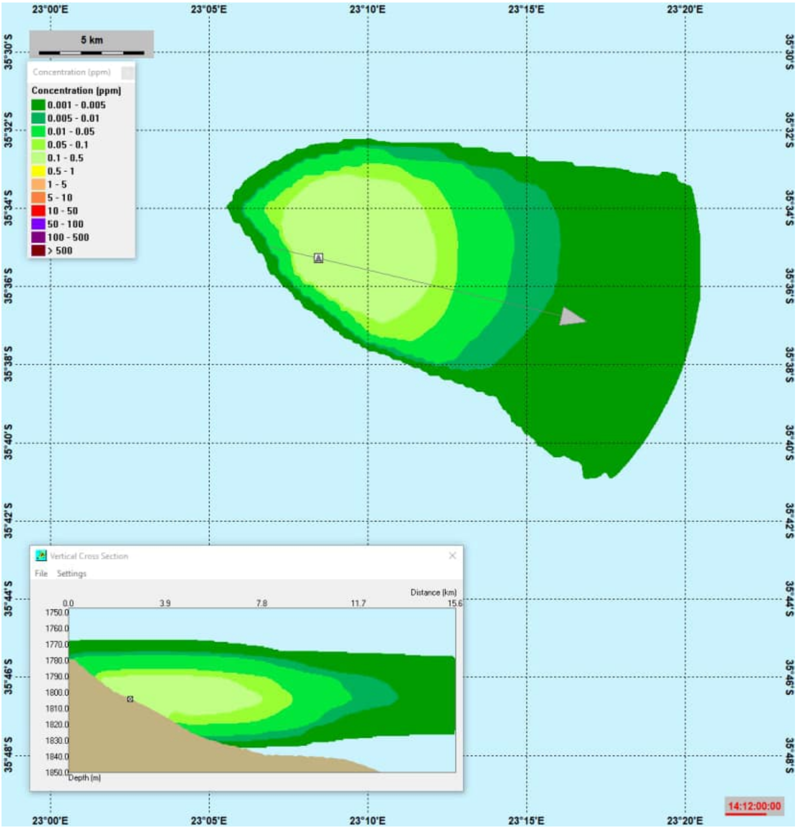

Figure 9.25 Concentration field for the component that gave the largest contribution to the environmental risk, namely the particle group barite, at the same time-step as for maximum EIF. A cross-section of the plume is shown in the smaller panel. Discharge location 5 - Winter.

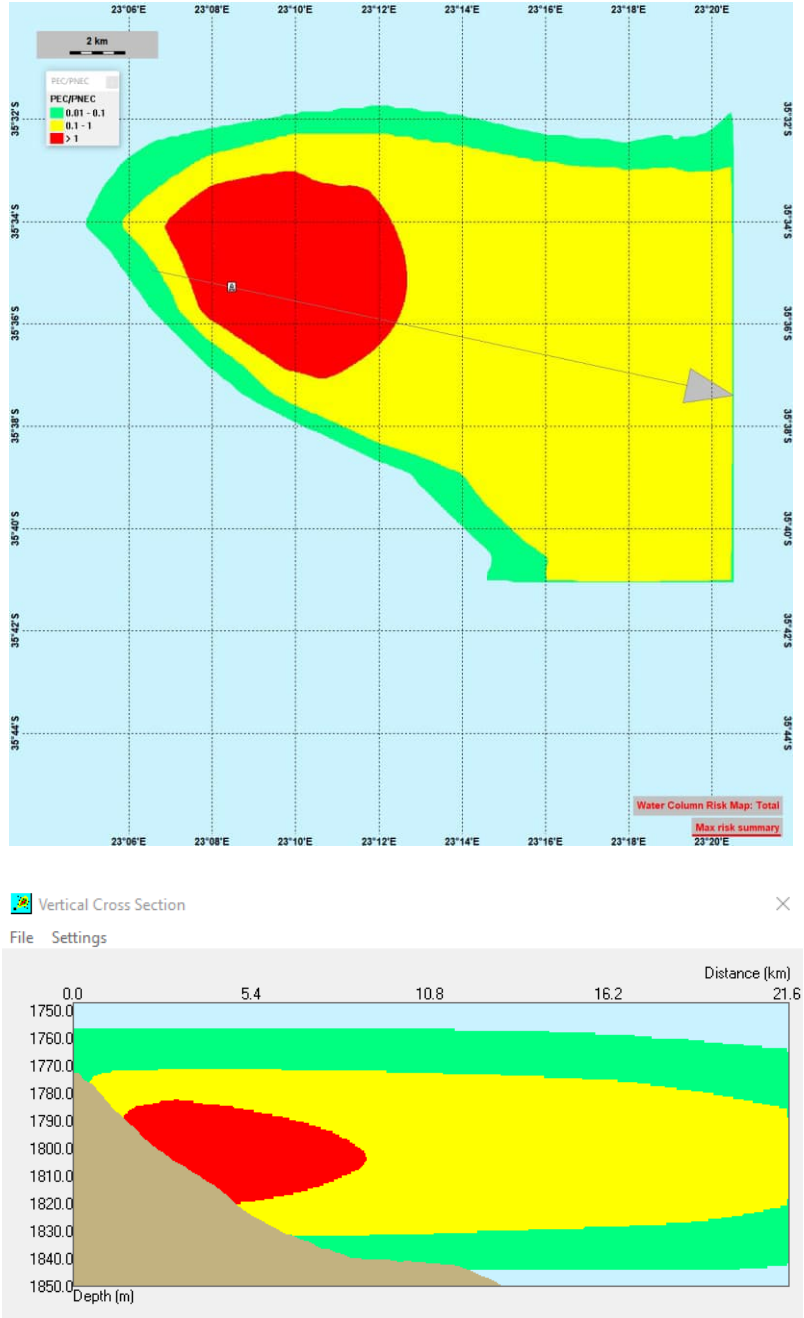

Figure 9.26 Maximum cumulative risk of drilling operations throughout the lower water column at any time for discharge location 5 (Start time August 12), discharge at the seafloor. Discharge location 5 – Winter.

9.3.2 Discharge location 5 - Upper water-column – Winter

The maximum EIF (water volume 100x100x10 m³) in the upper water-column 0-100 meter for discharge location 5, Winter, was 14220, while the time average EIF was 894. The contributions of the components of the discharge are listed in the table below (risk in % of EIF).

Table 9.9 Table and pie-chart with EIF results for the water column, upper 100 meter for discharge location 5, Winter.

Computed max. EIF:	**14220**				
Time averaged EIF:	894				
Components	Product	PNEC ppb	Contribution to risk %	Contribution max EIF	Contribution time averaged EIF
Total					
Soda Ash		200	0.03	4.26599787	0.26811681
Caustic Soda		20	0.36	51.19197444	3.21740172
Barazan D		420	0.08	11.37599432	0.71497816
Potassium Cloride		100	7.11	1011.041495	63.54368397
Sodium Chloride		1000000	0	0	0
GEM GP		188	0.03	4.26599787	0.26811681
Clayseal Plus		562.3	0	0	0
Clayseal Plus-2		0.45	1.38	196.235902	12.33337326
Clay Grabber		9.8	0.32	45.50397728	2.85991264
Clay Grabber-2		1.31	0.4	56.8799716	3.5748908
Clay Sync II		1160	0.02	2.84399858	0.17874454
Bore HIB		146	0	0	0
Dextrid E		1000	0.08	11.37599432	0.71497816
PAC-L		87.26	0.68	96.69595172	6.07731436
Cuttings		100000	0	0	0
Barite-Bariumsulfat		115	84.57	12025.848	755.8212874
Barite-Silica		440	0.83	118.0259411	7.41789841
Baracarb 150		115	2.06	292.9318537	18.41068762
Baracarb 50		115	2.06	292.9318537	18.41068762

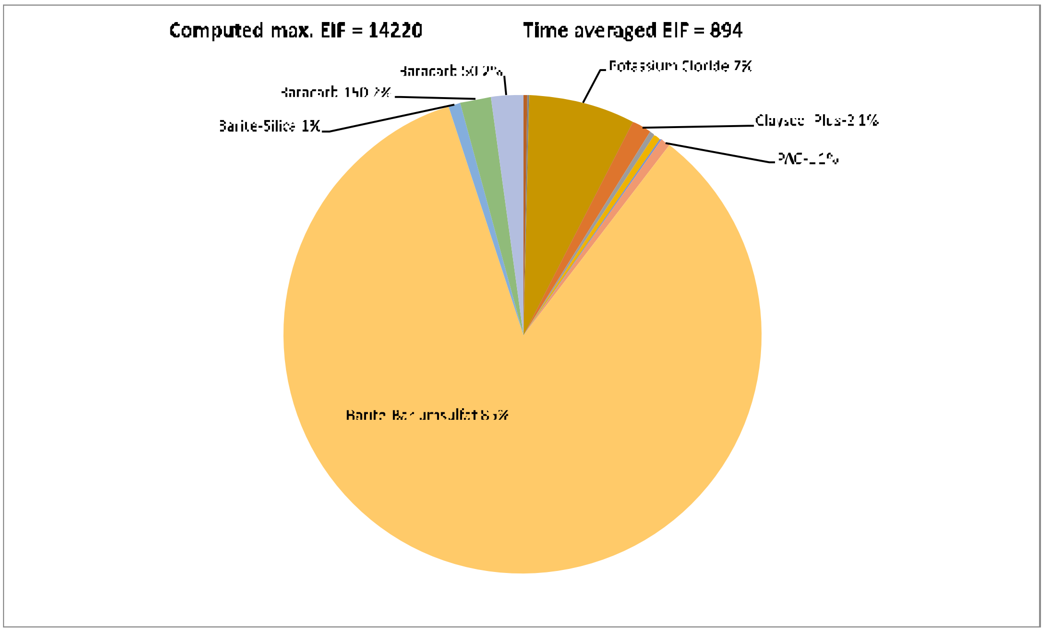

The results show that for the upper water column, effects caused by discharges of particle matter (essentially Barium sulfate 85%) are dominating the risk in the affected water volume. During the time of maximum EIF, the discharge is released from the rig 10 meters below sea-surface and sinks in the water-column.

Figure 9.27 shows the time development for the EIF in water-column. It shows that the duration with high environmental risk disappears shortly after discharge.

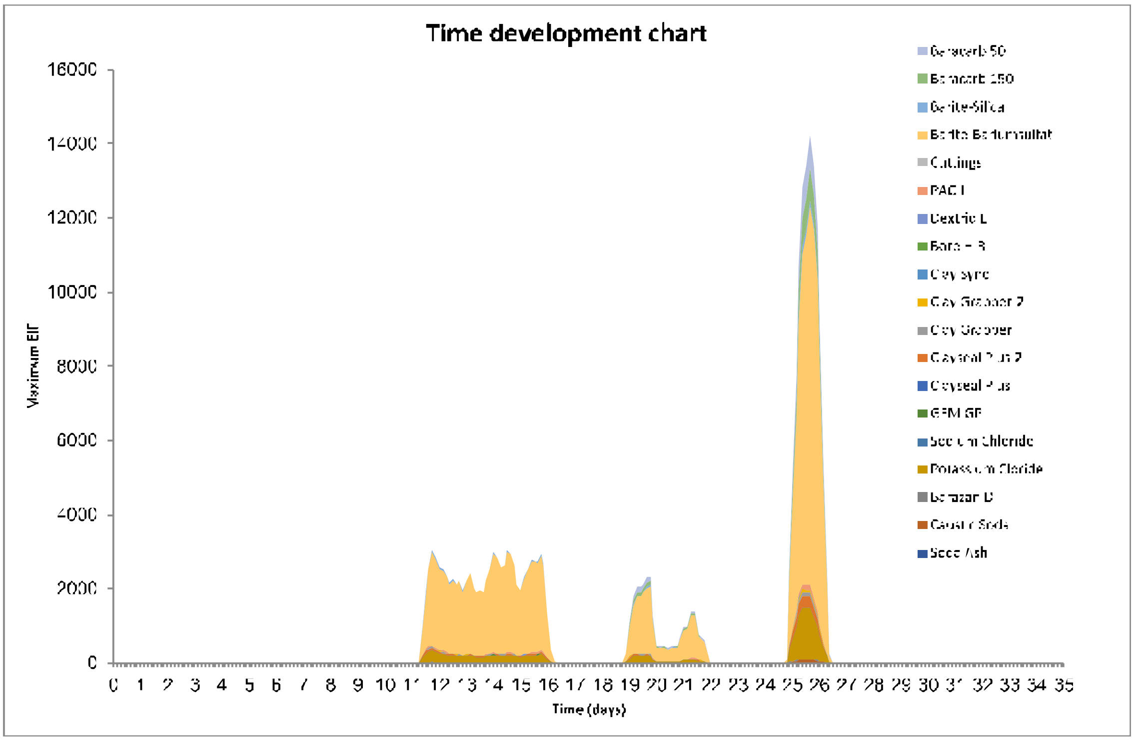

Figure 9.27 Time development of the EIF for the upper water column, for discharge location 5 - Winter.

Figure 9.28 shows the time instant with maximum EIF for the upper water column due to discharges from rig 10 m below sea surface, while Figure 9.30 shows the maximum cumulative risk (foot-print) throughout the upper water column at any time during the drilling operation with discharges from the rig.

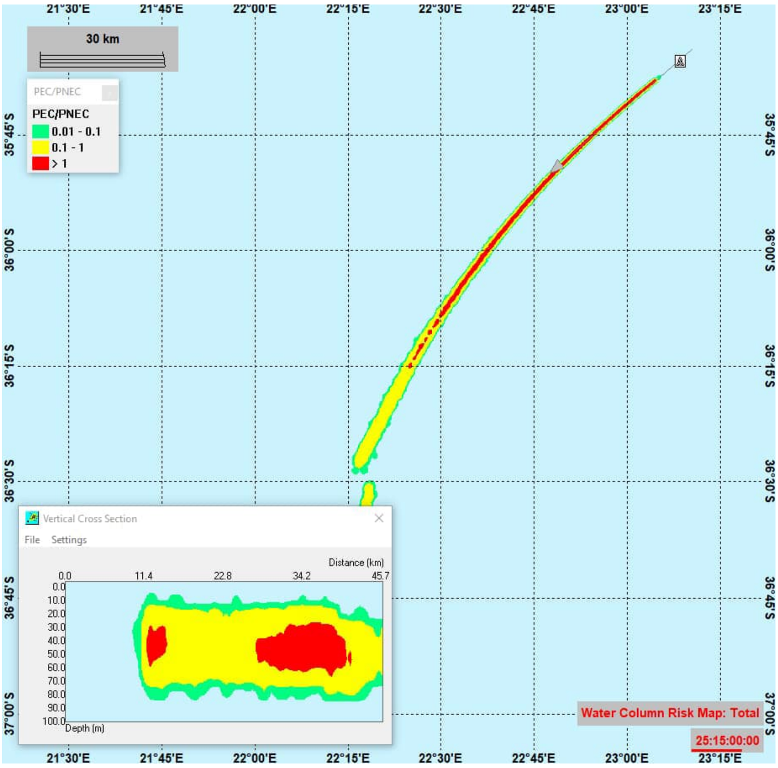

Figure 9.28 Snapshot showing the time instant with maximum EIF for the upper water column between 0-100 meters. Snapshot from 25.5 days after start, when the discharge is released from the rig. The vertical cross section shows the PEC/PNEC ratio in the water column along the grey arrow. Discharge location 5 - Winter.

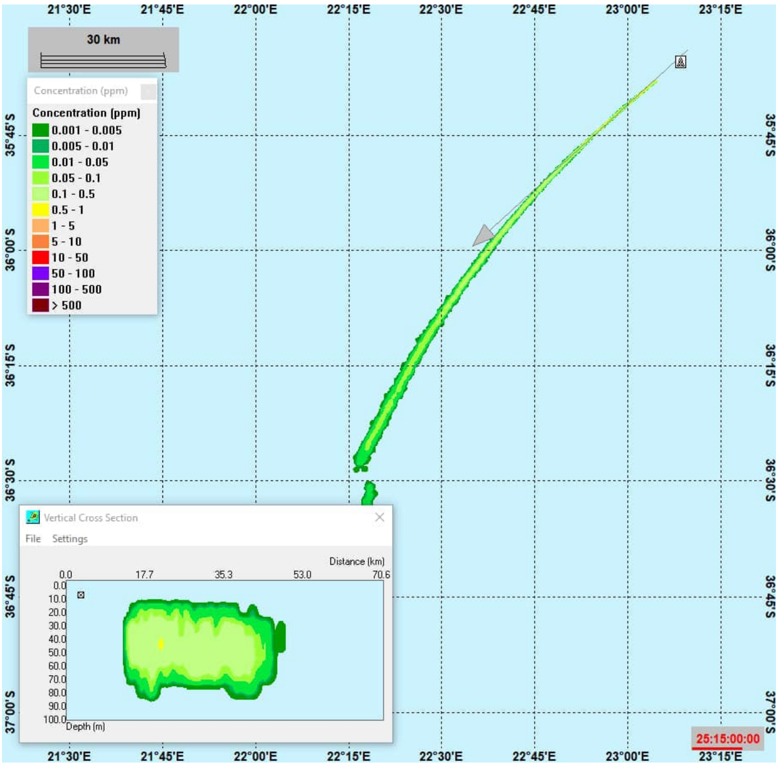

Figure 9.29 Concentration field for the component that gave the largest contribution to the environmental risk, namely the particle group Barium sulfate, at the same time-step as for maximum EIF. Discharge location 5 - Winter.

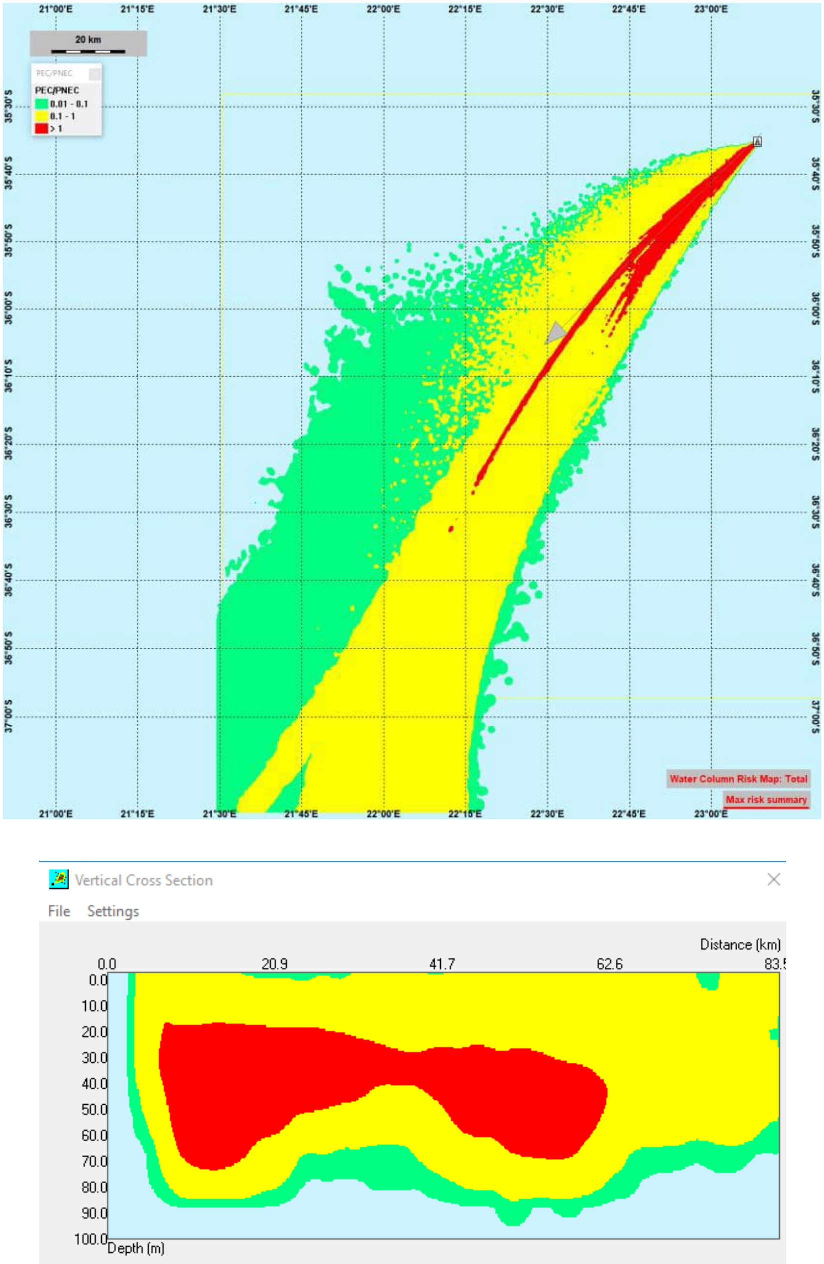

Figure 9.30 Maximum cumulative risk of drilling operations throughout the upper water column at any time for discharge location 5 (Start time August 12), discharge from rig 10 m below sea surface. Discharge location 5 – Winter.

9.3.3 Discharge location 5 - EIF results for the sediment – Winter

The maximum EIF (sea floor area 100x100 m^2) is computed with 0 impact by discharge from the rig, and 0.5 impacted by the top hole discharge. The contributions of the components of the discharge are listed in the table below (risk in % of EIF). The affected area on the sea floor is largest at the end of the transport and fate simulation, shortly after the sediment module starts. After that the sea floor will start to restore and the area (EIF) will get smaller.

Table 9.10 Table and pie-chart shows contributions to EIF from the components discharged from the top hole sections to the sediment for location 5 – Winter.

Simulated instantaneous EIF:	**0.5**				
Components	Product	PNEC ppb	Contribution to risk %	Contribution max EIF	Contribution time averaged EIF
Total					
Barazan D		420	0	0	0
Soda Ash		200	0	0	0
Caustic Soda		20	0	0	0
Potassium Cloride		100	0	0	0
Starcide		49	0	0	0
Thickness		0	64.99	0.32495	0.32495
Oxygen		0	0	0	0
Grain size		0	35.01	0.17505	0.17505

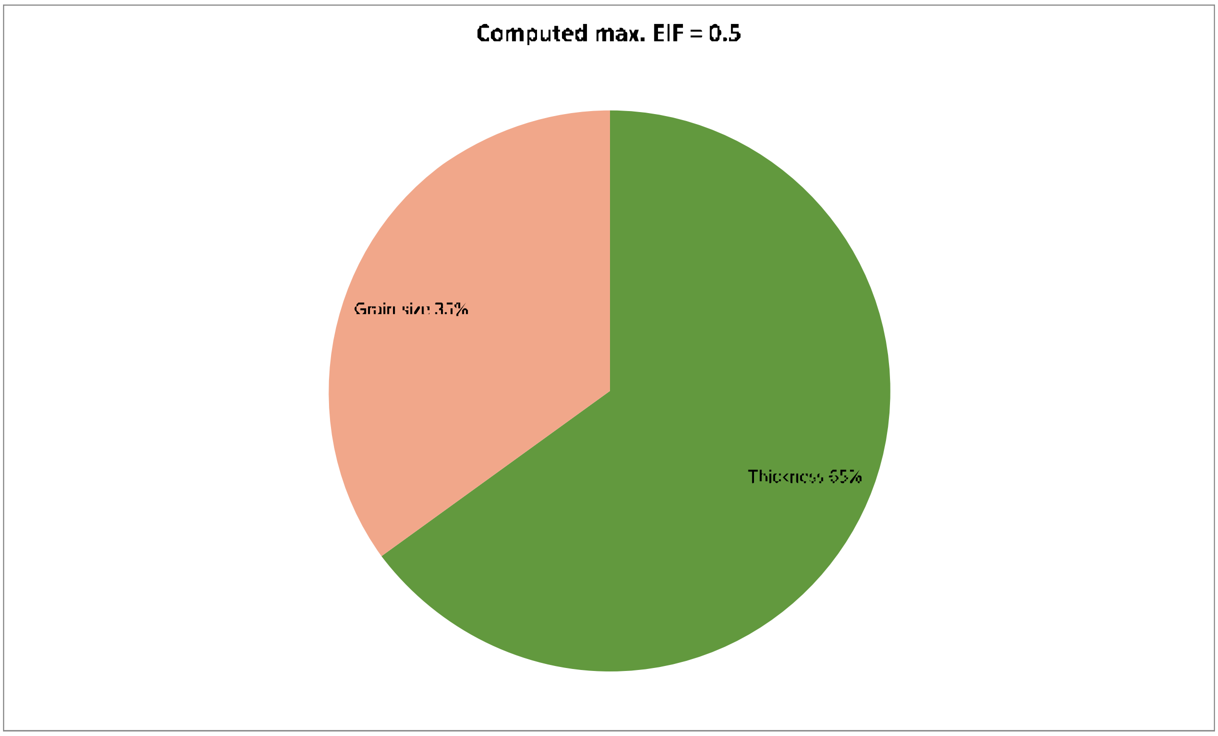

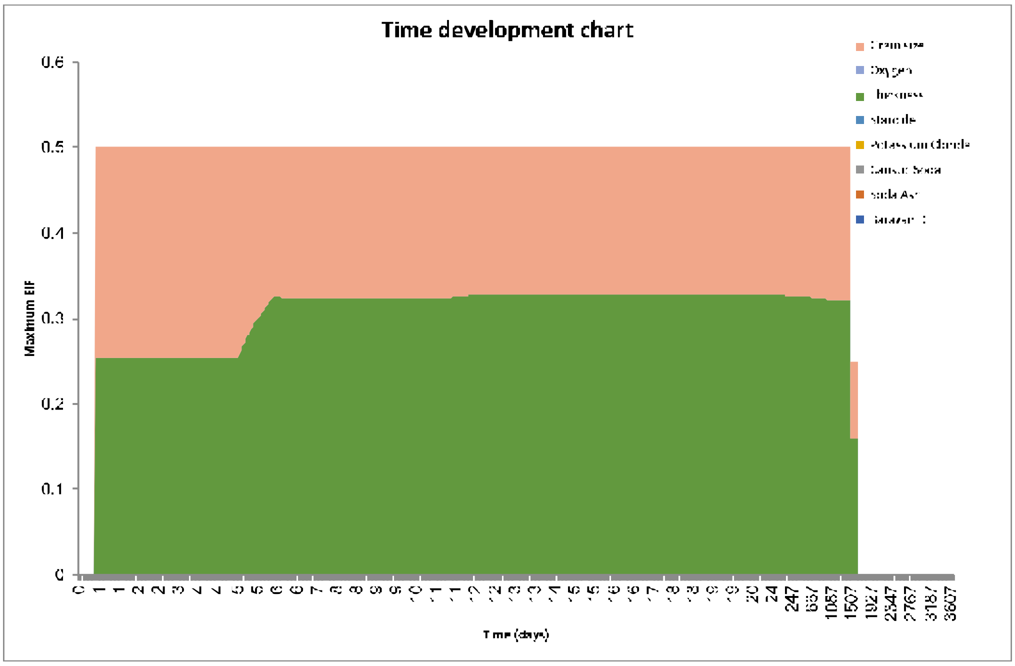

Figure 9.31 Time development of EIF for discharge from the top hole sections for the sediment for discharge location 5 – Winter.

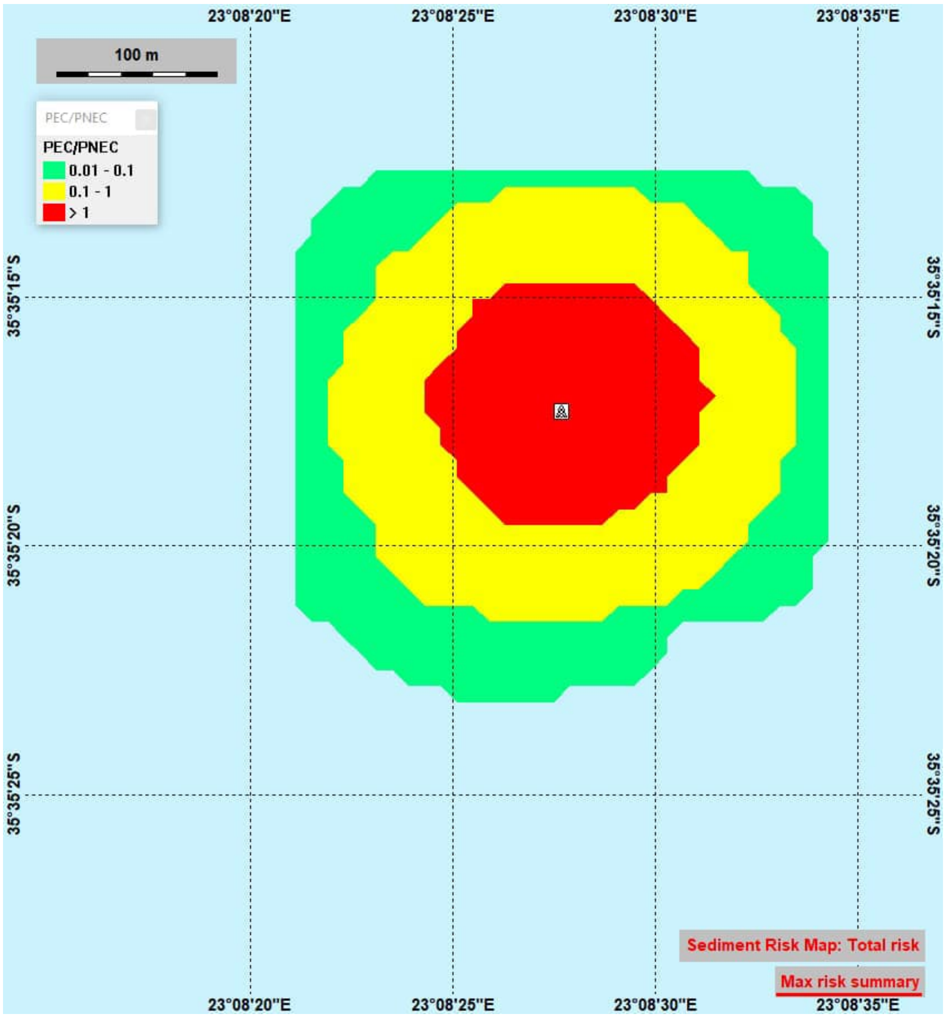

Figure 9.32 The total maximum EIF for the sediment (highest value at each location over simulation period) for discharge location 5 – Winter.

9.4 EIF results for discharge location 5, Spring

9.4.1 Discharge location 5 - Lower water-column – Spring

The maximum EIF (water volume 100x100x10 m^3) in the lower water-column 1750 - 1850 meters for discharge location 5, Spring was 3170, while the time average EIF was 731. The contributions of the components of the discharge are listed in the table below (risk in % of EIF).

Table 9.11 Table and pie-chart with EIF results for the lower water column, 1750 - 1850 meters. Discharge location 5 - Spring.

Computed max. EIF:	**8722**				
Time averaged EIF:	2028				
Components	Product	PNEC ppb	Contribution to risk %	Contribution max EIF	Contribution time averaged EIF
Total					
Barazan D		420	0.45	39.2489	9.1260
Soda Ash		200	0.14	12.2108	2.8392
Caustic Soda		20	1.84	160.4843	37.3151
Potassium Cloride		100	13.49	1176.5942	273.5763
Starcide		49	0.12	10.4664	2.4336
Cuttings		100000	0.01	0.8722	0.2028
Bentonite_ECHA		170	14.83	1293.4687	300.7515
Barite-Bariumsulfat		115	68.46	5971.0631	1388.3644
Barite-Silica		440	0.66	57.5650	13.3848

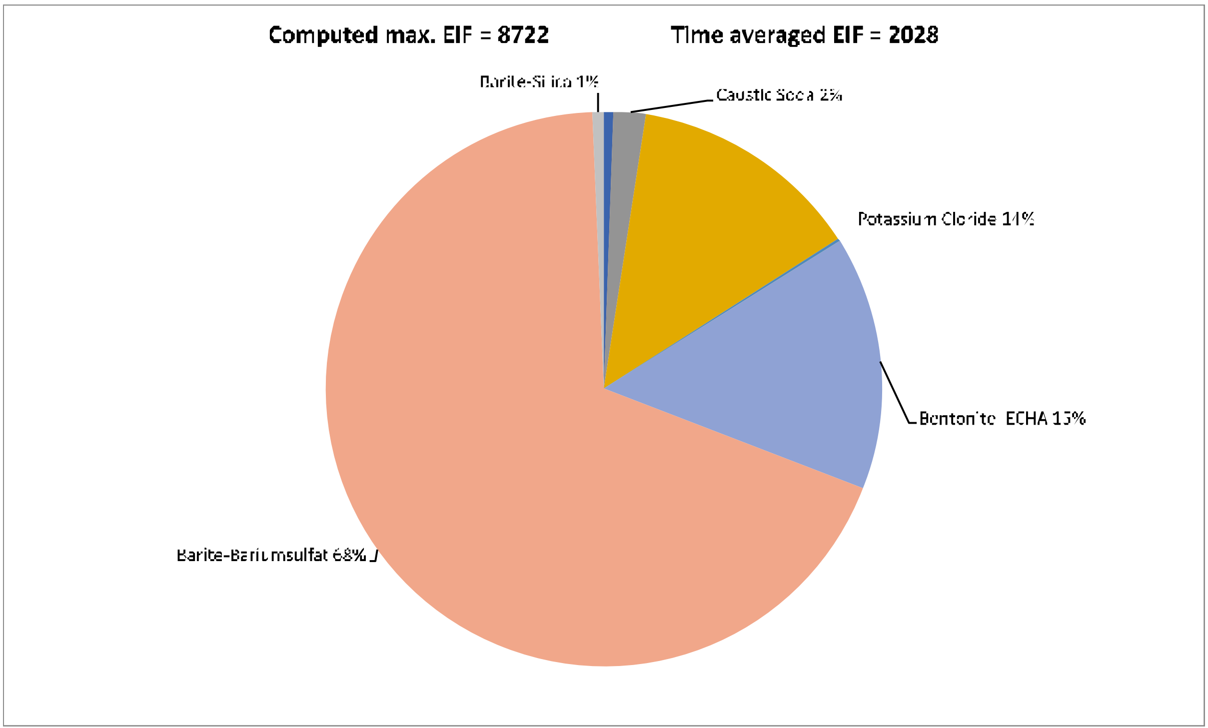

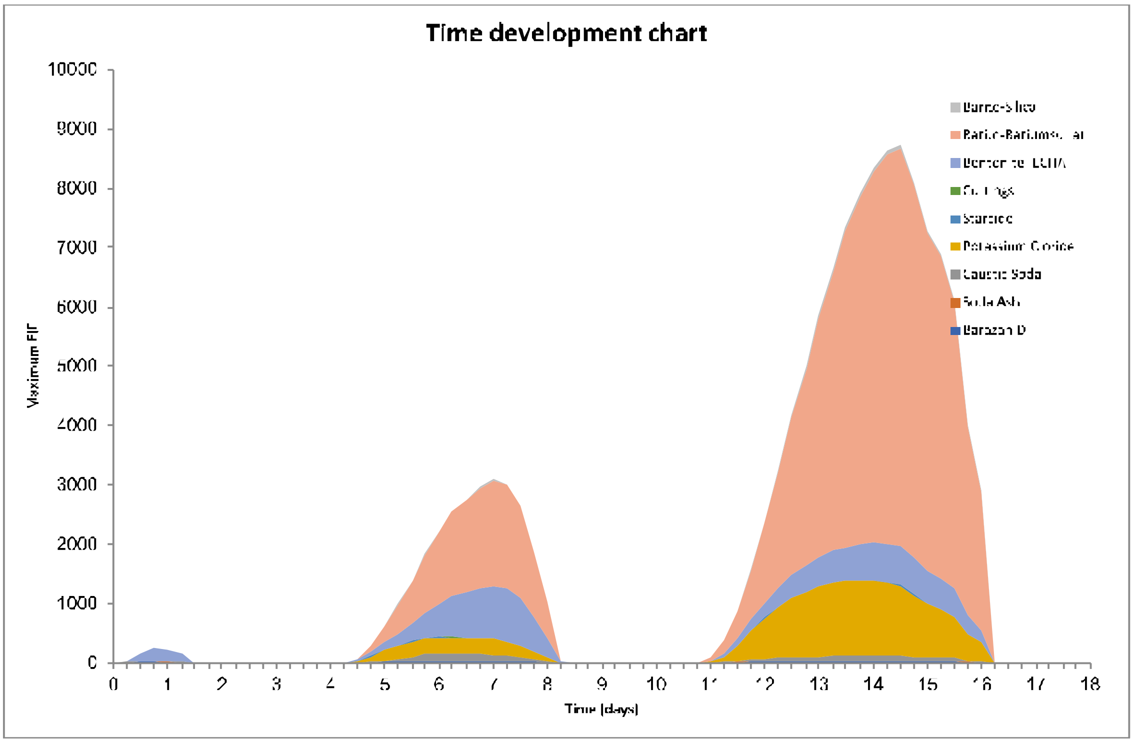

Figure 9.33 Time development of the EIF for the lower water column. Discharge location 5 - Spring.

Figure 9.34 shows the time instant with maximum EIF for the lower water column due to discharges from the top hole sections, while Figure 9.36 shows the maximum cumulative risk (foot-print) throughout the lower water column at any time during the drilling operation with discharges from the top hole sections.

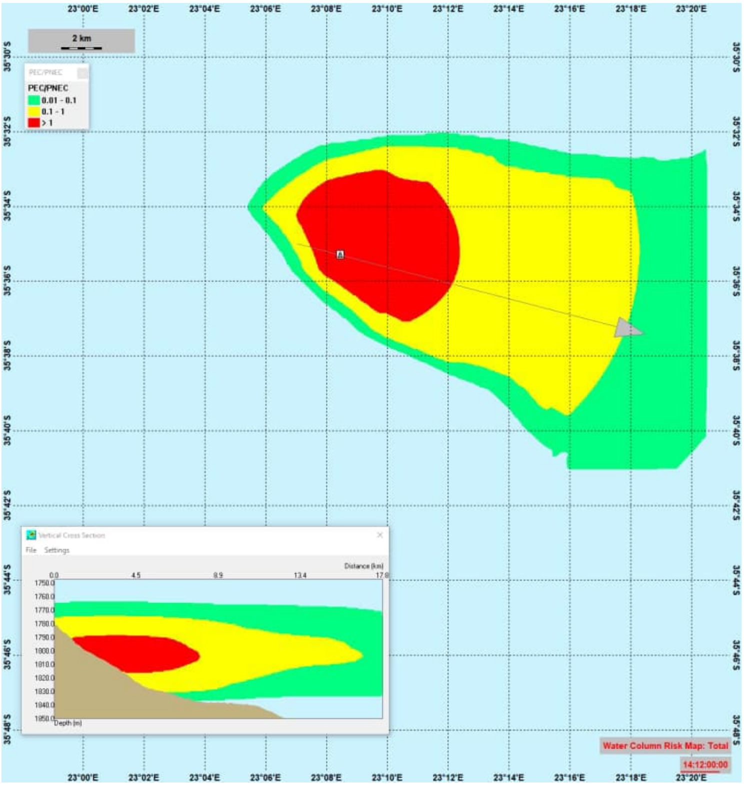

Figure 9.34 *Snapshot showing the time instant with maximum EIF for the lower water column at 1750 - 1850 meters. Snapshot at day 14.5, when the discharge is from the top hole sections on the sea floor. The vertical cross section shows the PEC/PNEC ratio along the grey arrow. Discharge location 5 - Spring.*

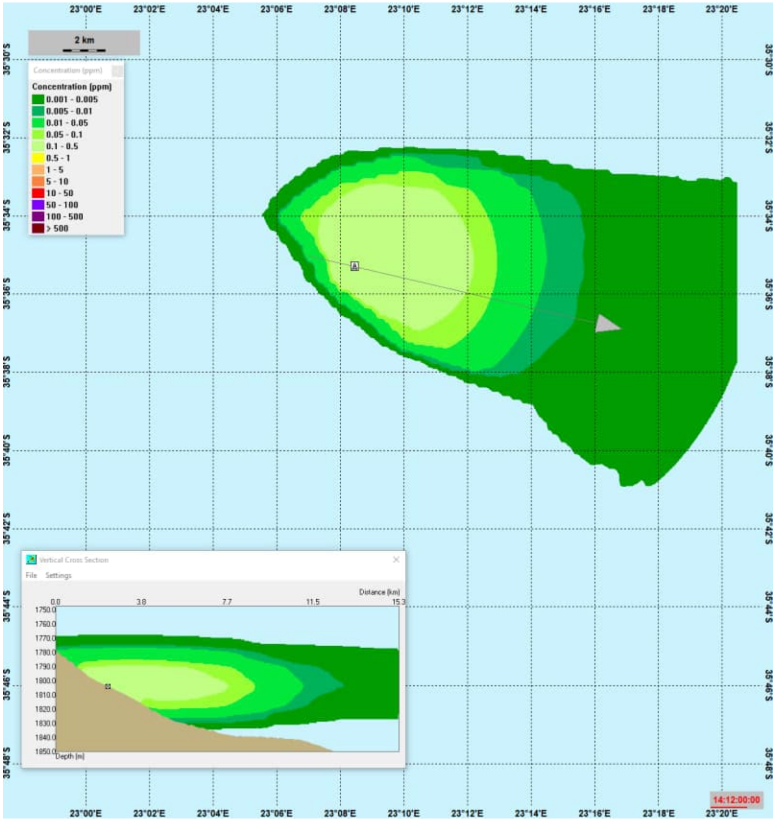

Figure 9.35 *Concentration field for the component that gave the largest contribution to the environmental risk, namely the particle group barite, at the same time-step as for maximum EIF. A cross-section of the plume is shown in the smaller panel. Discharge location 5 - Spring.*

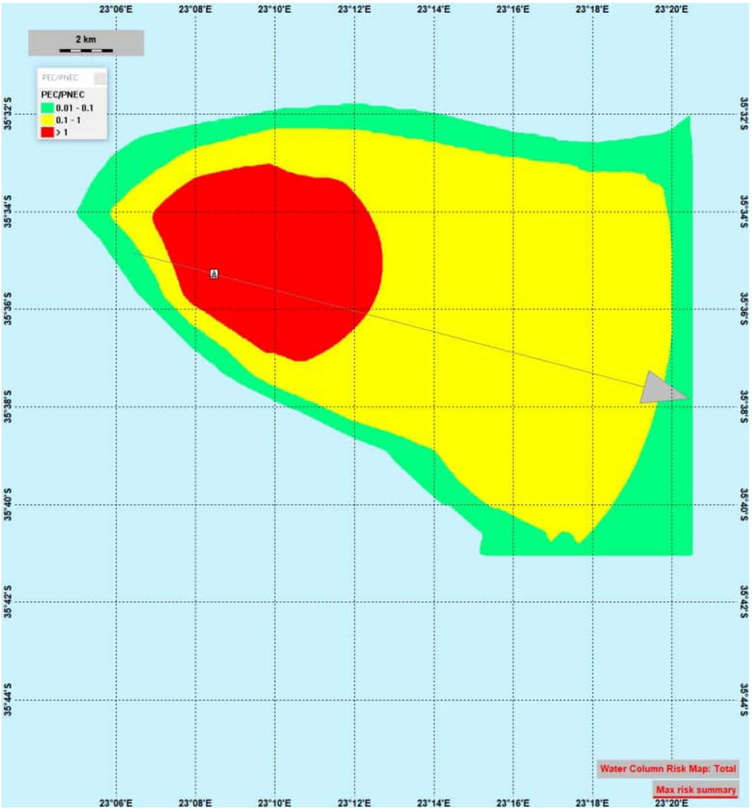

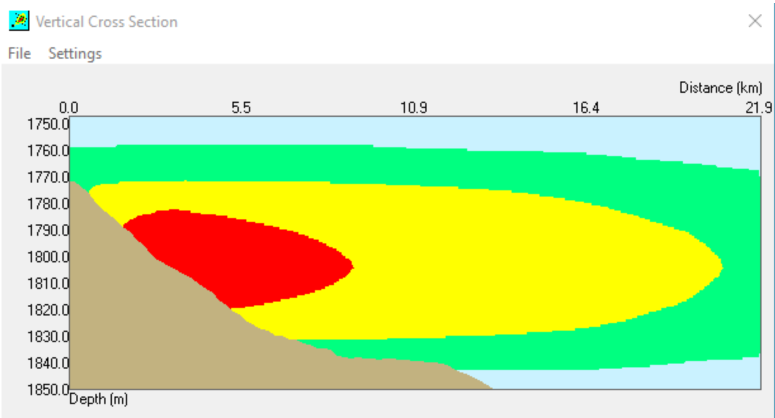

Figure 9.36 Maximum cumulative risk of drilling operations throughout the lower water column at any time for discharge location 5 (Start time October 15), discharge at the seafloor. Discharge location 5 – Spring.

9.4.2 Discharge location 5 - Upper water-column – Spring

The maximum EIF (water volume 100x100x10 m^3) in the upper water-column 0-100 meter for discharge location 5, Spring, was 14536, while the time average EIF was 979. The contributions of the components of the discharge are listed in the table below (risk in % of EIF).

Table 9.12 Table and pie-chart with EIF results for the water column, upper 100 meter for discharge location 5, Spring.

Computed max. EIF:	**14536**				
Time averaged EIF:	979				
Components	Product	PNEC ppb	Contribution to risk %	Contribution max EIF	Contribution time averaged EIF
Total					
Soda Ash		200	0.03	4.36079781	0.2935635
Caustic Soda		20	0.39	56.69037153	3.8163255
Barazan D		420	0.09	13.08239343	0.8806905
Potassium Cloride		100	7.68	1116.364239	75.152256
Sodium Chloride		1000000	0	0	0
GEM GP		188	0.03	4.36079781	0.2935635
Clayseal Plus		562.3	0	0	0
Clayseal Plus-2		0.45	1.66	241.2974788	16.243847
Clay Grabber		9.8	0.35	50.87597445	3.4249075
Clay Grabber-2		1.31	0.44	63.95836788	4.305598
Clay Sync II		1160	0.02	2.90719854	0.195709
Bore HIB		146	0	0	0
Dextrid E		1000	0.09	13.08239343	0.8806905
PAC L		87.26	0.75	109.0199453	7.3390875
Cuttings		100000	0	0	0
Barite-Bariumsulfat		115	82.59	12005.27637	808.1803155
Barite-Silica		440	0.92	133.7311328	9.002614
Baracarb 150		115	2.49	361.9462182	24.3657705
Baracarb 50		115	2.49	361.9462182	24.3657705

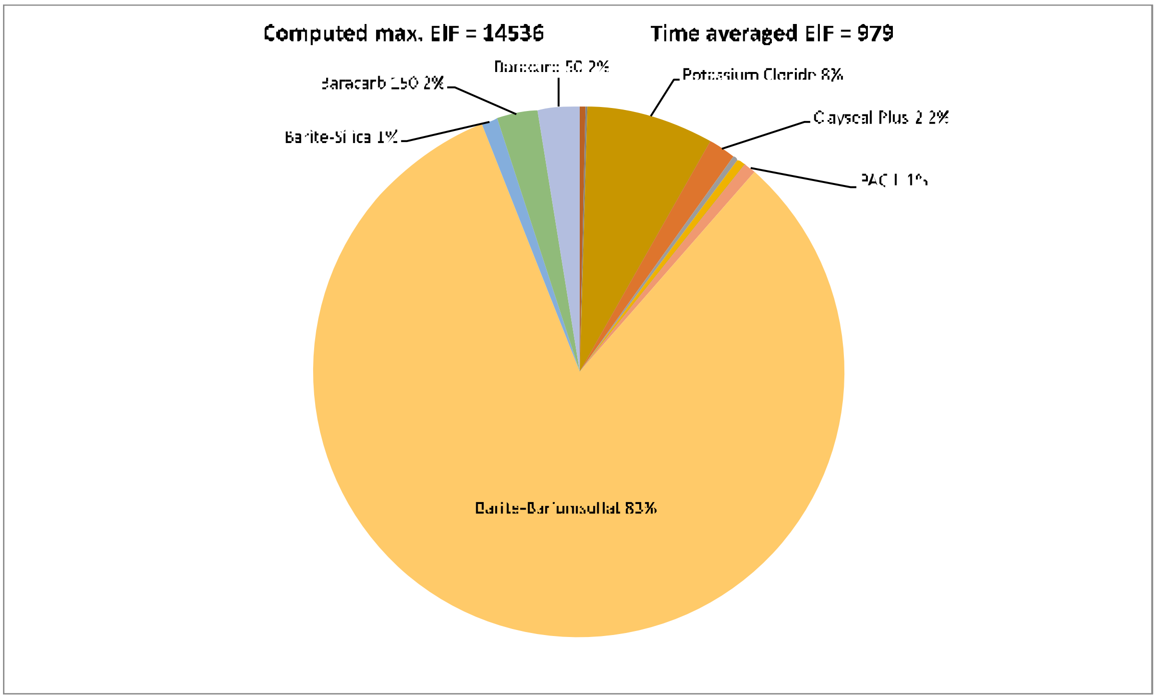

The results show that for the upper water column, effects caused by discharges of particle matter (essentially Barium sulfate 83%) are dominating the risk in the affected water volume. During the time of maximum EIF, the discharge is released from the rig 10 meters below sea-surface and sinks in the water-column.

Figure 9.37 shows the time development for the EIF in water-column. It shows that the duration with environmental risk disappears shortly after discharge.

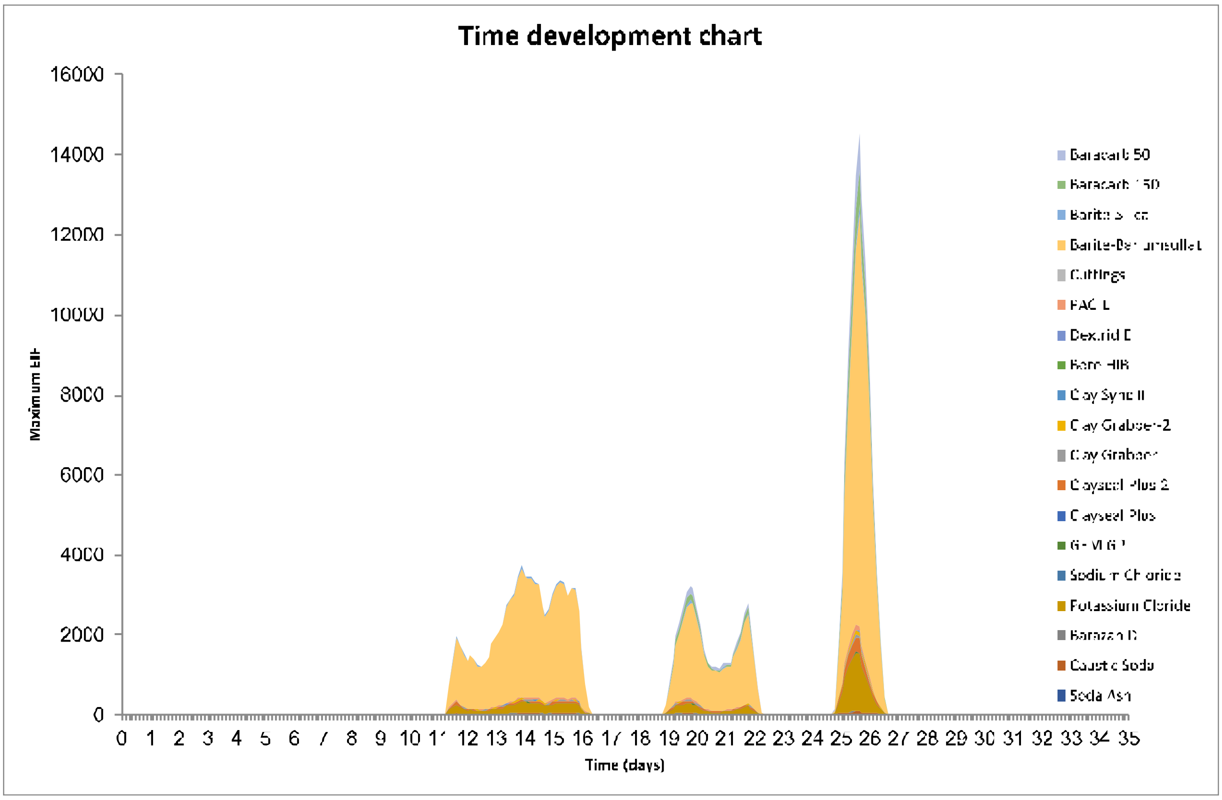

Figure 9.37 Time development of the EIF for the upper water column, for discharge location 5 Spring.

Figure 9.38 shows the time instant with maximum EIF for the upper water column due to discharges from rig 10 m below sea surface, while Figure 9.40 shows the maximum cumulative risk (foot-print) throughout the upper water column at any time during the drilling operation with discharges from the rig.

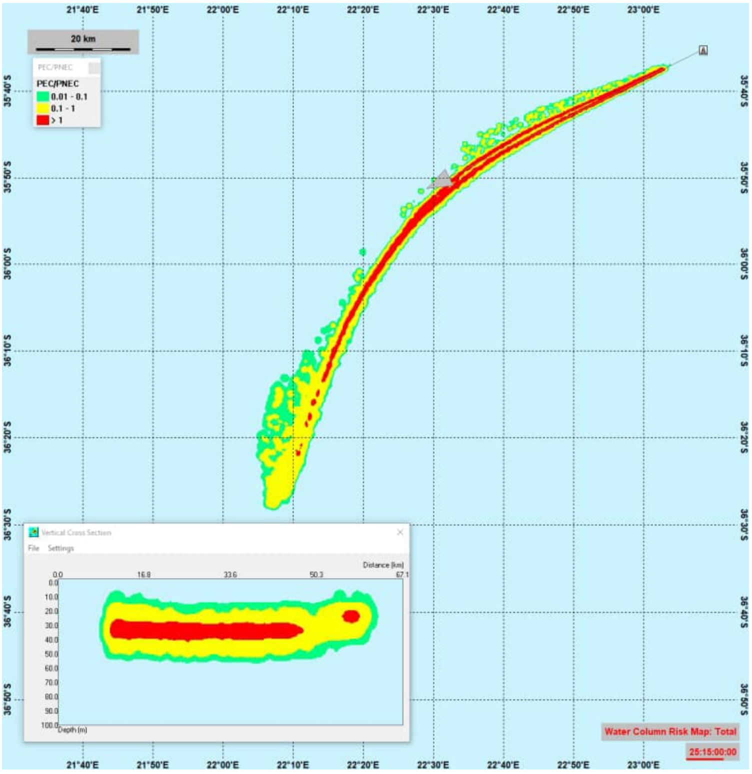

Figure 9.38 Snapshot showing the time instant with maximum EIF for the upper water column between 0-100 meters. Snapshot from 25.5 days after start, when the discharge is released from the rig. The vertical cross section shows the PEC/PNEC ratio in the water column along the grey arrow. Discharge location 5 - Spring.

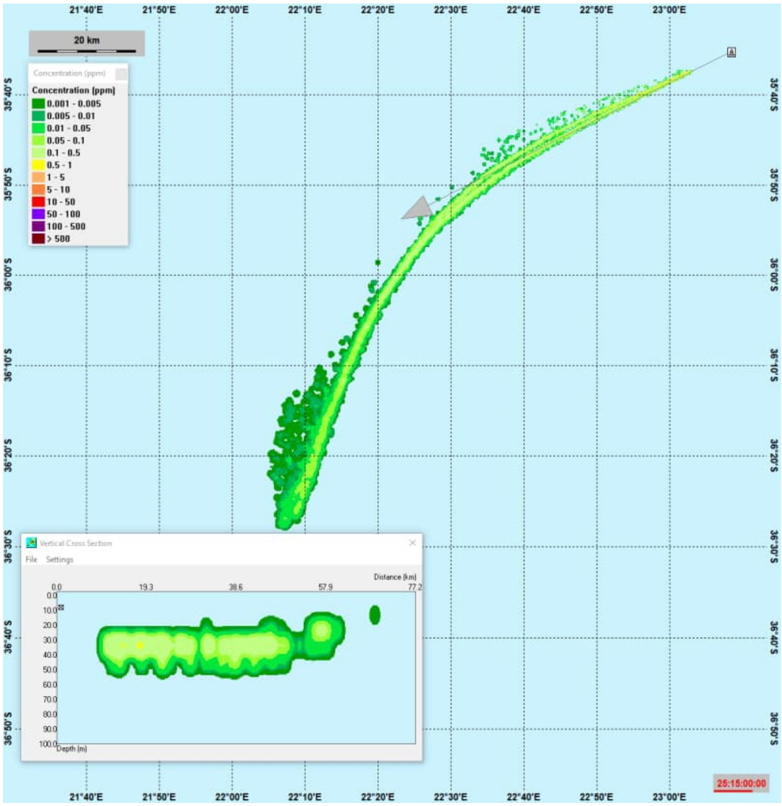

Figure 9.39 Concentration field for the component that gave the largest contribution to the environmental risk, namely the particle group Barium sulfate, at the same time-step as for maximum EIF. Discharge location 5 - Spring.

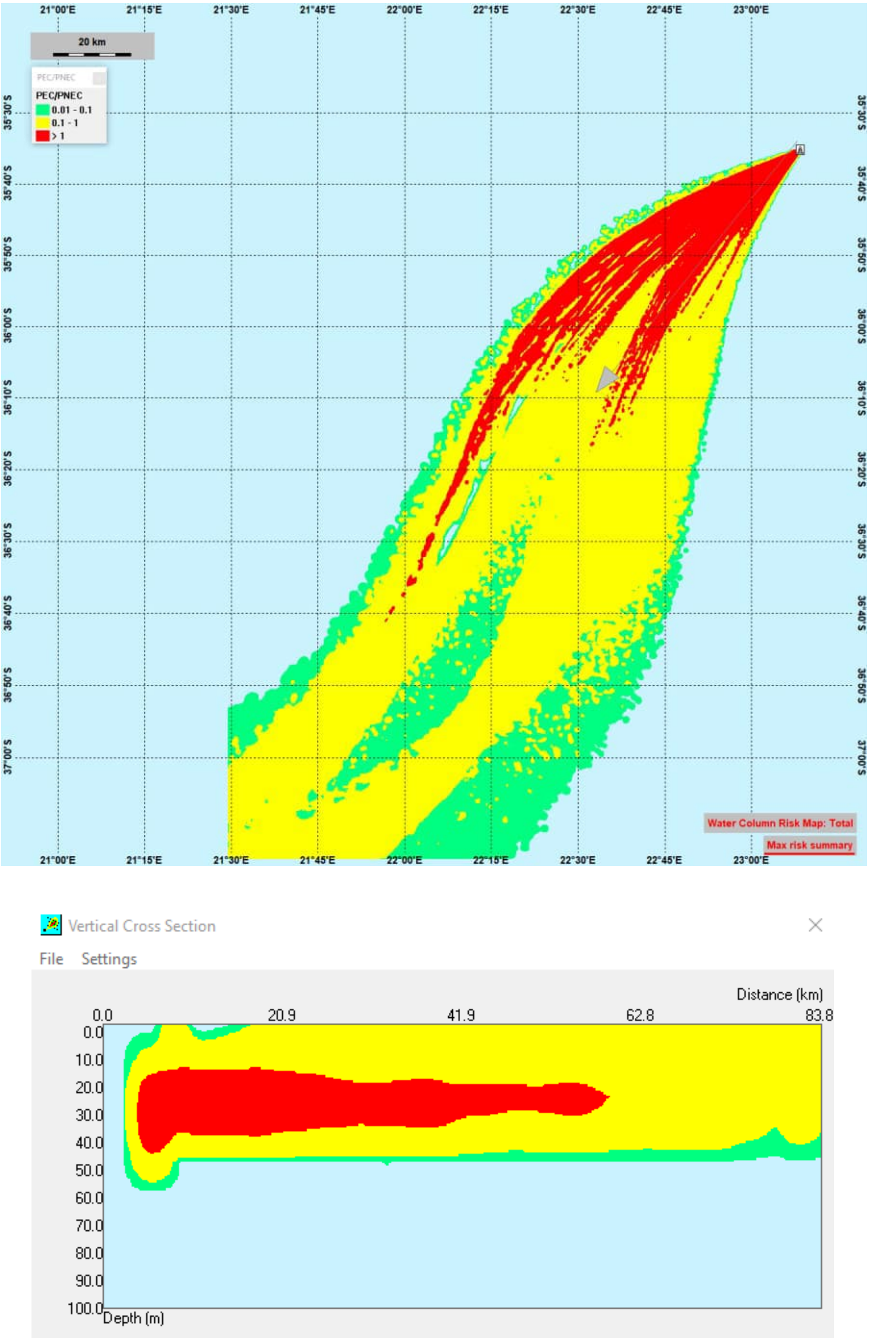

Figure 9.40 Maximum cumulative risk of drilling operations throughout the upper water column at any time for discharge location 5 (Start time October 15), discharge from rig 10 m below sea surface. Discharge location 5 – Winter.

9.4.3 Discharge location 5 - EIF results for the sediment – Spring

The maximum EIF (sea floor area 100x100 m^2) is computed with 0 impact for discharge from the rig, and 0.75 impacted by the top hole discharge. The contributions of the components of the discharge are listed in the table below (risk in % of EIF). The affected area on the sea floor is largest at the end of the transport and fate simulation, shortly after the sediment module starts. After that the sea floor will starts restoration and the area (EIF) decreases. The factor affecting risk for the rig discharge is only grain size as for discharge location 4, Summer.

Table 9.13 Table and pie-chart shows contributions to EIF from the components discharged from the top hole sections to the sediment for location 5 – Spring.

Simulated instantaneous EIF:	**0.75**				
Components	Product	PNEC ppb	Contribution to risk %	Contribution max EIF	Contribution time averaged EIF
Total					
Barazan D		420	0	0	0
Soda Ash		200	0	0	0
Caustic Soda		20	0	0	0
Potassium Cloride		100	0	0	0
Starcide		49	0	0	0
Thickness		0	63.64	0.4773	0.4773
Oxygen		0	0	0	0
Grain size		0	36.36	0.2727	0.2727

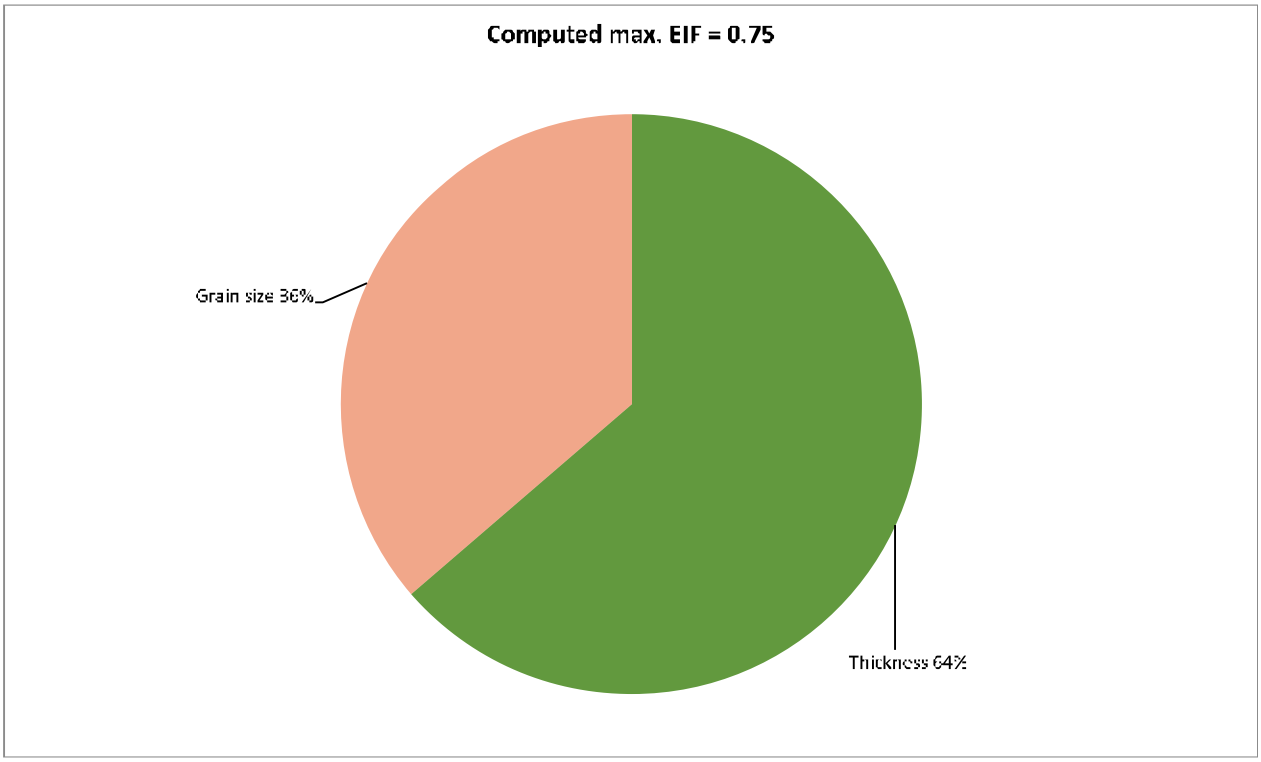

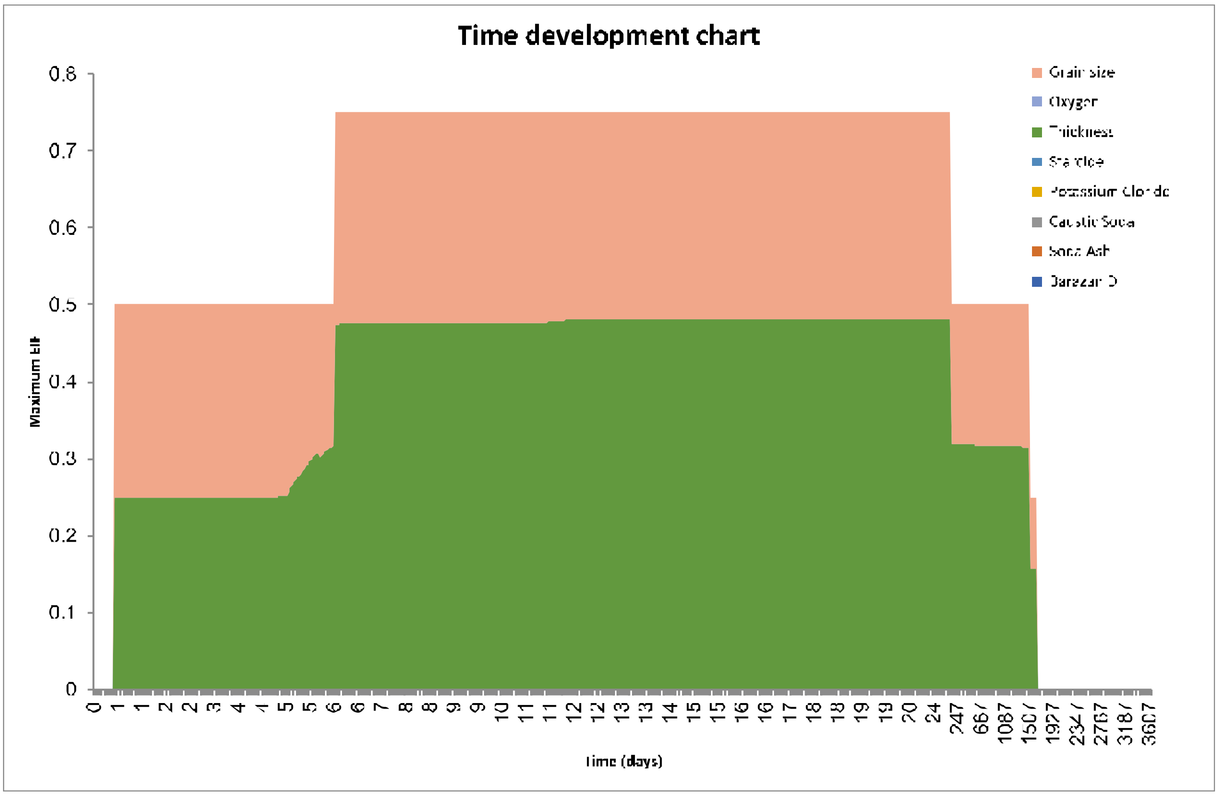

Figure 9.41 Time development of EIF for discharge from the rig for the sediment for discharge location 5 – Spring.

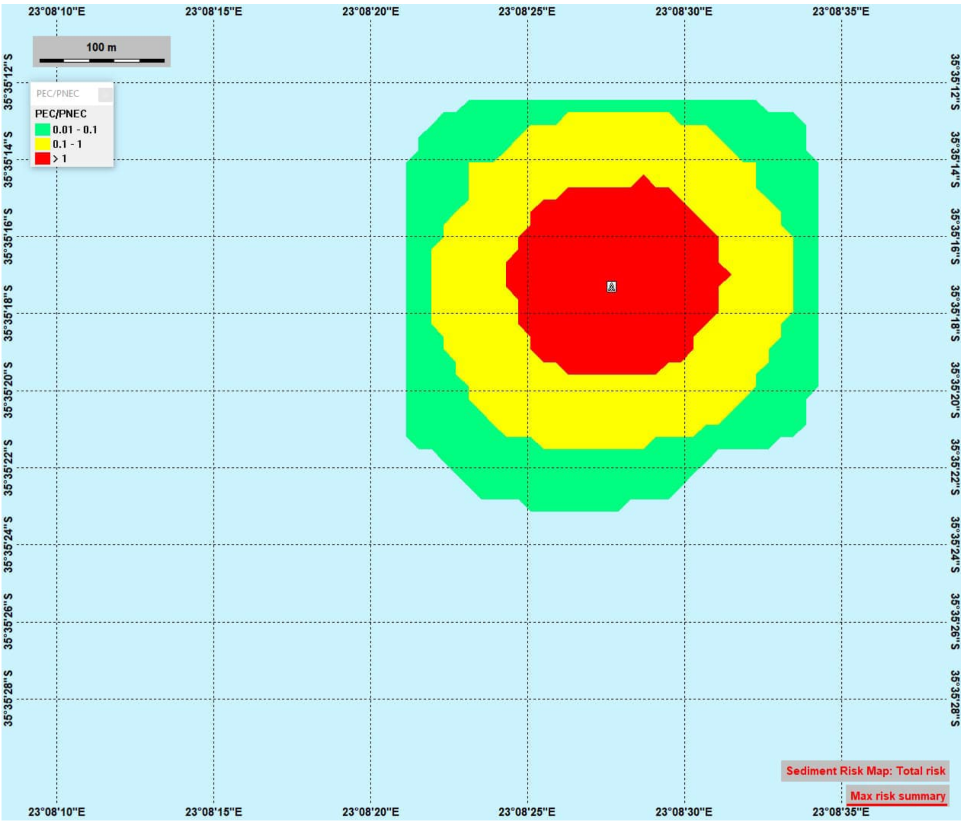

Figure 9.42 The total maximum EIF for the sediment (highest value at each location over simulation period) for discharge location 5 – Spring.

9.5 Risk results in the water column for location 5

The EIF results are a reference water volume and sea floor area, respectively, where the risk for an environmental effect is larger than 5%. The actual risk is computed by the PNEC and risk curves for each of the components and their combination. The figures below show this environmental risk from all components in % for the water-column at the time with maximum EIF for each section. Environmental risk below 5% (not contributing to the EIF) is colored as outline only.

9.5.1 Discharge location 5 – Summer: Risk results in the upper water column

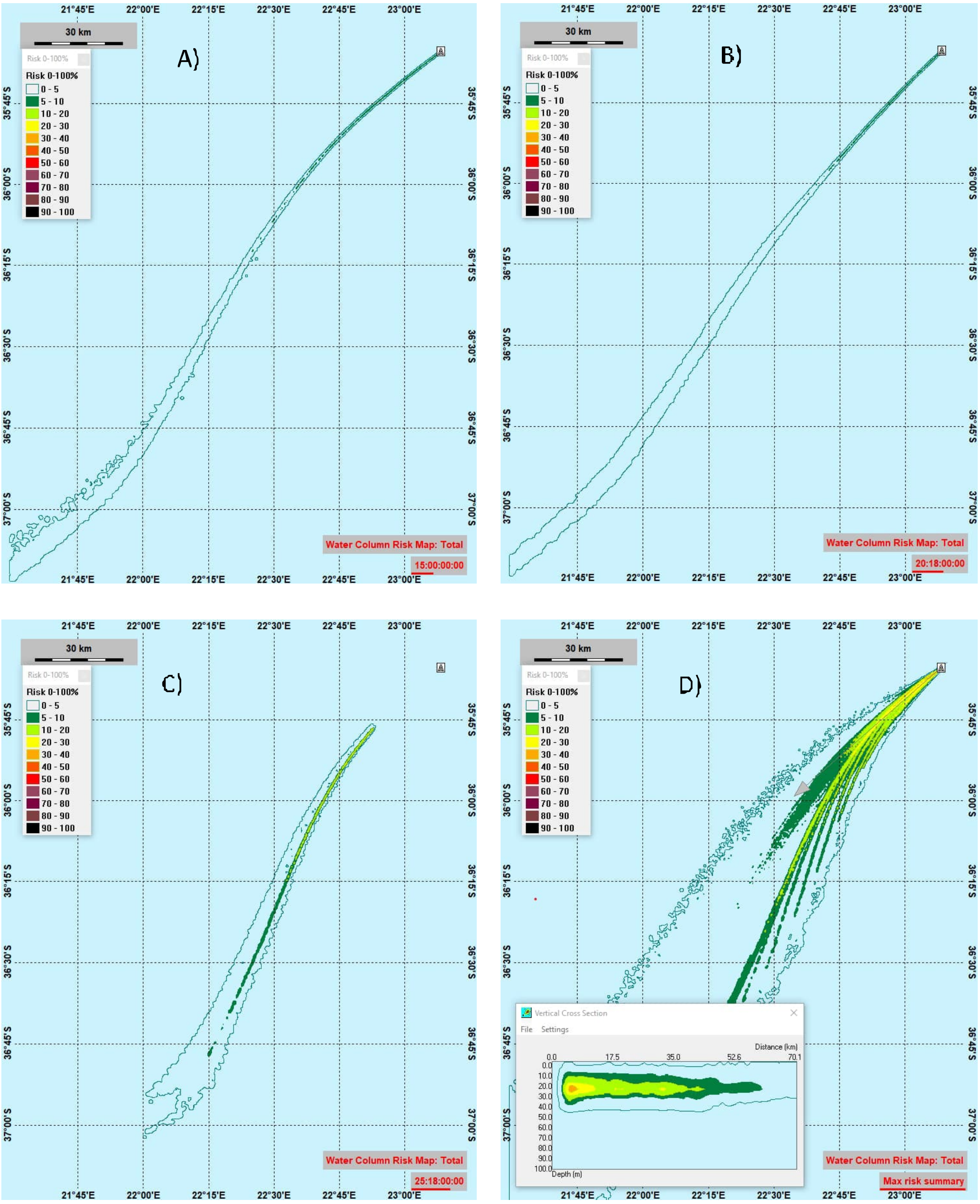

Figure 9.43 Discharge location 5 – Summer: Environmental risk > 5 % from all components for the upper water-column at the instant timestep with maximum risk for each discharge released from rig: A) Section 12 ¼" Cuttings + HPWBM, B) Section 8.5" Cuttings + HPWBM, C) Section 8.5 HPWBM, D) The total maximum risk summary for the upper water-column (highest value at each location over the whole simulation period).

9.5.2 Discharge location 5 – Summer: Risk results in the lower water column

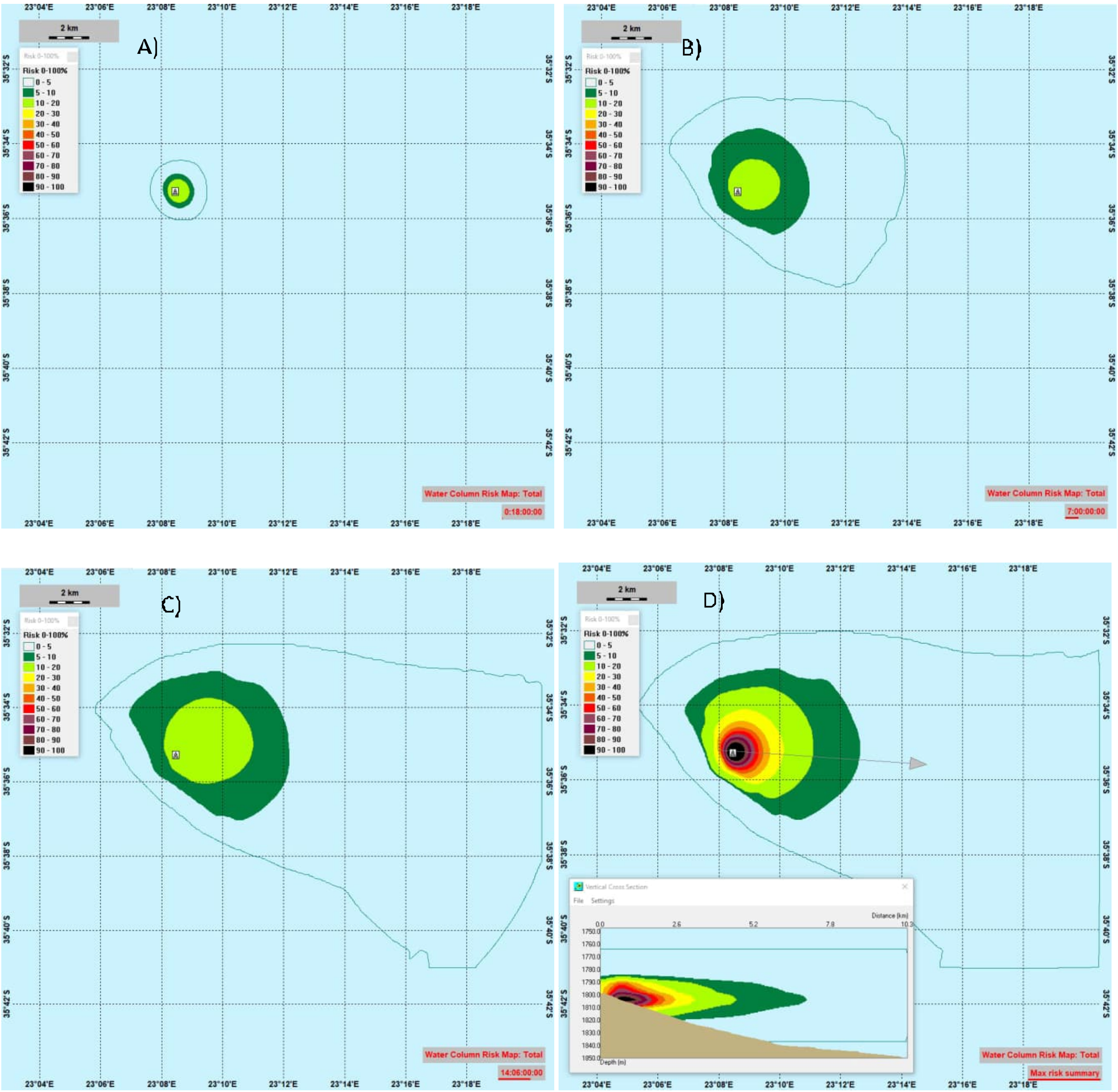

Figure 9.44 Discharge location 5 – Summer: Environmental risk > 5 % from all components for the lower water-column (1750 – 1850 meter) at the instant timestep with maximum risk for the discharges released at the sea floor: A) After Section 42", B) After Section 26". Figure C) Section 26" displacement. D) shows the total maximum risk summary for the lower water-column (highest value at each location over the whole simulation period).

9.5.3 Discharge location 5 – Autumn: Risk results in the upper water column

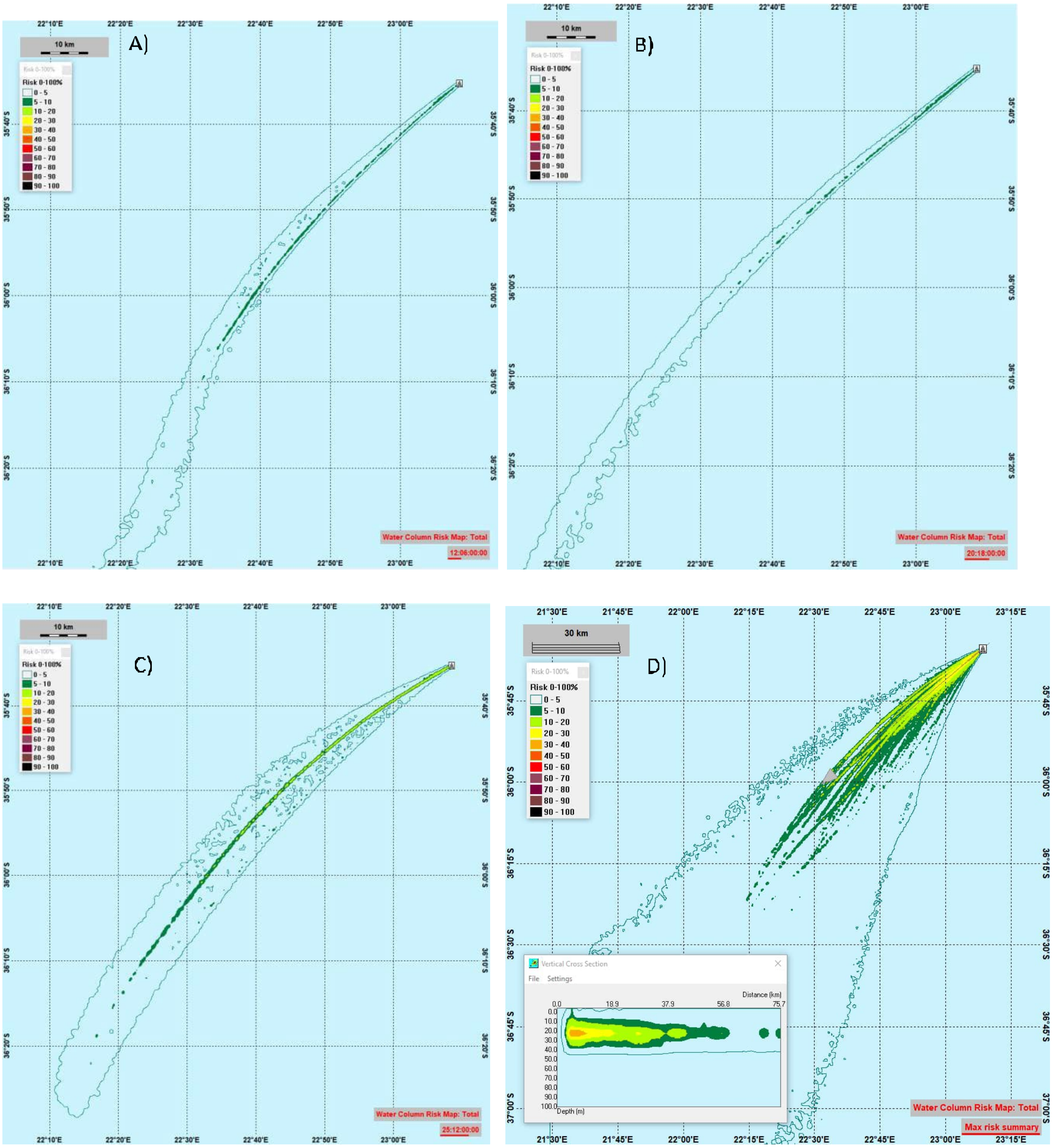

Figure 9.45 Discharge location 5 – Autumn: Environmental risk > 5 % from all components for the upper water-column at the timestep with maximum risk for the discharges released from rig: A) Section 12 ¼" Cuttings + HPWBM, B) Section 8.5" Cuttings + HPWBM, C) Section 8.5 HPWBM, D) The total maximum risk summary for the upper water-column (highest value at each location over the whole simulation period).

9.5.4 Discharge location 5 – Autumn: Risk results in the lower water column

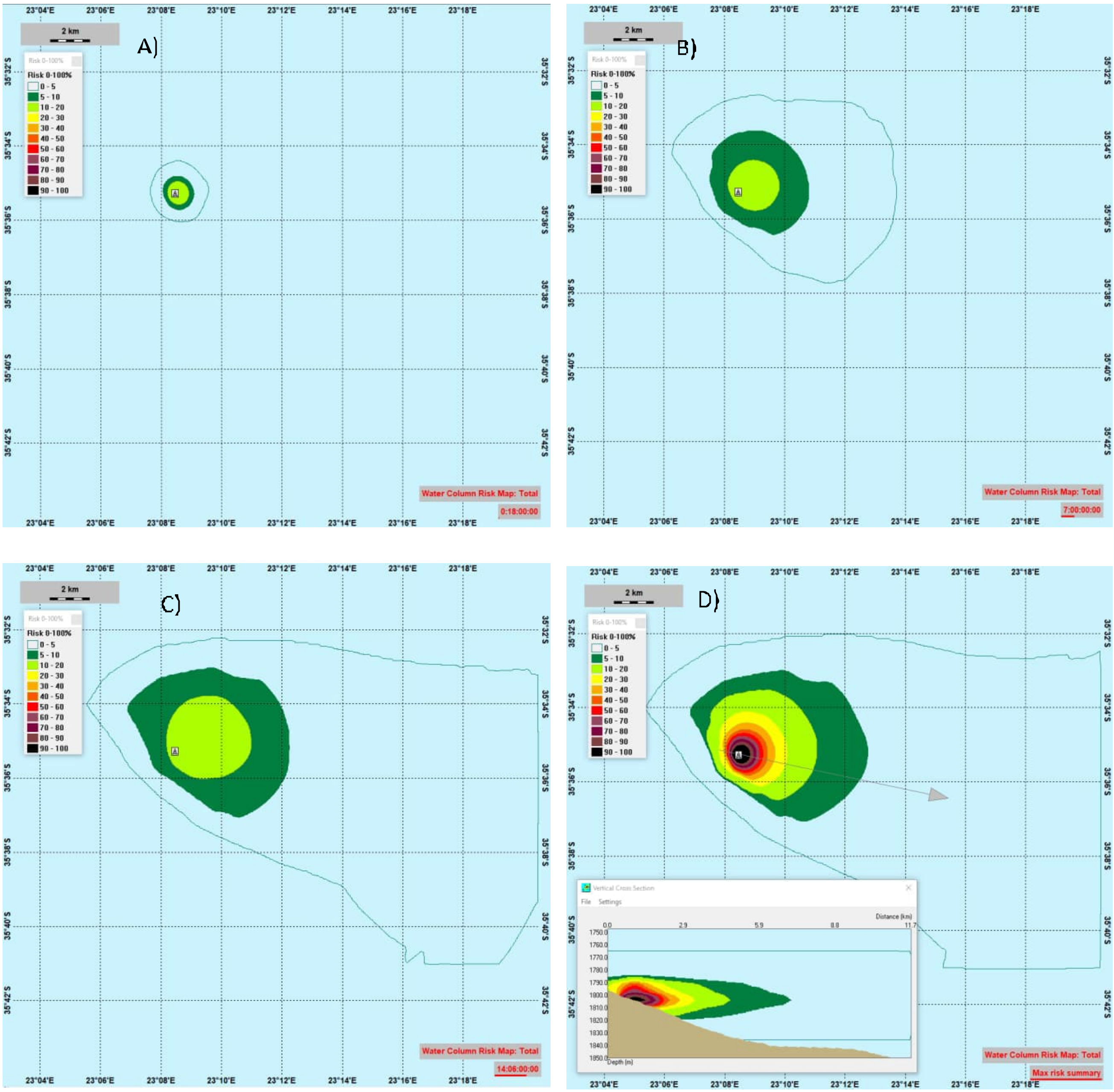

Figure 9.46 Discharge location 5 – Autumn: Environmental risk > 5 % from all components for the lower water-column (1750 – 1850 meter) at the instant timestep with maximum risk for the discharges released at the sea floor: A) After Section 42", B) After Section 26". Figure C) Section 26" displacement. D) shows the total maximum risk summary for the lower water-column (highest value at each location over the whole simulation period).

9.5.5 Discharge location 5 – Winter: Risk results in the upper water column

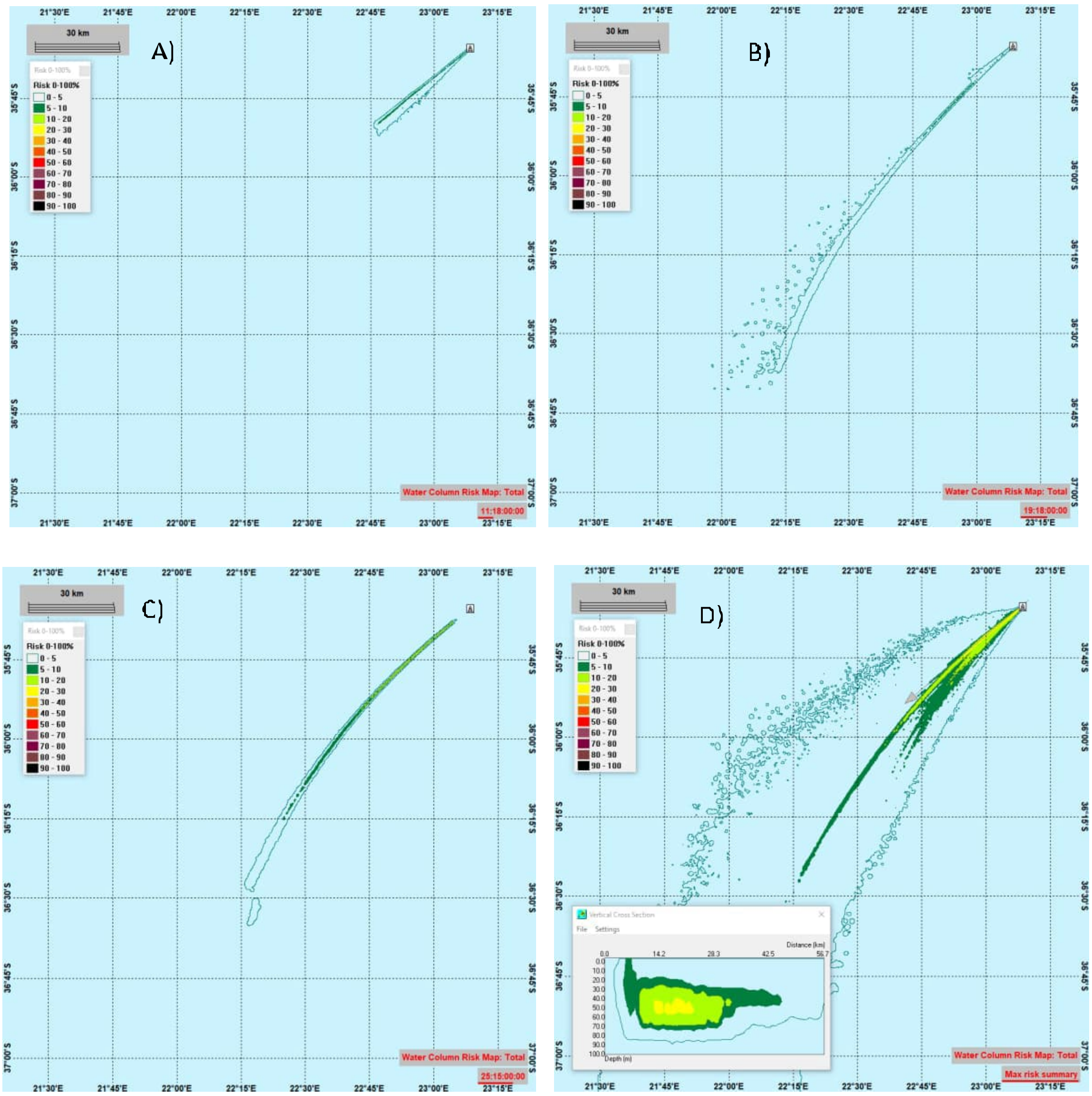

Figure 9.47 Discharge location 5 – Winter: Environmental risk > 5 % from all components for the upper water-column at the timestep with maximum risk for the discharges released from rig: A) Section 12 ¼" Cuttings + HPWBM, B) Section 8.5" Cuttings + HPWBM, C) Section 8.5 batch HPWBM , D) The total maximum risk summary for the upper water-column (highest value at each location over the whole simulation period).

9.5.6 Discharge location 5 – Winter: Risk results in the lower water column

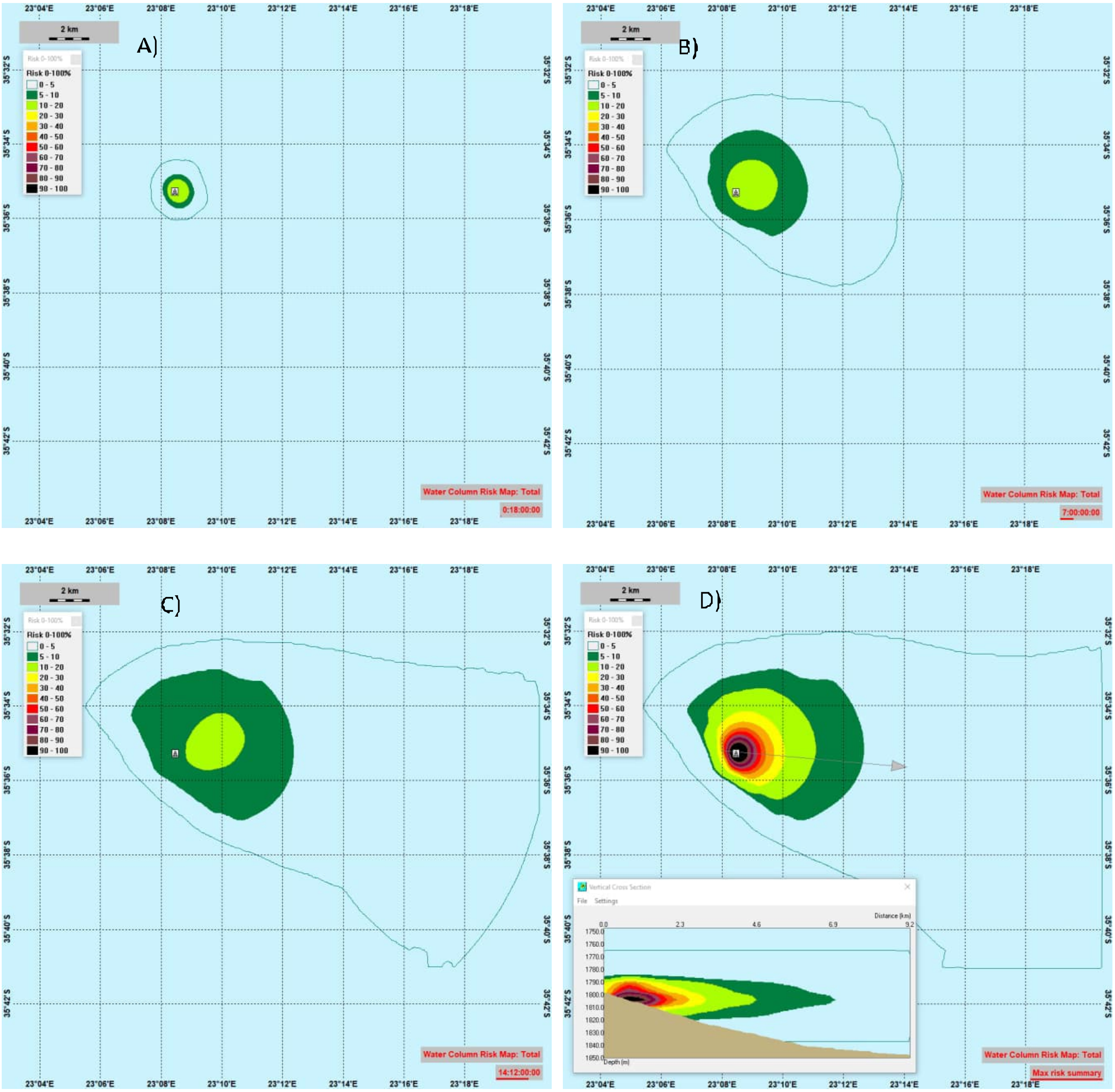

Figure 9.48 Discharge location 5 – Winter: Environmental risk > 5 % from all components for the lower water-column (1750 – 1850 meter) at the instant timestep with maximum risk for the discharges released at the sea floor: A) After Section 42", B) After Section 26". Figure C) Section 26" displacement. D) shows the total maximum risk summary for the lower water-column (highest value at each location over the whole simulation period).

9.5.7 Discharge location 5 – Spring: Risk results in the upper water column

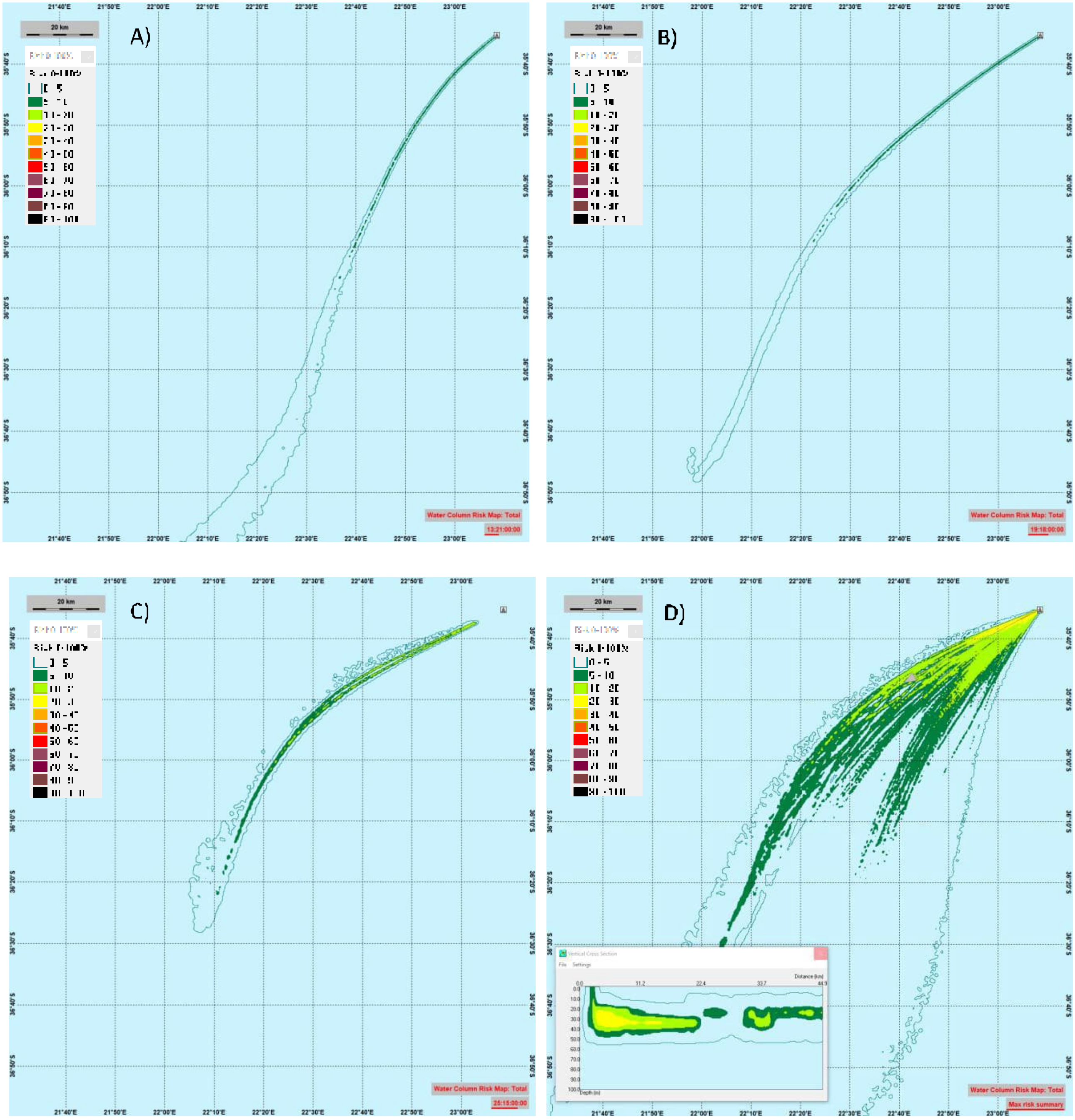

Figure 9.49 Discharge location 5 – Spring: Environmental risk > 5 % from all components for the upper water-column at the timestep with maximum risk for the discharges released from rig: A) Section 12 ¼" Cuttings + HPWBM, B) Section 8.5" Cuttings + HPWBM, C) Section 8.5 batch HPWBM , D) The total maximum risk summary for the upper water-column (highest value at each location over the whole simulation period).

9.5.8 Discharge location 5 – Spring: Risk results in the lower water column

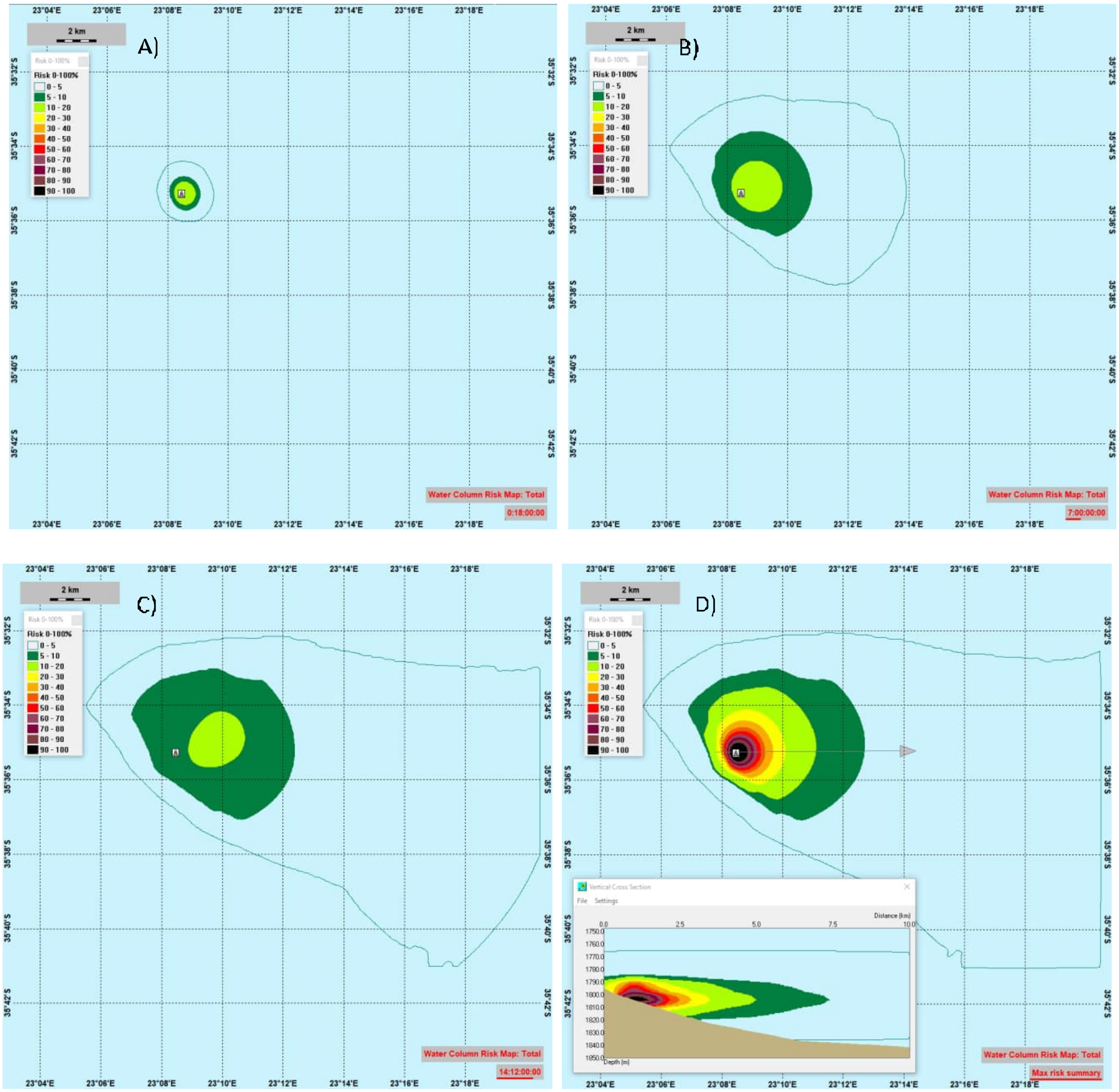

Figure 9.50 Discharge location 5 – Spring: Environmental risk > 5 % from all components for the lower water-column (1750 – 1850 meter) at the instant timestep with maximum risk for the discharges released at the sea floor: A) After Section 42", B) After Section 26". Figure C) Section 26" displacement. D) shows the total maximum risk summary for the lower water-column (highest value at each location over the whole simulation period.

9.6 Risk in the sediment for location 5

The environmental risk on the sea floor and in the sediment is presented as spatial distribution on a map and snapshots in time. The color scale is environmental risk in percent as the combination of all 4 stressors: toxicity, oxygen depletion, burial, and grain size change. Environmental risk below 5% (not contributing to the EIF) is indicated with an outline. The figures show the risk situation on day 11 the end of all discharges on the seafloor, after 2 years and after 4 years. Simulations show no risk in the sediment after 4 years. We note that changes to the sediment due to resuspension and transport by currents is not part of the simulation.

9.6.1 Discharge location 5 – Risk in sediment

Summer :

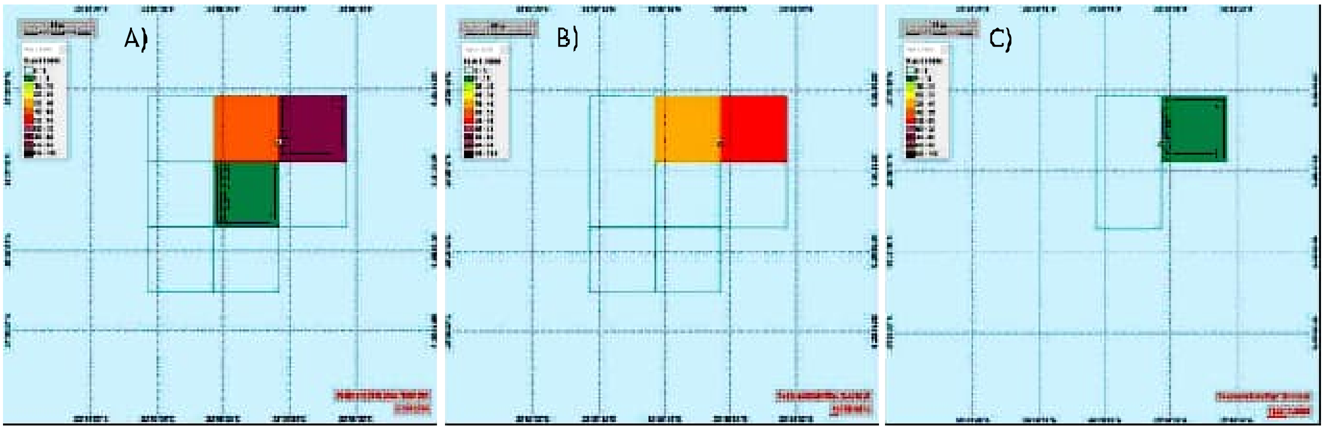

Autumn:

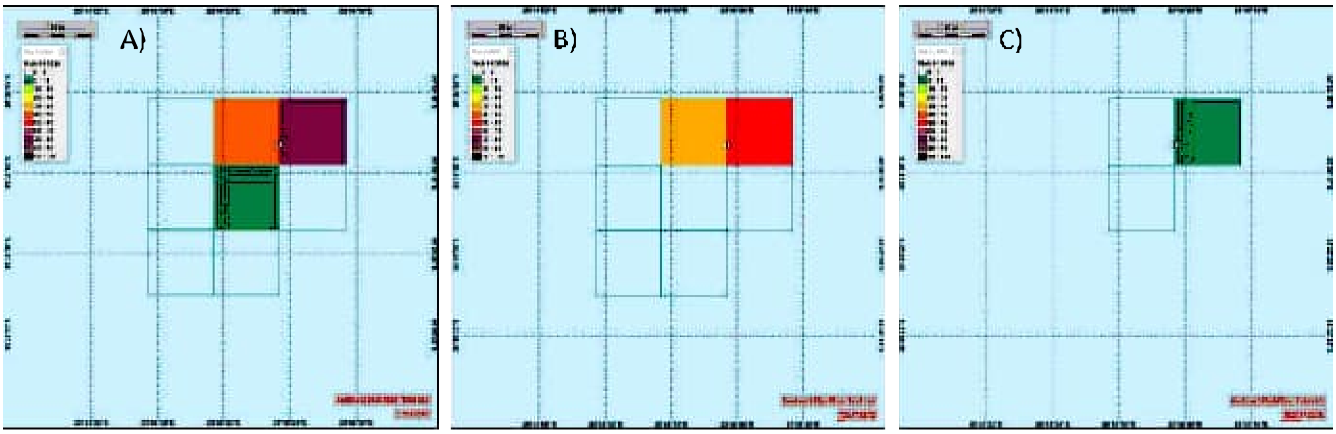

Winter:

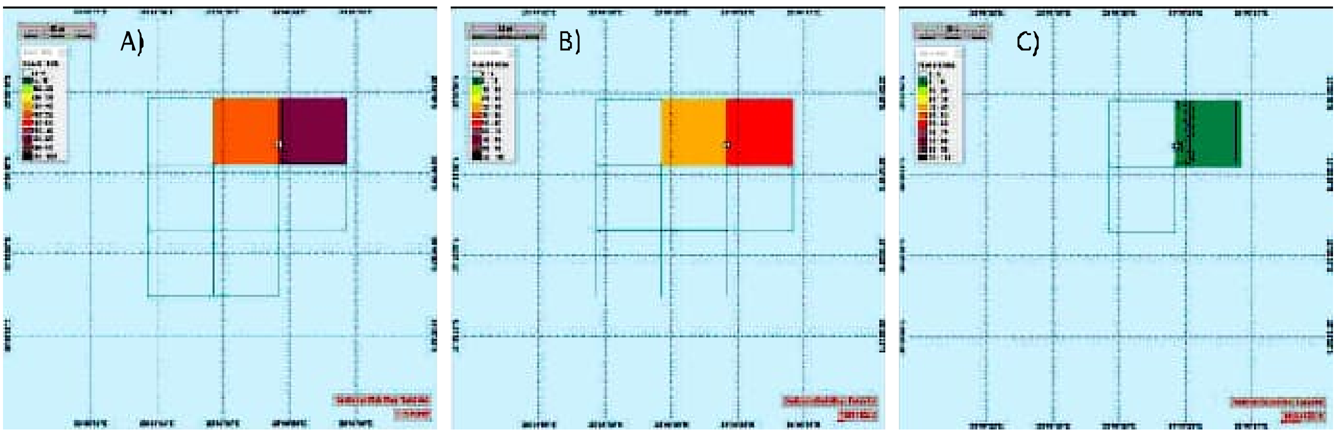

Spring:

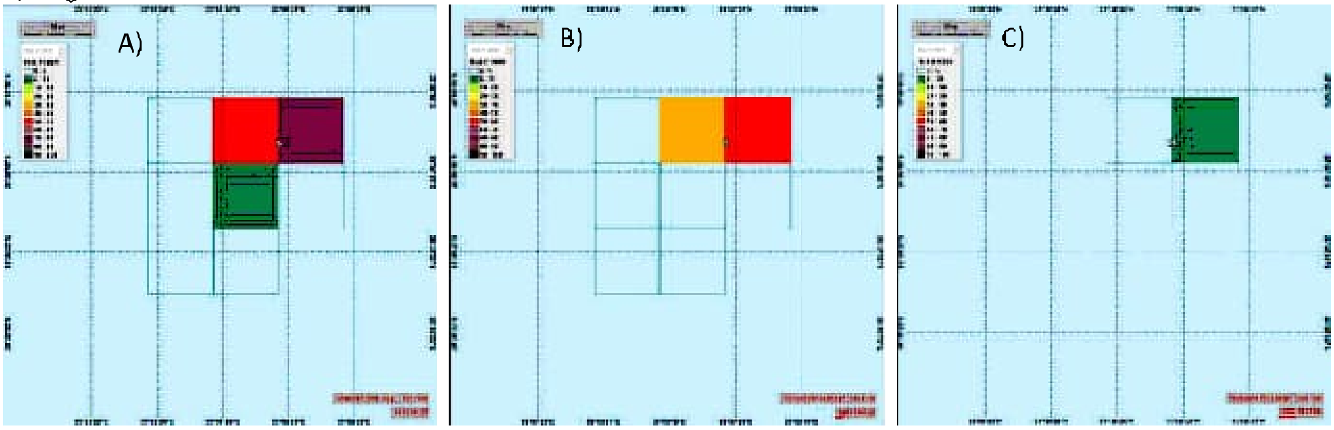

Figure 9.51 Risk as percent in the sediment A) Day 11, B) after 2 year, C) after 4 year for all four seasons.

9.7 Deposition on the sea floor for location 5

All chemicals in the discharge with a $logP_{OW} > 3$ will attach to the particulate material in the model and eventually end up at the sea floor. This also changes the particle size distribution of the discharged matter as particles agglomerate to bigger particles which affects the transport (sinking velocity) and eventually the footprint of the discharge on the seafloor. Figure 9.52- Figure 9.59 shows deposition on the seafloor for all particulate matter (cuttings, barite and bentonite) and any associated contaminants. The deposition is mainly caused by the cuttings particles discharged from the top hole sections on the sea floor. Discharges released from the rig gives only negligible footprint on the seafloor < 1 mm for all four seasons. The particles follow the currents and are widely dispersed higher in the water column and spreads over a larger area.

9.7.1 Discharge location 5 – Summer: Deposition on the seafloor

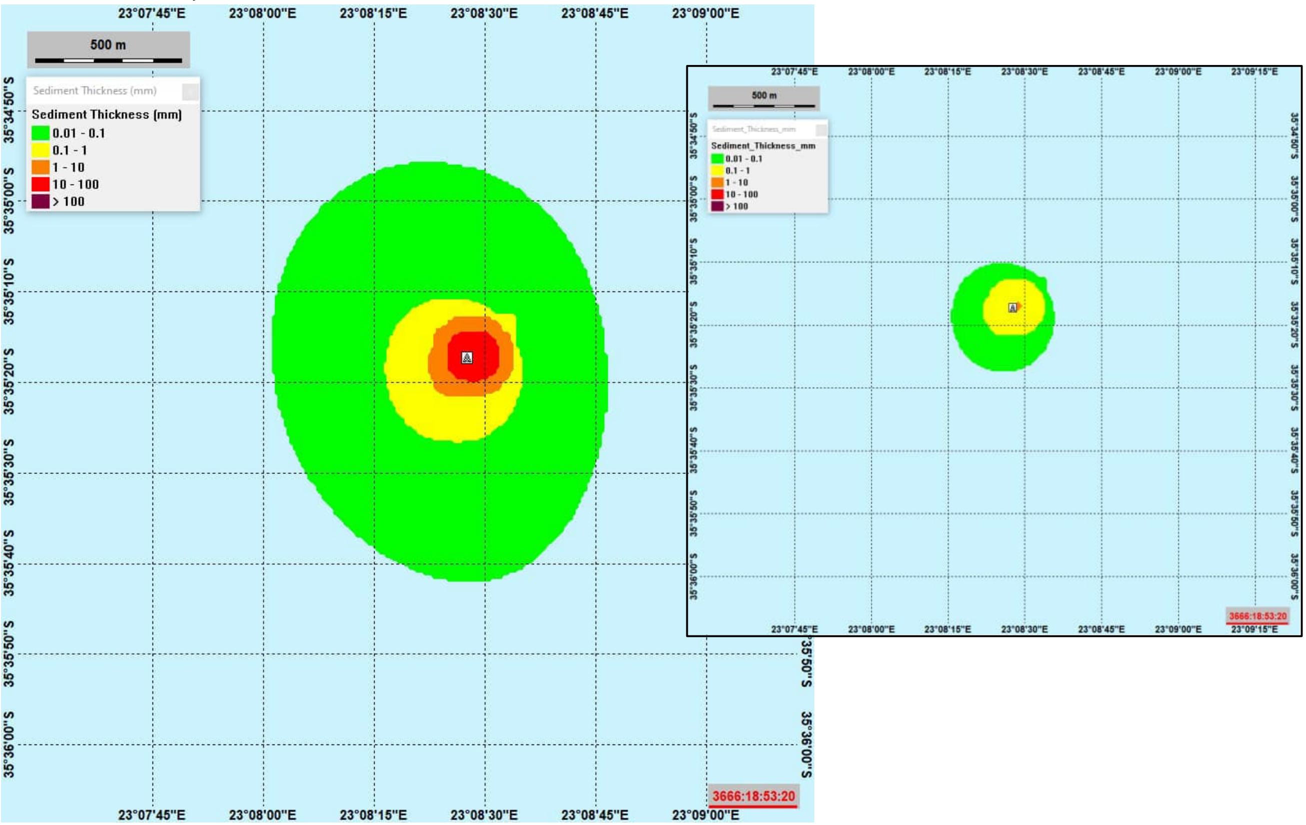

Figure 9.52 Discharge location 5 – Summer: Deposition of the total of particle matter on the sea floor (mm) (smoothed results) for discharge from the top hole sections. The inserted figure to the upper right shows deposition of barite and bentonite only. (Smoothing of gridded results leads to strange straight lines north and east of the figure).

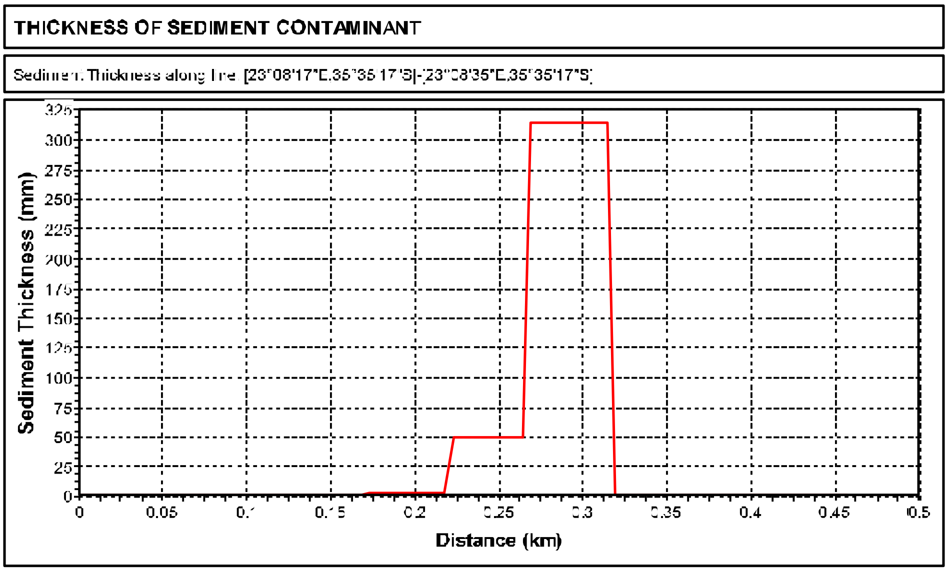

Figure 9.53 Discharge location 5 – Summer: Sediment thickness (mm) of total deposited matter on the sea floor (unsmoothed) through the release point from W towards E (release point 0.3 km on the scale). Grid cell size 50 x 50 meters.

9.7.2 Discharge location 5 – Autumn: Deposition on the seafloor

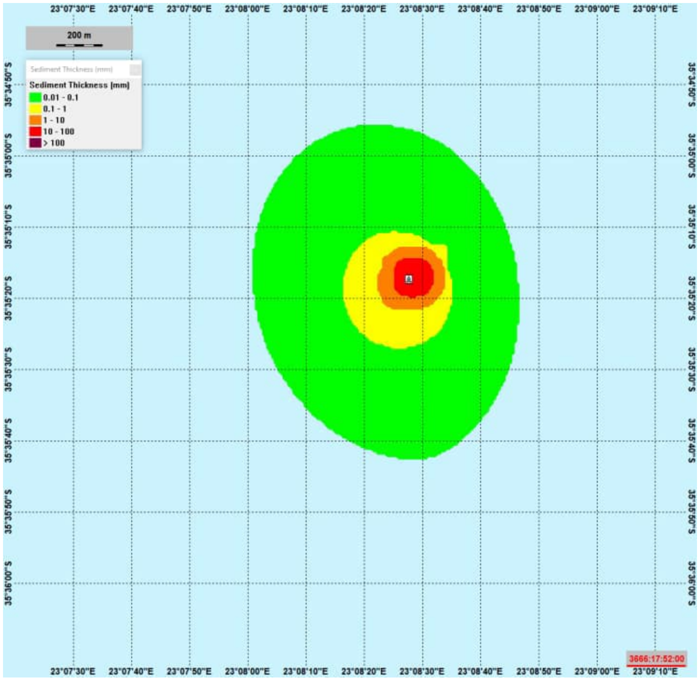

Figure 9.54 Discharge location 5 – Autumn: Deposition of particle matter on the sea floor (mm) (smoothed results) for discharge from the top hole sections.

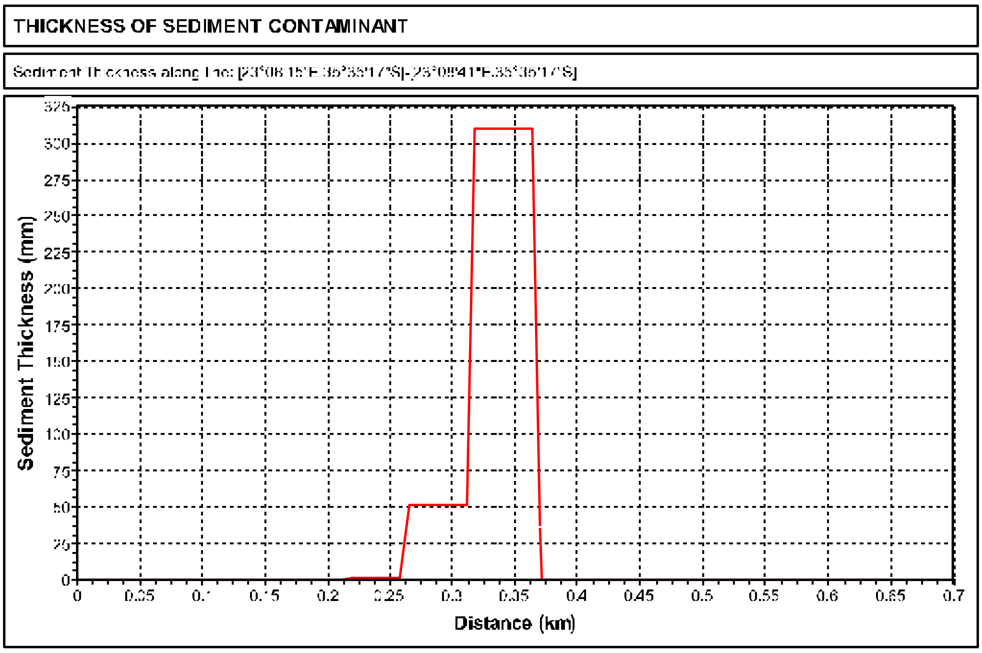

Figure 9.55 Discharge location 5 – Autumn: Sediment thickness (mm) of deposited matter on the sea floor (unsmoothed) through the release point from W towards E (release point 0.3 km on the scale). Grid cell size 50 x 50 meters.

9.7.3 Discharge location 5 – Winter: Deposition on the seafloor

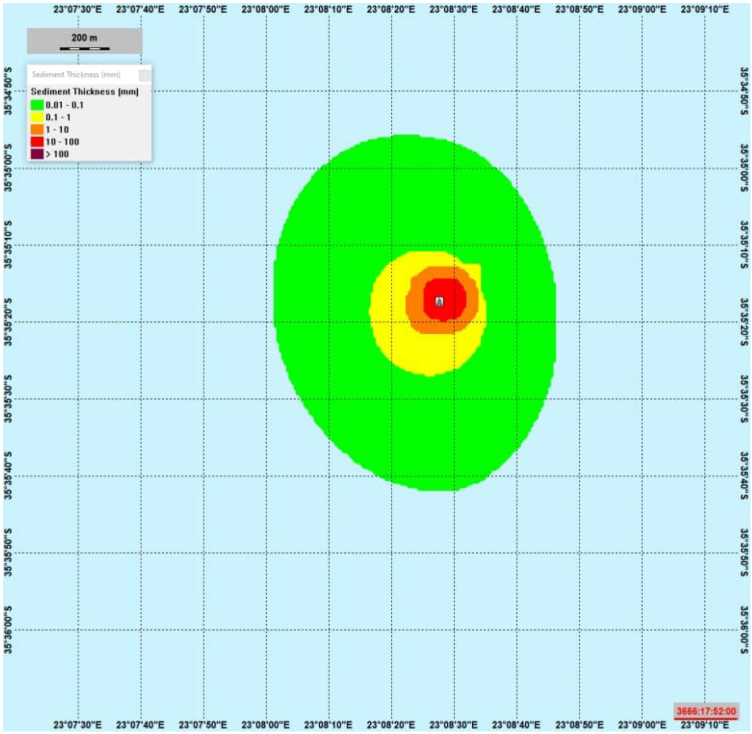

Figure 9.56 Discharge location 5 – Winter: Deposition of particle matter on the sea floor (mm) (smoothed results) for the discharge from the top hole sections.

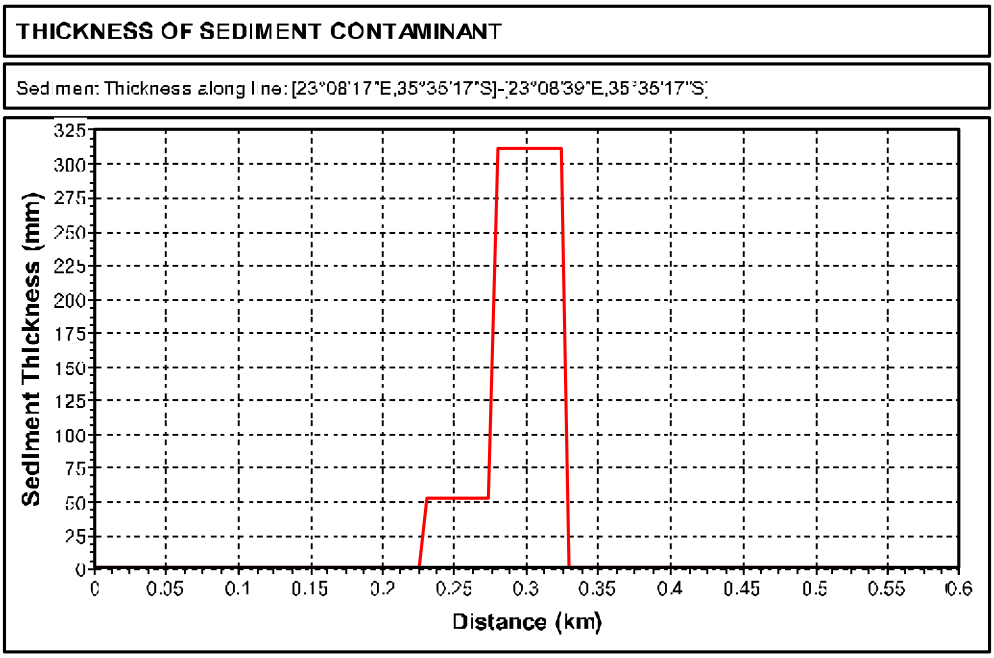

Figure 9.57 Discharge location 5 – Winter: Sediment thickness (mm)of deposited matter on the sea floor (unsmoothed) through the release point from W towards E (release point 0.3 km on the scale). Grid cell size 50 x 50 meters.

9.7.4 Discharge location 5 – Spring: Deposition on the seafloor

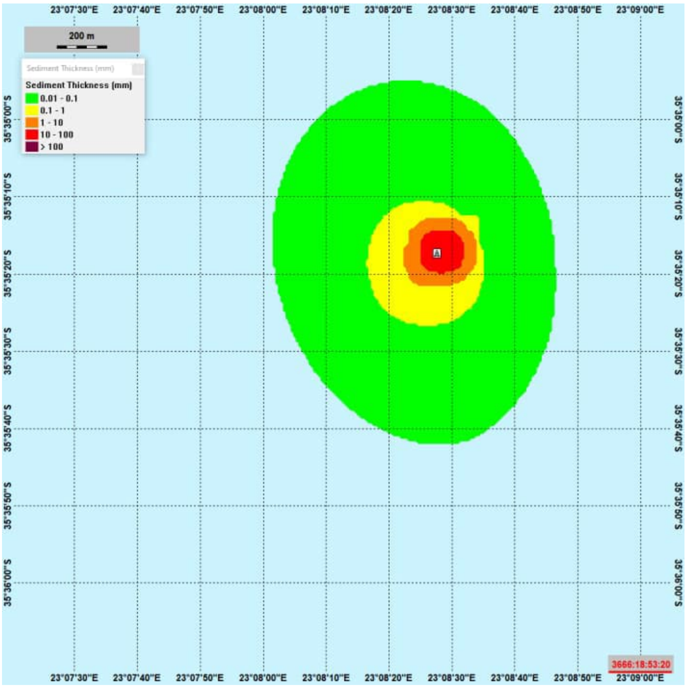

Figure 9.58 Discharge location 5 – Spring: Deposition of particle matter on the sea floor (mm) (smoothed results) for the discharge from the top hole sections.

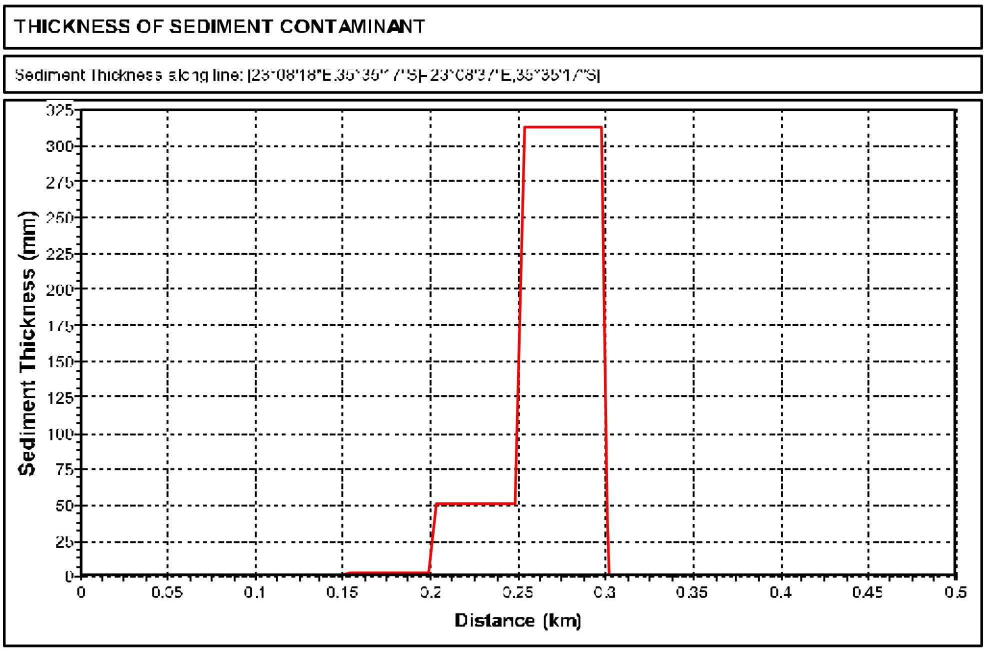

Figure 9.59 Discharge location 5 – Spring: Sediment thickness (mm)of deposited matter on the sea floor (unsmoothed) through the release point from W towards E (release point 0.3 km on the scale). Grid cell size 50 x 50 meters.

9.8 Sediment thickness at the sea floor from cuttings (mm) for location 5

The thickness of deposited cuttings is reported as a spatial map at the end of the simulation period (10 years). At this time, bioturbation will already have reduced the maximum thickness. Thickness below 6.5 mm (the PNEC for burial) is shown as an outline. Results are shown only for cuttings, since these represent essentially all of the risk from burial.

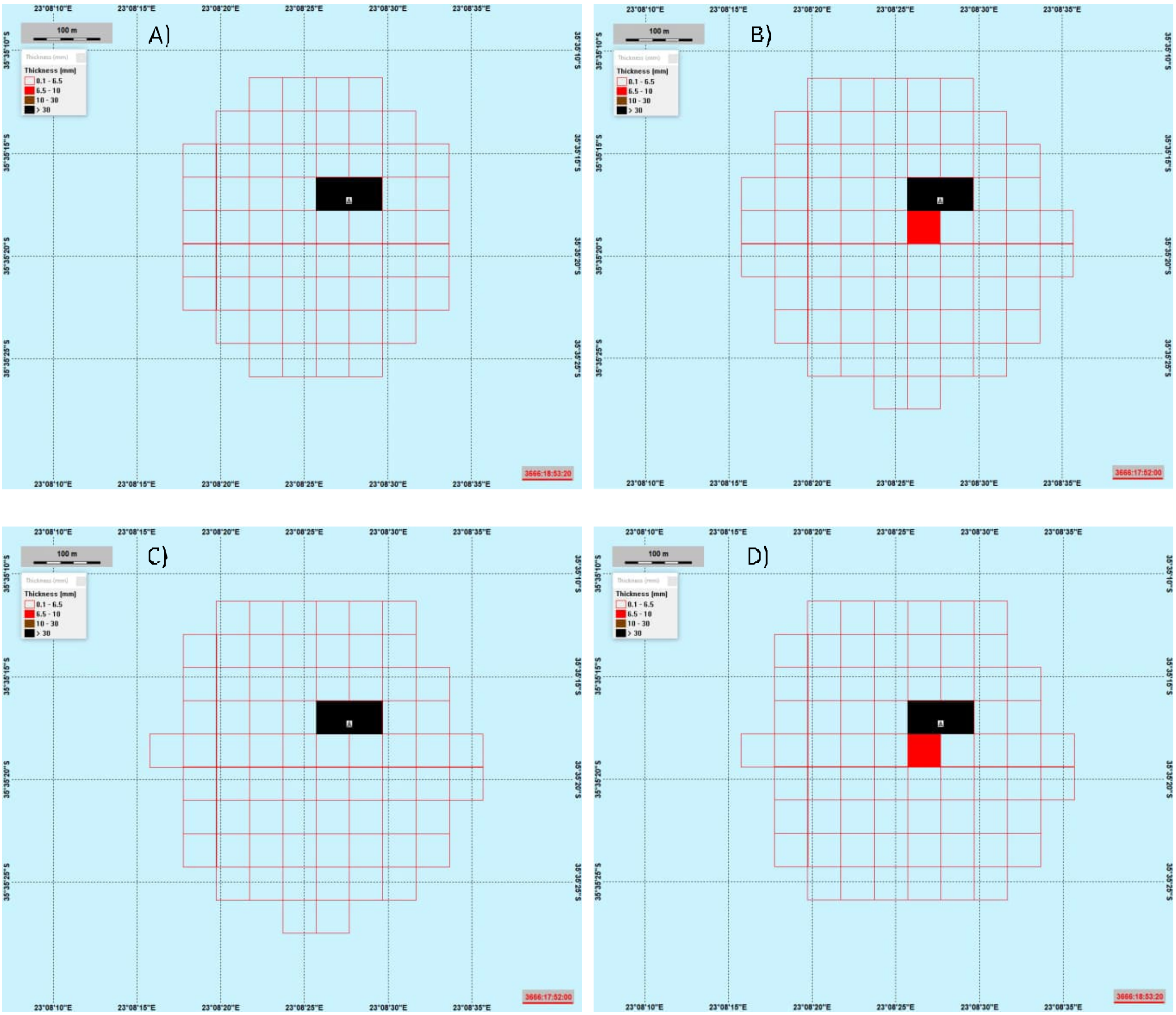

Figure 9.60 Sediment deposition at the seafloor from cuttings (thickness mm). Cell-size 50 x 50 meter, PNEC level for burial is 6.5 mm. A) Summer, B) Autumn, C) Winter, D) Spring.

9.9 Grain size change for location 5

The DREAM model calculates the stresses caused by the deposition of grains with sizes that are different from the natural grain sizes on the actual location. Therefore, the actual natural grain size on the location must be input to the sediment model. The median diameter of the natural grain size on site was assumed to be about 0.35 mm.

A change in median sediment grain size caused by deposited particle matter might result in a change of benthic communities. Exposure related to grain size change is defined as the change of the median grain size in the sediment, averaged over the upper three cm of the sediment layer (including the added sediment).

Figure 9.61 shows median grain size change in the upper sediment layer caused by cuttings discharge from the rig. The particle sizes on the seabed increase in areas closest to the rig with particle sizes of as much a **4** mm being observed approximately 4 km away from the rig.

Figure 9.61 Calculation of median grain size deposited at the sea floor after completion of the discharge from rig for discharge location 5 for all four seasons.

9.10 Oxygen change in the sediment for location 5

Environmental risk from oxygen depletion is reported as spatial distribution on a map and snapshots in time. Tones in grey show negative oxygen balances caused by biodegradation of mud chemicals. Green areas are neutral.

The figures show the risk situation at the end of discharge from the 8.5" HPWBM section discharged from rig, and after 26" displacement section discharged at the seafloor, after 3 years and at the end of the simulation period (10 years).

The PNEC for the change in oxygen content was set to 20% reduction of oxygen (in terms of mg O2/m2 sediment surface) based on NIVA Report no. 5188-2006, by considering the effect of reduced redox potential on the diversity of the benthic fauna.

The figures are very similar since the chemicals are attached to the cuttings, which are the same for all four seasons. None of the simulations gave results for oxygen change in the sediment that contributes to EIF > 1 (Risk over 5%). To give an overview of the development of oxygen change over time Figure 9.62 and Figure 9.63 are representative for all four seasons.

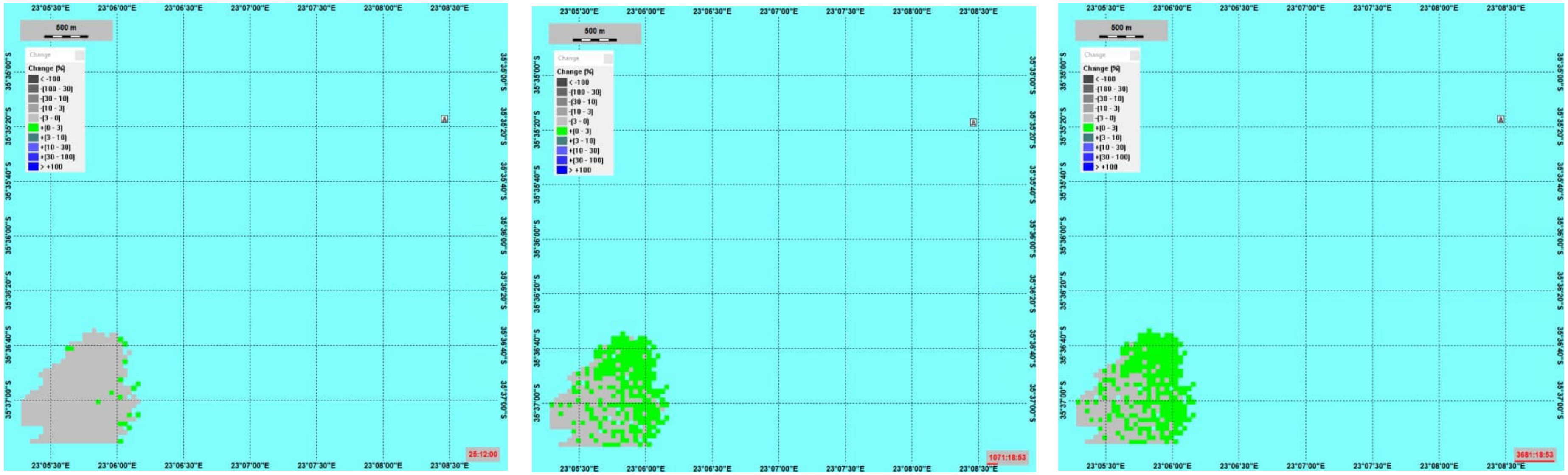

Figure 9.62 Oxygen change in the sediment layer caused by the degradation of chemicals attached to cuttings: A) timestep at the end of discharge from the 8.5" HPWBM section, B) after 3 years, C) after 10 years, for discharge location 5 discharge from rig. Summer conditions.

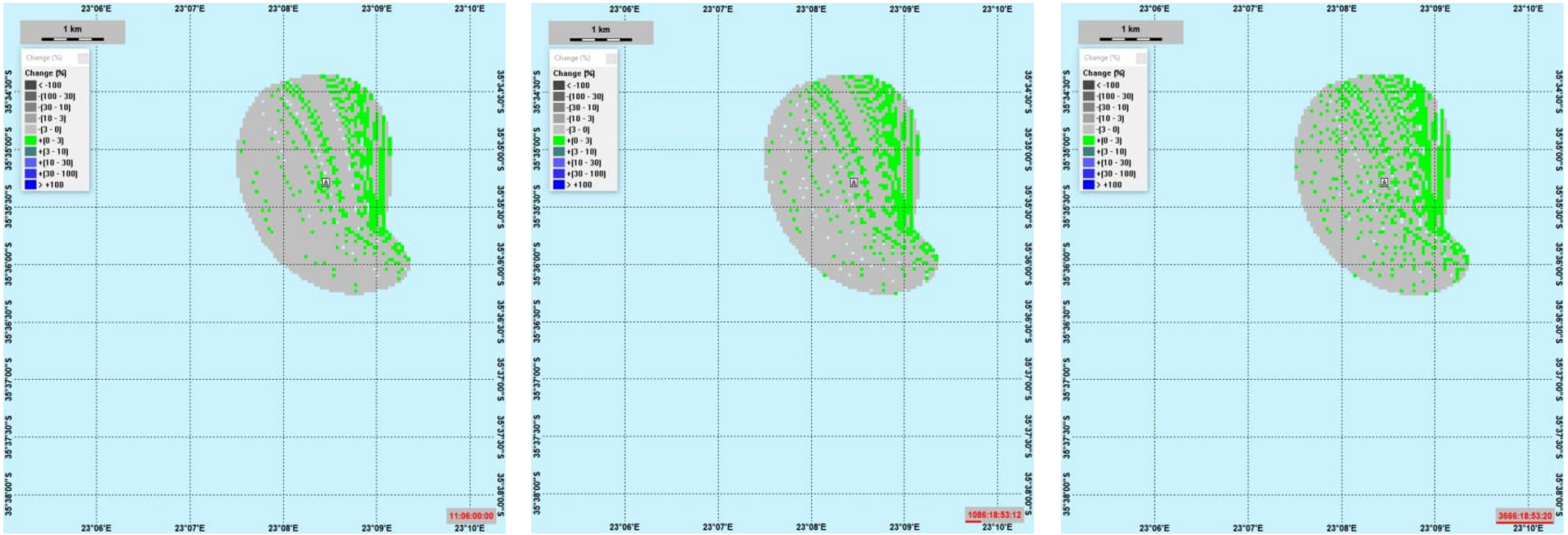

Figure 9.63 Oxygen change in the sediment layer caused by the degradation of chemicals attached to cuttings: A) timestep after 26" displacement section discharged at the seafloor, B) after 3 years, C) after 10 years, for discharge location 5 discharge at seafloor. Summer conditions.

10 Summary of EIF results and discussion.

Table 10.1 and Table 10.2 summarizes the results for EIF's calculated for the water column and for the sediment. The durations of impact are shown as well.

Both concentration in the water column and deposition on the sea floor are calculated, in addition to environmental risks expressed by the EIF (*Environmental Impact Factor*): The results from the EIF calculations can be summarized as shown in the table below. As can be seen, the differences between the seasons are small and not important.

Table 10.1 EIF results for discharge location 4.

Discharge location 4	Maximum EIF	Duration for discharge with max. EIF > 1	Dominant risk contributor
		Summer	
Upper water column (0-100 m)	12616	~ 1.25 days	Barium-sulfate 84%
Lower water column (1750-1850 m)	11639	~ 2.5 days	Barium-sulfate 63% Bentonite 20%
Sediment	1.5	~ 4.3 years	Burial 74% Grain size change 26%,
		Autumn	
Upper water column (0-100 m)	9232	~ 1.25 days	Barium-sulfate 86%
Lower water column (1750-1850 m)	12332	~2.5 days	Barium-sulfate 59% Bentonite 23%
Sediment	0.75	~ 4.3 years	Burial 73% Grain size change 27%
		Winter	
Upper water column (0-100 m)	12016	~ 1.25 days	Barium-sulfate 83%
Lower water column (1750-1850 m)	11972	~2.5 days	Barium-sulfate 59% Bentonite 22%
Sediment	1.5	~ 4.3 years	Burial 73% Grain size change 27%
		Spring	
Upper water column (0-100 m)	9032	~ 1.25 days	Barium-sulfate 85%
Lower water column (1750-1850 m)	11265	~2.5 days	Barium-sulfate 66% Bentonite 16%
Sediment	1	~ 4.3 years	Burial 73% Grain size change 27%

Table 10.2 EIF results for discharge location 5.

Discharge location 5	Maximum EIF	Duration for discharge with max. EIF > 1	Dominant risk contributor
		Summer	
Upper water column (0-100 m)	10148	~ 2 days	Barium-sulfate 82%
Lower water column (1750-1850 m)	8605	~ 5 days	Barium-sulfate 70% Bentonite 14%
Sediment	0.75	~ 4.5 years	Burial 65% Grain size change 35%,
		Autumn	
Upper water column (0-100 m)	8156	~ 1.25 days	Barium-sulfate 84%
Lower water column (1750-1850 m)	8623	~5 days	Barium-sulfate 70% Bentonite 14%
Sediment	0.75	~ 4.5 years	Burial 64% Grain size change 36%
		Winter	
Upper water column (0-100 m)	14220	~ 1.5 days	Barium-sulfate 85%
Lower water column (1750-1850 m)	8773	~5 days	Barium-sulfate 71% Bentonite 14%
Sediment	0.5	~ 4.5 years	Burial 65% Grain size change 35%
		Spring	
Upper water column (0-100 m)	14536	~ 2 days	Barium-sulfate 83%
Lower water column (1750-1850 m)	8722	~5 days	Barium-sulfate 68% Bentonite 15%
Sediment	0.75	~ 4.5 years	Burial 64% Grain size change 36%

For the water column, effects caused by discharges of particle matter (essentially barium sulfate) are dominating the risk in the affected water volume. During the time of maximum EIF for the upper water-column the discharge is released from the rig 10 meters below sea-surface and sinks down to about 40 meters in the water-column. The discharge is driven by the currents in S/SW direction. For the lower water-column close to seafloor, barium-sulfate dominates the risk together with smaller contributions from bentonite and potassium chloride discharged from the top hole sections.

Time development for EIF in the upper water-column shows that the duration with environmental risk is intermittent and short, about 2 days due to ongoing mud discharge from 8.5" Log at the end of the drilling period. Concentrations in the water-column will spread rapidly and dilute with the currents.
For the lower water-column, the concentrations will remain high for a longer time due to lower current speed near the bottom.

For impact on the sediment the calculated EIF is low. Deposited material in the sediment is up to 1 mm within a radius of 250 – 300 meters from the discharge point. The largest thickness close to the discharge location will comprise cuttings discharged from the top hole sections. Because the discharges are located on the sea floor, the cuttings will deposit rather immediately after discharged to the sea. The duration of impact for 4.5 years is consisted with a scenario without resuspension and further transport. If resuspension takes place, the impact duration may be shorter.

11 References

Altin, D., T. K. Frost and I. Nilssen (2008). "Approaches for derivation of environmental quality criteria for substances applied in risk assessment of discharges from offshore drilling operations." Integr Environ Assess Manag 4(2): 204-214.

Durgut I. H.Rye, M.Reed, M.G.D. Smit, M.K. Ditlevsen (2015) Dynamic modeling of environmental risk associated with drilling discharges to marine sediments

EC, 2011, Technical Guidance For Deriving Environmental Quality Standards, Guidance Document No. 27, Common Implementation Strategy for the Water Framework Directive (2000/60/EC), Technical Report - 2011 - 055

ECHA, 2008, Guidance for determination of PNEC. Part B of the Guidance on Information Requirements and Chemical Safety Assessment). European Chemicals Agency, Ispra Italy.

Frost, T.K., Myrhaug, J.L., Ditlevsen, M.K., Rye, H., 2014: Environmental Monitoring and Modelling of Drilling Discharges at a Location with Vulnerable Seabed Fauna: Comparison between Field Measurements and Model Simulations. SPE 168328.

Johnsen S, Frost TK, Hjelsvold M, Røe Utvik T. 2000. The environmental impact factor—A proposed tool for produced water impact reduction, management and regulation. In: SPE International Conference on Health, Safety and Environment in Oil and Gas Exploration and Production; 26–28 June 2000; Stavanger, Norway. Richardson (TX): Society of Petroleum Engineers paper no. 61178.

Karman CC et al., 1994: Ecotoxicological Risk of Produced Water from Oil Production Platforms in the Statfjord and Gullfax Fields. TNO Environmental Sciences. Laboratory for Applied Marine Research, den Helder, The Netherlands. Report TNO-ES, February 1994.

Karman CC and Reerink HG, 1997: Dynamic Assessment of the Ecological Risk of the Discharge of produced Water from Oil and Gas producing Platforms. Paper presented at the SPE (Society of Petroleum Engineers) conference in 1997, Dallas, USA. SPE paper No. 37905.

OSPAR, 2012. Oslo Paris Commission: OSPAR Guidelines in support of Recommendation 2012/5 for a Risk-based Approach to the Management of Produced Water Discharges from Offshore Installations (Source: OSPAR 12/22/1, Annex 19). (OSPAR Agreement: 2012-7).

OSPAR (2020). OSPAR Guidelines for Completing the Harmonised Offshore Chemical Notification Chemical Format (HOCNF). OSPAR Agreement 2012-05. Update 2020. https://www.ospar.org/documents?v=33043

Redman, A. D., T. F. Parkerton, M. H. Comber, M. L. Paumen, C. V. Eadsforth, B. Dmytrasz, D. King, C. S. Warren, K. den Haan and N. Djemel (2014). "PETRORISK: A risk assessment framework for petroleum substances." Integrated Environmental Assessment and Management 10(3): 437-448.

Redman, A. D., T. F. Parkerton, M. Leon Paumen, J. D. Butler, D. J. Letinski and K. den Haan (2017). "A re-evaluation of PETROTOX for predicting acute and chronic toxicity of petroleum substances." Environmental Toxicology and Chemistry 36(8): 2245-2252.

Redman, A. D., T. F. Parkerton, J. A. McGrath and D. M. Di Toro (2012). "PETROTOX: An aquatic toxicity model for petroleum substances." Environmental Toxicology and Chemistry 31(11): 2498-2506.EC, 2003, Technical Guidance Document on Risk Assessment in support of Commission Directive 93/67/EEC on Risk Assessment for New Notified Substances Commission Regulation (EC) No 1488/94 on Risk Assessment for existing substances Directive 98/8/EC of the European Parliament and of the Council concerning the placing of biocidal products on the market. European Commission Joint Research Centre. EUR 20418 EN/2.

Reed M, Hetland B. 2002. DREAM: a Dose-Related Exposure Assessment Model. Technical description of physical-chemical fates components. SPE paper No. 73856. In: SPE International Conference on Health, Safety and Environment in Oil and Gas Exploration and Production; 20-22 March 2002; Kuala Lumpur, Malaysia. Society of Petroleum Engineers, Mail: P.O. Box 833836 Richardson, TX 75083-3836, USA

Rye H, Reed M, Frost TK, Smit MGD, Durgut I, Johansen Ø, and Ditlevsen MK. 2008. Development of a numerical model for calculating exposure to toxic and nontoxic stressors in the water column and sediment from drilling discharges. Integrated Environmental Assessment and Management Vol. 4 No. 2, pp 194 – 203. SETAC journal 2008.

Saga, 1994: "Miljøprogram i forbindelse med brønn 7219/8-1s i Barentshavet". Report from Saga Petroleum a.s. dated 10 March 1994. Saga report R-TIY-0003. Written by J.R. Hasle, H.N. Lie and K. Thorbjørnsen in Norwegian.

Singsaas et al (2008) Development of a Risk-Based Environmental Management Tool for Drilling Discharges. Summary of a Four-Year Project

Smit, M.G.D., J.E. Tamis, R.G. Jak, C.C. Karman, G. Kjeilen-Eilertsen, H. Trannum, J. Neff, 2006. Threshold levels and risk functions for non-toxic sediment stressors: burial, grain size changes and hypoxia. Summary. TNO Report no. TNO 2006-DH-0046/A – Open.

Smith, M.G.D., R.G.Jak, H.Rye, T.K.Frost, 2006. Framework for the Environmental Impact Factor for drilling discharges. TNO Report no. 2006-DH-R0045/B – Open.

Smit MGD, Jak RG, Rye H, Frost TK, Singsaas I, Karman CC. 2008. Assessment of environmental risks from toxic and nontoxic stressors; a proposed concept for a risk-based management tool for offshore drilling discharges. Integr Environ Assess Manag 4:173–183.

Smit M.G.D., T.K. Frost, S. Johnsen., 2011, Achievements of risk-based produced water management on the Norwegian continental shelf (2002-2008). Integr Environ Assess Manag 7:668-677.

Thorne Schaaning, M., T.Bakke, 2006. Remediation of sediments contaminated with drill cuttings. NIVA Report no. 5188-2006 – Open. ERMS report no. 22.

USEPA, 1998, Guidelines for ecological risk assessment. Washington (DC): US Environmental Protection Agency. Fed Reg 63:26846–26924.

12 Appendices

12.1 Appendix 1 - Service Request Form

DREAM-PARTRACK MODELLING SETUP – SUMMARY SHEET

IMPORTANT/ Information detailed here must be agreed and validated (signed) by client before commencement of the study

WARNING 1: Any changes to the information mentioned herein after validation will imply an impact on the delivery time and / or costs associated with the service."

WARNING 2: For studies related with preparation and/or updating of ESIA. the input data for the study as well as the results. shall be verified by STS/HSE/EP/ES before disclosure to client.

WARNING 3: Report or results being produced are not absolute values and needs to be interpreted by specialists. Any misunderstanding or misleading interpretation of results provided will be client responsibility.

WARNING 4: As the CFT have not been issued and the Mud, Waste and Cement Contractors have not been selected so far, the herebelow data are either generic either proposed as a reference for further environmental studies. When the Contractors will be known, an update should be carried out.

COUNTRY/AFFILIATE	South Africa - TEPSA	
BLOCK/WELL	11B/12B / Discharge 4 and Discharge 5	
CLIENT/REQUESTOR NAME AND ENTITY		
HEAD OFFICE & AFFILIATE CORRESPONDANTsS	☒ *Affiliate:Eduard Groenewald*	☒ *Head quarter representative: Cesar FUENMAYOR*
RFS REFERENCE		
SERVICE SCOPE OF WORK	☒ EIA support	☐ Operation support
	☐ OSCP	☐ Other ....
NUMBER OF SCENARIOS	1 Scenario	☐ OSR
DEADLINE	Deliverables deadline Ppt slides .... Draft report Final report	
AGREED DELIVERABLES	☒ Technical Report (ESIA purposes)	☒ Power-point presentation (ESIA purposes)
	☒ GIS maps (.nc or .shp)	☒ raw PARTRACK results
METOCEAN DATA	☐ Available	☐ To be purchased
	Already ordered for Oilspill	*LAT:* 32°S to 44°S
		LON: 13.5°E to 32°E
CONFIDENTIAL LEVEL	☐ Confidential (internal use)	☐ external use (ESIA purposes)

BASIC INFORMATION – RELEASE LOCATION (WGS84)	
LOCATION 1– CONFIRMED/TENTATIVE COORDINATES	Discharge 4: Lon : 22° 44' 43.9515" E Lat : 35° 46' 58.4526" S
LOCATION 2 - CONFIRMED/TENTATIVE COORDINATES	Discharge 5 (Luiperd development barycenter) : Lon : 23° 08' 27.6914" E Lat : 35° 35' 17.3071" S
LOCATION 3 - CONFIRMED/TENTATIVE COORDINATES	
SIMULATION PERIOD	(1) To be confirmed

NUMBER OF SCENARIOS & duration of model			
	[redacted]	duration of simulation– water column (days)	duration of simulation– sediments (days)
Scenario 1	Discharge Point#3 Vertical well 1x CP +2x Csg – Season 1	To be tested	To be tested
Scenario 2	Discharge Point#3 Vertical well 1x CP +2x Csg – Season 2	To be tested	To be tested
Scenario 3	Discharge Point#3 Vertical well 1x CP +2x Csg – Season 3	To be tested	To be tested
Scenario 4	Discharge Point#3 Vertical well 1x CP +2x Csg – Season 4	To be tested	To be tested

Wellbore diameter (")	42"	26"	12.25"	8.5"		
				Drilling	Log	P&A
Sections length (m)	122	510	1392	418		
Drilling rate (m/h)	20	30	25	15		
Mass of cuttings (T)	433	694	421	57		
Cuttings discharged (yes/No)	yes	yes	yes	yes		
Type of mud used while drilling	Seawater + Gel/Polymer Sweeps	Seawater + Gel/Polymer Sweeps + KCl Mud	HPWBM	HPWBM		
quantity of mud discharged while drilling, including OOC for NABM (T)	270	756	1200	500	1200	1200
Drilling duration (section length* drilling rate + circulating before and after connexion, circulate hole cleaning (hours) = operation duration (Hours)	5	25	96	50	0	0
Cuttings & mud Discharge duration (Hours)	5	25	110	70	10	10
Discharge DEPTH (m)	Seabed	Seabed	10 m below mean sea level	10 m below mean sea level		
Discharge diameter (in)			12"	12"		
Indicative time before next operation (hours) – (including time to prepare next operation. cementing operation.	4 days	5 days	3 days	3 days		

Liner. casing. pressure tests...) = no discharge						
Suspension/ displacement/kill mud before drilling next section (yes/No)	Yes	Yes	No	No	No	No
Type of mud used for Suspension/clean-up/displacement	1.3sg KCl/Polymer Mud	1.3sg KCl/Polymer Mud				
quantity of mud discharged for Suspension/clean-up/displacement (T)	260	1040				
Suspension/clean-up/displacement duration (hours) – Default value 12 Hrs	12	12				
Discharge DEPTH (m)	Seabed	Seabed				
Discharge diameter (in)	42" Open hole	26" Open hole				

MUD COMPOSITION *MSDS or HOCNF or bioassays results report must be provided to HSE/ENV/OPS, to allow to gather Ecotoxicological data* *Data could be provided in an Excel spreadsheet and SES/HSE/A.P/ENV team will populate the table below*														
	Input from Fluid team						Input from HSE/ENV/OPS based on MSDS, HOCNF or bioassays results provided by the project team							
Mud type	Density of mud	name	composition	Function	Concentration (kg/T)	Mass (T)	PNEC (ppb)	KOC	Solubility (ppm)	density	Biodegradation (%)	KOW	Vapour pressure	MW
26"x42" Seawater + Gel/Polymer Sweeps	1.06	Bentonite	bentonite	Clay Viscosifier	60	20	170	Calculated from KOW in MEMW	0	2.5	0	0	0	150
		Danzan-D	Polysaccharide/Xanthan Gum	Polymer Viscosifier	0	2	420		100000	1.6	93	0	0	
		Soda Ash	Sodium Carbonate	Hardness buffer	1	0.25	200		212500	2.52	0	0	0	106
		Caustic Soda	Sodium hydroxide	Alkaline/pH buffer	1	0.25	20		1000000	2.13	0	0	0	40
26"x42" 30sg KCL/Polymer Mud	1.3	Soda Ash	Sodium Carbonate	Hardness buffer	1	0.2	200		212500	2.52	0	0	0	106
		Caustic Soda	Sodium hydroxide	Alkaline/pH buffer	1	0.2	20		1000000	2.13	0	0	0	40
		Danzan-D	Polysaccharide/Xanthan Gum	Viscosifier	6	1.2	420		100000	1.6	93	0	0	
		Potassium Chloride	Potassium Chloride	Shale inhibitor	70	14	100		355000	1.98	0	0	0	
		Barite	Barium Sulfate	Weighting agent	350	96.5	115		3.1	4.5	0	0	0	233.4
			Crystalline silica, quartz			3.5	440		0	2.6	0	0	0	60
		Staricide	3, 3'-Methylene bis (5-methyl oxazolidine)	Bactericide	0.5	0.1	40		2800000	1.05	80.6	0.9	0.014 hPa	186.25
26" Seawater +	1.08	Bentonite	bentonite	Clay Viscosifier	60	56	170		0	2.5	0	0	0	150

Gel/Polymer Sweeps		Barazan-D	Polysaccharid e/Xanthan Gum	Bolymer Viscosifier	8	5.6	420		100000	1.6	93	0	0	
		Soda Ash	Sodium Carbonate	Hardness buffer	1	0.7	200		212500	2.52	0	0	0	106
		Caistic Soda	Sodium hydroxide	Alkaline/pH buffer	1	0.7	20		1000000	2.13	0	0	0	40
26" 30sq KCL/Polymer Mud	1.3	Soda Ash	Sodium Carbonate	Hardness buffer	1	0.8	200		212500	2.52	0	0	0	106
		Caistic Soda	Sodium hydroxide	Alkaline/pH buffer	1	0.8	20		1000000	2.13	0	0	0	40
		Barazan-D	Polysaccharid e/Xanthan Gum	Viscosifier	6	4.8	420		100000	1.6	93	0	0	1000000
		Potasium Chloride	Potassium Chloride	Shale inhibitor	70	56	100		355000	1.98	0	0	0	74.55
		Barite	Barium Sulfate	Weighting agent	350	266	115		3.1	4.5	0	0	0	233.4
			Crystalline silica, quartz			14	440		0	2.6	0	0	0	60
		Starcide	3, 3'-Methylene bis (5-methyl oxazolidine)	Bactericide	0.5	0.4	49		2800000	1.069	90	0.9	0,014 hPa	186.25
12-1/4" HPWBM	1	Soda Ash	Sodium Carbonate	Hardness buffer	1	2	200		212500	2.52	0	0	0	106
		Caistic Soda	Sodium hydroxide	Alkaline/pH buffer	1	2	20		1000000	2.13	0	0	0	40
		Barazan-D	Polysaccharid e/Xanthan Gum	Bolymer Viscosifier	6	12	420		100000	1.6	93	0	0	
		Potasium Chloride	Potassium Chloride	Shale inhibitor	70	140	100		355000	1.98	0	0	0	
		Barite	Barium Sulfate	Weighting agent	350	855	115		3.1	4.5	0	0	0	233.4
			Crystalline silica, quartz			45	440		0	2.6	0	0	0	60
		Sodium Chloride	NaCl	Shale inhibitor	40	80	1E+06		317000	2.17	100	0	0	
		GEM GP	Polyethylene glycol butyl ether	Shale inhibitor	1	2	188		989000	0.989	69	2.75	0	
		Clayseal Plus	Triethylenetetramine, polymer with oxirane	Shale inhibitor	2	1.2	562.3		500000	1.0411	100	0		
			Hydrochloric acid			0.2	0.45		500000	1.27	100	0	45.6	
		Clay Grabber	Hydrotreated light petroleum distillate	Shale inhibitor	2.5	1	9.8		12	0.798	58.6	1E+07	0.03	
			Ethoxylated branched C13 alcohol			0.15	1.31		1000	1	60	10	0	228.42
		Clay Sync II	?	Shale inhibitor	5	10	1160		500000	1.04	2.8	0	0	
		Bore HIB	Silicic acid, potassium salt	Fluid loss reducer	20	10	146		0	1.43	na	na	0	
		Dextrid E	Complex carbohydrate	Fluid loss reducer	8	40	1000		500000	1.5	70	0	0	
		PAC-L	Polyanionic Cellulose	Fluid loss reducer	8	16	87.26		500000	1.6	60	na	0	263
8/1/2" HPWBM	1	Soda Ash		Hardness buffer	1	1	200		212500	2.52	0	0	0	106
		Caistic Soda		Alkaline/pH buffer	1	1	20		1000000	2.13	0	0	0	40
		Barazan-D		Viscosifier	6	6	420		100000	1.6	93	0	0	
		Potasium Chloride		Shale inhibitor	70	70	100		355000	1.98	0	0	0	
		Barite	Barium Sulfate	Weighting agent	350	427.5	115		3.1	4.5	0	0	0	233.4
			Crystalline silica, quartz			22.5	440		0	2.6	0	0	0	60
		Sodium Chloride		Shale inhibitor	40	40	1E+06		317000	2.17	100	0	0	
		GEM GP		Shale inhibitor	1	1	188		989000	0.989	69	2.75	0	
		Clayseal Plus	Triethylenetetramine, polymer with oxirane	Shale inhibitor	2	0.6	562.3		500000	1.0411	100	0		
			Hydrochloric acid			0.1	0.45		500000	1.27	100	0	45.6	
		Clay Grabber	Hydrotreated light petroleum distillate	Shale inhibitor	2.5	0.5	9.8		12	0.798	58.6	1E+07	0.03	

			Ethoxylated branched C13 alcohol			0.075	1.31		1000	1	60	10	0	228.42
		Clay Sync II	?	Shale inhibitor	5	5	1160		500000	1.04	2.8	0	0	
		Bore HIB	Silicic acid, potassium salt	Fluid loss reducer	20	20	146		0	1.43	na	na	0	
		Dextrid E	Complex carbohydrate	Fluid loss reducer	8	8	1000		500000	1.5	70	0	0	
		PAC-L	Polyanionic Cellulose	Fluid loss reducer	8	8	87.26		500000	1.6	60	na	0	263
		BARACARB 150	Barium Sulfate	Loss Control Material/LCM	25	25	115		3.1	4.5	0	0	0	233.4
		BARACARB 50	Barium Sulfate	Loss Control Material/LCM	25	25	115		3.1	4.5	0	0	0	233.4

RELEASE PROPER TIES			
ORIENTATION of discharge	Vertical		
		RELEASE TEMPERATURE (°C)	Release salinity (g/L)
	42" Section:1	Close to seabed temperature	25 g/l Cl^-
	26"Section: 2	Close to seabed temperature	25 g/l Cl^- while drilling 35 g/l Cl^- after drilling & during cementing casing
	12 .25" Section: 3	25-35°C	70 g/l Cl^-
	8.5" Section: 4	25-35°C	70 g/l Cl^-

AMBIENT AVERAGE DATA (to be provided by affiliate or ENV/AOP)
If water profiles are available close to studied area; they should be provided; if not, default values or bibliography average values to be considered

comments	bibliography				EBS values (range)
	Monthly means values				
	January	March	June	Sept	January March June September
WATER COLUMN TEMPERATURE (°C)	0m: 22.6; 100m: 15.8; 200m: 12.7; 500m: 9.7; 800m: 7.4; 1000m: 5.7; 1500m: 3.4 1600m: 3.1	0m: 22.7; 100m: 15.5; 200m: 12.7; 500m: 8.6; 800m: 6.0; 1000m: 4.6; 1500m: 3.3 1600m: 3.1	0m: 19.5; 100m: 16.7; 200m: 14.7; 500m: 9.7; 800m: 6.4; 1000m: 5.1; 1500m: 3.3 1600m: 3.1	0m: 18.6; 100m: 14.3; 200m: 11.7; 500m: 7.7; 800m: 5.2; 1000m: 5.1; 1500m: 4.1 1600m: 3.1	No info
SALINITY (%)	0m: 35.4; 700m: 34.9 100m: 34.6 2000m: 34.7 2500m: 34.8	0m: 35.4; 700m: 34.9 100m: 34.6 2000m: 34.7 2500m: 34.8	0m: 35.4; 700m: 34.9 100m: 34.6 2000m: 34.7 2500m: 34.8	0m: 35.4; 700m: 34.9 100m: 34.6 2000m: 34.7 2500m: 34.8	No info
AIR TEMPERATURE (°C)	21.5	21.2	17.6	16.9	No info
OXYGEN CONTENT (mg/l)	0m: 7.68 250m: 7.36 500m: 6.88 1000m: 6.08 1500m: 5.44 2000m: 6.88	0m: 7.68 250m: 7.36 500m: 6.88 1000m: 6.08 1500m: 5.44 2000m: 6.88	0m: 7.68 250m: 7.36 500m: 6.88 1000m: 6.08 1500m: 5.44 2000m: 6.88	0m: 7.68 250m: 7.36 500m: 6.88 1000m: 6.08 1500m: 5.44 2000m: 6.88	No info
Median GRAIN SIZE (mm)	0.350				No info
SUSPENDED SEDIMENT (mg/l)	0				No info

12.2 **Appendix 2:**

ANALYSIS OF METOCEAN DATA FOR OIL SPILL AND DRILLING DISCHARGE MODELLING FOR BLOCK 11B/12B.

TotalEnergies E&P South Africa BV

OFFSHORE PRODUCTION RIGHT AND ENVIRONMENTAL AUTHORISATION APPLICATIONS FOR BLOCK 11B/12B

Analysis of Metocean Data for Oil Spill and Drilling Discharge Modelling.

41105306-358665-9
JULY 2023

PUBLIC

TotalEnergies E&P South Africa BV

OFFSHORE PRODUCTION RIGHT AND ENVIRONMENTAL AUTHORISATION APPLICATIONS FOR BLOCK 11B/12B

Analysis of Metocean Data for Oil Spill and Drilling Discharge Modelling.

TYPE OF DOCUMENT (VERSION) PUBLIC

PROJECT NO. .41105306

OUR REF. NO. 41105306-358665-9

DATE: JULY 2023

TotalEnergies E&P South Africa BV

OFFSHORE PRODUCTION RIGHT AND ENVIRONMENTAL AUTHORISATION APPLICATIONS FOR BLOCK 11B/12B

Analysis of Metocean Data for Oil Spill and Drilling Discharge Modelling.

WSP

Building 1, Maxwell Office Park
Magwa Crescent West, Waterfall City
Midrand, 1685
South Africa

Phone: +27 11 254 4800

WSP.com

QUALITY CONTROL

Issue/revision	Final
Date	04 July 2023
Prepared by	Ashwin Gadgil
Signature	
Checked by	Sundar Prasad
Signature	
Authorised by	Roy van Ballegooyen
Signature	
Project number	41105306
Report number	41105306-358665-9

CONTENTS

TABLES

FIGURES

APPENDICES

APPENDIX A

SATOCEAN HYDRODYNAMIC DATABASE: CALIBRATION AND VALIDATION

APPENDIX B

DOCUMENT LIMITATIONS

1 INTRODUCTION

A statistical assessment of wind and current data was carried out at three locations within License Block 11B/12B, located off the Southern Cape Coast of South Africa. The area of interest is approximately 12,000 km^2 and lies between Mossel Bay and Cape St. Francis in waters of depths of between 500 m and 2,300 m. The data was sourced from a SAT-OCEAN (TotalEnergies, 2022) hindcast model covering a 5-year period (Jan 2012 – Dec 2016). The SAT-OCEAN model has a resolution of 1/32 degree (about 3.5 km) in the study area. Model output is provided at 3-hour time steps. The vertical z-coordinates of the model (m) are 0, 5, 10, 20, 30, 40, 50, 75, 100, 125, 150, 200, 300, 400, 500, 750, 1000, 1250, 1500, 1750, 2000, 2250, 2500, 2750, 3000, 3250, 3500, 4000, 5000, and 5500. The calibration and validation of these data are reported in Appendix A. See also Russo *et al*. (2022) that has undertaken an intercomparison of re-analysis products (including HYCOM upon which the SATOCEAN data is based) for southern African Waters.

1.1 DISCHARGE LOCATIONS AND OVERVIEW OF METOCEAN CONDITIONS

Metocean statistics have been compiled to support the numerical modelling of condensate dispersion from a subsea blowout and a submarine pipeline leak, and dispersion of drilling mud and cuttings discharges at the seabed and near the water surface. Three locations, Discharge 4 and Discharge 5, on the southwest end of Block 11B/12B, and Pipe Leak on the shallower continental shelf and approximately 87 km northwest of Discharge 5, are considered for the present assessment, and are shown in Figure 1-1.

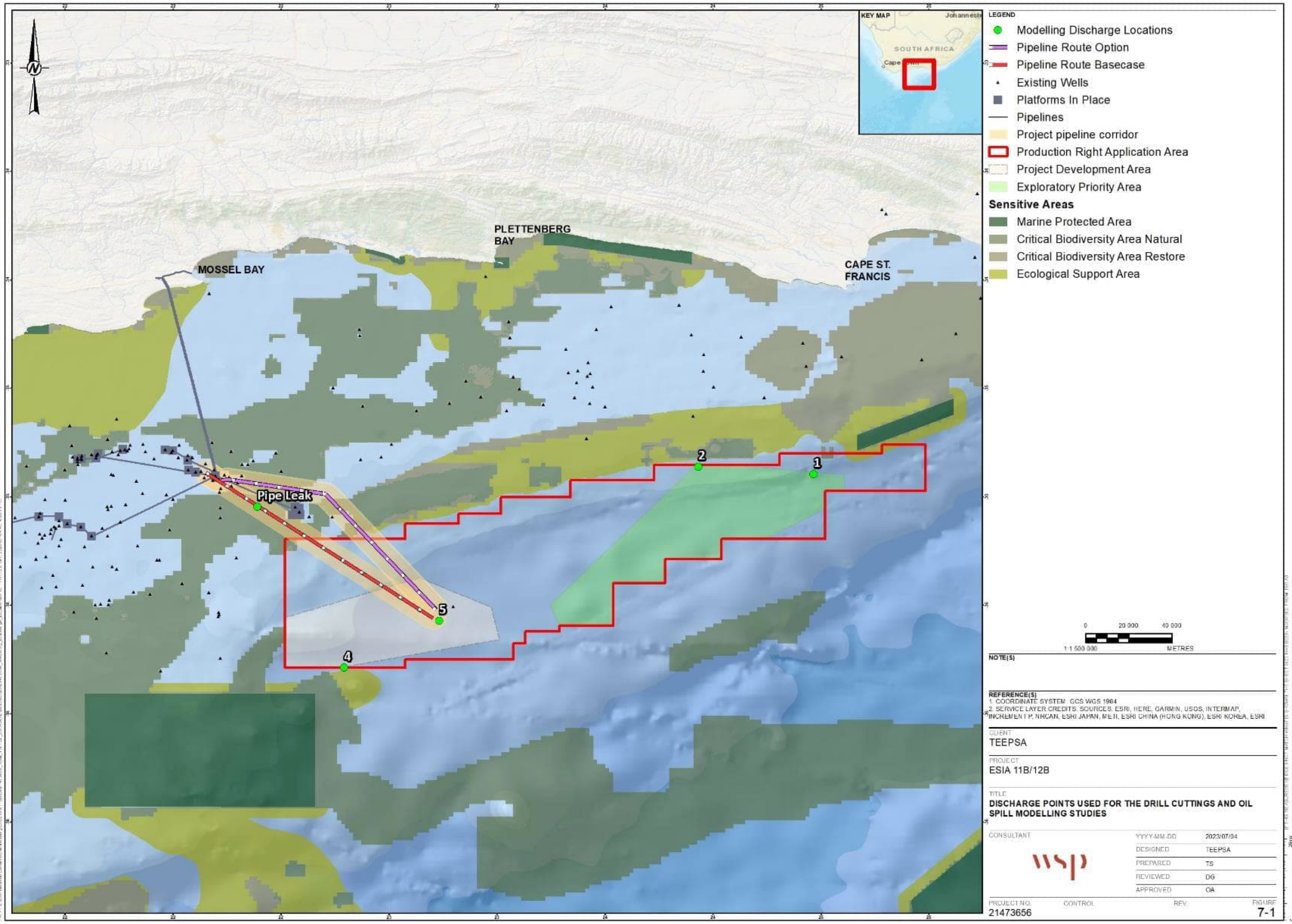

Figure 1-1 - Locations of Discharge 4, Discharge 5, and condensate Pipe Leak in the study area

The primary driver of ocean dynamics in Block 11B/12B is the strong Agulhas Current which flows southward along the east coast of Africa from 27°S to 40°S and is estimated to transport 70 million cubic metres of water per second. Figure 1-2 shows drifter derived surface current velocities and spatial extent of the flow. The eastward Agulhas Return Current at approximately 40°S can also be seen.

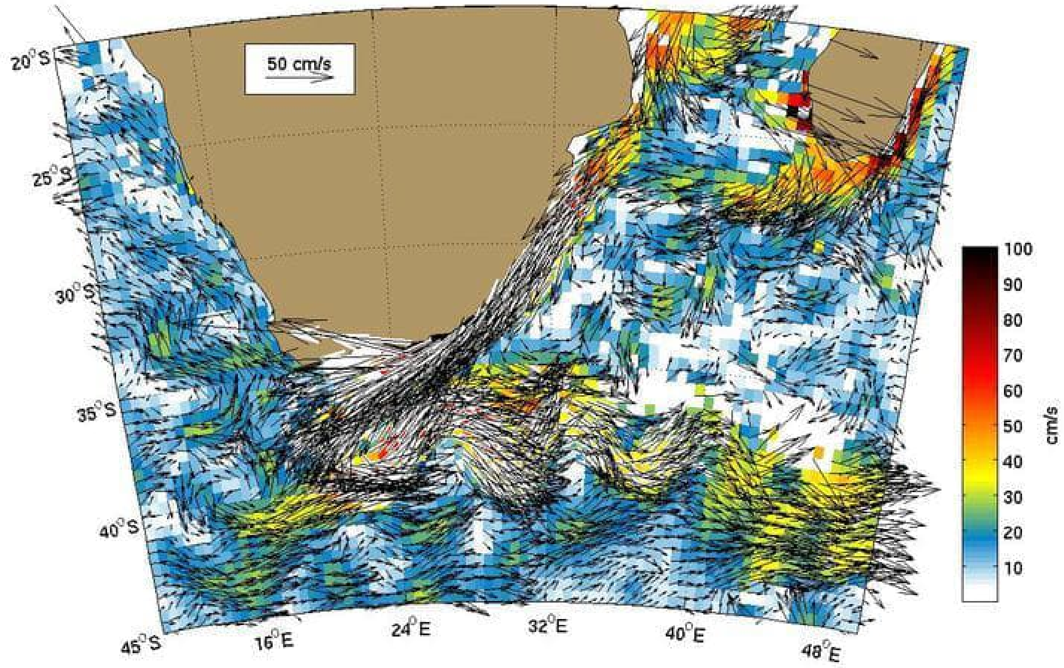

Figure 1-2 - Mean ocean surface velocities derived from satellite-tracked drifters following the ocean at 15 m depth (https://oceancurrents.rsmas.miami.edu/atlantic/agulhas_2.html)

The licence block 11B/12B is located on the inner edge of the Agulhas Current that is subject mainly to strong steady south-westward Agulhas Current flows but also flow reversals associated with:

- shear edge features (*e.g.,* Lutjeharms *et al*., 1988, 2003; Krug *et al*., 2014; Tedesco *et al*., 2019), and
- larger-scale variability due to occasional large-scale perturbations of the Agulhas Current such as the passing of Natal Pulses (*e.g.,* Lutjeharms and Roberts, 1988; Roualt and Penven, 2011) that are evidenced throughout the depth of the water column (Lutjeharms *et al*., 2001).

Such perturbations (Figure 1-3 and Figure 1-4) strongly influence the largely wind-driven flows and associated water column structures of the adjacent Agulhas Bank (Boyd and Shillington, 1994; Largier and Swart,1987; Swart and Largier, 1987; Largier *et al*., 1992; Bailey *et al*., 2022); . This influence extends into coastal embayments of the eastern Agulhas Bank (Schumann *et al*., 1988; Goschen and Schumann, 1990).

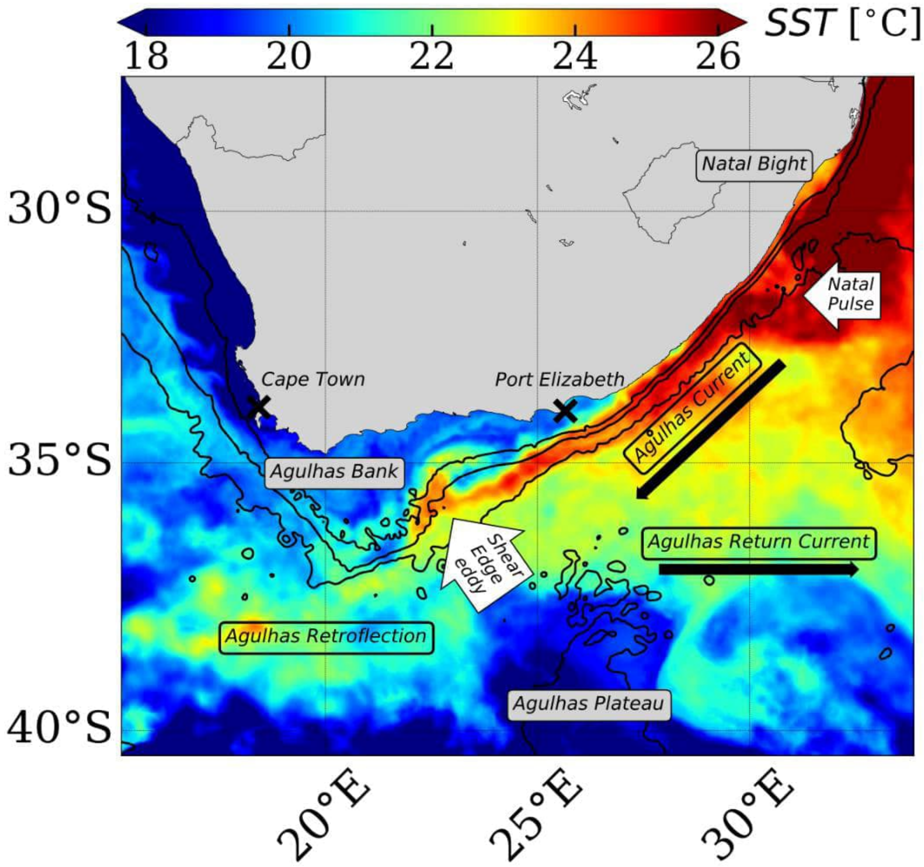

Figure 1-3 - Satellite-derived sea surface temperature (°C) for 4 June 2014 showing the main features of the Agulhas Current, including the shear edge features on the inner edge of the Agulhas Current and early evidence of an upstream Natal Pulse that will propagate downstream resulting in a major perturbation of flows in Block 11B/12B. The black lines represent the 200, 1000, and 3000 m isobaths (Source: Tedesco *et al*., 2019)

Discharge locations 4 and 5 are situated on the inner edge of the Agulhas Current that is strongly influenced by the predominantly strong south-westerly surface flows of the Agulhas Currents. These flows are significantly weaker at depth and more prone to current reversals. There is evidence of a more persistent current reversals in the deeper waters (> 1 500 m) on the inshore edge of the upstream regions of the Agulhas Current (Beal and Bryden, 1997; Beal, 2009; Beal *et al*., 2015), an influence that could extend into licence Block 11B/12B but at slightly greater depths (~ 1 800m).

The Pipe Leak (rupture) discharge location, in the shallower waters (~ 140 m to 150 m water depth) of the adjacent Agulhas Bank is more strongly influenced by wind driven flows, particularly in the surface waters where there is evidence of more persistent north-easterly wind-driven flows in the surface waters associated with the strong westerly winds associated with passing mid-latitude cyclones ("cold fronts") that occur during the winter months.

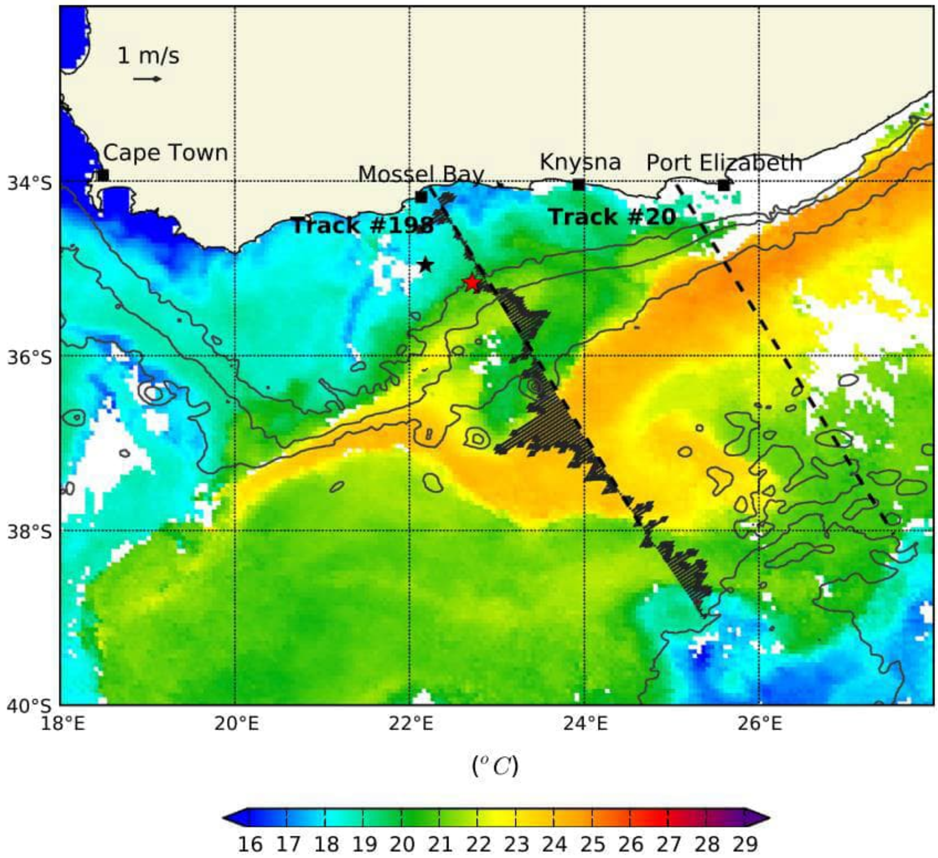

Figure 1-4 - Daily composite of SEVIRI SST on 13 May 2009, during the passage of a Natal Pulse. Overlaid vectors represent the cross-track absolute geostrophic current velocities derived from the high resolution along-track altimetry (Source: Krug and Dufois, 2014).

Early studies suggested based on limited data suggested a lack of seasonality in the surface core speeds of the Agulhas Current (Pearce and Gründlingh, 1982). More recent studies have indicated a seasonality in the volume fluxes of the Agulhas Current (Beal *et al*., 2015; Hutchinson, 2018), however it is not clear how this would influence current speeds in the region of interest to the drilling discharge and oil spill modelling studies. Despite this limited evidence of seasonality in the Agulhas Current speeds, it is rather the major changes in current speeds expected for the offshore discharge locations due to the onshore-offshore movement of the Agulhas Current, shear edge features and major episodic perturbations such as the passing of a Natal Pulse (Lutjeharms *et al*., 1989; 2003; Krug *et al*., 2014), that are of greatest relevance. However, as noted above, there is an increasing seasonality in the current flows upon moving further inshore into the increasingly shallow waters of the Agulhas Bank and coastal embayments, this being particularly true for the surface waters.

The drilling cutting discharge modelling is strongly influenced by the Agulhas Currents flows occurring throughout the water column. Given that the influences of drilling discharges mainly are confined to deeper waters, it is not expected that there will be evidence of significant seasonal variability in such influences. The major variability will be due to shear edge features (that have a greater influence in surface waters) and major perturbations of the of the Agulhas Current such as those due to Natal Pulses (that typically influence the full water column). The transport and fate of the condensate in the oil spill modelling, although influenced by deeper flows as the condensate rises through the water column, is predominantly determined by surface flows (whether those of the Agulhas Current in deeper waters or those of the mainly wind-driven flows in the shallower waters of the adjacent Agulhas Bank). The capturing of seasonal effects in the oil spill modelling therefore is important. This is adequately achieved by the use stochastic simulations undertaken throughout the year.

The key characteristics of wind and current at the three discharge locations are presented in Table 1-1. Note that oceanographic convention is used for current direction which indicates the direction *towards* which the current flows. Meteorological convention is used for wind direction and signifies the direction *from* which the wind blows. The wind speed is reported at the standard elevation of 10 m above MSL and corresponds to a 10-minute average.

Table 1-1 - Discharge location characteristics

Location	Longitude (Deg WGS 84)	Latitude (Deg WGS 84)	Depth (m)	Current - primary direction (to)	Wind - primary direction (from)
4	22.745542° E	35.782903° S	~1600	SW to WSW	WSW to WNW
5	23.141025° E	35.588141° S	~1815	SW to WSW	WSW to WNW
Pipe leak	22.383794° E	35.116225° S	~146	SW to WSW	WSW to W, E

1.2 ENVIRONMENTAL DATA

Environmental data at Discharge 4 and 5 are summarized in Table 1-2.

Table 1-2 - Environmental average data (Discharge 4 & 5 PARTRACK Modelling SRF, TEEPSA, 2022)

Environmental Parameter		Value
Upper water column temperature (°C)		20.9
Middle water column temperature (°C)		6.3
Lower water column temperature (°C)		3.1
Air Temperature (°C)		19.3
Salinity (PSU)	Surface (0 m)	35.4
	Middle (1250 m)	34.6
	Bottom (2500 m)	34.8
Seawater oxygen content (mg/l)	Upper	7.7
	Lower	6.9
Median grain size (mm)		0.3
Suspended sediment (mg/l)		0

1.3 DISPERSION MODELLING SIMULATION PERIODS

Metocean data was analysed for four seasons: Season 1 (December – February (Summer)); Season 2 (March – May (Fall)); Season 3 (June – August (Winter)); Season 4 (September – November (Spring)). Average metocean conditions for each discharge location and season are presented in Table 1-3. Sections 2 and 3 of this report provide the detailed results derived from data at Discharge 4 and Discharge 5, respectively.

Table 1-3 - Overview of metocean conditions by season at Discharge 4, 5, and Pipe Leak for 2012 - 2016

		Discharge 4				Discharge 5				Pipe Leak			
		S1	S2	S3	S4	S1	S2	S3	S4	S1	S2	S3	S4
Surface Current	Average (m/s)	1.4	1.2	1.1	1.4	1.5	1.4	1.2	1.5	0.4	0.4	0.6	0.5
	Maximum (m/s)	3.1	3.4	4.8	3.8	3.1	3.6	4.9	3.8	2.6	2.7	5.0	3.5
	Most frequent Direction	SW	SW	SW	SW	SW	SW	SW	SW	SW	SW	NE	SW
Winds	Average (m/s)	7.7	8.2	9.9	9.1	7.6	8.2	9.8	9.1	6.8	7.0	8.6	8.2
	Maximum (m/s)	23.2	24.1	27.8	23.5	21.9	24.1	27.8	23.7	21.0	19.9	24.5	22.5
	Most frequent Direction	E	W	W	W	E	ENE	W	W	E	W	W	WSW

2 DISCHARGE 4

The average metocean data at the Discharge 4 location over the five-year dataset is presented in Figure 2-1.

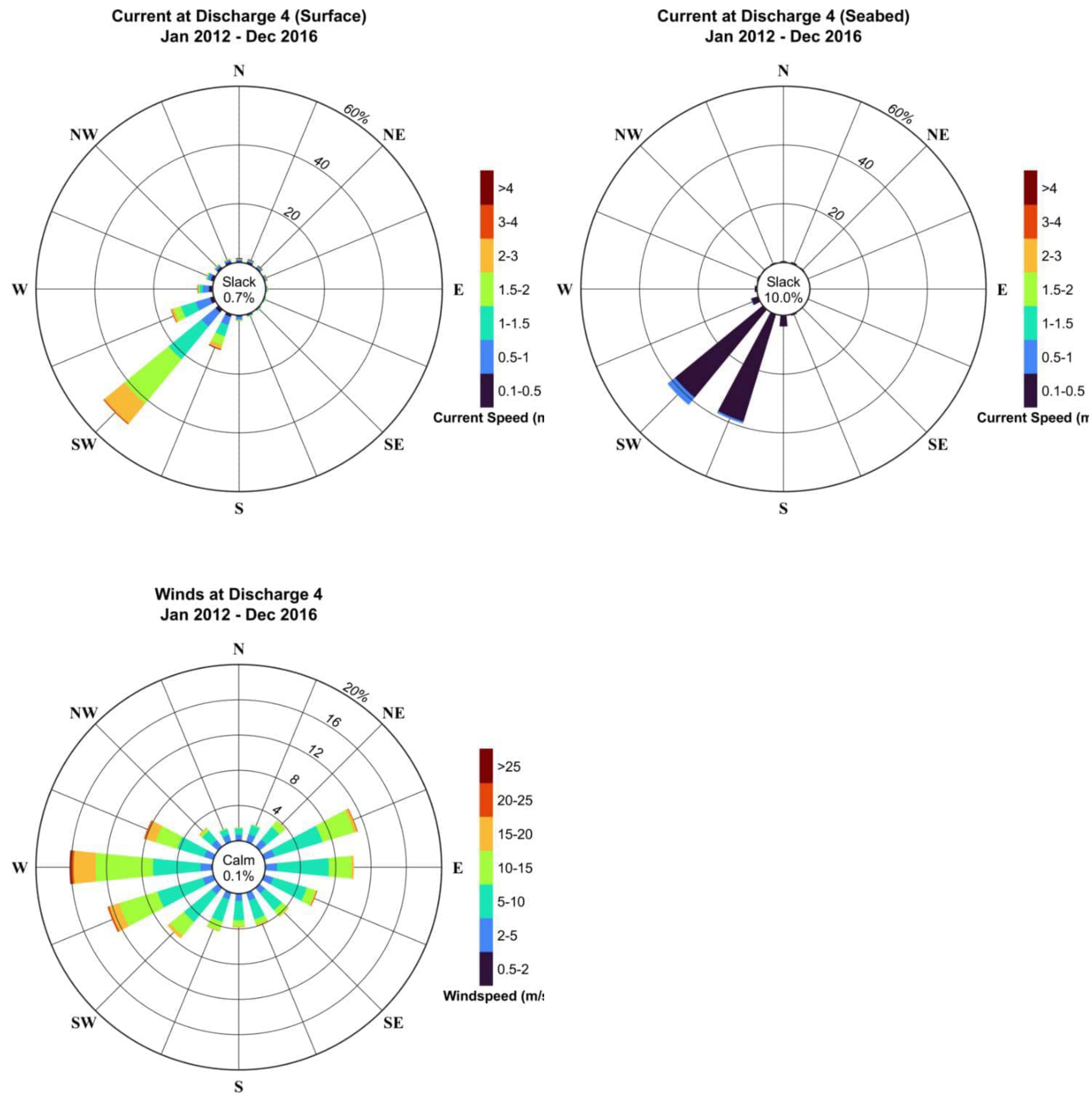

Figure 2-1 - Average annual current and wind speed roses at Discharge 4 for 2012-2016

The dominant direction for surface current at Discharge 4 is towards SW for the 2012 to 2016 period with an occurrence probability greater than approximately 50%. Current speeds can reach up to 4 m/s at the surface.

Dominant current direction at the seabed is towards SSW and SW for approximately 80% of the time. Part of the drill cuttings are discharged at the seabed, which makes seabed currents an important factor in drilling discharge modelling.

Dominant wind directions are from between WSW and WNW (approximately 36% of the time), and ENE and ESE (approximately 27% of the time). Wind speeds are mostly in the 5 m/s to 20 m/s range.

Figure 2-2 and Table 2-1 present the average monthly current roses at the surface for 2012 to 2016 and the associated statistics, respectively. The surface current at Discharge 4 is predominantly directed to the southwest in all months. There are periods of the year (Feb, May and June) when occurrences of flow towards the north are also observed. The peak monthly surface current speed of 4.8 m/s to NNE, and 4.2 m/s to SSW occur in June and July, respectively. These comprise strong wind-driven flows associated with the passing "cold fronts" that occur during the winter season. The nearest coastal regions lie to the north and NNE of Discharge 4.

Table 2-1 - Yearly and monthly surface current speed and direction statistics at Discharge 4

SPEED (M/S)	YRLY	JAN	FEB	MAR	APR	MAY	JUN	JUL	AUG	SEP	OCT	NOV	DEC
Median	1.2	1.5	0.7	1.4	1.3	0.8	1.0	1.1	1.1	1.3	1.2	1.6	1.8
Mean	1.3	1.6	0.9	1.4	1.3	0.9	1.1	1.1	1.2	1.3	1.2	1.6	1.7
Std. deviation	0.0	0.5	0.6	0.6	0.6	0.6	0.6	0.6	0.6	0.6	0.6	0.5	0.5
Minimum	0.0	0.1	0.0	0.1	0.1	0.0	0.0	0.0	0.1	0.0	0.1	0.1	0.1
Maximum	4.8	3.1	2.9	3.4	3.0	3.0	4.8	4.2	3.1	3.6	3.8	3.0	3.1
Most frequent direction	SW	SW	SW	SW	SW	SW	SW	SW	SW	SW	SW	SW	SW
Strongest current direction	NNE	SSW	SSW	SW	SW	SW	NNE	SSW	SW	SW	NNE	SW	WSW

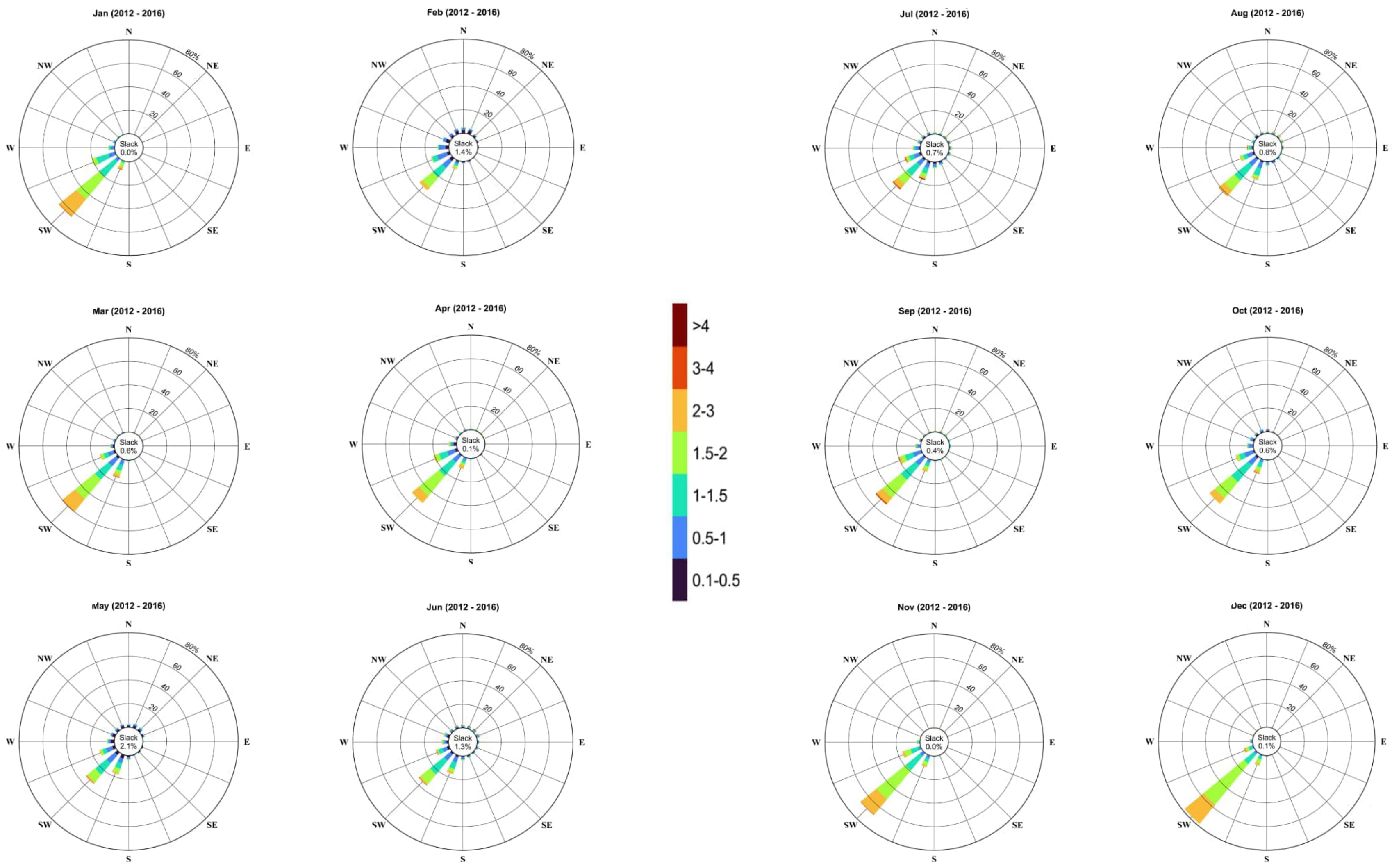

Figure 2-2 - Average monthly surface current roses at Discharge 4 for 2012 – 2016 (colour bar represents current speed in m/s)

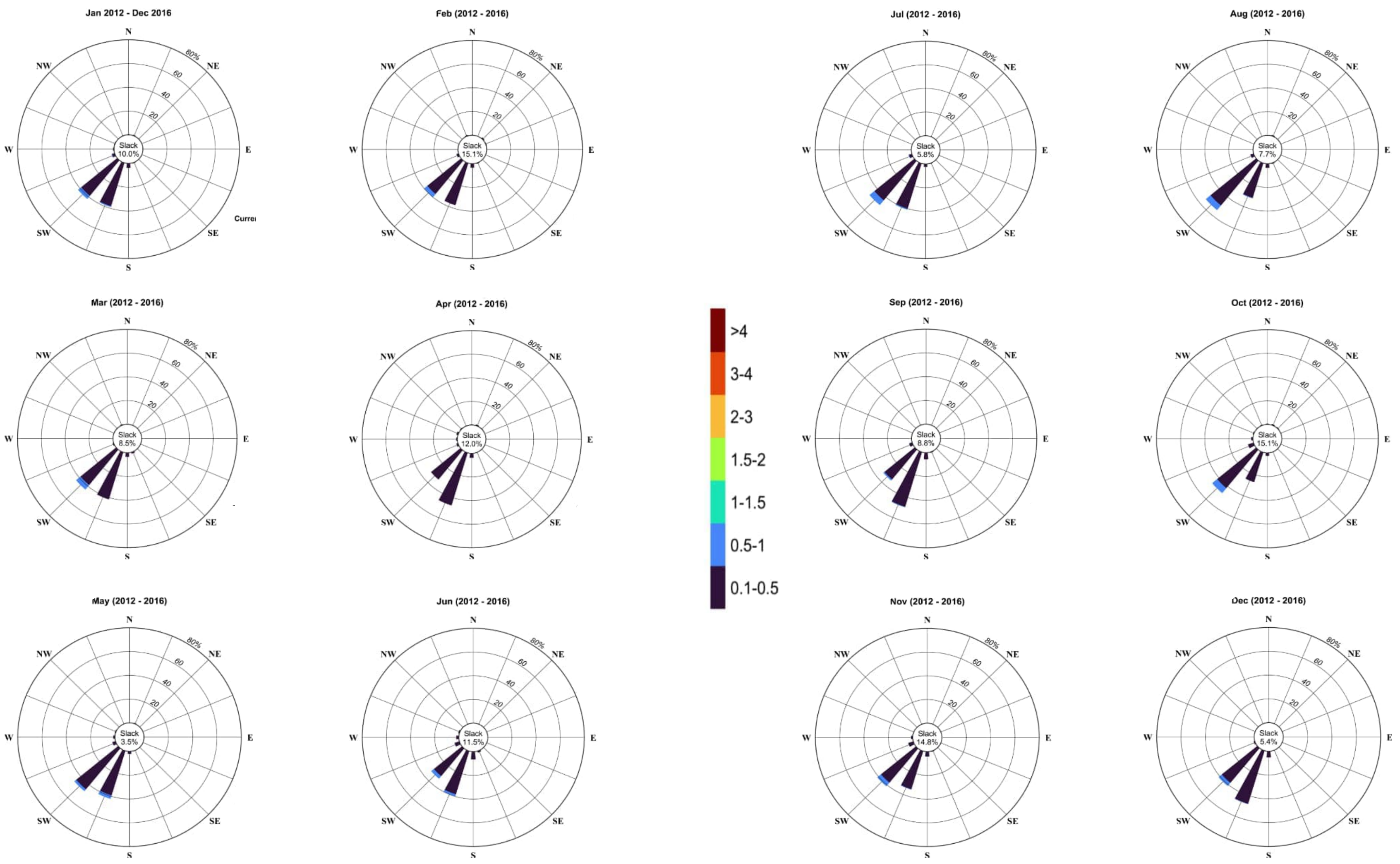

Figure 2-3 - Average monthly seabed current roses at Discharge 4 for 2012 – 2016 (colour bar represents current speed in m/s)

Figure 2-3 and Table 2-2 present the monthly current roses at the seabed for 2012 to 2016 and their associated statistics, respectively. The seabed currents present a low directional variability compared to the surface currents (Figure 2-3) and the dominant flow direction is to the southwest. Table 2-2 shows that the current speed is higher in the period from May to September (end of Q2 and Q3), and the dominant direction is largely SW.

Table 2-2 - Yearly and monthly seabed current speed and direction statistics at Discharge 4

SPEED (M/S)	YRLY	JAN	FEB	MAR	APR	MAY	JUN	JUL	AUG	SEP	OCT	NOV	DEC
Median	0.2	0.2	0.3	0.2	0.2	0.3	0.2	0.2	0.2	0.2	0.2	0.2	0.2
Mean	0.2	0.2	0.3	0.3	0.2	0.3	0.2	0.3	0.3	0.2	0.3	0.2	0.3
Std. deviation	0.0	0.1	0.1	0.1	0.1	0.1	0.1	0.1	0.1	0.1	0.1	0.1	0.1
Minimum	0.0	0.0	0.0	0.0	0.0	0.0	0.0	0.0	0.0	0.0	0.0	0.0	0.0
Maximum	0.9	0.6	0.6	0.6	0.5	0.7	0.7	0.9	0.6	0.5	0.6	0.7	0.6
Most frequent direction	SW	SW	SW	SSW	SSW	SW	SW	SW	SW	SSW	SW	SW	SSW
Strongest current direction	SW	SW	SW	SW	SW	SSW	SW	SW	SW	SW	SW	SW	SW

Figure 2-4 and Table 2-3 present the average monthly wind speed and direction statistics at 10 m elevation above sea level. Winds mainly occur in the east and west quadrants. The most frequent direction for stronger winds (>15 m/s) is from W over the five-year analysis period. The period from May to September also experiences mostly westerly winds.

Table 2-3 - Yearly and monthly wind speed and direction statistics at Discharge 4

SPEED (M/S)	YRLY	JAN	FEB	MAR	APR	MAY	JUN	JUL	AUG	SEP	OCT	NOV	DEC
Median	8.3	7.5	7.5	8.2	7.8	7.8	9.7	9.7	9.2	9.7	9.0	8.4	7.7
Mean	8.7	7.5	7.7	8.2	8.0	8.3	10.0	10.1	9.7	9.9	8.9	8.6	7.8
Std. deviation	0.6	3.1	3.1	3.1	3.6	3.9	4.7	4.6	4.5	3.9	3.3	3.5	3.1
Minimum	0.2	0.3	0.3	0.5	0.6	0.3	0.5	0.2	0.6	0.8	0.4	0.3	0.3
Maximum	27.8	19.4	19.4	24.1	20.5	19.7	27.8	23.8	24.9	23.5	22.1	23.0	23.2
Most frequent direction	W	E	ENE	ENE	ENE	W	W	W	W	W	ENE	WSW	E
Strongest wind direction	W	W	W	W	W	W	W	W	W	W	W	WSW	WSW

In summary, the current data at Discharge 4 for the years 2012 to 2016 indicates flow at the sea surface mostly towards the SW for all months with some variability in speed, and mostly constant SW flow direction and speed at the seabed for all months. There are periods of the year (Feb, May and June) when occurrences of surface flow towards the north are also observed. The months of May to September also see an increase in the frequency and strength of winds from the west compared to other times in the year

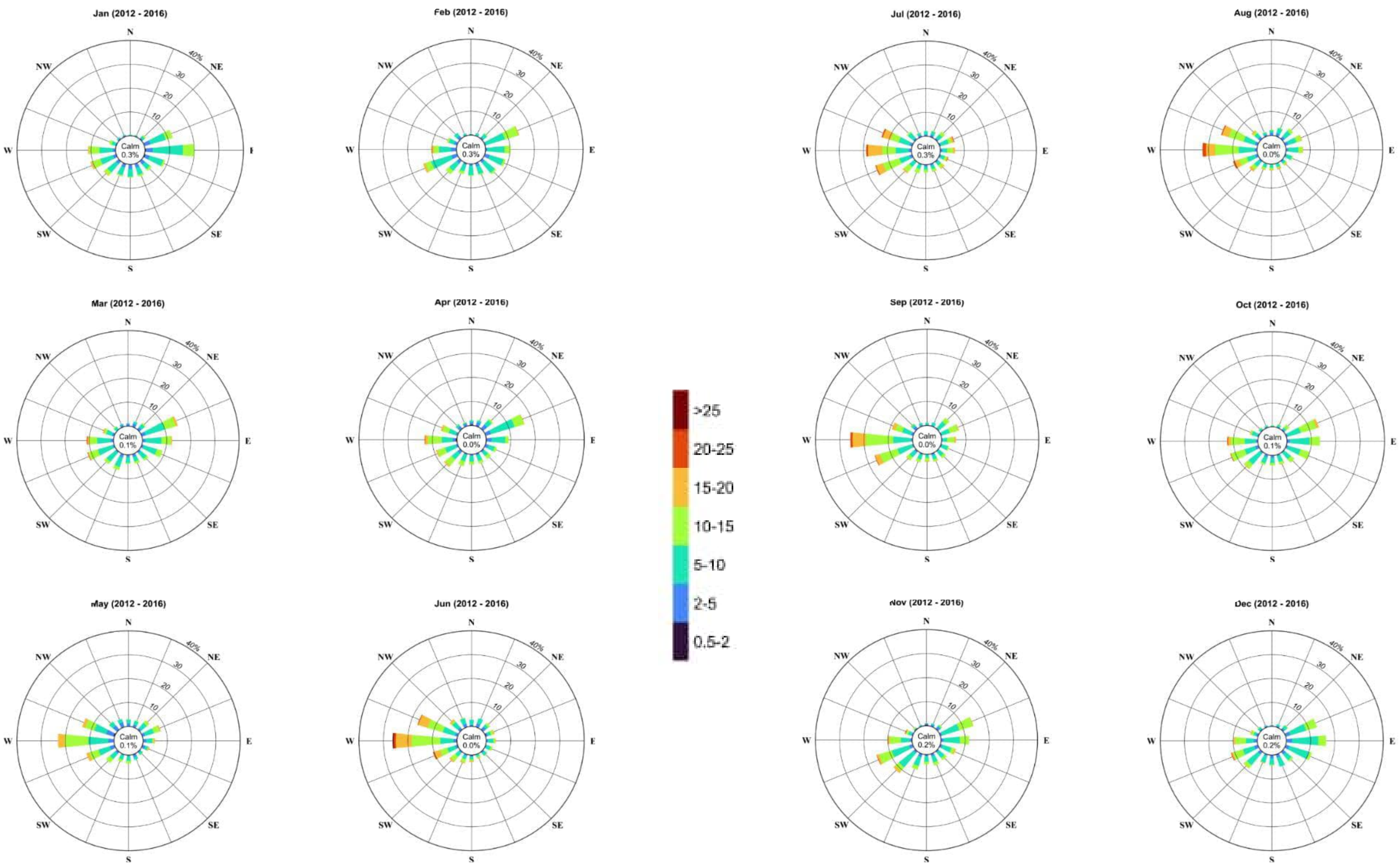

Figure 2-4 - Average monthly wind roses at Discharge 4 for 2012 – 2016 (colour bar represents wind speed in m/s)

2.1 SELECTION OF DRILLING DISCHARGE SIMULATION PERIODS FOR DISCHARGE 4

Simulations for the dispersion of drill cuttings and drilling muds from well drilling operations at Discharge 4 require the selection of a suitable model start time in each season. The methodology to identify the start time for each season in the present study involved an examination of the near-seabed and surface current speed and direction which would lead to maximum transport of drilling discharges towards the nearest Marine Protected Area (MPA). For Discharge 4, the nearest MPA is the Southwest Indian Seamount Marine Protected Area, whose NE corner lies approximately 18.1 km to the SW as shown in Figure 2-5.

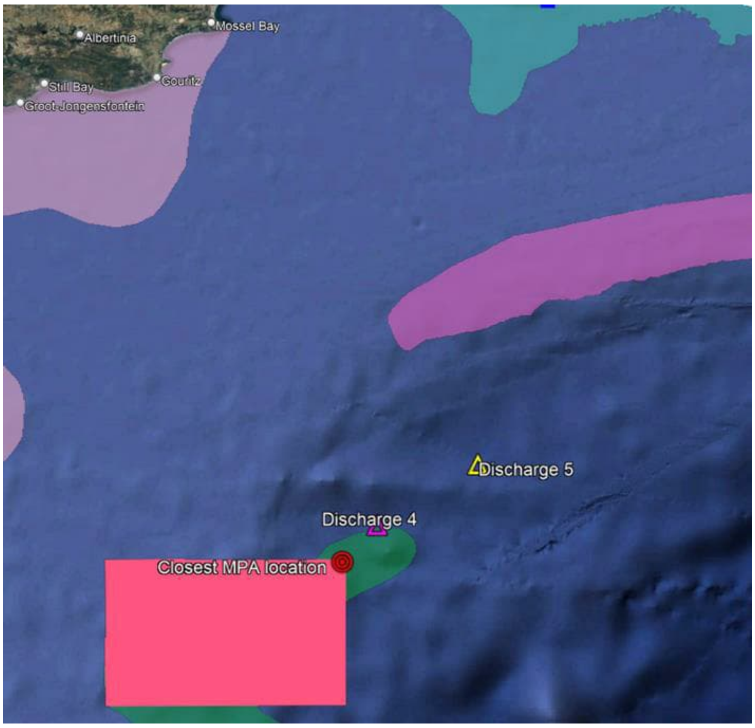

Figure 2-5 - Locations of Discharge 4 and Discharge 5 relative to Southwest Indian Seamount MPA

Based on information provided by Total, there are two distinct discharge phases over the course of drilling a well:

- Riserless phase – representing the first 270 hrs of operations, which includes 54 hrs of discharge at the seabed and 216 hrs (9 days) of no discharge. The total mass of cuttings and drilling mud released at the seabed during this phase is 1127 tonnes and 2326 tonnes, respectively.
- Riser phase – representing the next 344 hrs of drilling operations, which includes 200 hrs of discharge at 10 m below the water surface and 144 hrs (6 days) of no discharge. The total mass of cuttings and drilling mud released during this phase is 478 tonnes and 4100 tonnes, respectively.

Figure 2-6 illustrates the sequence of drilling discharge operations and the time spent for each operation. Figure 2-7 shows the quantity (mass in tonnes) of the drilling muds and cuttings discharged from the commencement of drilling to the final HPWBM mud discharge at the end of the 8.5" diameter section of the well.

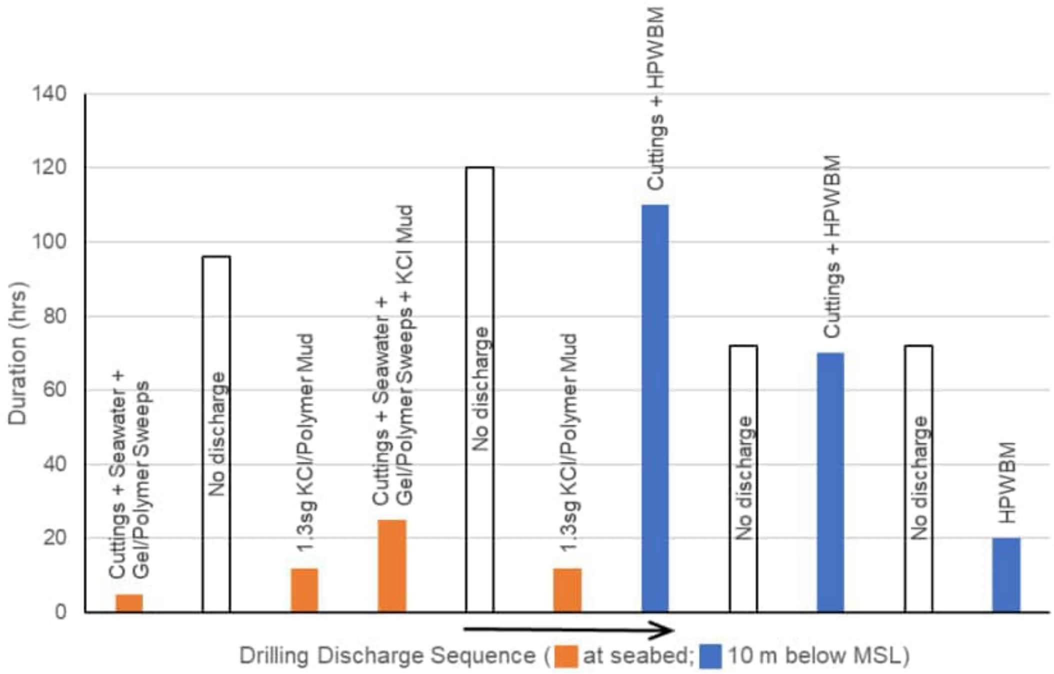

Figure 2-6 - Typical sequence and duration of mud and cuttings discharges

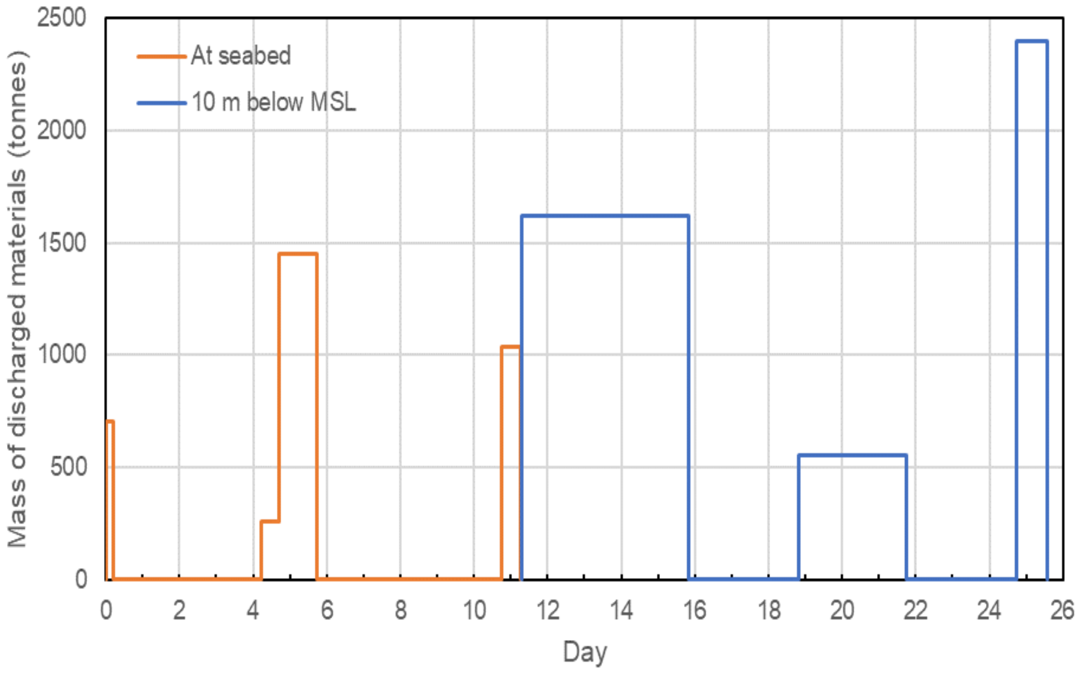

Figure 2-7 - Variation of discharged mud and cuttings quantity with time at drilling location

Since discharges at both the seabed and close to the water surface have the potential to reach the MPA, the current speed and direction data at these elevations were analysed to estimate the periods of time when the maximum combined seabed and surface transport of seawater towards the MPA occurred during each season in the 5-year metocean dataset. It is these periods that were used for the model simulations.

2.1.1 SEASON 1- DECEMBER TO FEBRUARY

Figure 2-8 presents summary statistics of current speed and direction at the seabed for each month of Season 1. Maximum current speed tends to mostly remain in the range of 0.4 m/s to 0.6 m/s, while average speed mostly lies in the 0.2 m/s to 0.3 m/s range. The most frequently occurring flow direction for the strongest 10% of the seabed currents is almost always to the southwest with a couple of months in 2016 showing stronger flows to the SSW. These observations are most probably related to large-scale perturbation of the Agulhas Currents due to the passing of a Natal Pulse.

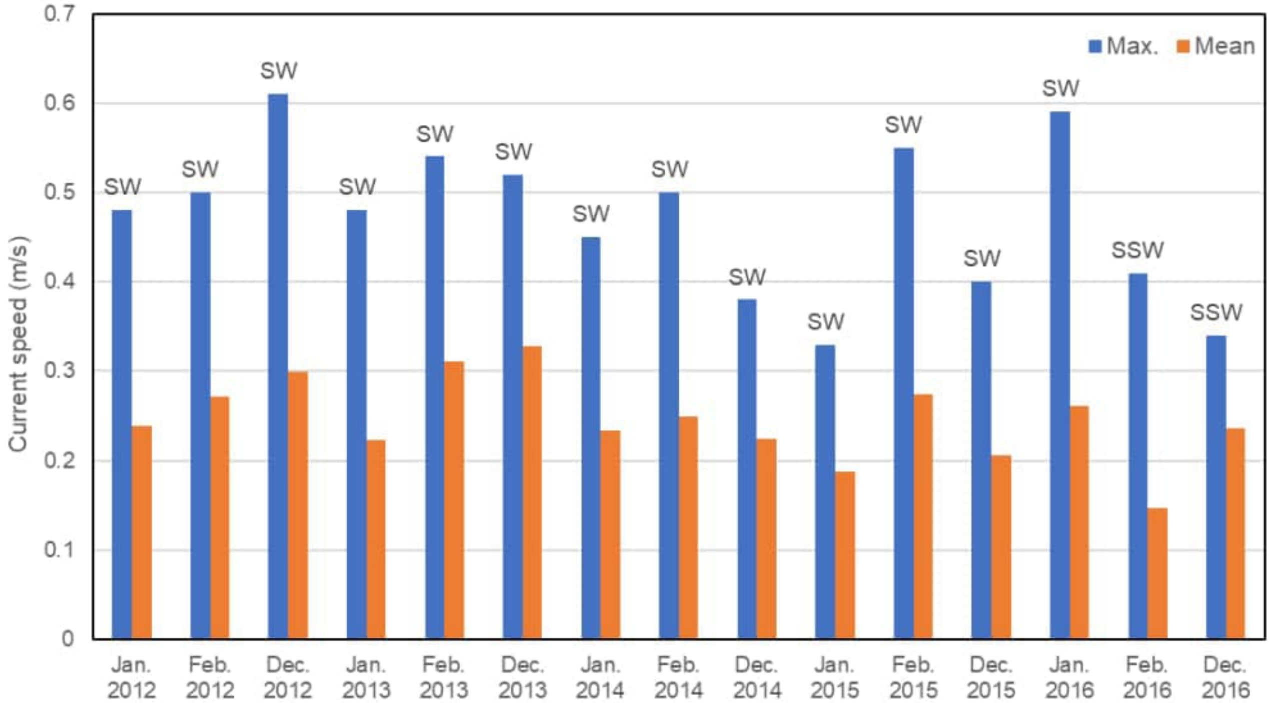

Figure 2-8 - Bottom current mean and maximum speed, and primary direction at Discharge 4 for Season 1 (2012 – 2016)

Figure 2-9 shows the current vectors at the seabed and surface at Discharge 4 for a 45-day period from 17 Dec 2015 to 30 Jan 2016. For clarity, the seabed and surface current vectors are scaled independently. The selected start time for the drilling discharge simulation in **Season 1 is 26 Dec 2015 at 1500 hrs**, as it yields the maximum combined seabed and surface transport of seawater towards the nearest MPA. The simulation periods for the riserless and riser phases of the well drilling are shown in Figure 2-9.

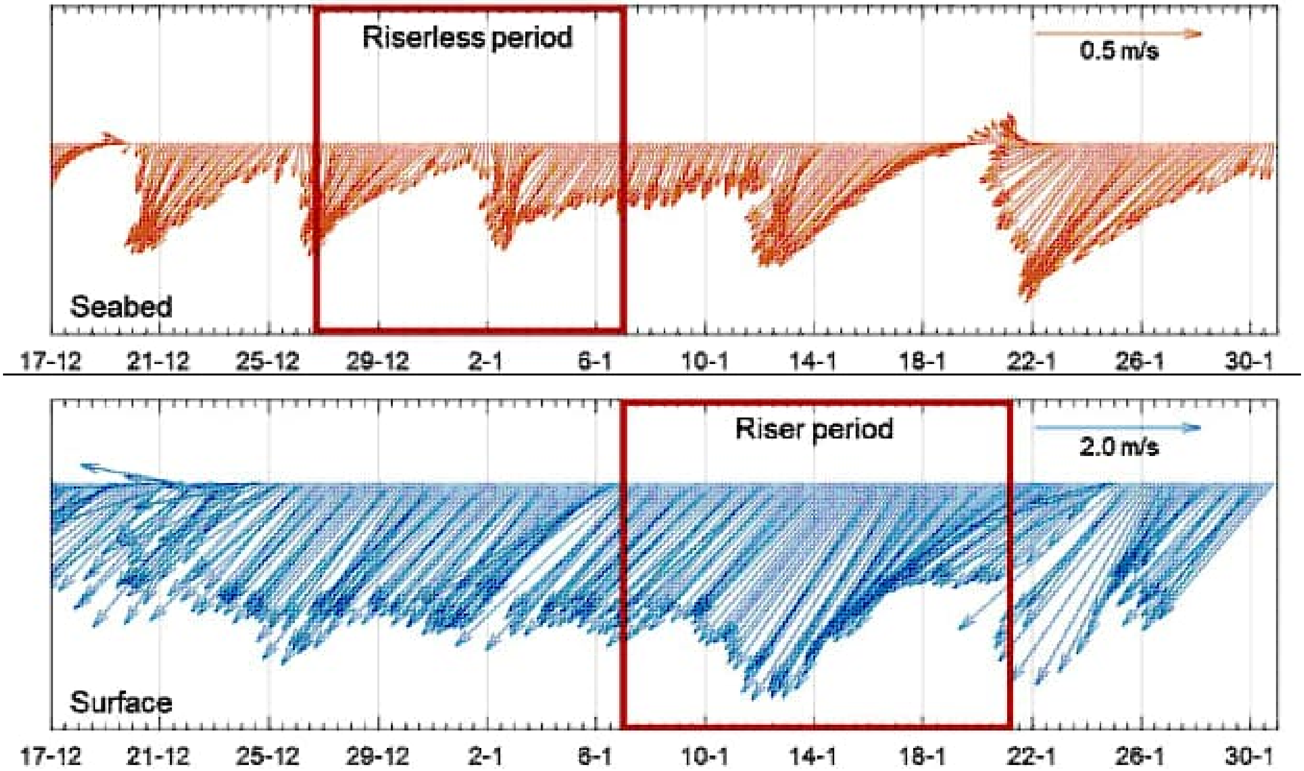

Figure 2-9 - Seabed and surface current vectors at Discharge 4 from 17 Dec 2015 to 30 Jan 2016 with boxes showing the period selected for drilling discharge simulation in Season 1

2.1.2 SEASON 2- MARCH TO MAY

Figure 2-10 presents summary statistics of current speed and direction at the seabed for each month of Season 2. In comparison with Season 1, there is a wider range in the maximum current speed which typically varies between 0.3 m/s to 0.6 m/s. The maximum speed of approximately 0.7 m/s occurs in May 2012. Average current speed is like Season 1 and mostly lies in the 0.2 m/s to 0.3 m/s range. The most frequently occurring flow direction for the strongest 10% of the seabed currents is almost always to the southwest although 2012 and April 2016 had stronger flows to the SSW.

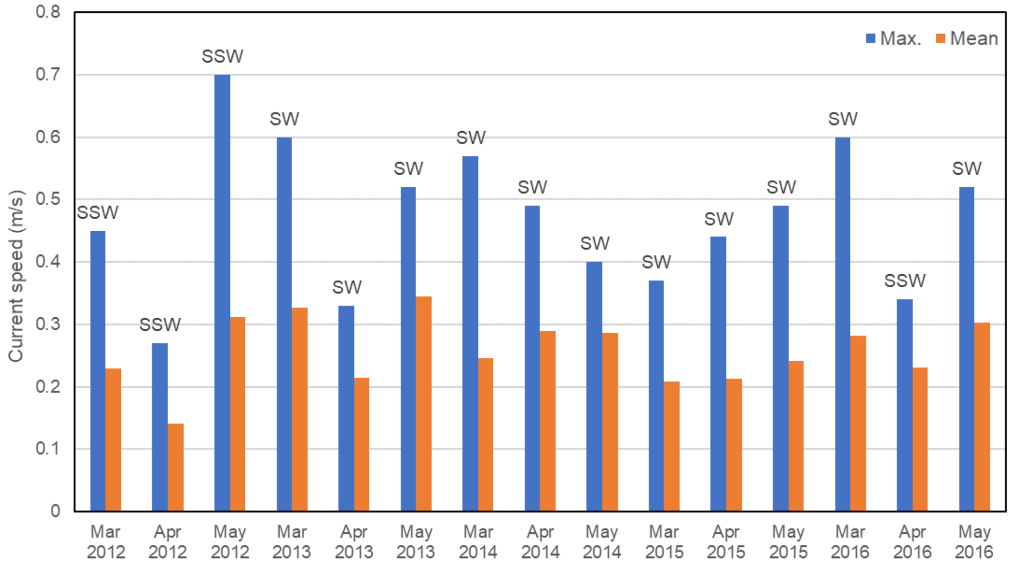

Figure 2-10 - Bottom current mean and maximum speed, and primary direction at Discharge 4 for Season 2 (2012 – 2016)

Figure 2-11 shows the current vectors at the seabed and surface at Discharge 4 for a 45-day period from 3 Mar 2013 to 16 Apr 2013. For clarity, the seabed and surface current vectors are scaled independently. The selected start time for the drilling discharge simulation in **Season 2 is 12 Mar 2013 at 0900 hrs**, as it yields the maximum combined seabed and surface transport of seawater towards the nearest MPA. The simulation periods for the riserless and riser phases of the well drilling are shown in Figure 2-11.

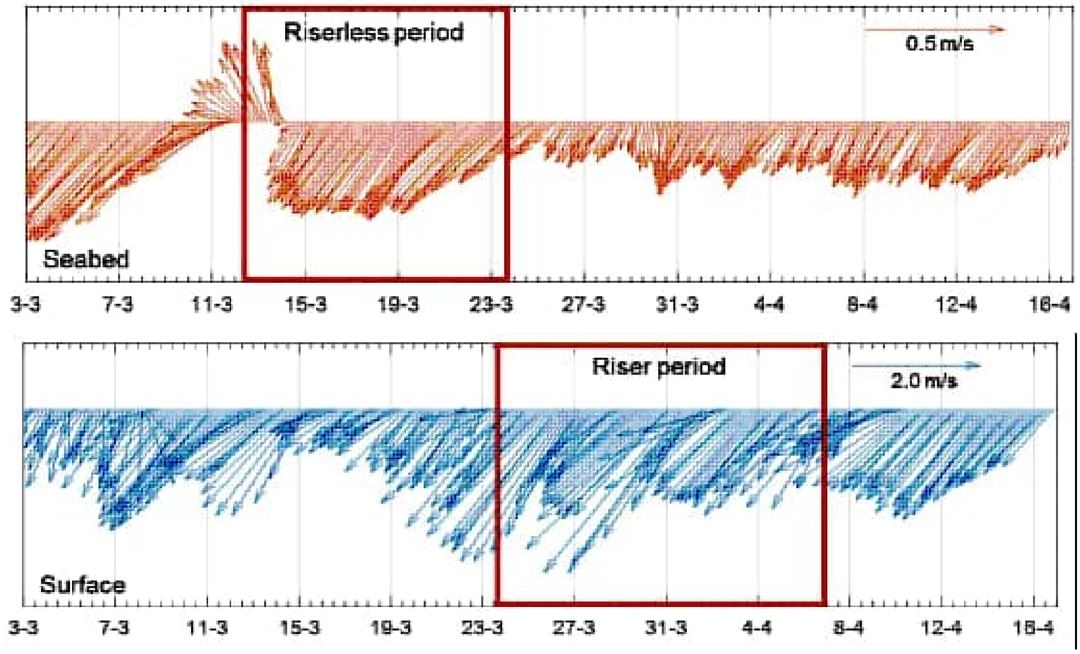

Figure 2-11 - Seabed and surface current vectors at Discharge 4 from 3 Mar 2013 to 16 Apr 2013 with boxes showing the period selected for drilling discharge simulation in Season 2

2.1.3 SEASON 3- JUNE TO AUGUST

Figure 2-12 presents summary statistics of current speed and direction at the seabed for each month of Season 3. The maximum current speed typically varies between 0.4 m/s to 0.6 m/s with a notable outlier of approximately 0.85 m/s occurring in July 2016. Average current speed mainly lies between 0.2 m/s and 0.3 m/s. The most frequently occurring flow direction for the strongest 10% of the seabed currents is almost always to the southwest except in July 2012 when this direction was to the SSW.

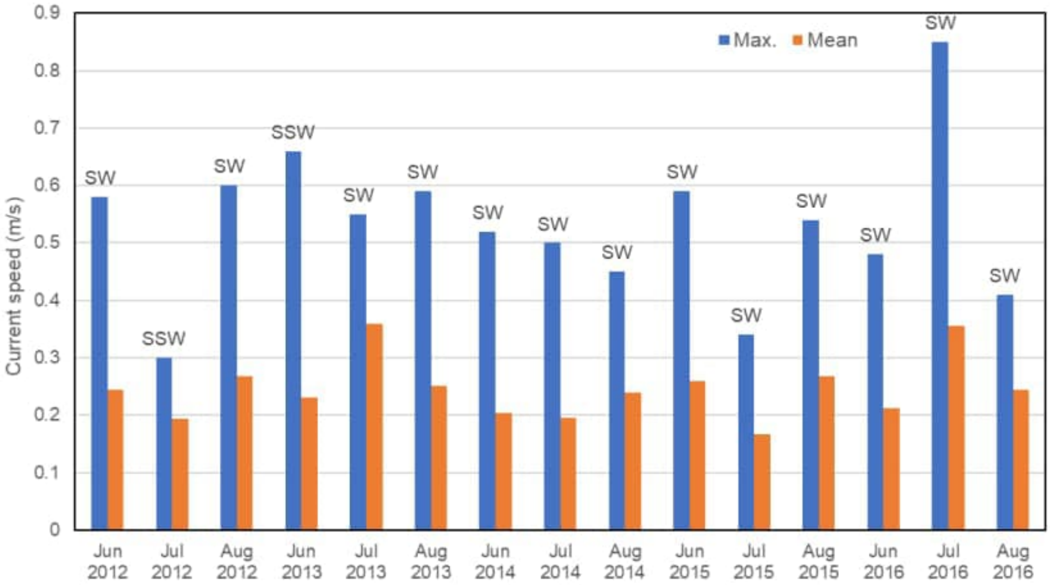

Figure 2-12 - Bottom current mean and maximum speed, and primary direction at Discharge 4 for Season 3 (2012 – 2016)

Figure 2-13 shows the current vectors at the seabed and surface at Discharge 4 for a 45-day period from 5 Aug 2016 to 18 Sep 2016. For clarity, the seabed and surface current vectors are scaled independently. The selected start time for the drilling discharge simulation in **Season 3 is 14 Aug 2016 at 0900 hrs**, as it yields the maximum combined seabed and surface transport of seawater towards the nearest MPA. The simulation periods for the riserless and riser phases of the well drilling are shown in Figure 2-13.

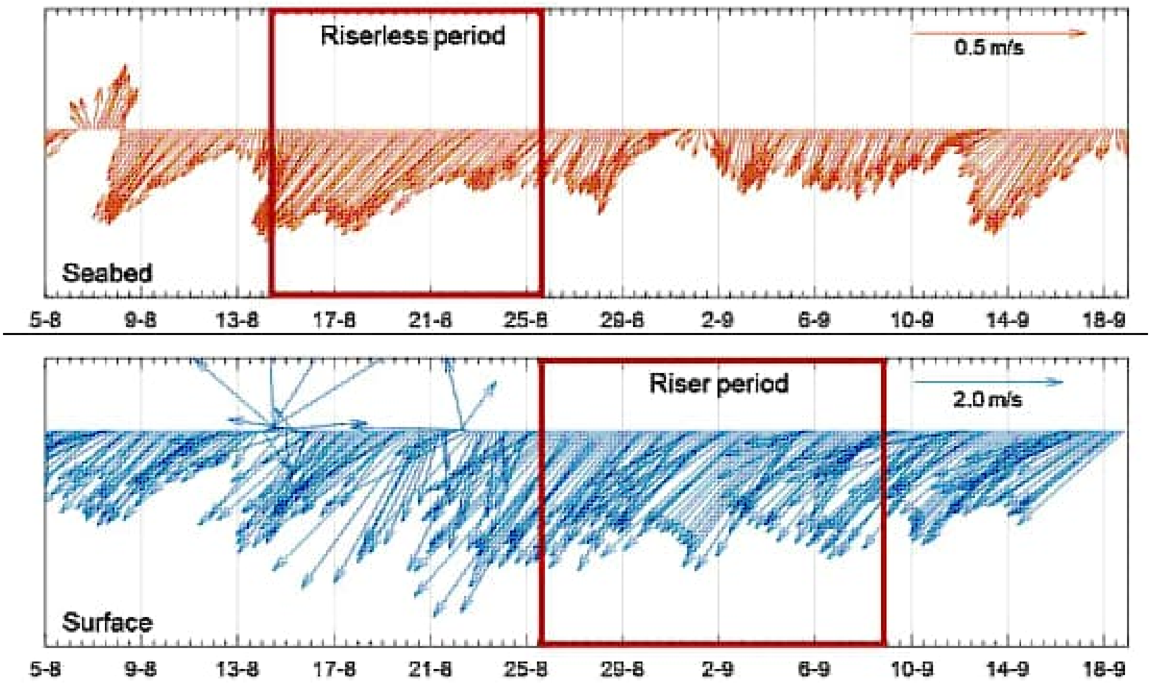

Figure 2-13 - Seabed and surface current vectors at Discharge 4 from 5 Aug 2016 to 18 Sep 2016 with boxes showing the period selected for drilling discharge simulation in Season 3

2.1.4 SEASON 4- SEPTEMBER TO NOVEMBER

Figure 2-14 presents summary statistics of current speed and direction at the seabed for each month of Season 4. The maximum current speed typically varies between 0.4 m/s to 0.5 m/s although Oct and Nov 2012 contain maximum speeds exceeding 0.6 m/s. Average current speed mainly lies between 0.2 m/s and 0.3 m/s. The most frequently occurring flow direction for the strongest 10% of the seabed currents is almost always to the southwest except in Sep and Nov 2016 when this direction was to the SSW.

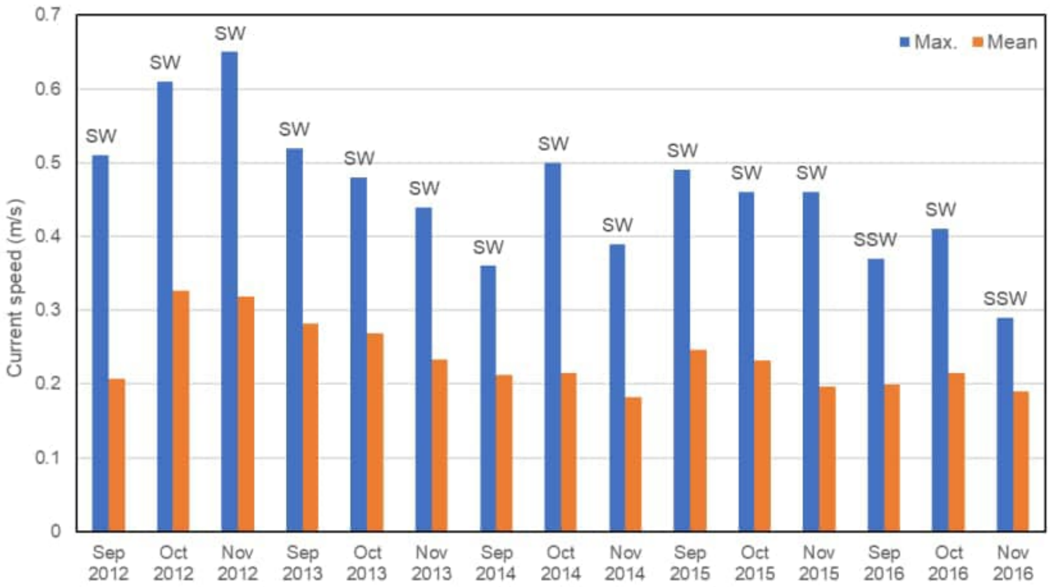

Figure 2-14 - Bottom current mean and maximum speed, and primary direction at Discharge 4 for Season 4 (2012 – 2016)

Figure 2-15 shows the current vectors at the seabed and surface at Discharge 4 for a 45-day period from 10 Oct 2014 to 23 Nov 2014. For clarity, the seabed and surface current vectors are scaled independently. The selected start time for the drilling discharge simulation in **Season 4 is 19 Oct 2014 at 1200 hrs**, as it yields the maximum combined seabed and surface transport of seawater towards the nearest MPA. The simulation periods for the riserless and riser phases of the well drilling are shown in Figure 2-15.

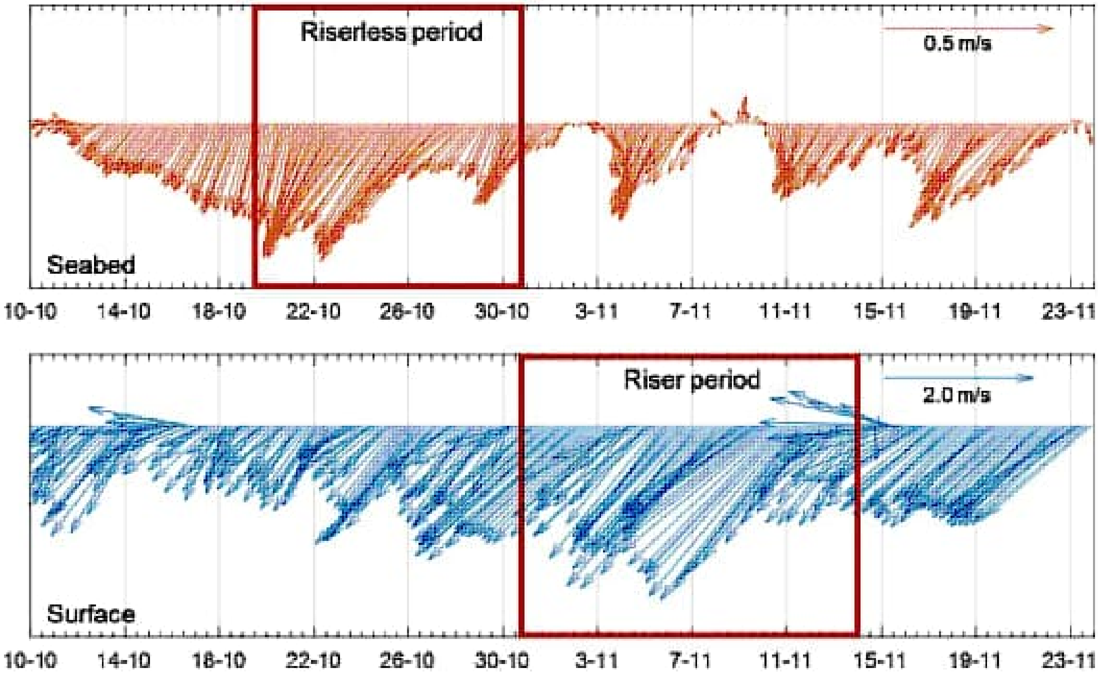

Figure 2-15 - Seabed and surface current vectors at Discharge 4 from 10 Oct 2014 to 23 Nov 2014 with boxes showing the period selected for drilling discharge simulation in Season 4

3 DISCHARGE 5

The average metocean data at the Discharge 5 location over the five-year data is presented in Figure 3-1

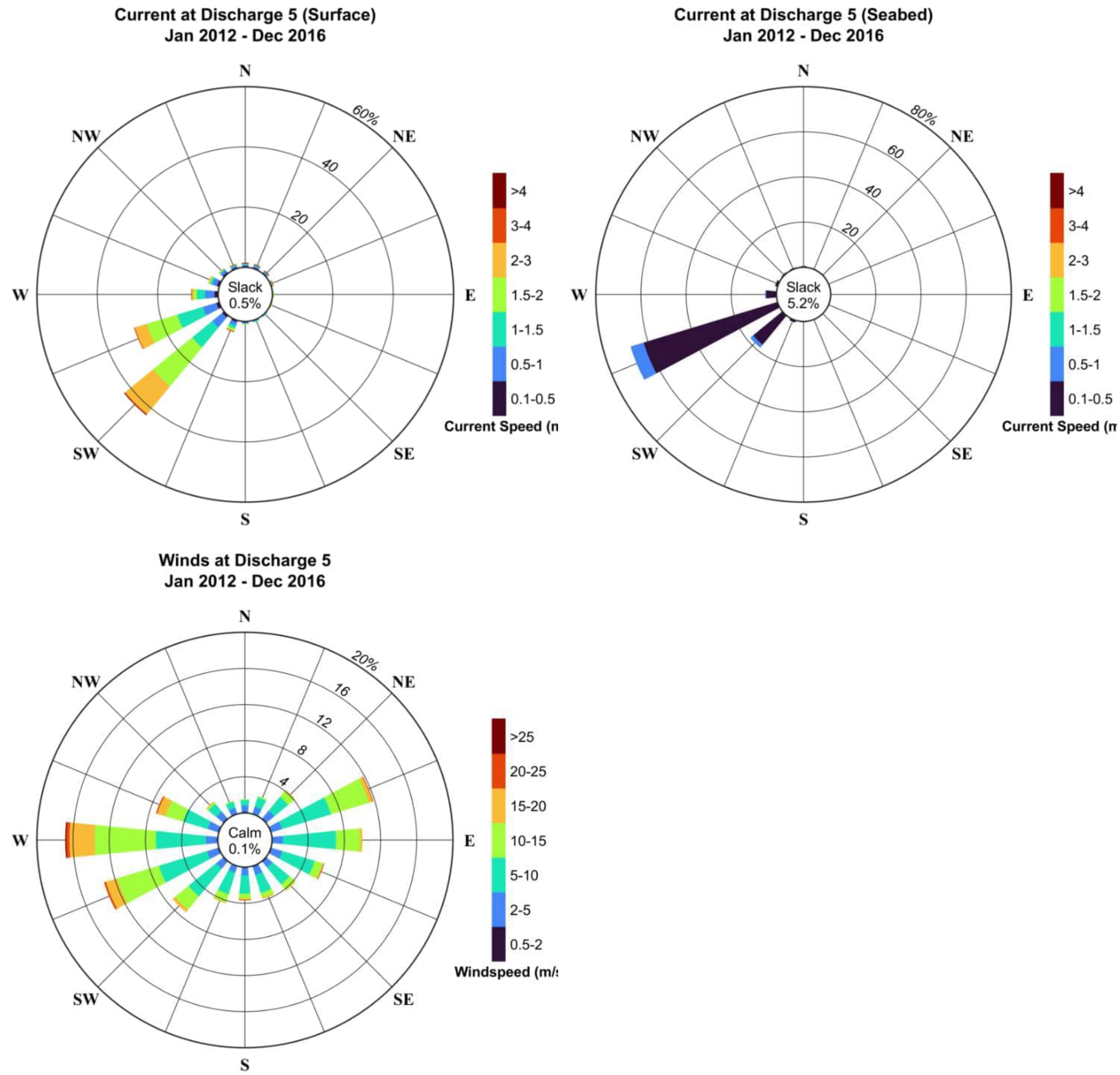

Figure 3-1 - Average annual current and wind speed roses at Discharge 5 for 2012-2016

The dominant direction for surface current at Discharge 5 is towards SW and WSW for the 2012 to 2016 period with an occurrence probability greater than approximately 70%. Current speeds can reach up to 4 m/s at the surface.

Dominant current direction at the seabed is towards WSW and SW for approximately 80% of the time. Part of the drill cuttings are discharged at the seabed, which makes seabed currents an important factor in drilling discharge modelling.

Dominant wind directions are from between WSW and WNW (approximately 36% of the time), and ENE and ESE (approximately 28% of the time). Wind speeds are mostly in the 5 m/s to 20 m/s range.

Figure 3-2 and Table 3-1 present the average monthly current roses at the surface for 2012 to 2016 and the associated statistics, respectively. The surface current at Discharge 5 is predominantly directed to the southwest in all months. There are periods of the year (Feb, May and June) when occurrences of flow towards the north are also observed. The peak monthly surface current speed of 4.9 m/s to N, and 4.4 m/s to SW occur in June and July, respectively. The nearest coastal regions lie to the north of Discharge 5.

Table 3-1 - Yearly and monthly surface current speed and direction statistics at Discharge 5

SPEED (M/S)	YRLY	JAN	FEB	MAR	APR	MAY	JUN	JUL	AUG	SEP	OCT	NOV	DEC
Median	1.4	1.6	0.9	1.7	1.4	1.1	1.2	1.1	1.3	1.4	1.4	1.8	1.9
Mean	1.4	1.6	1.0	1.6	1.4	1.1	1.2	1.2	1.3	1.4	1.4	1.8	1.9
Std. deviation	0.1	0.6	0.6	0.6	0.6	0.6	0.6	0.7	0.6	0.6	0.6	0.5	0.4
Minimum	0.0	0.1	0.0	0.1	0.1	0.0	0.0	0.0	0.0	0.1	0.1	0.1	0.4
Maximum	4.9	3.0	2.6	3.6	3.1	2.8	4.9	4.4	4.1	3.5	3.8	3.1	3.1
Most frequent direction	SW	SW	SW	SW	SW	SW	SW	SW	SW	WSW	SW	SW	SW
Strongest current direction	N	SW	SW	SW	WSW	SW	N	SW	SW	SW	NNE	WSW	W

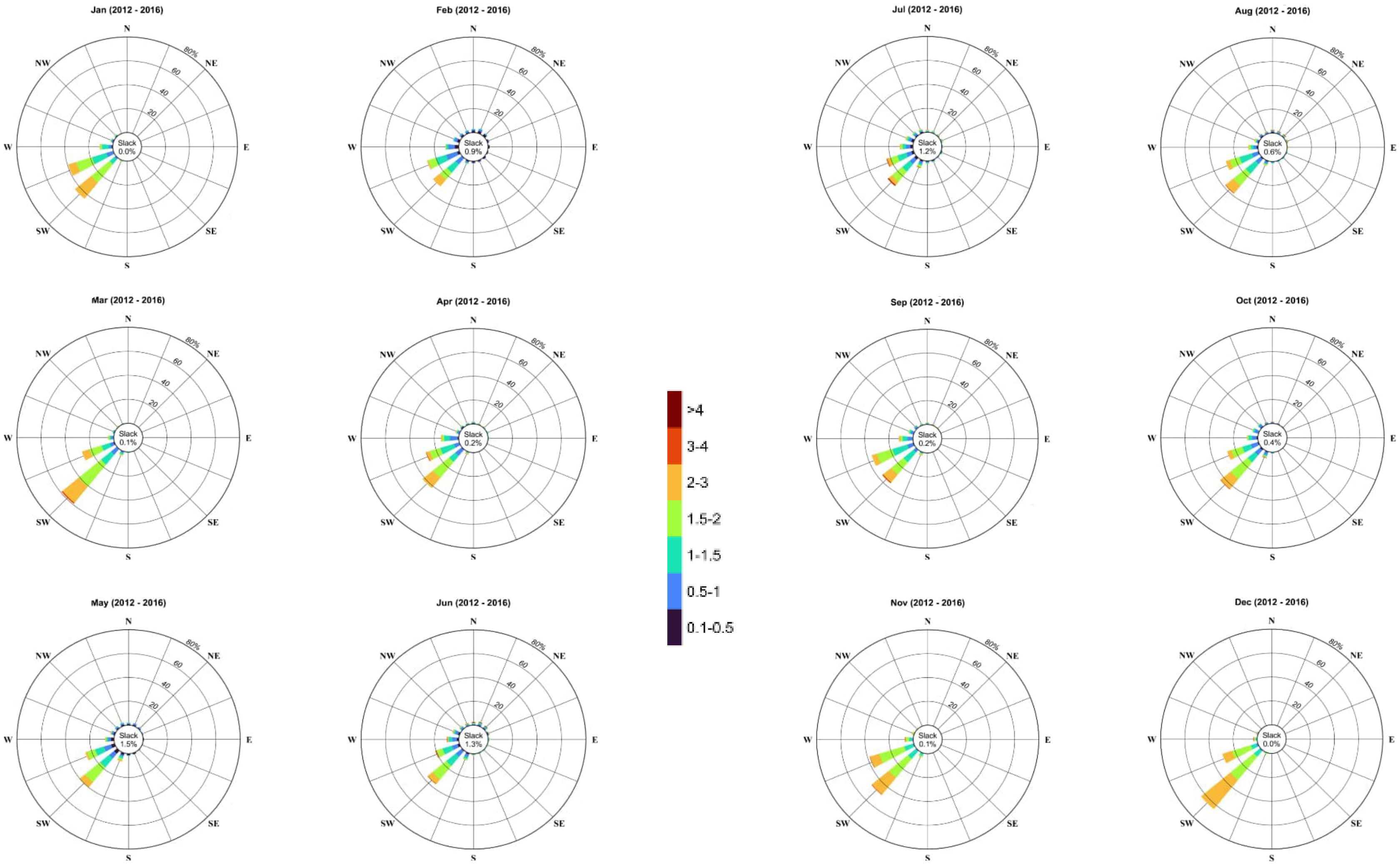

Figure 3-2 - Average monthly surface current roses at Discharge 5 for 2012 – 2016 (colour bar represents current speed in m/s)

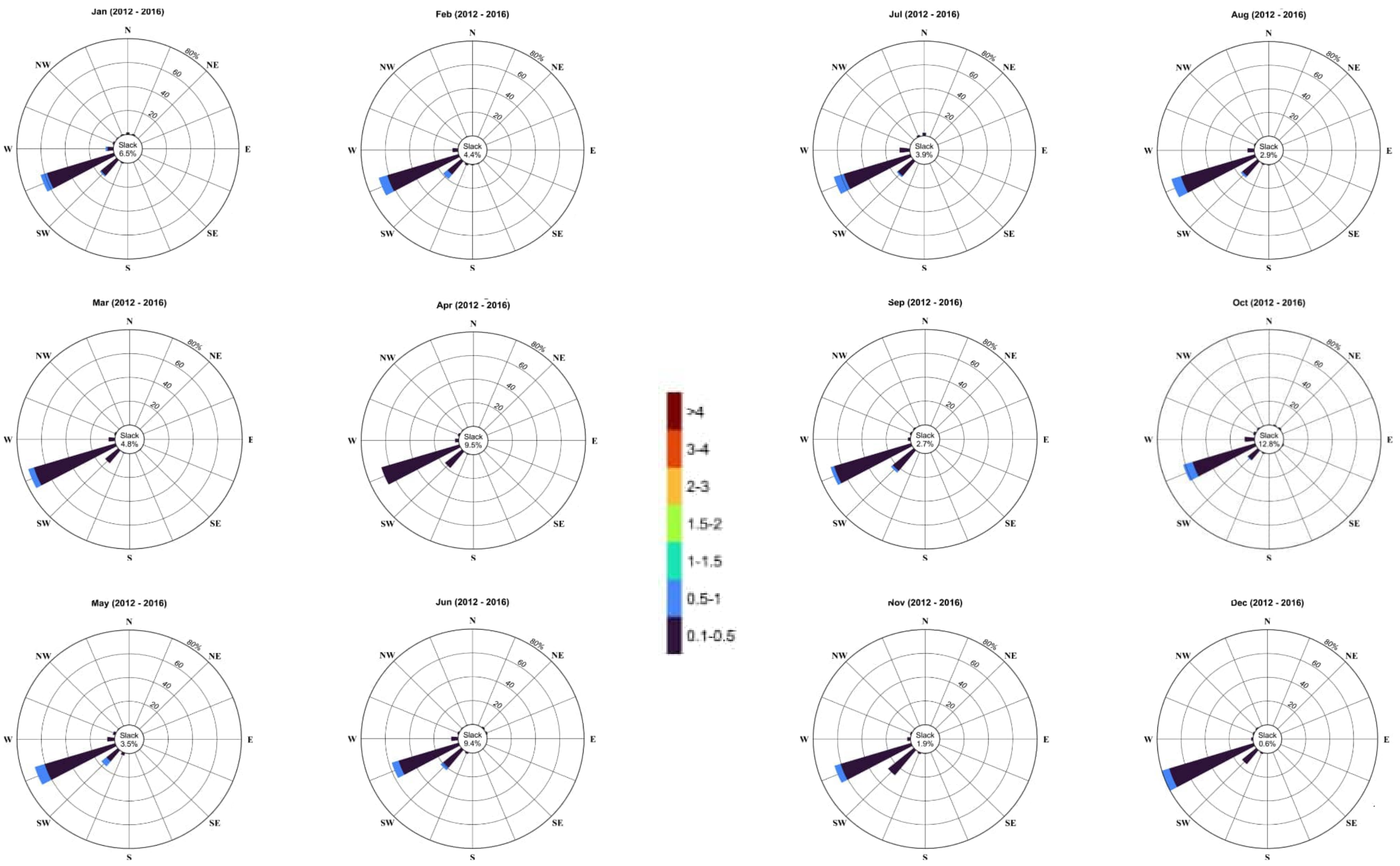

Figure 3-3 - Average monthly seabed current roses at Discharge 5 for 2012 – 2016 (colour bar represents current speed in m/s)

Figure 3-3 and Table 3-2 present the monthly current roses at the seabed for 2012 to 2016 and their associated statistics, respectively. The seabed currents present a low directional variability similar to the surface currents (Figure 3-3) and the dominant flow direction is to the WSW.

Table 3-2 - Yearly and monthly seabed current speed and direction statistics at Discharge 5

SPEED (M/S)	YRLY	JAN	FEB	MAR	APR	MAY	JUN	JUL	AUG	SEP	OCT	NOV	DEC
Median	0.3	0.3	0.4	0.3	0.3	0.4	0.3	0.3	0.3	0.3	0.3	0.3	0.3
Mean	0.3	0.3	0.3	0.3	0.3	0.4	0.3	0.3	0.3	0.3	0.3	0.3	0.3
Std. deviation	0.0	0.1	0.1	0.1	0.1	0.1	0.1	0.1	0.1	0.1	0.1	0.1	0.1
Minimum	0.0	0.0	0.0	0.0	0.0	0.0	0.0	0.0	0.0	0.0	0.0	0.0	0.1
Maximum	0.8	0.6	0.7	0.6	0.5	0.7	0.7	0.8	0.7	0.6	0.6	0.6	0.7
Most frequent direction	WSW	WSW	WSW	WSW	WSW	WSW	WSW	WSW	WSW	WSW	WSW	WSW	WSW
Strongest current direction	WSW	WSW	SW	WSW	WSW	SW	WSW	WSW	WSW	WSW	WSW	WSW	WSW

Figure 3-4 and Table 3-3 present the average monthly wind speed and direction statistics at 10 m elevation above sea level. Winds mainly occur in the east and west quadrants. The most frequent direction for stronger winds (>15 m/s) is from W over the five-year analysis period. The period from May to September also experiences mostly westerly winds.

Table 3-3 - Table 4: Yearly and monthly wind speed and direction statistics at Discharge 5

SPEED (M/S)	YRLY	JAN	FEB	MAR	APR	MAY	JUN	JUL	AUG	SEP	OCT	NOV	DEC
Median	8.4	7.5	7.5	8.2	7.7	7.7	9.6	9.6	9.2	9.7	8.9	8.6	7.8
Mean	8.7	7.5	7.6	8.3	8.0	8.2	9.9	10.1	9.6	9.9	8.9	8.6	7.8
Std. deviation	0.6	3.1	3.2	3.2	3.6	4.0	4.8	4.6	4.5	4.0	3.4	3.6	3.1
Minimum	0.1	0.2	0.3	0.4	0.3	0.3	0.4	0.3	0.5	0.4	0.6	0.6	0.1
Maximum	27.8	19.8	19.5	24.1	19.0	18.8	27.8	24.3	26.0	23.7	23.0	22.5	21.9
Most frequent direction	WSW	E	ENE	ENE	ENE	W	W	W	W	W	ENE	WSW	E
Strongest wind direction	W	W	W	W	W	W	W	ENE	W	W	W	W	WSW

In summary, the current data at Discharge 5 for the years 2012 to 2016 indicates flow at the sea surface mostly towards the SW for all months with some variability in speed, and mostly constant SW flow direction and speed at the seabed for all months. There are periods of the year (Feb, May and June) when occurrences of surface flow towards the north are also observed. The months of May to September also see an increase in the frequency and strength of winds from the west compared to other times in the year.

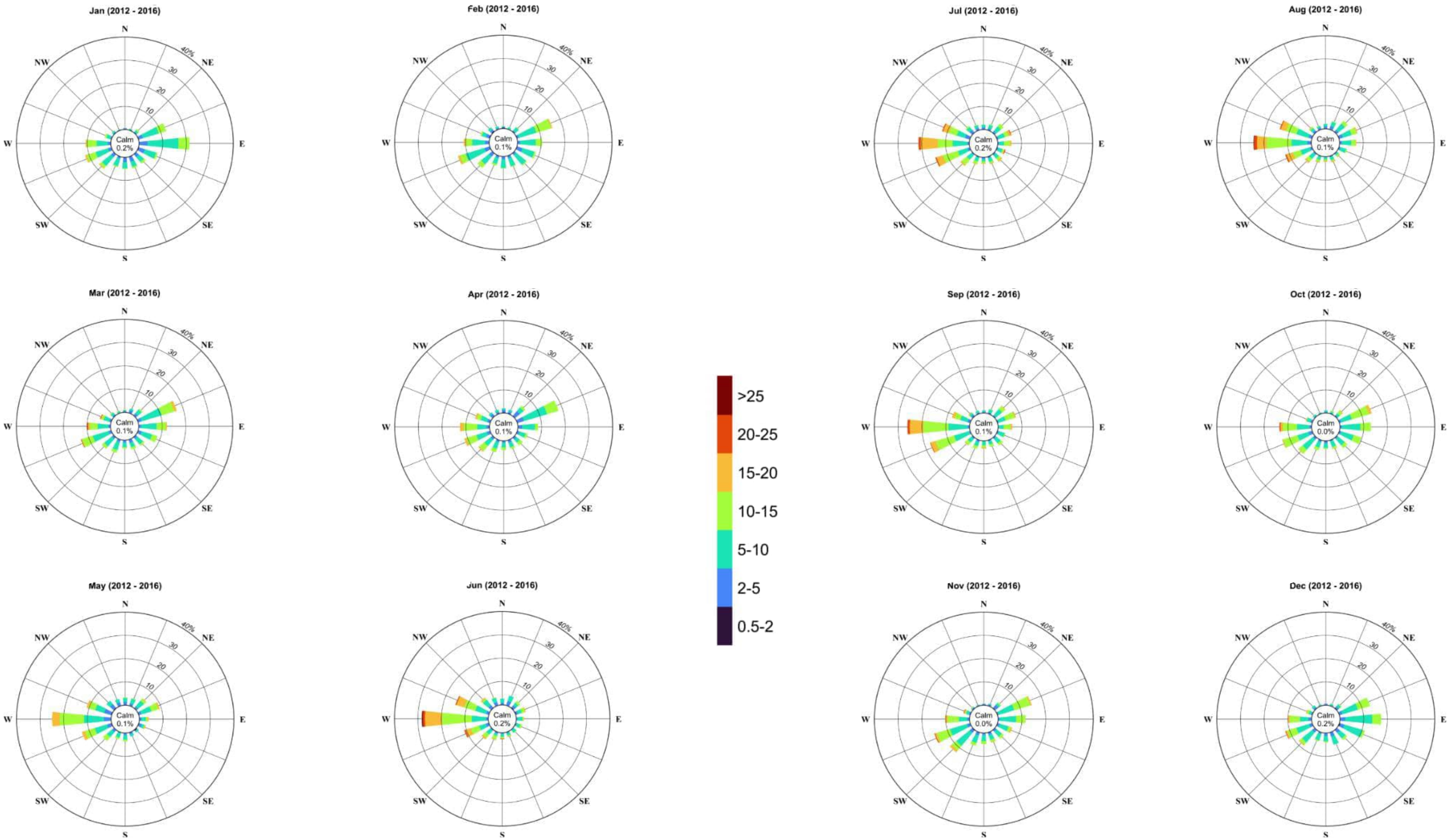

Figure 3-4 - Average monthly wind roses at Discharge 5 for 2012 – 2016 (colour bar represents wind speed in m/s)

3.1 SELECTION OF DRILLING DISCHARGE SIMULATION PERIODS FOR DISCHARGE 5

The methodology for identifying a suitably conservative start time for the drilling discharge simulations at Discharge 5 for Seasons 1 to 4 is identical to that described in Section 2.1. Similar to Discharge 4, the nearest MPA to Discharge 5 is the Southwest Indian Seamount Marine Protected Area, whose NE corner lies approximately 60.4 km to the SW as shown in Figure 2-5.

The two stages of well drilling at Discharge 5 are the same as for Discharge 4 and repeated below:

- Riserless phase – representing the first 270 hrs of operations, which includes 54 hrs of discharge at the seabed and 216 hrs (9 days) of no discharge. The total mass of cuttings and drilling mud released at the seabed during this phase is 1127 tonnes and 2326 tonnes, respectively.
- Riser phase – representing the next 344 hrs of drilling operations, which includes 200 hrs of discharge at 10 m below the water surface and 144 hrs (6 days) of no discharge. The total mass of cuttings and drilling mud released during this phase is 478 tonnes and 4100 tonnes, respectively.

The current speed and direction data at the seabed and ocean surface were analysed at Discharge 5 to estimate the periods of time when the maximum combined seabed and surface transport of seawater towards the MPA occurred during each season in the 5-year metocean dataset.

3.1.1 SEASON 1- DECEMBER TO FEBRUARY

Figure 3-5 presents summary statistics of current speed and direction at the seabed for each month of Season 1. Maximum current speed tends to mostly remain in the range of 0.5 m/s to 0.7 m/s, while average speed mostly lies in the 0.3 m/s to 0.4 m/s range. The most frequently occurring flow direction for the strongest 10% of the seabed currents is almost always to the WSW with a couple of months in 2014 and 2016 showing stronger flows to the W and SW.

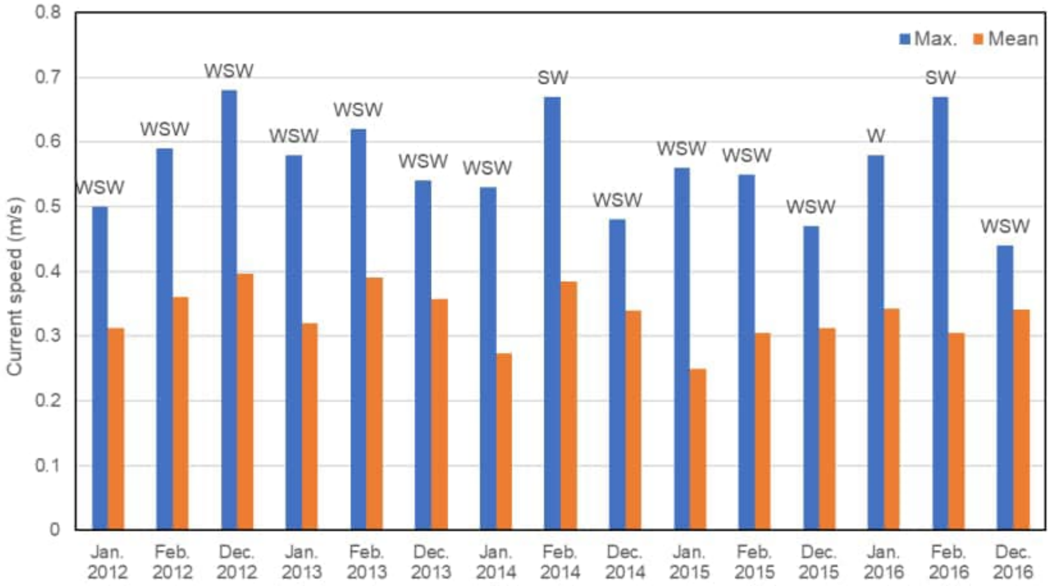

Figure 3-5 - Bottom current mean and maximum speed, and primary direction at Discharge 5 for Season 1 (2012 – 2016)

Figure 3-6 shows the current vectors at the seabed and surface at Discharge 5 for a 45-day period from 14 Dec 2015 to 27 Jan 2016. For clarity, the seabed and surface current vectors are scaled independently. The selected start time for the drilling discharge simulation in **Season 1 is 24 Dec 2015 at 0300 hrs**, as it yields the maximum combined seabed and surface transport of seawater towards the nearest MPA. The simulation periods for the riserless and riser phases of the well drilling are shown in Figure 3-6.

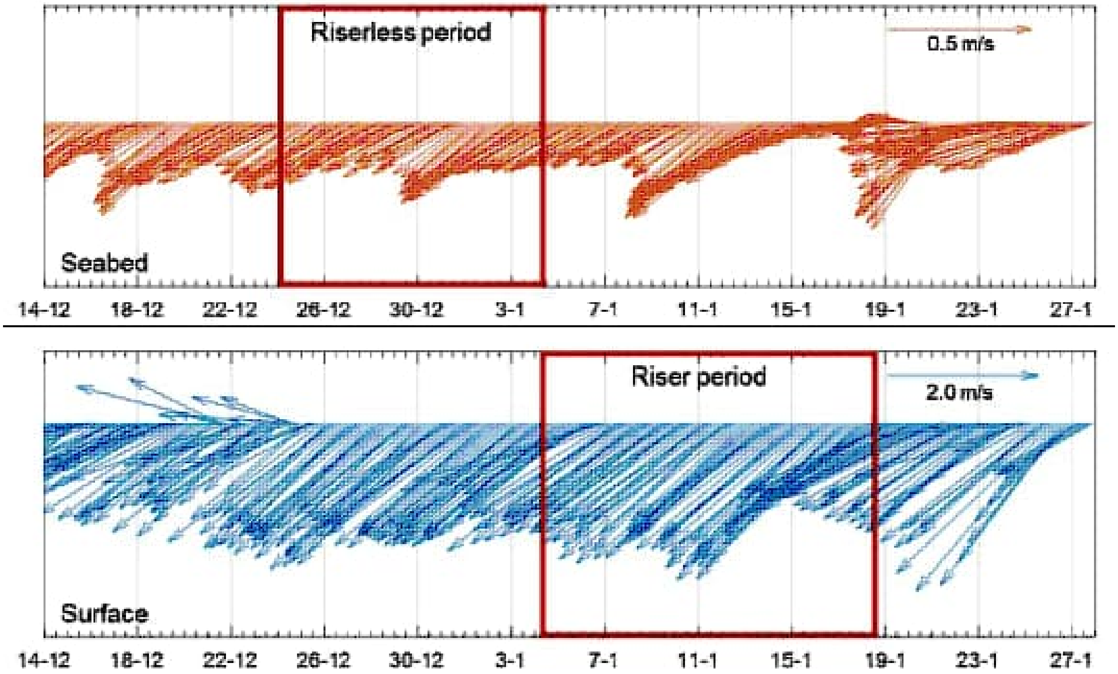

Figure 3-6 - Seabed and surface current vectors at Discharge 5 from 14 Dec 2015 to 27 Jan 2016 with boxes showing the period selected for drilling discharge simulation in Season 1

3.1.2 SEASON 2- MARCH TO MAY

Figure 3-7 presents summary statistics of current speed and direction at the seabed for each month of Season 2. Maximum current speed tends to mostly remain in the range of 0.5 m/s to 0.7 m/s, while average speed mostly lies in the 0.2 m/s to 0.4 m/s range. The most frequently occurring flow direction for the strongest 10% of the seabed currents is almost always to the WSW with a couple of months showing stronger flows to the SW.

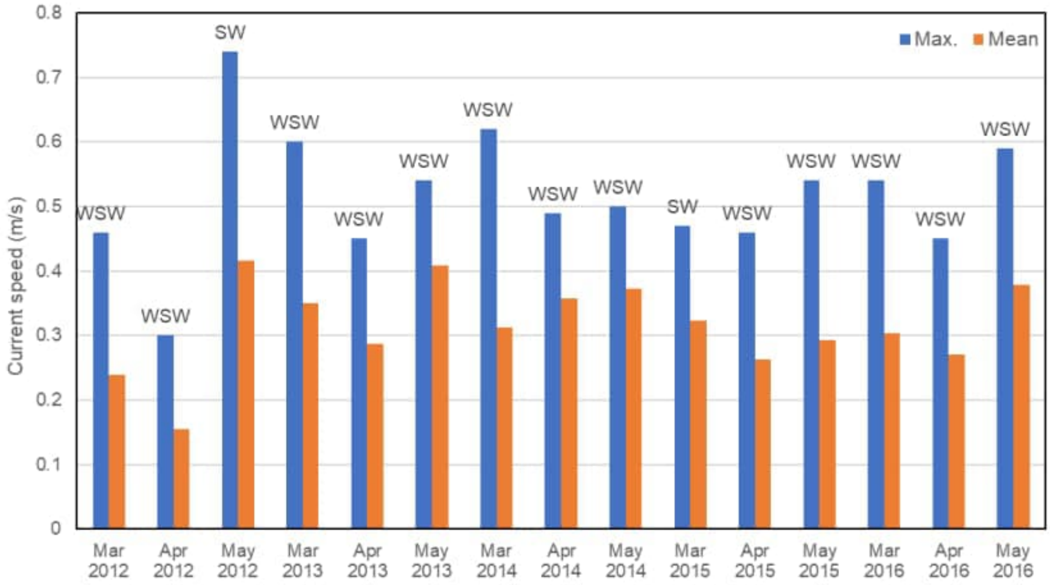

Figure 3-7 - Bottom current mean and maximum speed, and primary direction at Discharge 5 for Season 2 (2012 – 2016)

Figure 3-8 shows the current vectors at the seabed and surface at Discharge 5 for a 45-day period from 3 Mar 2013 to 16 Apr 2013. For clarity, the seabed and surface current vectors are scaled independently. The selected start time for the drilling discharge simulation in **Season 2 is 12 Mar 2013 at 0900 hrs**, as it yields the maximum combined seabed and surface transport of seawater towards the nearest MPA. The simulation periods for the riserless and riser phases of the well drilling are shown in Figure 3-8.

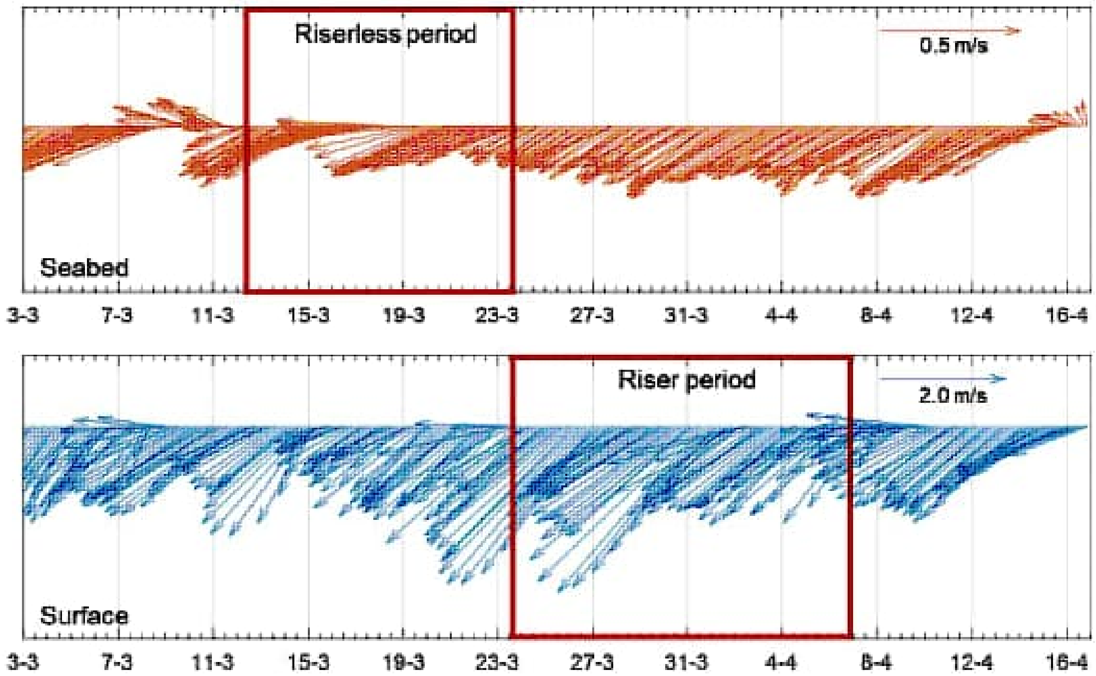

Figure 3-8 - Seabed and surface current vectors at Discharge 5 from 3 Mar 2013 to 16 Apr 2013 with boxes showing the period selected for drilling discharge simulation in Season 2

3.1.3 SEASON 3- JUNE TO AUGUST

Figure 3-9 presents summary statistics of current speed and direction at the seabed for each month of Season 3. Maximum current speed tends to mostly remain in the range of 0.5 m/s to 0.8 m/s, while average speed mostly lies in the 0.2 m/s to 0.4 m/s range. The most frequently occurring flow direction for the strongest 10% of the seabed currents is almost always to the WSW with just one month of June 2016 showing stronger flows to the SW.

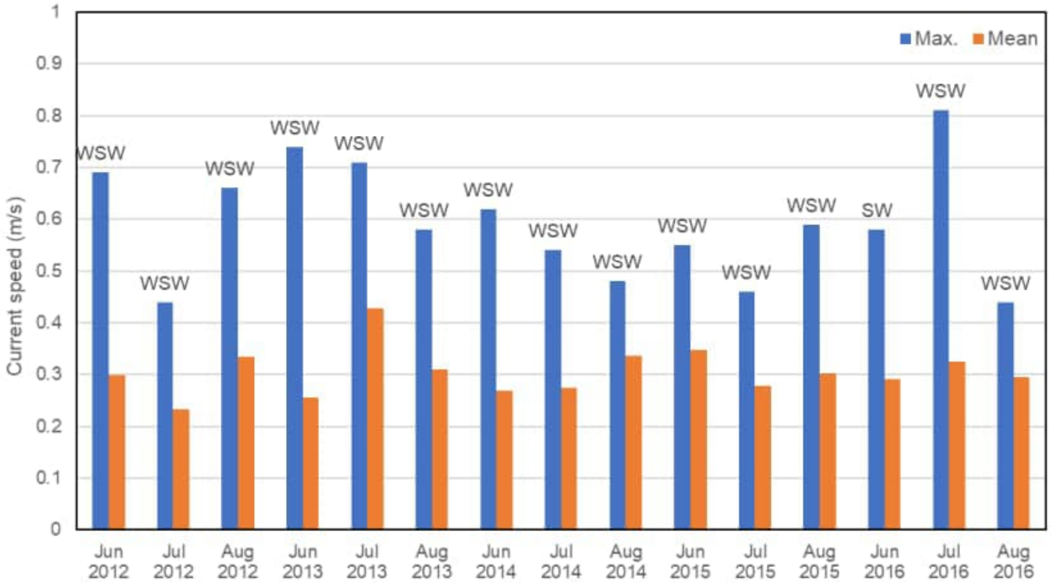

Figure 3-9 - Bottom current mean and maximum speed, and primary direction at Discharge 5 for Season 3 (2012 – 2016)

Figure 3-10 shows the current vectors at the seabed and surface at Discharge 5 for a 45-day period from 2 Aug 2015 to 15 Sep 2015. For clarity, the seabed and surface current vectors are scaled independently. The selected start time for the drilling discharge simulation in **Season 3 is 12 Aug 2015 at 0000 hrs**, as it yields the maximum combined seabed and surface transport of seawater towards the nearest MPA. The simulation periods for the riserless and riser phases of the well drilling are shown in Figure 3-10.

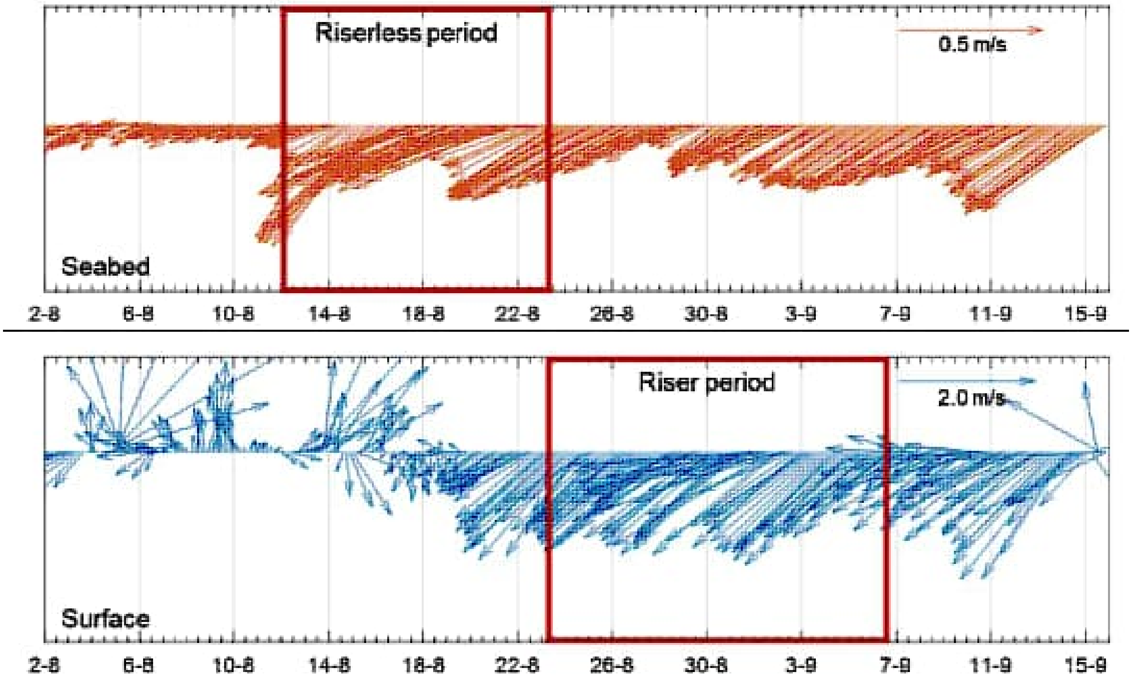

Figure 3-10 - Seabed and surface current vectors at Discharge 5 from 2 Aug 2015 to 15 Sep 2015 with boxes showing the period selected for drilling discharge simulation in Season 3

3.1.4 SEASON 4- SEPTEMBER TO NOVEMBER

Figure 3-11 presents summary statistics of current speed and direction at the seabed for each month of Season 4. Maximum current speed tends to mostly remain in the range of 0.5 m/s to 0.7 m/s, while average speed mostly lies in the 0.2 m/s to 0.4 m/s range. The most frequently occurring flow direction for the strongest 10% of the seabed currents is almost always to the WSW with a couple of months showing stronger flows to the SW.

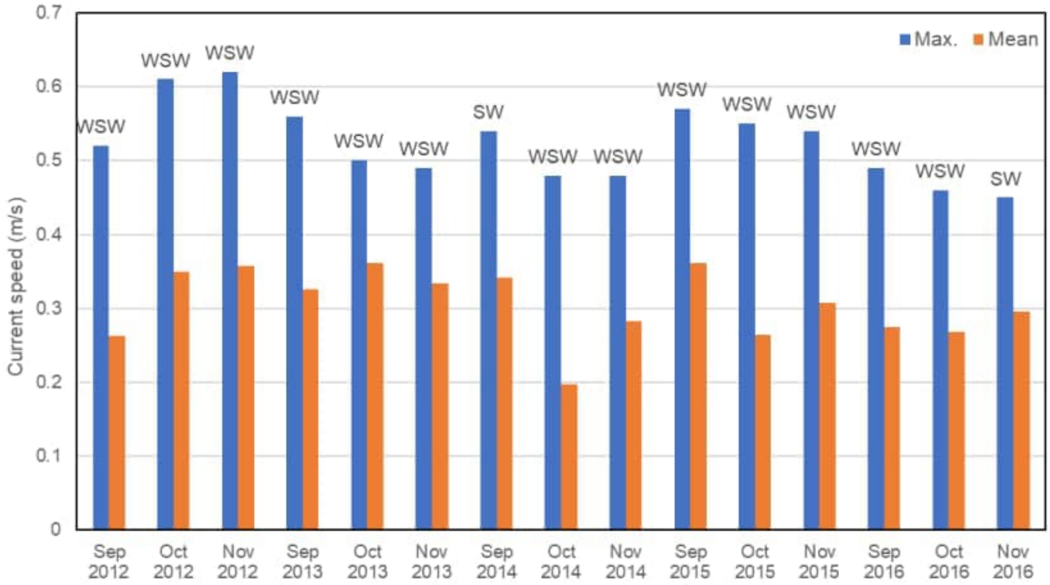

Figure 3-11 - Bottom current mean and maximum speed, and primary direction at Discharge 5 for Season 4 (2012 – 2016)

Figure 3-12 shows the current vectors at the seabed and surface at Discharge 5 for a 45-day period from 5 Oct 2015 to 18 Nov 2015. For clarity, the seabed and surface current vectors are scaled independently. The selected start time for the drilling discharge simulation in **Season 4 is 15 Oct 2015 at 0300 hrs**, as it yields the maximum combined seabed and surface transport of seawater towards the nearest MPA. The simulation periods for the riserless and riser phases of the well drilling are shown in Figure 3-12.

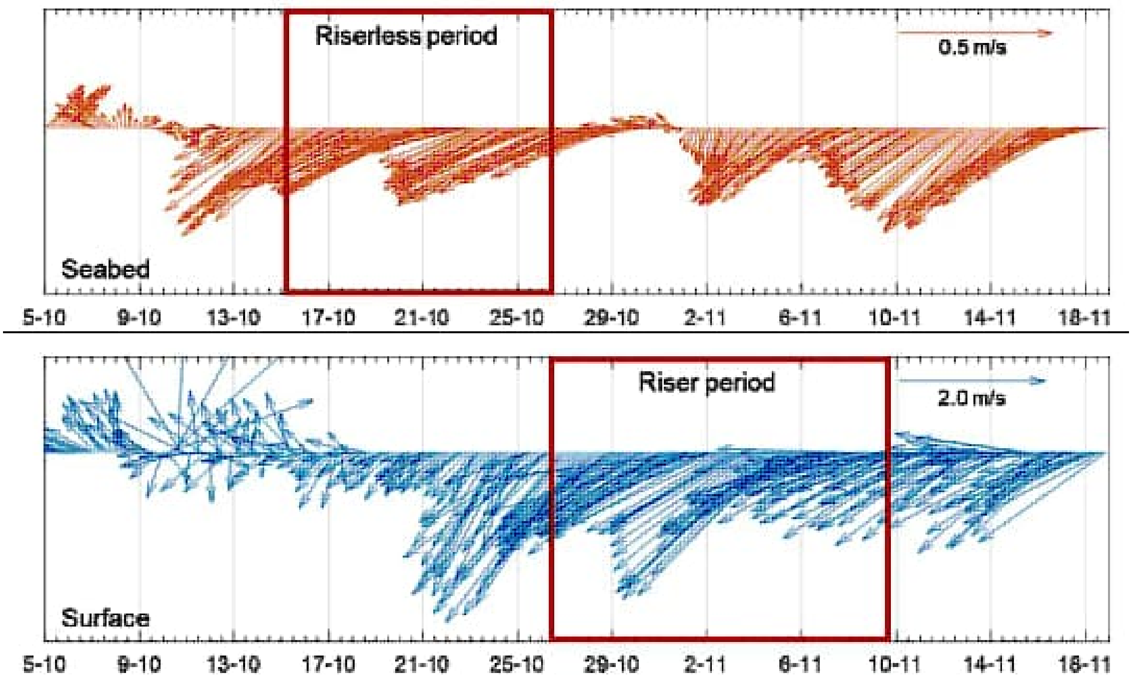

Figure 3-12 - Seabed and surface current vectors at Discharge 5 from 5 Oct 2015 to 18 Nov 2015 with boxes showing the period selected for drilling discharge simulation in Season 4

4 CONDENSATE PIPE LEAK LOCATION

Figure 4-1 shows the annual current and wind roses at the condensate pipe leak location - 35°6'58.41" S, 22°23'1.66" E. The surface current flows more often towards the SW like at Discharge 4 and 5, but there is more frequent occurrence of strong flows to the NE and NNE. Current speeds at the seabed are mainly to the WSW and SW and rarely exceed 0.5 m/s. Winds are mostly E-W and display similar characteristics as at Discharge 4 and 5.

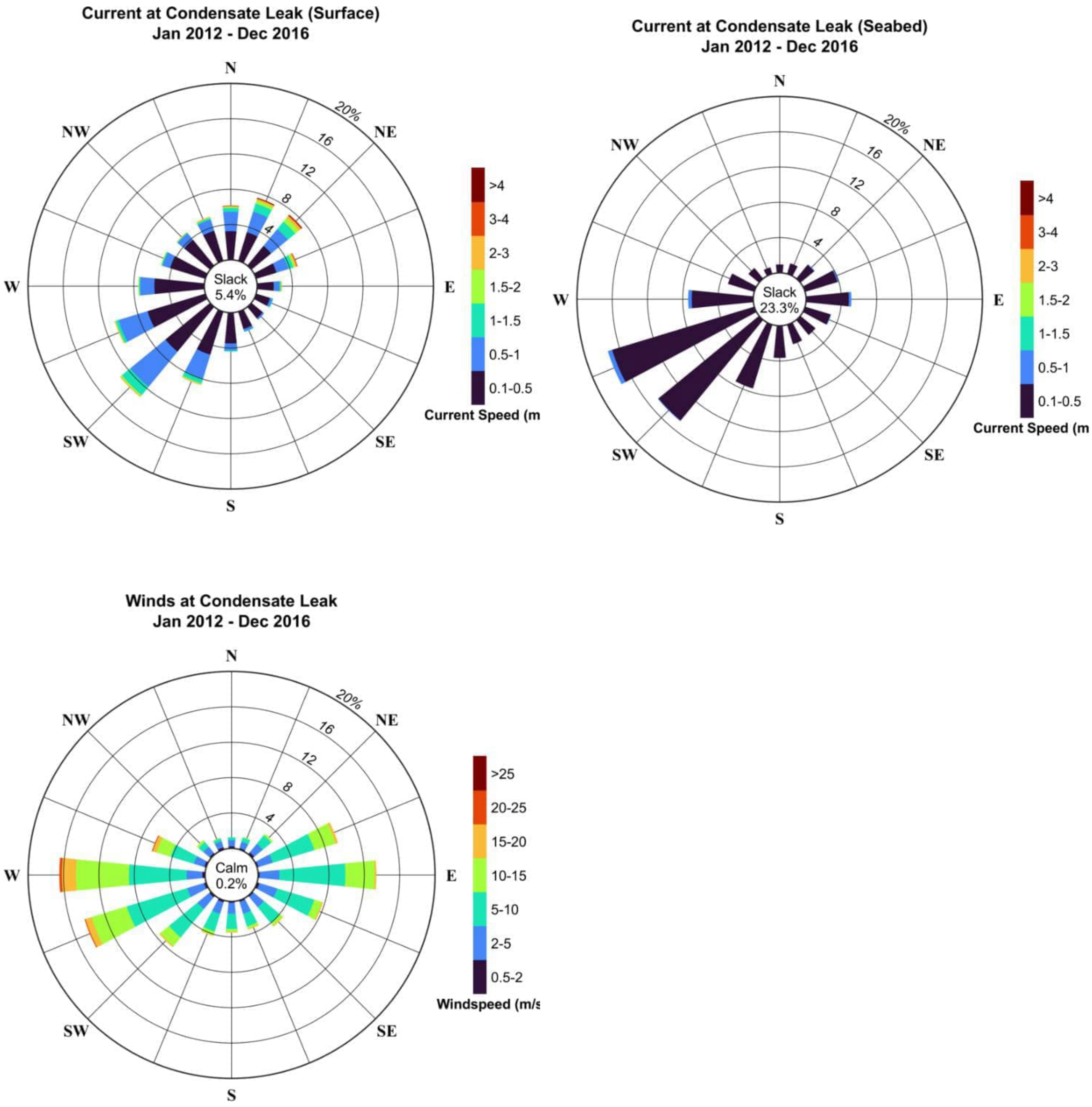

Figure 4-1 - Average annual current and wind speed roses at Pipe Leak location for 2012-2016

Table 4-1 summarises statistics of surface current at the Pipe Leak location. While the surface current usually flows to the SW for most of the year, the direction switches to the NE quadrant during the months of May to Aug. The strongest flows are almost always towards the NNE or NE. Peak current speed reached almost 5 m/s in the 5-year dataset although monthly median speeds generally vary between around 0.3 m/s and 0.5 m/s over the course of the year.

Table 4-1 - Yearly and monthly surface current speed and direction statistics at Pipe Leak location

SPEED (M/S)	YRLY	JAN	FEB	MAR	APR	MAY	JUN	JUL	AUG	SEP	OCT	NOV	DEC
Median	0.4	0.3	0.4	0.4	0.4	0.3	0.4	0.5	0.4	0.4	0.4	0.4	0.3
Mean	0.5	0.4	0.4	0.4	0.5	0.4	0.6	0.6	0.6	0.6	0.5	0.5	0.4
Std. deviation	0.4	0.3	0.3	0.3	0.3	0.3	0.6	0.5	0.5	0.5	0.3	0.4	0.3
Minimum	0.0	0.0	0.0	0.0	0.0	0.0	0.0	0.0	0.0	0.0	0.0	0.0	0.0
Maximum	5.0	2.0	1.9	2.3	2.7	2.3	5.0	3.3	3.8	3.5	3.5	3.0	2.6
Most frequent direction	SW	SW	SW	SW	SW	NNE	NE	NE	NE	SW	SW	SW	SW
Strongest current direction	NNE	NE	NNE	SW	NNE	ENE	NNE	NE	NE	NNE	NE	NNE	NE

Figure 4-2 shows average monthly surface current roses at the Pipe Leak location for 2012 to 2016. The surface current flows towards the SW quadrant in the months of January to April and October to December. The surface current is directed towards the NE and SW quadrants in the months of May to September, however the north-easterly currents are consistently stronger in those months.

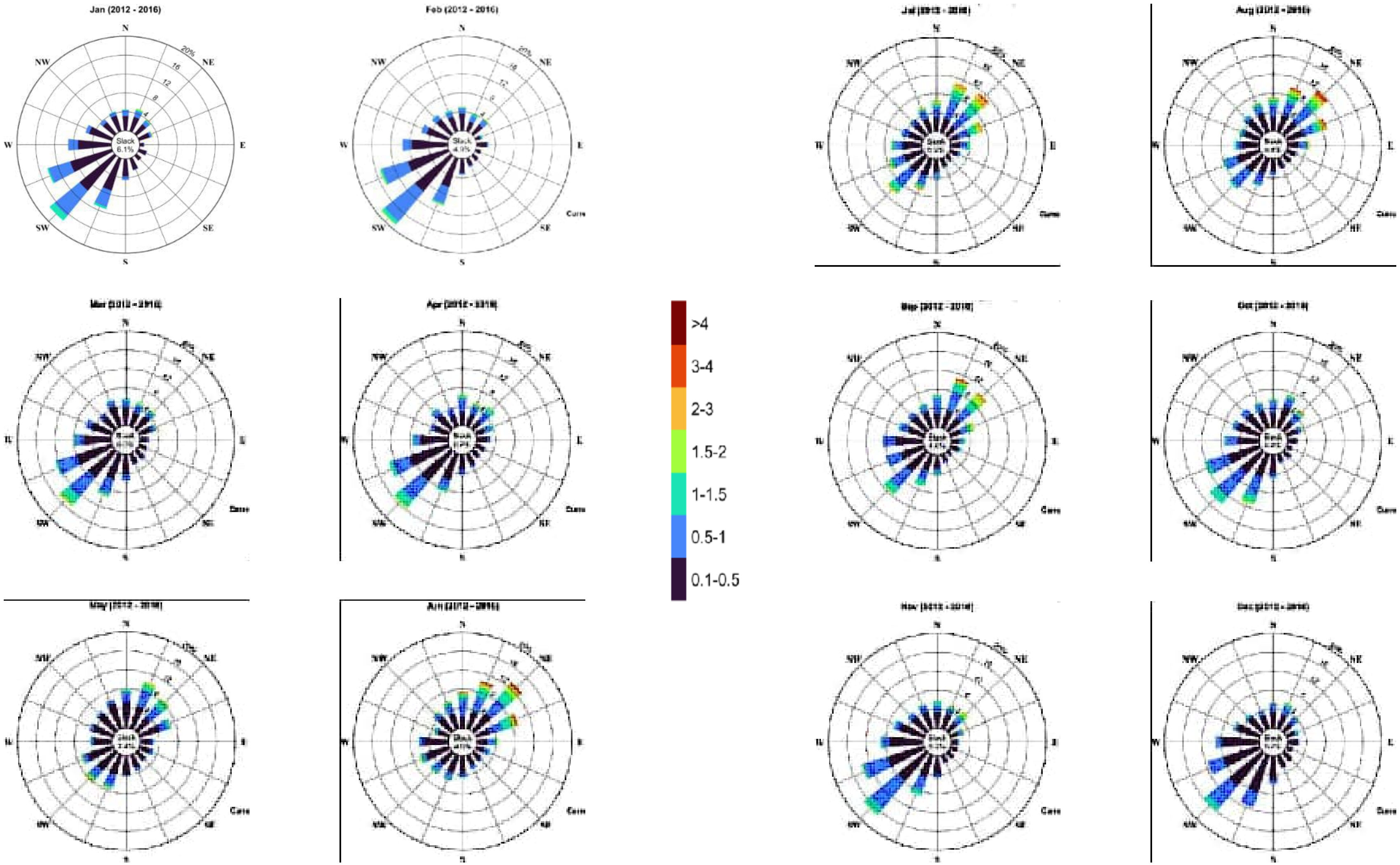

Figure 4-2 - Average monthly surface current roses at Pipe Leak for 2012 – 2016 (colour bar represents current speed in m/s)

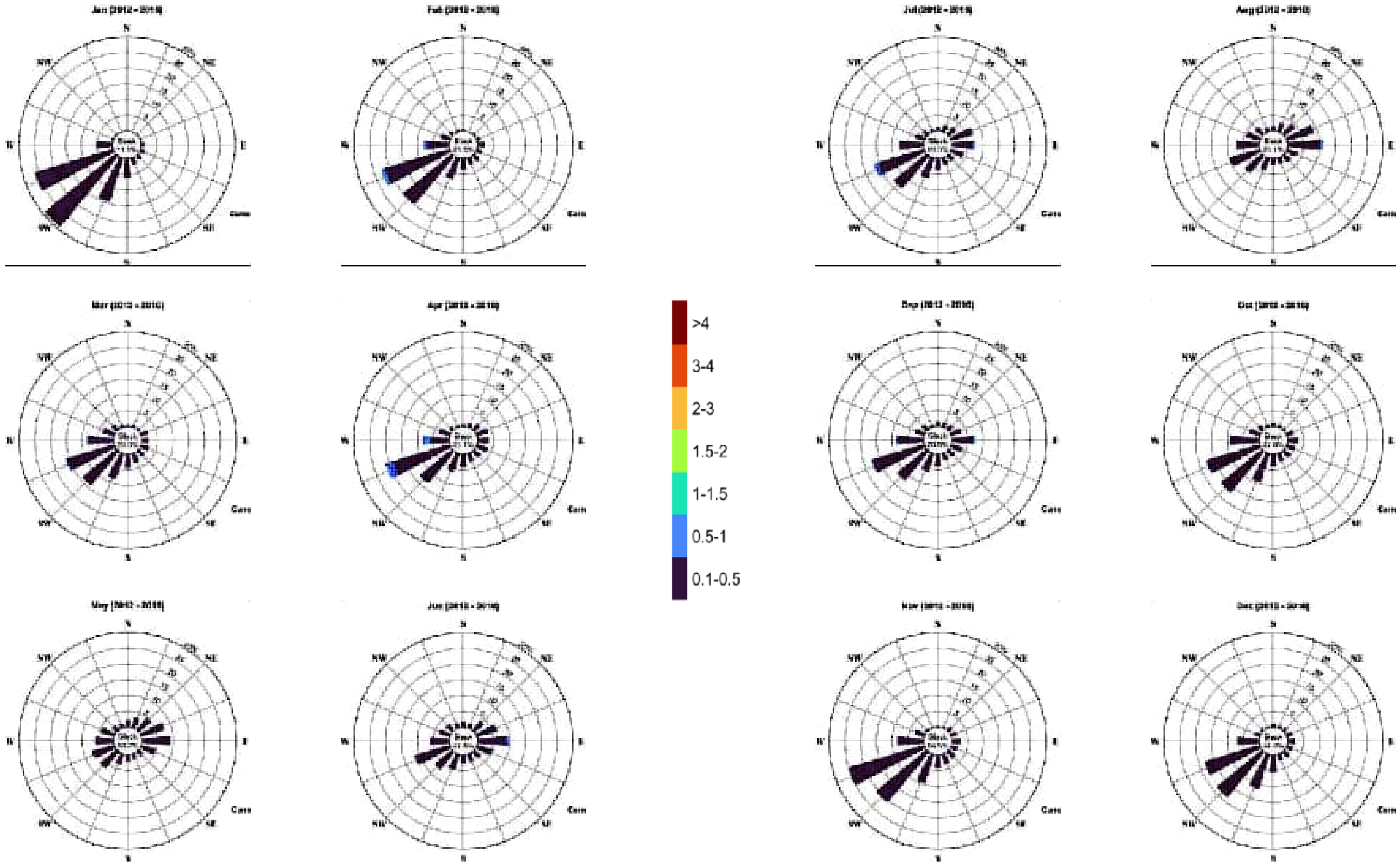

Figure 4-3 - Average monthly seabed current roses at Pipe Leak for 2012 – 2016 (colour bar represents current speed in m/s)

Statistics of the seabed current at the Pipe Leak location are summarised in Table 4-2. The seabed current is directed to the SW quadrant for most of the year except for the months of May and August, which see the most frequently occurring seabed current direction switching to an easterly flow. The strongest flows are almost always towards the east or WSW. Peak current speed reached 0.8 m/s in the 5-year dataset although monthly median speeds generally remain at 0.2 m/s over the course of the year.

Table 4-2 - Yearly and monthly seabed current speed and direction statistics at Pipe Leak location

SPEED (M/S)	YRLY	JAN	FEB	MAR	APR	MAY	JUN	JUL	AUG	SEP	OCT	NOV	DEC
Median	0.2	0.2	0.2	0.1	0.2	0.1	0.2	0.2	0.2	0.2	0.2	0.2	0.2
Mean	0.2	0.2	0.2	0.2	0.2	0.1	0.2	0.2	0.2	0.2	0.2	0.2	0.2
Std. deviation	0.1	0.1	0.1	0.1	0.1	0.1	0.1	0.1	0.1	0.1	0.1	0.1	0.1
Minimum	0.0	0.0	0.0	0.0	0.0	0.0	0.0	0.0	0.0	0.0	0.0	0.0	0.0
Maximum	0.8	0.5	0.7	0.6	0.8	0.6	0.7	0.7	0.7	0.6	0.6	0.5	0.5
Most frequent direction	WSW	SW	WSW	WSW	WSW	E	WSW	WSW	E	WSW	WSW	WSW	WSW
Strongest current direction	W	WSW	W	ENE	W	E	E	WSW	E	E	E	WSW	WSW

Figure 4-3 shows the average monthly seabed current roses at the Pipe Leak location for 2012 to 2016. The seabed current at the Pipe Leak location is directed towards the southwest quadrant in the months of January to April and September to December. The seabed current flows both eastward and to the southwest quadrant in the months of May to August.

Table 4-3 and Figure 4-4 present the statistics of hourly-average wind speed at 10 m elevation for the Pipe Leak location. Winds mainly blow from the eastern and western sectors from October to April. However, in the months of May to September westerly winds dominate in frequency of occurrence as well as strength. The most frequent direction for stronger winds (>15 m/s) is from W over the five-year dataset.

Table 4-3 - Yearly and monthly wind speed and direction statistics at Pipe Leak location

SPEED (M/S)	YRLY	JAN	FEB	MAR	APR	MAY	JUN	JUL	AUG	SEP	OCT	NOV	DEC
Median	7.3	6.6	6.5	7.2	6.6	6.4	8.0	8.6	8.0	8.6	8.1	7.6	6.8
Mean	7.6	6.8	6.7	7.2	6.9	6.9	8.4	8.9	8.5	8.7	8.0	7.7	6.9
Std. deviation	3.7	2.9	3.1	3.3	3.4	3.7	4.5	4.4	4.3	3.8	3.3	3.5	3.0
Minimum	0.1	0.2	0.4	0.5	0.2	0.1	0.3	0.2	0.1	0.6	0.6	0.1	0.3
Maximum	24.5	18.1	17.5	19.9	19.3	18.2	24.5	21.7	22.6	22.3	21.8	22.5	21.0
Most frequent direction	W	E	E	E	ENE	W	W	W	W	W	E	E	E
Strongest wind direction	W	W	W	W	W	WSW	W	W	W	W	W	WSW	WSW

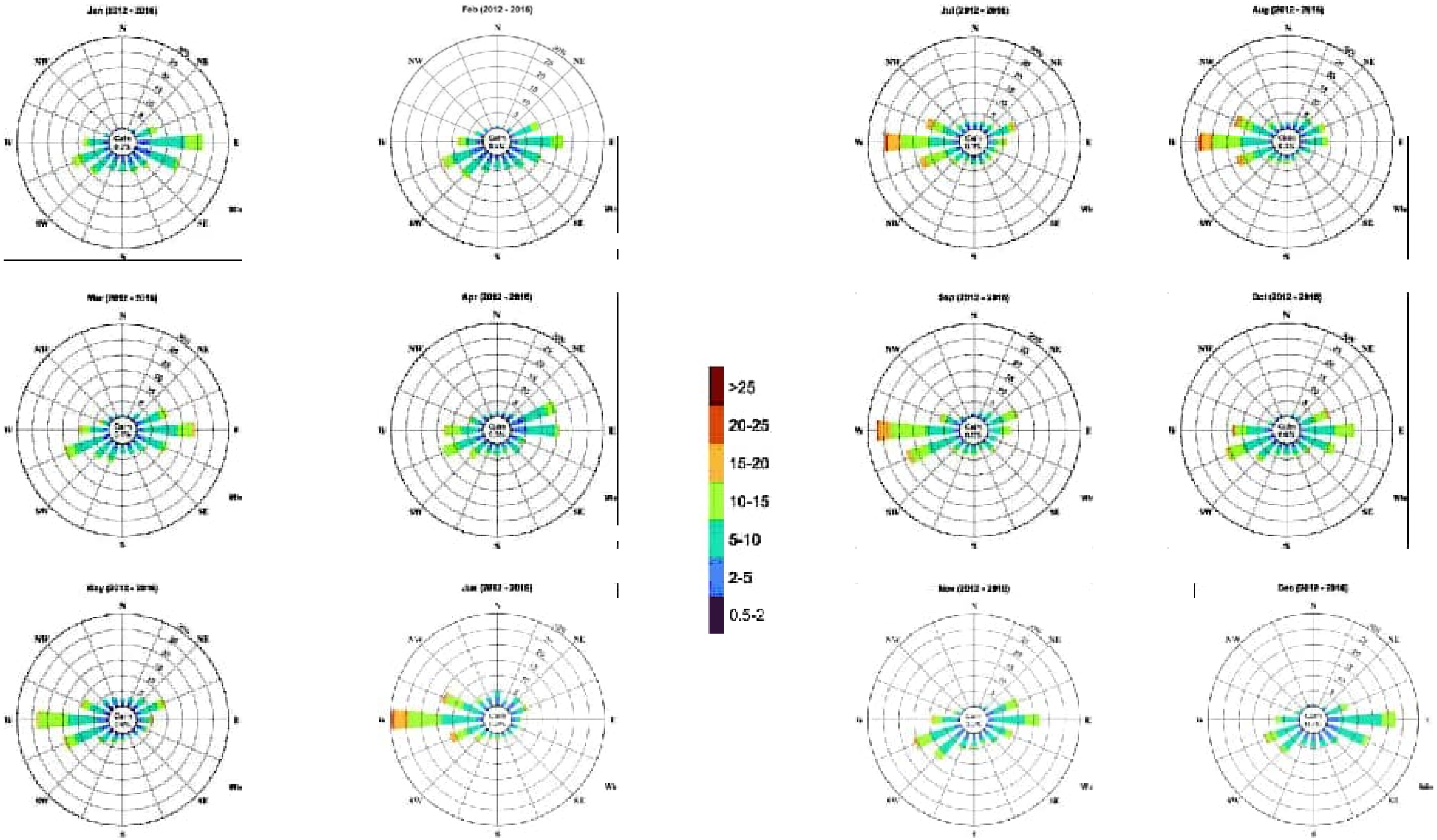

Figure 4-4 - Average monthly wind roses at Pipe Leak for 2012 – 2016 (colour bar represents wind speed in m/s)

5 STUDY LIMITATIONS

WSP Canada Inc. (WSP) has prepared this document in a manner consistent with the level of care and skill ordinarily exercised by members of the engineering and science professions currently practising under similar conditions in the jurisdiction in which the services are provided, subject to the time limits and physical constraints applicable to this document. No warranty, express or implied, is made.

This document, including all text, data, tables, plans, figures, drawings, and other documents contained herein, has been prepared by WSP for the sole benefit of Total Energies. This report represents WSP's professional judgement based on the knowledge and information available at the time of completion. WSP is not responsible for any unauthorized use or modification of this document. All third parties relying on this document do so at their own risk.

The factual data, interpretations, suggestions, recommendations, and opinions expressed in this document pertain to the specific project, site conditions, design objective, development and purpose described to WSP by Total Energies and are not applicable to any other project or site location. In order to properly understand the factual data, interpretations, suggestions, recommendations, and opinions expressed in this document, reference must be made to the entire document.

This document, including all text, data, tables, plans, figures, drawings, and other documents contained herein, as well as all electronic media prepared by WSP are considered its professional work product and shall remain the copyright property of WSP. Total Energies may make copies of the document in such quantities as are reasonably necessary for those parties conducting business specifically related to the subject of this document or in support of or in response to regulatory inquiries and proceedings. Electronic media is susceptible to unauthorized modification, deterioration, and incompatibility and therefore no party can rely solely on the electronic media versions of this document.

6 REFERENCES

Bailey, D.F., J. Hermes, P. Penven, T. Bornman, W. Goschen (2022). An investigation of sea level and circulation response during a coastal trapped wave event on the Eastern Agulhas Bank, South Africa. *Continental Shelf Research*, **240,** 104698.

Beal, L.M. and H. L. Bryden (1997). Observations of an Agulhas Undercurrents, *Deep-Sea Res.*, **44(9)**, 1715-1735.

Beal, L.M. (2009). A time series of Agulhas undercurrent transport. *J. Phys. Oceanography*, **30**, 2436-2450.

Beal, L.S. S. Elipot, A. Houk and G.M. Leber (2015). Capturing the Transport Variability of a Western Boundary Jet: Results from the Agulhas Current Time-Series Experiment (ACT),. *Journal of Physical Oceanography*, **45**, 1302-1324.

Boyd, A.J. and F.A. Shillington (1994). Physical frocing and circulation patterns on the Agulhas Bank. *S.A. J. Sci*, **90**, 114-122.

Goschen, W. and E.H. Schumann (1990). Agulhas Current variability and structure off the Cape province, South Africa. *J. Geophys. Res*., **95(C1)**, 667-678.

Hutchinson, K. (2018). Seasonality of the Agulhas Current with respect to near- and far-field winds. *Phd Thesis*, University of Cape Town, 176pp.

Krug, M. J. Tournadre and F. Dufois (2014). Interactions between the Agulhas Currents and the eastern margin of the Agulhas Bank, *Continental Shelf Research*, **81**, 67-79.

Largier, J.L. and V.P. Swart, V.P.(1987). East -west variation in thermocline breakdown on the Agulhas Bank. In: *The Benguela and Comparable Ecosystems*, Payne, A. I. L., Gulland, J. A. and K. H. Brink (Eds). *S. Afr. J. mar. Sci*., **5**, 263-272.

Largier, J. P. Chapman, W.T. Peterson and V.P. Swart (1992). The western Agulhas Bank: circulation, stratification and ecology, *South African Journal of Marine Science*, **12(1)**, 319-339, DOI: 10.2989/02577619209504709

Lutjeharms, J.R.E. and M.J. Roberts (1988). The Natal Pulse: An extreme transient on the Agulhas Current., *J. Geophys.* Res,, **93 (C1)**, 631-645.

Lutjeharms, J.R.E., R. Catzel and H.R. Valentine (1989). Eddies and other boundary phenomena of the Agulhas Currents, *Cont. Shelf. Res*., **9(7)**, 597-616.

Lutjeharms, J.R.E., O. Boebel, P.F.C. van der Vaart, W.P.M. de Ruijter, T. Rossby and H.L. Bryden (2001). Evidence that the Natal Pulse involves the Agulhas Current to its full depth. *Geophysical Research Letters*, **28(18)**, 2449-2452.

Lujeharms, J.R.E., P. Penven and C. Roy (2003). Modelling the shear edge eddies of the southern Agulhas Current. *Cont. Shelf Res*., **23**, 1099-1115.

Pearce, A.F and M.L. Gründlingh (1982). Is there a seasonal variation of the Agulhas Current? *Journal of Marine Research*, **40(1)**, 177-184.

Russo S.R., J. Veitch, M. Carr, G. Fearon and C. Whittle (2022) An intercomparison of Global Re-analysis products for southern Africa's major oceanographic features. Front. Mar. Sci. 9:837906. doi: 10.3389/fmars.2022.837906.

Roualt, M.J. and F. Penven (2011). New perspectives on the Natal Pulse from Satellite observations, *J. Geophys. Res*., **116**, C07013, doi:10.1029/2010JC006866.

Schumann, E.H., G.J.B . Ross and W.S. Goschen (1988) Cold water events in Algoa Bay and alog the Cape south coast, South Africa, in Marc/April 1987. S.A. J. Sci., 84, 581-584.

Swart, V.P. and J.L. Largier (1987). Thermal structure of the Agulhas Bank water. In: *The Benguela and Comparable Ecosystems*, Payne, A. I. L., Gulland, J. A. and K. H. Brink (Eds). *S. Afr. J. mar. Sci*., **5**, 243-253

Tedesco, P., J. Gula, C., Ménesguen, P. Penven and M. Krug (2019). Generation of submesoscale frontal eddies in the Agulhas Current. *Journal Geophysical Research: Oceans*, **124**, 7606–7625. https://doi.org/10.1029/2019JC015229.

TotalEnergies. (2022). *Drilling Discharge Modeling Technical Report.*

7 CLOSURE

We trust the above meets your present requirements. If you have any questions or requirements, please contact the undersigned.

Ashwin Gadgil, PhD, EIT

Coastal Engineer & Hydrodynamic Modeller

Sundar Prasad, PhD

Senior Principal Coastal Engineer

Marieh Rajaie, PhD, EIT

Water Resources Specialist

Appendix A

SATOCEAN HYDRODYNAMIC DATABASE: CALIBRATION AND VALIDATION

MEMO

Exploration & Production

TEPSA/OPS – TEPSA/2020-0098/OPS.PL

Destinataire : C. MICHEL (EP/AF/A-FE/ZA-TEP/HSEQ) *To* E. GROENEWALD (EP/AF/A-FE/ZA-TEP/HSEQ)	Expéditeur : P. LATTES (EP/AF/A-FE/ZA-TEP/OPS) T. MAJA (EP/AF/A-FE/ZA-TEP/OPS) *From*
Copie : *Copy*	Date : April 21th 2020
Object : 3D current model calibration and methodology – South Blocks - South Africa. *Subject*	Philippe LATTES Signature numérique de Philippe LATTES Date : 2020.06.09 13:20:38 +02'00'

1 Background

Block 11B/12B is characterized by harsh environmental conditions. Total Hs and surface winds show clear seasonality signals with best conditions occurring during austral summer. Another aspect that affects Block 11B/12B is the core of the Agulhas Current. This warm and saline current is formed by several oceanic currents in the Indian ocean and is the second strongest current in the world.

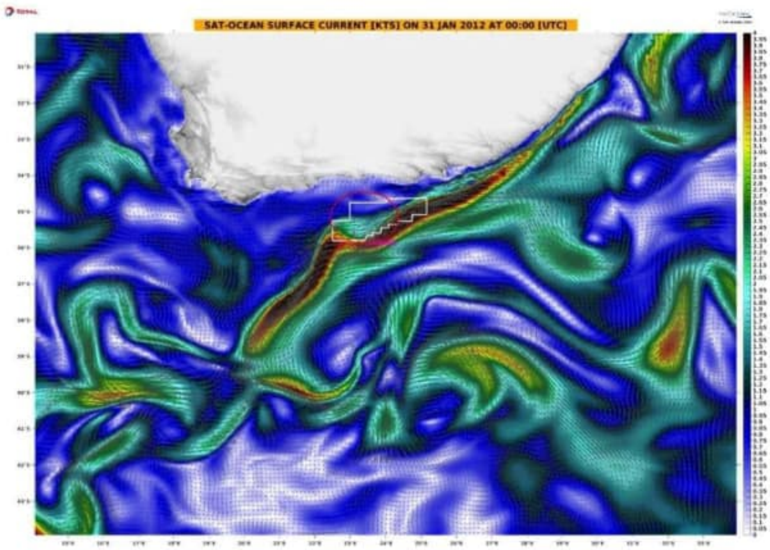

Figure 1: Current speed map of current flow over the southern African region showing the Agulhas Current system for January 2012. A shear edge eddy (red circle) cross the 11B/12B block is demarcated by a white polygon.

TOTAL Classification: Restricted Distribution

TOTAL MEMO

A great portion of the 11B/12B block lies on the pathway of the Agulhas Current, a fast and narrow western boundary current flowing along the eastern and southern coasts of South Africa. The core of the current is generally positioned across the block and is occasionally perturbed by shear edge eddies (see Figure 1) generated upstream south of Port Elizabeth (34° S) and or Natal pulse anomalies generated offshore Durban. During passage of these anomalies, the current speeds over the block are either weakened or reinforced with an associated change in flow direction and depending on the behavior of the anomaly (see Figure 2).

Current speeds of up to and exceeding 6 knots have been recorded within the core of the current associated with meanders. Current direction can change in response to change in winds and or progression of large eddies. The Agulhas Current does not present any seasonality as the anomalies impacting the current flow, in addition to weather, are sporadic and difficult to predict.

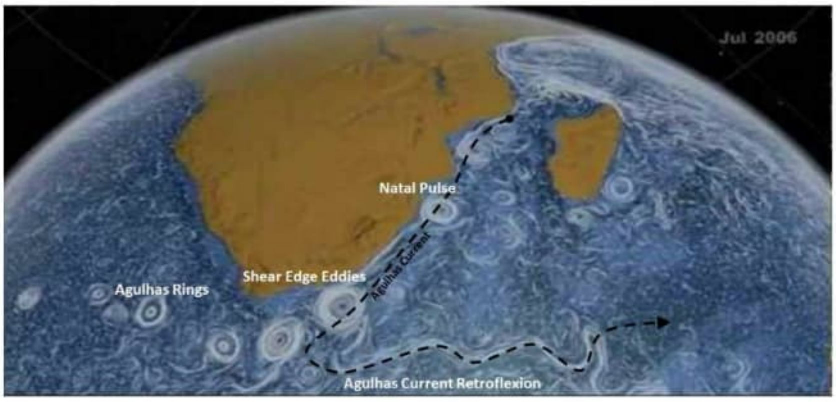

Figure 2 Large current eddies due to shear stress induced by the coast and continental shelf in South Africa

2 SAT-OCEAN Model description

SAT-OCEAN have developed innovative and exclusive technologies based on in-situ, satellite sea surface temperature, wind and altimetric data by which absolute ocean currents and winds are computed, anywhere in the world.

In effect, coupled inverse/direct modeling approaches combined with the data allow us to measure these quantities from space with very high spatial (1/32°) and temporal resolutions (3-hour output time step) over the model emprise (see Figure 1Figure 1: Current speed map of current flow over the southern African region showing the Agulhas Current system for January 2012. A shear edge eddy (red circle) cross the 11B/12B block is demarcated by a white polygon.).

Several studies have shown that upper layer oceanic features can be monitored from satellite measurements over long periods of time. SAT-OCEAN merge up to 9 sensor data sets and produce analyzed SST fields accurate to 0.3°C on average compared to surface drifting buoys' temperature measurements. Monitoring the ocean's surface at such resolutions yields the ability to compute absolute 3-dimensional currents

TOTAL MEMO

worldwide. In addition, SAT-OCEAN model data are cloud free and can be produced up to every 3 hours at a 7-10 km resolution in space from 1998.

SAT-OCEAN inverse/direct model is controlled by very accurate SST analyzed fields, together with wind satellite analyzed data and altimetric data, leading to high resolution current fields. Over several areas of the world including offshore South Africa, this new approach has yielded accurate current estimates with respect to simultaneous on-site measurements (ADCP, HF radars, current meter and buoys' velocities).

SAT-OCEAN also provides high quality analyzed satellite wind data, either in real time or spanning over the past 25 years. The data can be used for design or to assist offshore operations.

3 Satellite observations and Ocean Currents Monitoring

3.1 Satellite data

SAT-OCEAN bases its ocean current computations on several data sets, stemming from scatterometers (for the model forcing winds) as well as from altimeter-based and Sea Surface Temperature satellite observations (to be assimilated in the HYCOM based ocean current model).

3.2 QSCAT and SSMI satellite wind data

Satellite wind scatterometry data are processed for the purpose of forcing the 3D Navier-Stokes direct circulation model.

The data are extracted from the GSFC database (public access), and wind magnitude and direction images are processed (flagged for rainy areas, bad data, projected and calibrated against anemometer data).

The processed data are then merged via objective mapping and spectral fusion. Analyzed wind fields are produced in real time every 3 hours at a 0.125° spatial resolution.

3.3 Geostationary imagery

The geostationary raw data are routinely obtained from the GMS satellite series which cover the area of interest. SAT-OCEAN produces SST images via a methodology analogous to the one described for the AVHRR imagery (section 3.4).

The GOES image series presents a 5 km spatial resolution over the area of concern and 24 to 48 images are available each day, depending on the availability of the data.

3.4 TRMM TMI and AQUA AMSR-E imagery

MEMO

The TRMM (Tropical Rainfall Measuring Mission), TMI (TRMM Microwave Imager) and AMSR-E AQUA SST image series are extracted in real time from the GSFC (Goddard Space Flight Center) data base (public access). The SSTs are already computed and the projection, geolocation and error correction are already applied. The TMI and AMSR-E measurement technology is such that the ocean is always visible no matter the cloud coverage, except over regions where it is raining. The TMI and AMSR-E image spatial resolution is about 25 km and the area is covered twice a day.

3.5 Polar Orbiting NOAA Satellite AVHRR imagery

Satellite AVHRR (Advanced Very High Resolution Radiometer) Level 1b high resolution imagery is extracted in real time from the NOAA (US National Oceanographic and Atmospheric Agency) Satellite Active Archive server (public access). The level 1b data is very similar to the Level 0 on-board recorded measurement.

The AVHRR image series presents a 1 km (Local Area Coverage) to 4 km (Global Area Coverage) spatial resolution and 10-12 images are available each day, depending on the number of orbiting satellites.

The raw satellite data are processed in real time at SAT-OCEAN including: channels 1 to 5 linear and non-linear calibrations, geolocation, clock drift and satellite attitude (roll, pitch and yaw) error corrections, Lambert Azimuthal Equal Area projection, multi-channel cloud detection and sea surface temperature (SST) will be computed using split, dual or triple window algorithms from the 5 processed channels.

3.6 Satellite altimeter data

Several altimeters are and have been orbiting with a worldwide coverage. Among those, some are performing measurements in spectral bands dedicated to ocean circulation.

SAT-OCEAN will process the data set over the area of concern for the study, calibrate and cross-calibrate all the data to construct an altimeter-based series over the area.

3.7 HF radars and ADCP

ADCP data have been recorded during seismic campaigns and dedicated surveys over the 11B/12B block and have been used for SAT-OCEAN model calibration. In addition, several HF radars installed and operated by TOTAL located along the coast (between Mossel Bay and Port Elizabeth) allowed to monitor surface current since February 2018 over a large offshore area. These data are available every 30 minutes at 6km resolution. This monitoring allows accurate historical and real time monitoring of the surface currents over the block 11B/12B and has been used for model validation/calibration.

TOTAL MEMO

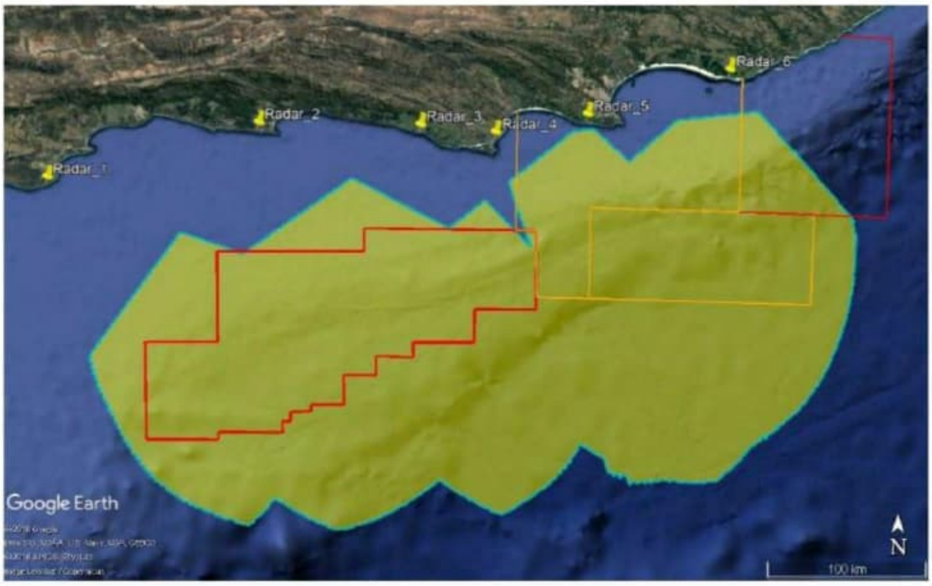

Figure 3 Coverage with 6 radar stations

4 Methodology

4.1 Ocean current computation

SAT-OCEAN ocean current modeling is based on HYCOM (Hybrid Coordinate Ocean Model - Bleck, 2001). HYCOM is a generalized hybrid vertical coordinate model widely recognized as a powerful and efficient tool for ocean modeling. To this state of the art model, SAT-OCEAN brings a significant methodology innovation in using it in an inverse way: the "data" drives the model where the dynamics is fitted onto it to yield 3D absolute ocean currents.

SST cloud-free fields are produced from merged sensor data sets with a very high spatial and temporal resolution and a 0.2°C rms error compared to simultaneous *in situ* measurements. From there, a regression coefficient calculation derived from simultaneous altimetric fields and historical Temperature / Salinity (T/S) profiles yields 3D temperature and salinity, daily: the obtained 3D T/S is called SAT-OCEAN dynamic climatology and represents as closely as possible the 3D state of the ocean over a given region.

The 3D T/S data is then strongly being assimilated in HYCOM/SAT-OCEAN model, strongly in the sense that it is given very little freedom to the model, and are very close to performing an inversion of forcing data, for the ocean circulation (except in the mixed layer which is highly driven by the forcing wind stress). Another way to present this is to say that ocean currents is fitted with high quality 3D satellite data, rather than obtaining current "data" from a model.

MEMO

SAT-OCEAN also make a quantitative use of *in situ* data to calibrate the model when available (section 4.2).

A first 1/16° assimilated global model in-house run is used that covers the global ocean domain. Then, a fine resolution 1/32nd degree configuration of the assimilated model will cover a very large target area covering the offshore South Africa area of concern. The run will encompass 34 layers, with an about 10-layer sampling of the thermocline and a 3-hour output time step.

4.2 Calibration

Where TOTAL HF Radar and ADCP *in situ* current measurements are available, SAT-OCEAN performs a calibration and validation of their 3D ocean current model against the field data. Many mooring data as possible are used to perform the model calibration, including previous drilling campaigns and extensive seismic survey-based hull mounted ADCP on site current measurements. However, model calibration and validation at the deeper layers remain always more challenging due to the lack of measurements and are generally less reliable than at the surface where a larger quantity of data measurements are available. For each data set, current speed and direction measurements are extracted at all times and depths from all the provided files, and time-depth arrays are built. Specific procedures are then developed and applied (SVD decomposition, Kalman filtering etc.) to process the data at each measurement site such that it can be used for quantitative comparison and assimilation into the current model.

The pre-processed measurements are then used by SAT-OCEAN to extract the best calibration scheme for obtaining an improved time-depth dataset at each of the mooring sites. The outcome of this approach significantly improves the correlation between the modeled currents and the measurement series. Typically, SAT-OCEAN derive a calibration scheme over a learning data subset and evaluate the result over the remainder set, providing solid ground for the calibration scheme generalization to periods beyond learning periods. The final calibration scheme is applied to the entire ocean current historical/hindcast period to obtain calibrated hindcast datasets at every mooring location.

A calibration of the full South African south blocks dataset is finally performed. Spatial correction fields are derived in order to quantify at all ocean locations the influence of the locally calibrated currents at the mooring sites and of the modeled currents at each grid point of the hindcast domain.

The methodology results in a fully calibrated ocean current data set that takes the best advantage of the HF radar and ADCP on-site data available and of the assimilated model hindcast.

MEMO

4.3 Validation: currents and winds

4.3.1 Surface current

The SAT-OCEAN model currents were compared against observational data from HF radar for the purpose of validation. Only currents at the surface could be validated due to limited or no data at the sub-surface and for this exercise, 30 days of surface current observations from a single point were extracted from the HF radar dataset. The comparison of modelled currents with observations offers an opportunity to assess the ability of the SAT-OCEAN model to represent the current variability from the extracted data. Time series data starting from 10/03/2020 and ending on 10/04/2020 is presented in Figure 4 below.

From the visual inspection of the presented time-series in Figure 4 and scatter plots in Figure 5, surface current observations are generally coherent with SAT-OCEAN currents during the 30-day period. The SAT-OCEAN current presents a relative error RMS of 0.32kt. The increasing and decreasing patterns are consistent between the model and observations although there are slight differences in the magnitude of current speeds. The absolute mean bias between the SAT-OCEAN model and HF radar observations generally should not exceed 1 knot and there are occasional and slightly differences in the direction of the surface current flow.

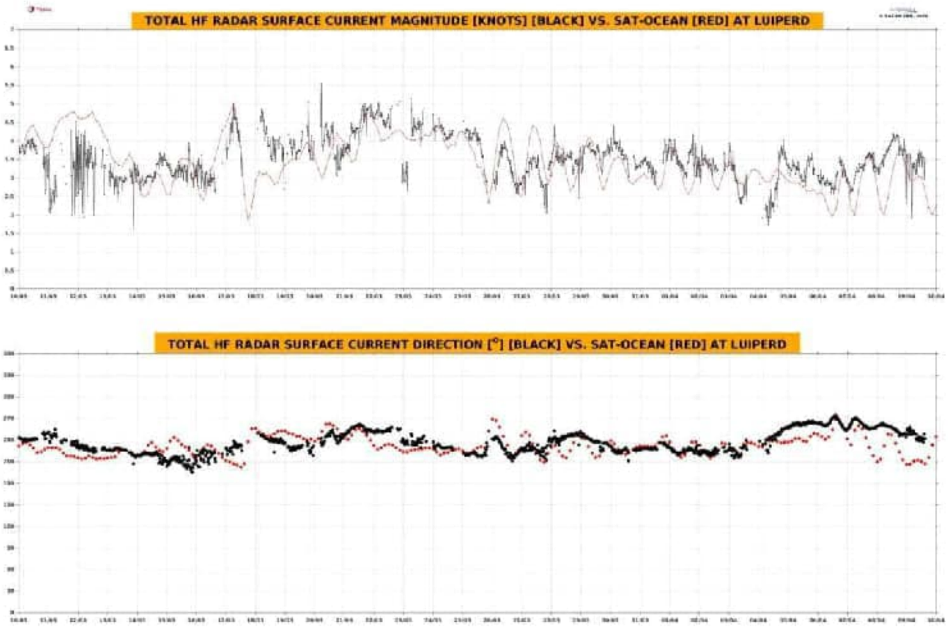

Figure 4: Surface currents time-series from SAT-OCEAN (model) vs HF Radar (observations) for 30 days.

TOTAL Classification: Restricted Distribution

TOTAL MEMO

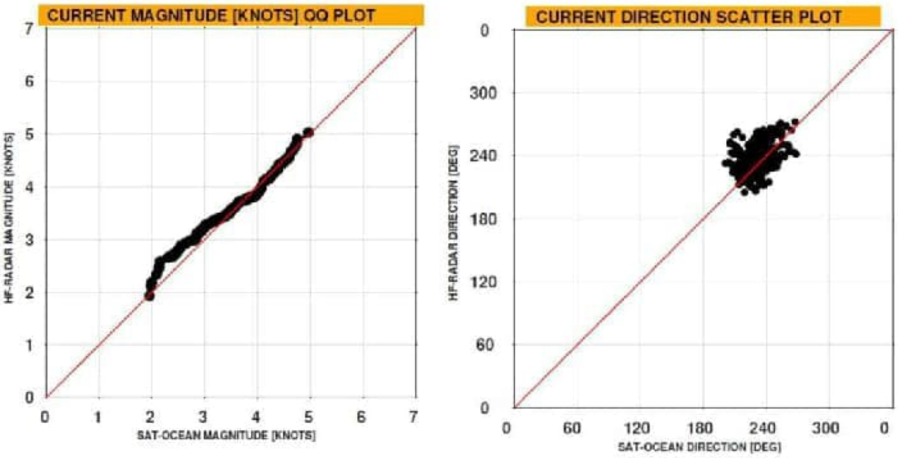

Figure 5 Current speed QQ plot and current direction scatter plot of SATOCEAN model vs observation for the considered period

For the given location, SAT-OCEAN modelled currents performed adequately indicating a reasonably fair representation of the surface current conditions over the 11B/12B block. The performance of the model may vary depending on features impacting the current flow e.g. a meandering core vs jet-regime state. Caution should be exercised when interpreting these results as they only represent validation at a single point within the block area (i.e. the Luiperd well location).

4.3.2 Winds

For the wind model validation, METAR (METeorological Airport Report) wind observations are used as reference to compare with the model output. The comparison is made from a weather station wind dataset from Port Elizabeth which is located north-east outside the11B/12B block along the South African coast. The Port Elizabeth location is within our observation area of interest with HF radars and therefore a relevant position for validation of the wind model. The time series comparison between the dates 10/03/2020 and 10/04/2020 is presented below in Figure 6.

Strong correlation between wind observations and model (see Figure 7) is recorded from the 30-day time series with the model explaining more than 88% of the variability in wind observations (r = 0.94 and rms = 13 kt). The SAT-OCEAN wind model provides coherent and consistent representation of the winds and is accurate in both magnitude and direction. Although the extreme wind conditions at 11B/12B can often exceed that of Port Elizabeth, the SAT-OCEAN model has proven its adequacy in capturing and representing wind conditions over a larger area including the full extent of the 11B/12B block.

MEMO

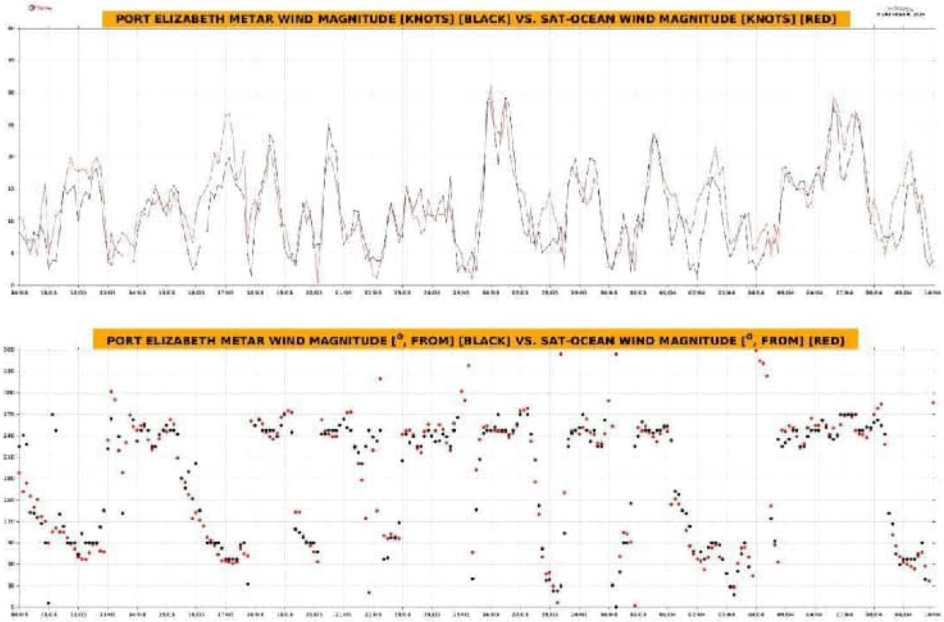

Figure 6 Surface winds time-series from SAT-OCEAN (model) vs METAR (observations) for 30 days.

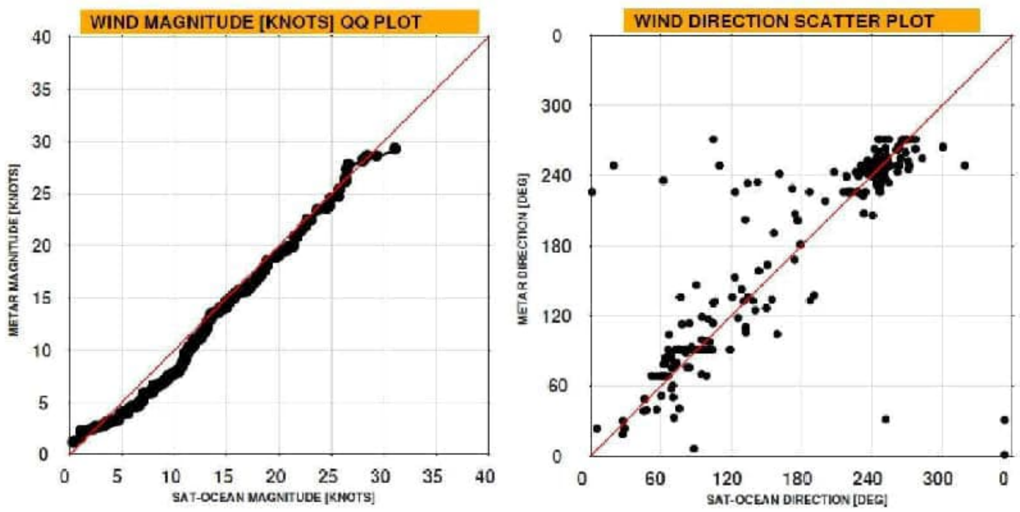

Figure 7 Wind speed QQ plot and wind direction scatter plot of SATOCEAN model vs observation for the considered period

Appendix B

DOCUMENT LIMITATIONS

DOCUMENT LIMITATIONS

This document has been provided by WSP Group Africa Pty Ltd ("WSP") subject to the following limitations:

i) This Document has been prepared for the particular purpose outlined in WSP's proposal and no responsibility is accepted for the use of this Document, in whole or in part, in other contexts or for any other purpose.

ii) The scope and the period of WSP's Services are as described in WSP's proposal, and are subject to restrictions and limitations. WSP did not perform a complete assessment of all possible conditions or circumstances that may exist at the site referenced in the Document. If a service is not expressly indicated, do not assume it has been provided. If a matter is not addressed, do not assume that any determination has been made by WSP in regard to it.

iii) Conditions may exist which were undetectable given the limited nature of the enquiry WSP was retained to undertake with respect to the site. Variations in conditions may occur between investigatory locations, and there may be special conditions pertaining to the site which have not been revealed by the investigation and which have not therefore been taken into account in the Document. Accordingly, additional studies and actions may be required.

iv) In addition, it is recognised that the passage of time affects the information and assessment provided in this Document. WSP's opinions are based upon information that existed at the time of the production of the Document. It is understood that the Services provided allowed WSP to form no more than an opinion of the actual conditions of the site at the time the site was visited and cannot be used to assess the effect of any subsequent changes in the quality of the site, or its surroundings, or any laws or regulations.

v) Any assessments made in this Document are based on the conditions indicated from published sources and the investigation described. No warranty is included, either express or implied, that the actual conditions will conform exactly to the assessments contained in this Document.

vi) Where data supplied by the client or other external sources, including previous site investigation data, have been used, it has been assumed that the information is correct unless otherwise stated. No responsibility is accepted by WSP for incomplete or inaccurate data supplied by others.

vii) The Client acknowledges that WSP may have retained sub-consultants affiliated with WSP to provide Services for the benefit of WSP. WSP will be fully responsible to the Client for the Services and work done by all its sub-consultants and subcontractors. The Client agrees that it will only assert claims against and seek to recover losses, damages or other liabilities from WSP and not WSP's affiliated companies. To the maximum extent allowed by law, the Client acknowledges and agrees it will not have any legal recourse, and waives any expense, loss, claim, demand, or cause of action, against WSP's affiliated companies, and their employees, officers and directors.

viii) This Document is provided for sole use by the Client and is confidential to it and its professional advisers. No responsibility whatsoever for the contents of this Document will be accepted to any person other than the Client. Any use which a third party makes of this Document, or any reliance on or decisions to be made based on it, is the responsibility of such third parties. WSP accepts no responsibility for damages, if any, suffered by any third party because of decisions made or actions based on this Document.

WSP GROUP AFRICA (PTY) LTD

Building 1, Maxwell Office Park
Magwa Crescent West, Waterfall City
Midrand, 1685
South Africa

wsp.com